Functional Polypyrrole Core-Shell Particles and Flexible Membranes for Biomedical Applications

Thèse

Jifu Mao

Doctorat en Médecine Expérimentale

Philosophiae Doctor (Ph.D.)

Québec, Canada

Functional Polypyrrole Core-Shell Particles and Flexible Membranes for Biomedical Applications

Thèse

Jifu Mao

Sous la direction de :

Ze Zhang, directeur de recherche

Résumé

Le polypyrrole (PPy), l'un des polymères conducteurs de type p, a démontré un potentiel considérable dans les applications biomédicales et le stockage d'énergie en raison de sa conductivité électrique intrinsèque, sa facilité de synthèse, son potentiel de modification chimique et sa biocompatibilité. En raison de la conjugaison étendue dans ses chaînes moléculaires et de son état d'agrégation, les mauvaises propriétés mécaniques et le manque de processabilité du PPy ont été des défis scientifiques et technologiques exceptionnels. En outre, le PPy possède une bioconductivité, mais aucune bioinductivité, c'est-à-dire une absence de biofonctionnalité, ce qui constitue un autre défi pour le PPy lorsqu'il est utilisé pour des applications biomédicales. Cette thèse se concentre principalement sur ces deux défis auxquels le PPy fait face, c'est-à-dire le manque de biofonctionnalité et la mauvaise performance mécanique.

En se basant sur la différence des réactivités chimiques des comonomères, les particules de poly(pyrrole-co-(1- (2-carboxyéthyl)pyrrole structurées en noyaux-coquilles (P(Py-PyCOOH)) ont été synthétisées. Elles sont constituées d'un noyau composé d'un copolymère de P(Py-PyCOOH) riche en PPy et d'une coque composée de PPy-COOH. Les paramètres expérimentaux de polymérisation en émulsion ont été étudiés pour définir les conditions optimales. L'anticorps d'albumine de sérum humain (anHSA), en tant que molécule modèle a été immobilisé par des liaisons covalentes sur la surface des particules et a été prouvé réactif aux antigènes. Un schéma a été proposé pour illustrer la formation des particules de cœur-coquille (P(Py-PyCOOH)) selon un nouveau mécanisme basé sur les réactivités du comonomère. Cette méthode de fabrication peut permettre de préparer des particules de PPy fonctionnelles en grande quantité. La chimie de surface et de masse, la conductivité et le rendement global des particules peuvent être régulés.

Pour la première fois, une membrane en PPy souple et mécaniquement traitable (PPy-N) a été préparée par polymérisation interfaciale assistée par modèle (TIP) sans modification chimique des monomères ni autres matériaux. Les structures uniquement interconnectées et multicouches ont été considérées comme responsables de l'excellente souplesse aux températures ambiante et à -196 °C. Un mécanisme basé sur la nature exothermique de la polymérisation du pyrrole a été suggéré pour expliquer les morphologies du PPy-N. Cette

membrane en PPy flexible a un poids léger (9 g m^{-2}), une grande surface (14,5 m^2 g^{-1}), un comportement électrothermique stable, une amphiphilicité et une excellente cytocompatibilité.

Enfin, une nouvelle approche modulaire a été proposée pour immobiliser les protéines sur une surface micro/nano structurée. L'albumine de sérum bovin (BSA) et la HSA ont été immobilisées de manière covalente sur la surface des particules (P(Py-PyCOOH) avant qu'elles soient assemblées sur la surface de la membrane PPy-N pour construire une surface biofonctionnée avec la coexistence de deux types de biomolécules. Cette approche sépare la greffe de protéines et l'immobilisation en deux étapes indépendantes, fournissant ainsi une méthode simple et hautement flexible pour concevoir et fabriquer une surface ou un échafaudage multi-biofonctionnalisé.

Summary

Polypyrrole (PPy), one of p-type conducting polymers, has shown considerable potential in biomedical applications and energy storage owing to its inherent electrical conductivity, ease of synthesis, possibility of further chemical modification, and biocompatibility. Due to the extensive conjugation in PPy chains and the aggregation state, the poor mechanical property and processability of pristine heterocyclic PPy have been the outstanding scientific and technological challenges. Moreover, PPy only possesses bioconductivity but no bioinductivity, i.e., lack of biofunction, which is another challenge for PPy when it is applied in biomedical applications. This thesis mainly focuses on these two issues of PPy, i.e., the lack of biofunctionality and the poor mechanical performance.

Based on the difference in comonomer reactivity, the core-shell structured poly(pyrrole-co-(1-(2-carboxyethyl)pyrrole)) (P(Py-PyCOOH)) particles were synthesized, comprising the pyrrole (Py) dominated P(Py-PyCOOH) copolymer as the core and PPyCOOH homopolymer as the shell. Experimental parameters of emulsion polymerization were investigated to define the optimal conditions. Anti-human serum albumin antibody (anHSA) as a model molecule was covalently immobilized onto the particle surface and proven reactive to its antigen. A schema was proposed to illustrate the formation of the core-shell (P(Py-PyCOOH)) particles based on a new reactivity-driven mechanism. This fabrication method can be used to prepare functional PPy particles in large-scale. The surface and bulk chemistry, conductivity, and the overall yield of the particles can be regulated.

For the first time, a soft and mechanically processable PPy membrane (PPy-N) was prepared by template assisted interfacial polymerization (TIP) with neither chemical modification of the monomers nor compounding with any other materials. The uniquely interconnected and multilayered structures were considered responsible for the excellent flexibility at both room temperature and -196 °C. A mechanism based on the exothermic nature of pyrrole polymerization was suggested to explain the morphology of the PPy-N. Such a flexible PPy membrane has lightweight (9 g m^{-2}), large surface area (14.5 m^2 g^{-1}), stable electrothermal behavior, amphiphilicity, and excellent cytocompatibility.

Finally, a novel modular approach was proposed to immobilize proteins to a micro/nano structured surface. Bovine serum albumin (BSA) and HSA were covalently immobilized onto the surface of the (P(Py-PyCOOH)) particles prior to their assembly onto the surface of the PPy-N membrane, to construct a biofunctionalized surface with the coexistence of two types of biomolecules. This approach separates protein grafting and immobilization into two independent steps, providing an easy and highly flexible method to design and fabricate multi-biofunctionalized surface or scaffold.

CONTENTS

List of Tables

List of Figures

List of Abbreviations

anti-HSA	Human serum albumin antibody
ATP	Adenosine triphosphate
BC	Bacterial cellulose
BET	Brunner-Emmet-Teller Measurement
BSA	Bovine serum albumin
CNF	Carbon nanofiber
CNT	Carbon nanotube
Col	Collagen
CP	Conducting polymer
CS	Chondroitin sulphate
DBS	Dodecylbenzenesulfonic acid sodium salt
DEHS	Di(2-ethylhexyl) sulfosuccinate
DMEM	Dulbecco's modified Eagle's medium
DS	Dextran sulphate
dsDNA	Double stranded DNA
DTG	Derivative thermogravimetric analysis
ECM	Extracellular matrix
ECP	Electrically conducting polymer
EDC	N-(3-Dimethylaminopropyl)-N′-ethylcarbodiimide hydrochloride
EDLC	Electric double layer supercapacitor
EIS	Electrochemical impedance spectroscopy
EO	Ethylene oxide
EP	Electrochemical polymerization
FTIR	Fourier transform infrared spectroscopy
GOD	Glucose oxidase
GOx	Glucose oxidase
HA	Hyaluronic acid
HCG	Human chorionic gonadotropin
HE	Heparin
HSA	Human serum albumin

IC	Indigo carmine
ICP	Intrinsically conductive polymer
LDH	Layered double hydroxides
LIB	Lithium-ion battery
MO	Methyl orange
NGC	Nerve guidance conduit
NGF	Nerve growth factor
NHS	N-Hydroxysuccinimide
NMP	N-methylphenothiazine
NMR	Nuclear Magnetic Resonance
P(Py-PyCOOH) or PPy-co-PPyCOOH	Poly(pyrrole-co-(1-(2-carboxyethyl)pyrrole))
PA	Polyacetylene
PAN	Polyacrylonitrile
PANI	Polyaniline
PBS	Phosphate buffered saline
PC	Polycarbazole
PCL	Polycaprolactone
PDLLA	Poly (D,L-lactide)
PEDOT	Poly(3,4-ethylenedioxythiophene)
PEG	Polyethylene glycol
PET	Poly(ethylene terephthalate)
PF	Polyfluorene
PI	Polyindole
PLA	Polylactic acid
PLGA	Poly(lactic-co-glycolic acid)
PMAS	Poly(2-methoxyaniline-5-sulfonic acid)
PPP	Polyphenylene
PPV	Poly(phenylene-vinylene)
PPy	Polypyrrole
PPyCOOH	Poly(1-(2-carboxyethyl)pyrrole))
PPy-N	Flexible PPy membrane with nanotubes

PPy-NH_2	Poly (pyrrole-co-N-3-aminopropylpyrrole)
PPy-NHS	Poly(pyrrole-co-succinimidyl pyrrole)
PPy-P	PPy membrane with particles
PPy-PO	Poly(pyrrole-co-N-glycidylpyrrole)
PS	Polystyrene
PSS	Poly(styrenesulfonate)
PTH	Polythiophene
pTS	Para-toluenesulfonic acid
PU	Polyurethane
PVA	Polyvinyl alcohol
PyCN or Py-CN	N-(2-cyanoethyl)pyrrole
PyCOOH or Py-COOH	1-(2-carboxyethyl)pyrrole
$PyNH_2$ or Py-NH_2	N-3-aminopropylpyrrole
PyOH or Py-OH	2-(1H-Pyrrol-1-yl)ethanol
PyPO or Py-PO	N-glycidylpyrrole
RGD	Arg-Gly-Asp
rGO	Reduced graphene oxide
SEM	Scanning electron microscopy
ssDNA	Single stranded DNA
TEM	Transmission electron microscopy
Tg	Glass transition temperature
TGA	Thermal gravity analysis
TIP	Template assisted interfacial polymerization
XPS	X-ray photoelectron spectroscopy

Acknowledgements

To achieve one of my dreams and great objectives, I came from as far as oriental China to defend a PhD at Université Laval, Canada, nearly 5 years ago. While I owned nothing when I came here and I still do now, the delightful experience of studies and life in Québec makes me have strong mental qualities and knowledge to meet the next phase of my life. Although being a personal achievement, such an honor and a privilege cannot be accomplished without countless academic, educational and psychological help, encouragement and supports from many special people surrounding me.

First of all, I would like to express my deepest appreciation and thanks to Prof. Ze Zhang for inviting me to join his research group, for bringing me into the field of conductive polymers, and for the continuous and patient guidance in my research. As an eminent scientist, Ze inspired me and provided me numerous valuable suggestions on my research and paper writing. My gratitude is also extended to a great deal of freedom on my research that he gave me, as well as the encouragement and trust. Furthermore, Ze always encourages and supports financially me to attend the academic conferences to keep up to date with new developments of biomaterials and to improve my social and communicative competence. Here, I would also like to thank Madam Jin Yang for inviting me to join the family parties during Spring Festival that gave me a home feeling in Québec City.

I would also like to address my sincere thanks to Prof. Robert Guidoin for offering an opportunity to join his project on artificial heart valve and stent graft. He helps me deeply understand from basic research of biomaterials to clinical applications of medical device. His perpetual energy and enthusiasm on academic research shall inspire my future research life. I am grateful to Prof. Mahmoud Rouabhia from faculty of dentistry of Université Laval, Prof. Xingyi Xie from Sichuan University, and Prof. Shiyun Meng from Chongqing Technology and Business University for their valuable discussions and suggestions.

I also wish to thank all my colleagues for their friendship and great help: Dr. Hyun Jin Park and Dr. Yongliang Wang contributed to the work of cell culture involved in my thesis; Dr. Bin Li, Dr. Olexandr Bondarenko, Madam Dingkun Wang, and Mr. Zhiyong Du provided generous discussions on immunology; Madam Yiwei Tong helped to prepare attractive

graphic abstracts and polish manuscripts; Madam Chaojing Li assisted with mechanical measurements and analysis; Dr. Yingchao Su and Madam Mahrokh Dorri taught me how to perform electrochemical impedance spectroscopy test and analysis. And I am also very gratefully for the technical assistances from Dr. Stéphane Turgeon, Dr. Pascale Chevallier, Dr. Sébastien Meghezi, and Madam Andrée-Anne Guay-Bégin. The help from Dr. Xu Dong on BET (Brunauer-Emmett-Teller mearsurement) surface area measurement is also greatly appreciated.

I highly appreciate the financial support from the Natural Sciences and Engineering Research Council of Canada (NSERC), the Canadian Institutes of Health Research (CIHR), and scholarships from Medicine Faculty of Université Laval and from Fondation du CHU de Québec.

My thanks and wishes are also extended to my close Chinese friends in Université Laval and the exchange students from Shanghai Jiao Tong University and Sichuan University for their helpc encouragement, and support.

Special thanks to my parents, godmother, younger brother, and relatives for their continuous love and support throughout my life. Every Sunday, telephone calls and video chats through internet made me feel the warmth of my family. In particular, I would like to express gratitude to my godmother Madam Ximeng Zhang for guiding me with a positive attitude towards life, love and career.

To my parents, Guixia Gao and Chuanwen Mao

To my godmother, Ximeng Zhang

To my brother, Jicai Mao

《Heaven helps those who help themselves》

Samuel Smiles (1812-1904)

Foreword

This PhD thesis contains six chapters, including four scientific articles (Chapter II to V) that either have been published, submitted or to be submitted. The research work was conducted in the Centre de Recherche du CHU de Québec located in l'Hôpital Saint-François d'Assise.

Chapter I reviews the background knowledge related to the research project, including the preparation and properties of PPy, its potential applications and challenges, and how to biofunctionalize and manufacture PPy-based materials. The hypotheses and objectives of the thesis are presented at the end of this chapter.

Chapter II reveals a novel reactivity-driven mechanism in the synthesis of the core-shell structured conductive polymer particles. The reactions are based on the difference in comonomer reactivity via a simple one-step and one-pot emulsion polymerization. Chapter II was published in ***J. Mater. Chem. B***, 2016, 4, 5429-5436 authored by Jifu Mao and Prof. Ze Zhang. Jifu Mao: experiments and manuscript writing; Prof. Ze Zhang: supervision of the experiments, revision of the manuscript and the financial support.

Chapter III demonstrates the optimization of experimental parameters in the one step emulsion polymerization of the functional PPy particles, including the ratio of water/oil, feeding of $FeCl_3$ and functional monomers, as well as reaction time, based on a balance in the quantity of carboxyl groups on particles surface, conductivity and overall yield. This part of the work has been published in ***Polymer*** 2016,105,113-123 authored by Jifu Mao and Prof. Ze Zhang. Jifu Mao: experiments and manuscript writing; Prof. Ze Zhang: supervision of the experiments, revision of the manuscript and the financial support.

Chapter IV presents a new approach named template assisted interfacial polymerization that was used to prepare a mechanically processable pristine PPy membrane possessing a remarkable softness and flexibility even in liquid nitrogen, despite the fact that the glass transition temperature of PPy is above 100 ^{o}C. Jifu Mao: experiments and manuscript writing; Prof. Ze Zhang: supervision of the experiments, revision of the manuscript and the financial support; Madam Chaojing Li: mechanical measurements and analysis; Dr. Hyun Jin Park: cell culture; Prof. Mahmoud Rouabhia: providing useful suggestions and discussion on the

results. This research has been published in ***ACS Nano*** 2017 (DOI: 10.1021/acsnano.7b05546).

Chapter V reports a straightforward strategy to prepare a functional and flexible electrically conducting PPy membrane, taking the advantages of the topology of nanotubes on the PPy membrane and the pea-like structure of the P(Py-PyCOOH) particles. This work is to be submitted to a scientific peer reviewed journal.

Finally, Chapter VI presents the general discussion, general conclusion and also the perspectives.

CHAPTER I

INTRODUCTION

1.1 Polypyrole (PPy)

1.1.1 Intrinsically conductive polymers

Intrinsically conductive polymers (ICPs), also known as conducting polymers (CPs) or electrically conducting polymers (ECPs), are conjugated polymers possessing unique electrical conductivity, electron affinity, and redox activity, which are different from carbon-based and metal filler-based conductive polymeric composites. The backbone of CPs always consists of π-conjugated chains allowing unpaired electrons delocalizing along the polymer chain, which is one of the basic requirements for CPs [1]. Another requirement is doping treatment which was systematically investigated in 1970s [2]. Following the accidental discovery of the silvery polyacetylene (PA), Heeger, Macdiarmid and Shirakawa cooperatively indicated that after a doping process, the conductivity of PA membrane was increased remarkably to 10^3 S cm^{-1}, an increase of around 8 orders of magnitude [2], for which they were awarded the Chemistry Nobel Prize in 2000. Since the discovery of doping, numerous CPs of high conductivity were synthesized successively [1, 3, 4], such as PPy, polyphenylene, polythiophene, poly(3,4-ethylenedioxythiophene), poly(phenylene-vinylene), and polyaniline. Their chemical structures are shown in Figure 1.1.

For an overwhelming majority of CPs, a treatment with suitable dopants can make them remarkably conductive. A neutral CPs can be *p*-doped with anions (oxidizing) or *n*-doped with cations (reducing). The dopants not only neutralize and stabilize the positive charges of the oxidized polymer backbone, but more importantly also delocalize the valence electrons to prompt the charge flux through the polymer upon an electrical potential applied to the polymer [5]. That is, the doping process introduces charge carriers moving along the backbone of CPs to generate electrical conductivity. The conductivity of CPs depends on the energy of the band gap, which is the distance between conducting band and valence band. The smaller band gap energy is, the better conductivity is considered to be. Band gap is affected mainly by the nature of dopant, doping level, synthesis method and temperature [6]. For example, the band gap of PPy decreases with the increasing of doping level [7]. Among all CPs, because of its superiority in conductivity, ease of synthesis, chemical stability and biocompatibility, PPy

has been in the focus of investigations, particularly for biomedical applications, energy storage, antistatic, and electric heating elements [8-11].

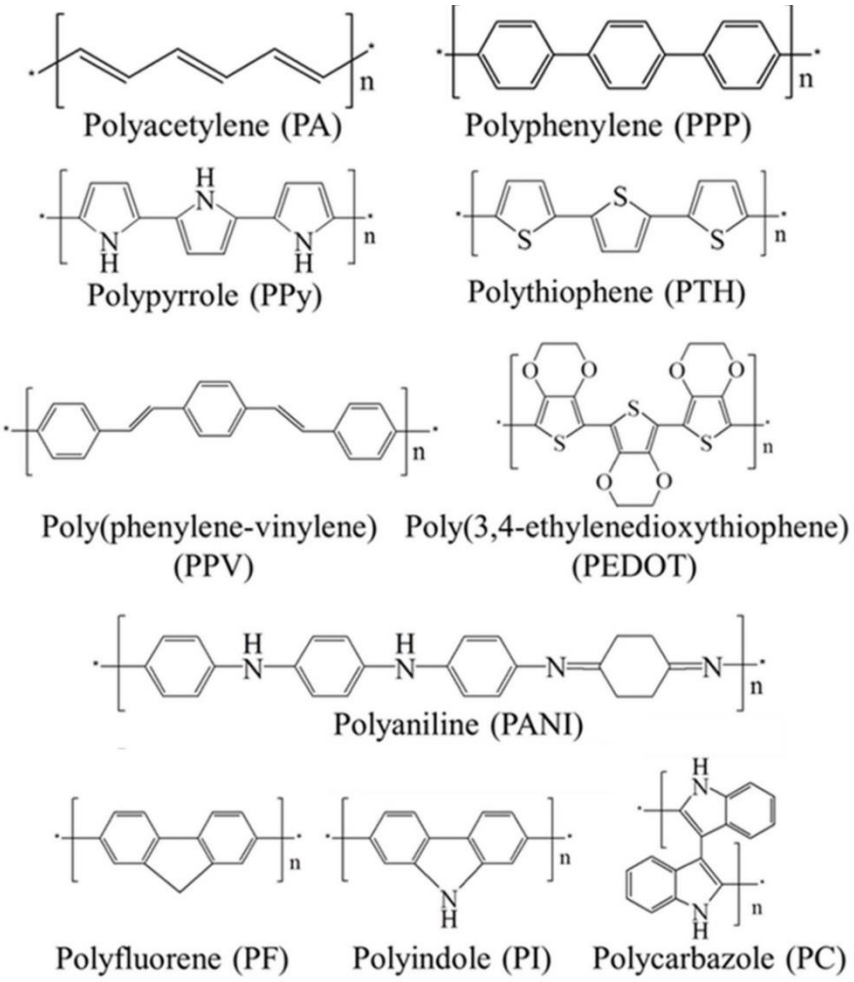

Figure 1.1 Chemical structures of some common conducting polymers [3].

1.1.2 History and chemical structure of PPy

Though the preparation of PPy could date back to early 1910s, the electrically conducting PPy was first discovered and reported only in the early 1960s [12], while the significantly conductive PPy had not been studied extensively until the electrochemistry method became employed in 1980s [13]. As shown in Figure 1.1, the ideal chemical structure of PPy was formed by a number of pyrrole rings repeatedly connected through the carbon at α position of the monomers. However, linear molecules formed by α-α linkages can only be achieved at the beginning of the polymerization. With the growth of a PPy molecule, the activation of β sites allows different arrangement of pyrrole rings, thus forming a three-dimensional (3D) cross-

linked network. Moreover, the insertion of dopants and the distortion of chains will lead to different inclinations such as cones or helices [14]. Highly cross-linked structures reduce the conjugation length, electrical conductivity, and solubility of PPy. Therefore, it is generally known that PPy is very difficult to further process once synthesized, presenting non-thermoplastic, mechanically rigid, brittle and insoluble characteristics [15]. In general, the heterogeneity of PPy structure due to the nonlinear polymerization makes it inferior in conductivity, mechanical properties and processability. Because of this, instead of being used as a single component, PPy has to be composed with other types of materials to form composites (in form of filler, coating, or suspension).

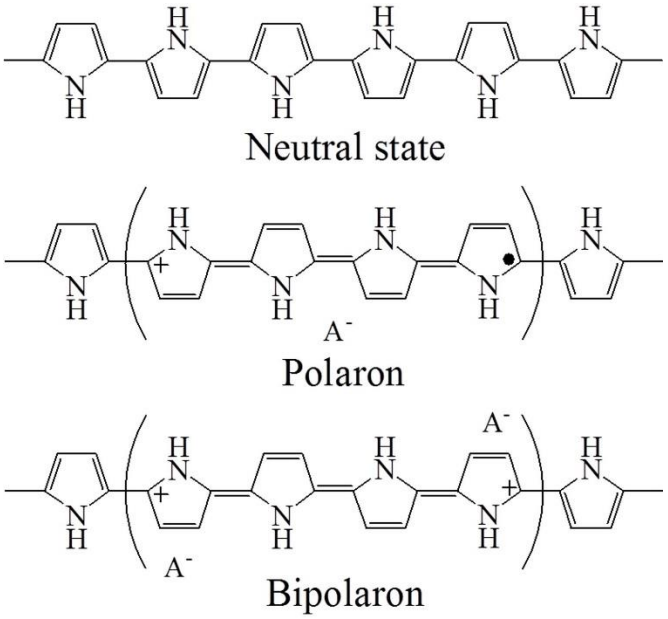

Figure 1.2 Neutral, polaron and biopolaron chemical structures of PPy. +: charge; •: unpaired electron; A-: dopant.

Because the backbone of the oxidized PPy is positively charged [16], understandably, it is necessary for conducting PPy to possess suitable anionic counterions. Previous studies have concluded that, depending on the level of oxidation, conduction via polarons or bipolarons (Fig. 1.2) is the dominant mechanism of charge transport in PPy [8, 16]. Bipolaron is generated either by the further oxidation and removal of the unpaired electron in polaron, or by the union of two independent polarons between the adjacent chains through a charge transfer reaction. Comparing to polarons, bipolarons are more favorable to transfer along the PPy chains and are considered the dominant charge carrier. Based on the doping ratio of nitrogen

in pyrrole rings, oxidized PPy normally has one charge for every three or four pyrrole repeating units [17]. Noticeably, the morphology and properties of PPy are inextricably linked to its synthesis methods, generally including electropolymerization and chemical polymerization.

1.1.3 Preparation methods of PPy

1.1.3.1 Electrochemical polymerization

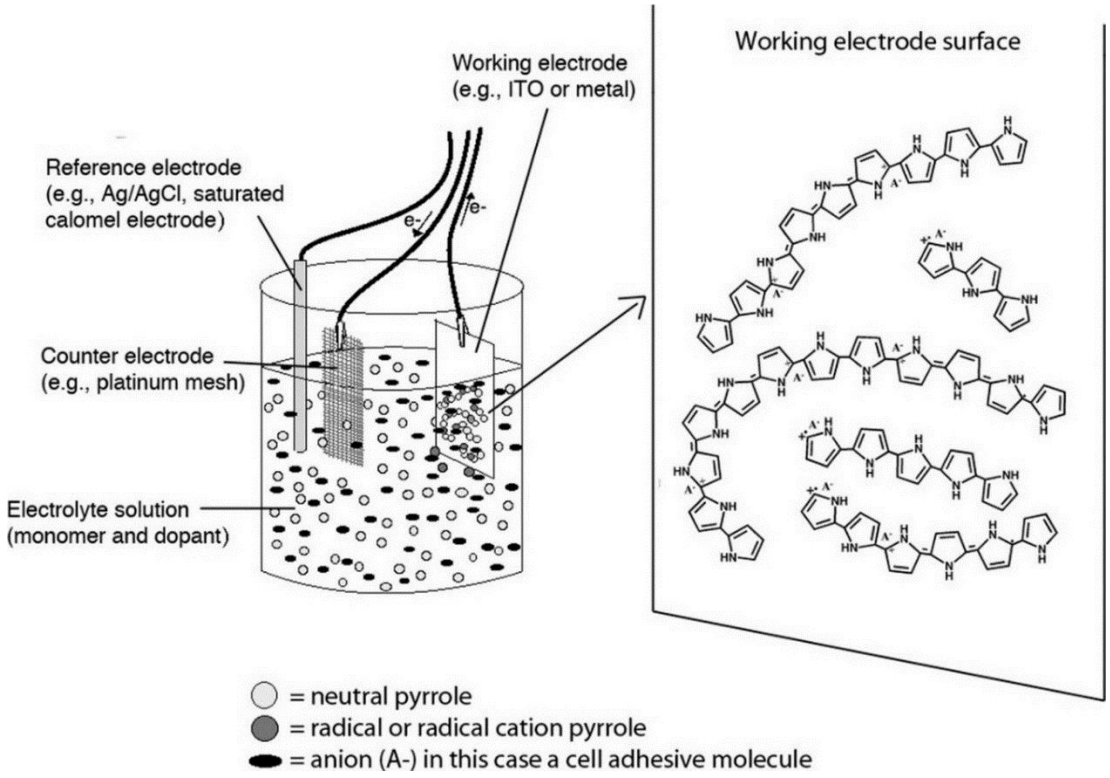

Figure 1.3 Three-electrode system for electrochemical polymerization: reference, working, and counter electrodes submersed in a monomer and electrolyte solution[8, 18].

Although PPy was first synthesized through chemical oxidation, the first well recognized conductive PPy film (100 S cm^{-1}) was prepared by Diaz via electro-oxidation on a platinum electrode in acetonitrile at 1979 [19]. This historic finding opened the prologue of research on CPs using EP. As shown in Fig. 1.3, PPy prepared through EP is in the form of a film on the working electrode of a three-electrode configuration (working, counter, and reference electrodes), which usually shows a uniform structure and high conductivity. In the solution, there are Py monomer, solvent, and electrolyte (dopant) [8]. Various modes of EP were

developed to synthesize PPy including potentiostatic (constant potential), galvanostatic (constant current), and potentiodynamic (potential scanning, i.e. cyclic voltammetry) [20, 21]. The main advantages of EP lie on [16, 22]: a). The product is an electroactive film with high conductivity; b). The product is generally obtained in the doped state after synthesis. For example, biological molecules can be used as dopant and directly incorporated into polymer during polymerization; c). The mass and thickness of the film can be controlled by the total charge via regulating potential/current and polymerization time; d). The in situ coating of PPy on complex substrate is particularly useful for preparing sensors. Though various mechanisms have been proposed to explain the mechanism of EP, two of them received the greatest attention, that is, the oxidative coupling of monomer molecules[23] and the free radical reaction[24].

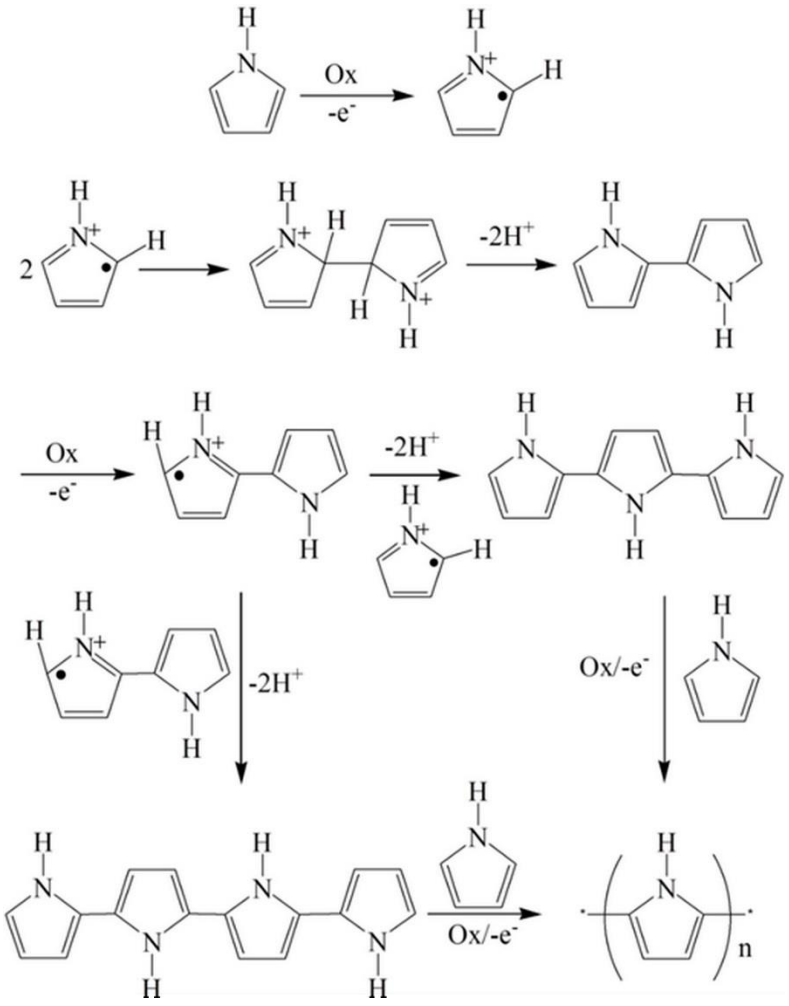

Figure 1.4 Scheme of the electrochemical (chemical) polymerization mechanism of PPy[23, 25, 26].

For now, a pseudo-polycondensation mechanism presented by Diaz [23] is most commonly accepted in the literature, which is considered appropriate for both EP and chemical polymerization of PPy. There are 7 steps in this mechanism [23, 25, 26], as shown in Fig.1.4, including the formation of a cation radical monomer, coupling between two radicals, loss of two protons to form an aromatic dimer, oxidation of the dimer to form a cation radical, coupling between the radical dimer themselves or with an active monomer, and the propagation that continues via the same sequence till termination. Termination happens when no further monomer left or side reactions terminate the propagation [27].

In conventional EP of PPy, the monomers were oxidized at the working electrode surface forming an insoluble and thin polymer film. The morphology and properties of the PPy film depend on a number of variables including the nature of the solvent, pH, temperature, electrolyte, electrode system, the purity and the concentration of monomer, and deposition time and charge [8, 22]. Stripping the PPy film off the working electrode is not always feasible because of the strong adhesion and the brittleness of the PPy film that is normally only several micrometers in thickness. Meanwhile, the area of the film totally depends on the size of the substrate or electrode, which is one of the main restrictions. To produce large films, a free-standing PPy film was generated at the air/liquid interface through EP [28]. Li also electrochemically synthesized free-standing PPy film at the three-phase interline, and evaluated the effect of potential, counterion and pyrrole concentration [29]. However, the disadvantages of EP lie in the low productivity, high cost, and specialized equipment, and the requirement for the carefully processed electrode and high-purity chemicals. Therefore EP is a more promising method to prepare electronic devices and sensors.

1.1.3.2 Chemical polymerization

Chemical polymerization is one of the first and still the most widely used approach for the preparation of PPy. Due to its solubility and the low oxidation potential that is less than 0.8V, pyrrole is vulnerable to oxidation and so can be synthesized chemically in a series of aqueous and non-aqueous solvents [30]. The chemical polymerization of PPy takes place when pyrrole meets the oxidant in a solvent according to the mechanism illustrated in Fig. 1.4, in which monomer oxidation is realized by the oxidant instead of oxidative electrical potential. In general, in solution polymerization, PPy precipitates as insoluble matter in forms of either

the deposition on the surface of various substrates or homogeneous powder. Compared to EP, chemical synthesis is preferred when a large quantity of CPs is required, which is particularly true for commercial applications. Furthermore, all types of CPs can be synthesized by chemical polymerization, including several novel CPs made of modified monomers that cannot be polymerized with EP [8, 15]. The products of chemical polymerization, in form of powder or surface coating, can serve as filler or coating layer to provide conductive property to the composites. In addition, chemical polymerization also offers many advantages such as low cost, simple process, high efficiency, and great yield. The properties of PPy prepared through chemical polymerization are inextricably linked to the nature and feeding of oxidant, the concentration of pyrrole, the solvent, reaction temperature and time, and also the selection of surfactant and additives [22, 30-34].

Plenty of oxidants such as H_2O_2, $(NH_4)_2S_2O_8$, $K_2S_2O_8$, and many kinds of salt containing transition metal ions or their mixtures, for instance, Fe^{3+}, Cu^{2+}, Cr^{6+}, Ce^{4+}, Ru^{3+}, Mn^{7+}, could be used as oxidant to chemically synthesize PPy [35-38]. Among them, extensive studies have been devoted to the use of $FeCl_3$ as oxidant for the polymerization of PPy [30, 31, 36]. In this way, the polymer is automatically doped by Cl^- anions during the process of synthesis. The overall stoichiometric reaction can be represented by Figure 1.5 [17, 22, 30], where y is the doping level that represents the oxidation degree of PPy. The general steps of chemical polymerization of PPy also follow what illustrated in Fig 1.4, that is, cation radical monomer formation, coupling of radicals, aromatic dimer formation, cation radical dimer formation, coupling between radical dimer themselves or with the active monomer, propagation, and the termination. However, as mentioned above, the polymerization of PPy does not only lead to a linear propagation [14]. Linear PPy molecules only form at the beginning of the polymerization, which allows the formation of α-α linkages. With the growth of polymer chains, the activated β sites enable the creation of α-β linkages leading to insoluble 3D cross-linked structures and making it difficult to evaluate the polymerization degree of the final PPy. The linear PPy molecules are favored for high conductivity due to their regular π-conjugation allowing a better charge carrier movement. In fact, variations in orders of magnitude in PPy conductivity can be gained by adjusting only the polymerization time [33, 39-41]. Reaction temperature mainly impacts on both the polymerization kinetics and the side reactions [41]. That is, a reasonably linear PPy with good conductivity can be synthesized at

low reaction temperature. Meanwhile, protic solvents possessing hydroxyl groups are recommended to synthesize PPy with high conductivity. When the ratio of Fe^{3+}/pyrrole is 2.33 and the reaction takes place in methanol for a short reaction time at low temperature, the highest conductivity of PPy can reach 220 S cm^{-1} [33]. The use of suitable surfactant in emulsion polymerization can further improve the conductivity and yield [32, 42]. Surfactant plays an important role to create the emulsion and improve the physical properties of PPy. For example, dodecylbenzenesulfonic acid sodium salt (DBS) can act as an additional dopant (counterion) to improve PPy stability and conductivity [43].

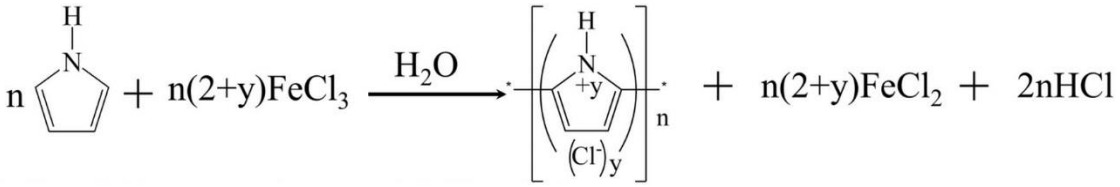

Figure 1.5 A stoichiometric chemical polymerization of PPy with ferric chloride oxidant [17, 22, 30].

Furthermore, it is especially noteworthy that chemical polymerization has a superiority in preparation of PPy with designed nanostructures via template method. The nanostructures can render PPy high in conductivity, large specific surface area, light-weight, fast in ion exchange, and enhanced mechanical properties [9, 44-46]. The template synthesis of PPy generally includes soft template and hard template methods. The soft template strategy typically consists of self-assembled micelles formed by surfactants that can guide the growth of PPy molecules to prepare low dimensional nanomaterials. According to the solvent system and selection of surfactant, soft template method involves emulsion, reversed-emulsion and self-template polymerization. In this type, the morphology and properties of PPy could be well controlled by the nature and concentration of surfactants [42, 46]. As for the hard template synthesis, the PPy polymer with controllable shape can be fabricated using physical scaffolds, such as colloidal particles and nanoarrays of metal, oxides, silica, and carbon [9]. Though some template-free chemical polymerization methods were also designed to generate nano-structural PPy [47], template synthesis has received increasing interest for its capacity to produce well-defined nanostructures. In general, the combination of chemical polymerization and template offers a flexible, simple, and efficient route to fabricate nano-sized PPy, with many advantages such as low cost, large quantity and one-pot synthesis. By changing the

templates and chemical polymerization systems, as shown in Fig 1.6, PPy can be prepared into different nano-sized morphologies, such as cauliflower-like particles, nanoparticles, nanocapsules, nanowires, nanofibers, nanotubes, thin film, hydrogel, and sponge.

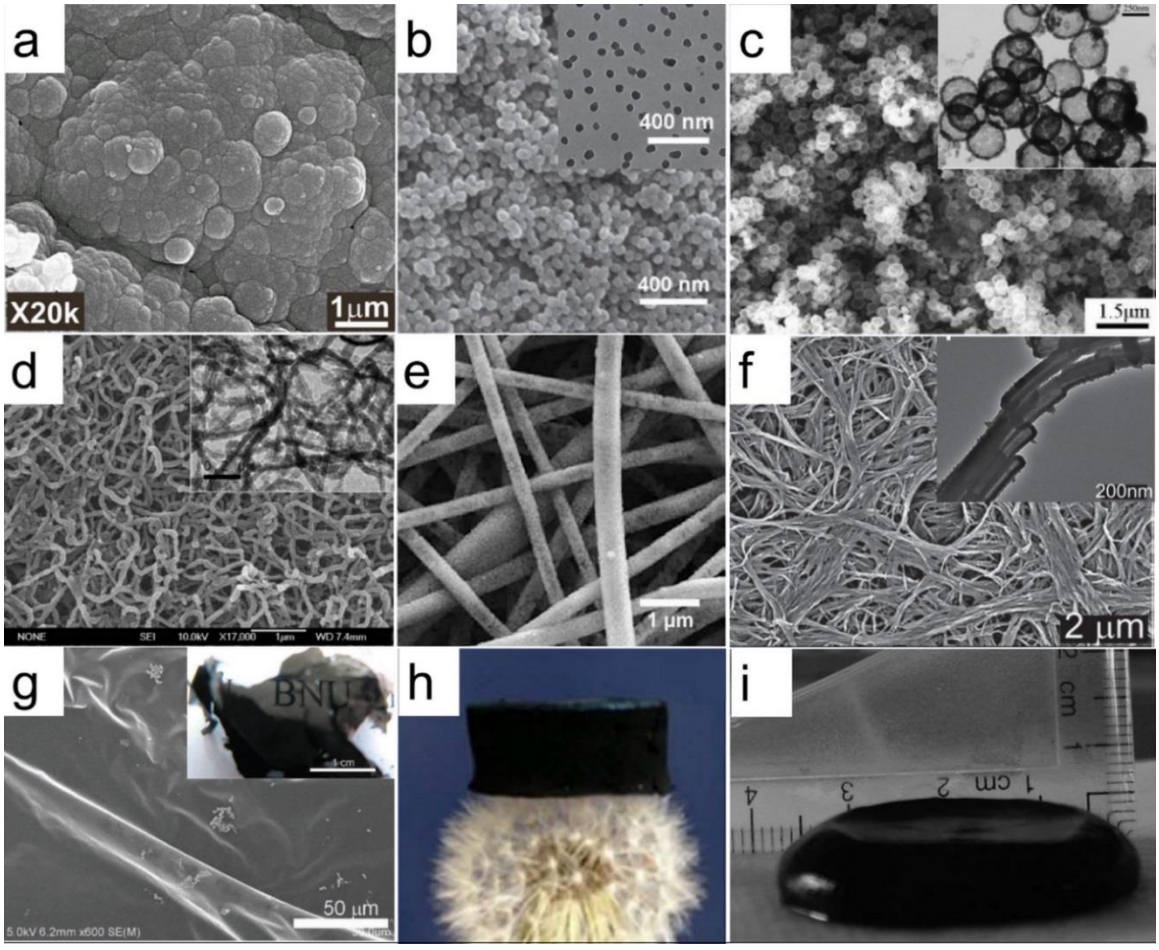

Figure 1.6 Morphology of PPys: a, cauliflower-like particles [48]; b, nanoparticles [49]; c, nanocapsules [50]; d, nanowires [51]; e, nanofibers [52]; f, nanotubes [53]; g, film [54]; h, sponge [55]; I, hydrogel [56].

1.1.4 Morphology of PPys

Cauliflower-like nodules are the most general morphology of PPy especially for the coating layer electrochemically polymerized on a substrate [57]. By controlling the chemical polymerization conditions, such nodular PPy can also be formed [48]. Actually, the cauliflower-like nodular PPy can be considered as the aggregation of PPy nanoparticles; and most PPy films obtained by electrochemical and chemical polymerizations are constructed by nodular

PPy. So this part will be splitted into nanoparticles and films in order to logically illustrate the morphology of PPys from zero dimension (0D) to 3D.

1.1.4.1 Nanoparticles/nanocapsules

During past decades, various synthesis methods have been developed to prepare nano-sized PPy spheres (0D) since they promise great potential in wide applications especially for the preparation of the highly dispersed heterophase composite materials [58-60]. PPy nanoparticles in 100-200 nm were first polymerized in aqueous in the presence of methylcellulose in the 1980s [61]. After that, monodisperse PPy nanopparticles of 20-400 nm in diameter were obtained by controlling the chemical synthesis parameters [60, 62]. The soft template assisted dispersion polymerization and emulsion polymerization are the main routes to prepare the homogeneous PPy nanoparticles. Various water-soluble steric or amphiphilic polymer stabilizers are introduced in dispersion polymerization to prevent macroscopic precipitation by adsorption of the stabilizers onto PPy nanoparticles [63]. And the size and morphology of the PPy nanoparticles depend on the nature and feeding of the stabilizer. By adjusting the molecular weight and concentration of polyvinyl alcohol (PVA), PPy nanoparticles of 20-60 nm in diameter were prepared without using any surfactant [60]. However, PPy nanoparticles prepared in dispersion show a relatively low conductivity because of the steric stabilizer that is difficult to remove. Thus, more attention has been paid to emulsion polymerization using surfactants as stabilizer to form PPy nanoparticles. A range of different surfactants have been employed [62]. PPy nanoparticles of 30-50 nm in diameter and 2.1 S cm^{-1} in conductivity were obtained by emulsion polymerization with DBS as surfactant [64]. Furthermore, Reung-U-Rai et al. improved the conductivity of PPy nanoparticles to 61.9 S cm^{-1} by using an alternative oxidant (ammonium peroxydisulfate) and surfactant (sodium dodecyl sulfate), and introducing a n-amyl alcohol additive [42]. In comparison, hard template synthesis is more effective in fabricating core-shell structural nanoparticles and nanocapsules. Hard template@PPy core-shell nanoparticles can be easily generated through similar dispersion or emulsion polymerization, and numerous hard templates have been investigated, such as polystyrene latex spheres [65], SiO_2 spheres [66], metal [67], metal oxide [68], and inorganic metal salt [69]. The incorporation of the core gives PPy nanoparticles additional specific physicochemical

characteristics. Moreover, some of the cores used as hard template can be subsequently removed to obtain PPy nanocapsules [50, 70].

1.1.4.2 Nanowires/nanofibers/nanotubes

One dimensional (1D) nanostructural PPy materials, i.e., nanowires, nanofibers, and nanotubes, have attracted a great attention recently owing to their high specific surface area and efficient charge and energy transport [46, 71, 72]. Soft template synthesis is the normal choice to prepare PPy nanowires using special surfactants as template. Zhang designed a lamellar inorganic/organic system (cetyltrimethylammonium bromide/ammonium persulfate) as template to fabricate PPy nanowires of 20-60 nm in diameter [72]. Afterwards, Zhong et al. optimized the reaction conditions to improve the yield and morphology [51]. Meanwhile, the alumina membrane with nanochannels inside was also adopted as hard template to form PPy nanowire arrays with high surface areas of 75.66-172.90 m^2/g [73]. PPy nanofiber is easily obtained by hard template polymerization. Abundant PPy nanofibers [52, 74] have been prepared by electrospinning, where natural nanofibres (bacterial cellulose [39]) and carbon nanomaterials [75] were used as templates. Removal of the hard templates from the PPy coated nanofibers is one of the methods to obtain PPy nanotubes[76]. Also, PPy nanotubes were synthesized by emulsion polymerization using sodium bis(2-ethylhexyl) sulfosuccinate as surfactant[77]. Recently, as a hard template method, reactive template has been developed to initiate the polymerization of pyrrole through oxidative reaction and effectively transfer its morphology to PPy at the same time. The V_2O_5 [76] or MnO_2 [78] nanowires/fibers, and the fibrillar complex of $FeCl_3$ and methyl orange (MO) [53] have been widely investigated as the reactive template to polymerize PPy nanotubes. Noticeably, the MO complex template cannot be formed when ammonium peroxodisulphate is used instead of $FeCl_3$ [79].

1.1.4.3 Film

It has been impossible to prepare large-sized two dimensional (2D) PPy without supporting substrate, owing to the infusible and insoluble nature of PPy. There are a small number of reports on the chemical synthesis of PPy film. Photopolymerisation and interfacial chemical polymerisation were designed to obtain PPy film. PPy-Ag nanocomposite films were photopolymerized at dichloromethane-water (200 μm in thickness) and air-water interfaces

(<1 μm in thickness) [80]. Wang's group recently reported free-standing PPy films (100 nm in thickness) with up to 2000 S cm^{-1} in conductivity at a solid-liquid interface via an *in situ* freezing interfacial polymerization method [54]. Additionally, they took the reaction system at room temperature and obtained the PPy film at the cyclohexane/water interface. The semitransparent free-standing PPy films with varied thickness (50-500 nm) and conductivity (150-560 S cm^{-1}) were synthesized by controlling reaction time and pyrrole monomer concentration [81]. Similarly, PPy films were also generated at n-hexane/water interface using Bmim [$FeCl_4$] (1-butyl-3-methylimidazolium tetrachloroferrate) as the oxidant [82]. However, all those PPy films are thin and frail resulting in the difficulty in collecting them from the reaction system, as well as in the further handling and drying processes. Therefore, most flexible and large-sized PPy films or membranes in literatures are constructed by coating PPy onto the support substrates, which are the major contributor to the mechanical properties and processability [83, 84]. Actually, there has been no report of any large-sized, highly flexible and free-standing film of intrinsically conductive polymers.

1.1.4.4 Hydrogel/sponge

PPy hydrogel possesses a high level of porosity made of three dimensional (3D) micro/nano networks resembling natural tissues. Traditionally, PPy hydrogels are formed by polymerization of pyrrole monomers onto the framework of a nonconductive hydrogel, or by blending PPy nanomaterials with the hydrogel component [56, 85]. But, some issues limit the performance of those composite PPy hydrogels, such as the separation of PPy from the substrate during the swelling or shrinking of the hydrogel, and the decrease of conductivity. So, pure PPy hydrogel is highly desired. To date, PPy hydrogels were fabricated by using the reactive MO-Fe^{3+} complex templates under static condition, presenting much faster swelling-shrinking behaviors and size changes compared with the conventional polymer gels [56]. The effective connections among PPy nanotubes and granules via π-π interaction and hydrogen bonding were suggested to be the reason for the formation of PPy hydrogel. Based on that, via long time secondary growth (30 days) without any template, Lu attempted to slow down the reaction by using the deficient oxidant $Fe(NO_3)_3$ to regulate joint density to fabricate an elastic PPy hydrogel [55]. The reduced joint density and coarsened joints of initial network make PPy hydrogel less stiff even in dry condition. Moreover, a copper phthalocyanine-

3,4',4'',4'''-tetrasulfonic acid tetrasodium salt was introduced as both crosslinker and dopant to enhance the conductivity and pseudocapacitance of the PPy hydrogel [86]. As a fledgling research area, for now, there are a few reports about the single component PPy hydrogel. In-depth research is still needed to improve the mechanical properties and processability of 3D PPy materials, especially in dry condition.

1.2 Potential applications of PPy and challenges

1.2.1 PPy in biomedical applications

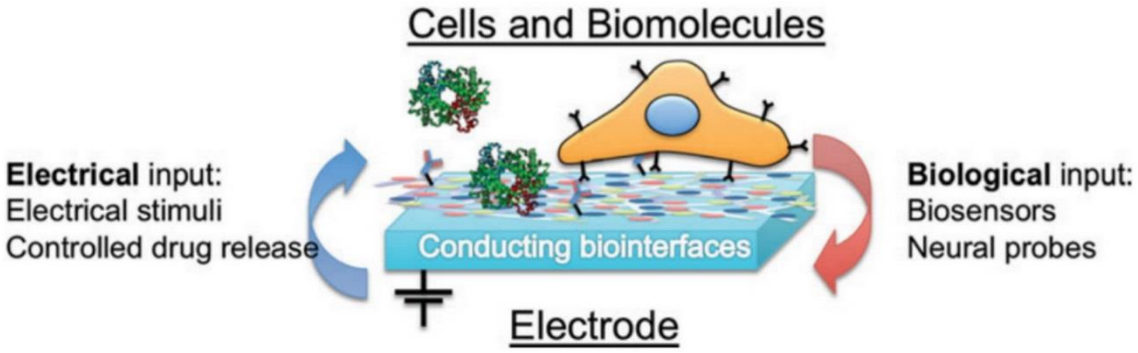

Figure 1.7 PPy serving as a conducting biointerface for various biomedical applications [87].

CPs have been investigated for biomedical applications largely because of the following reasons or expectations: a) CPs can interface the electrical exchange between living organism and external control; b) Biocompatibility; c) CPs are capable of immobilizing and releasing biomolecules [88]; d) Numerous human cells including nerve, bone, muscle, and cardiac cells, are responsive to CPs mediated electrical stimulation [8]; f) Electrical stimulation has already been used in the clinical practices [89]. Biocompatibiliy is essential for CPs to be used in biomedicine. The biocompatibility of PPy has been confirmed by numerous studies in the last decades. Williams and Doherty demonstrated that PPy is cytocompatible [90]. The systemic toxicity of PPy extract was evaluated according to ISO 10993 and ASTM 1748-82, showing no sign of acute toxicity, mutagenesis, pyregen, haemolysis or allergic response [91]. Furthermore, PPy has been shown to support the adhesion, growth and differentiation of a number of different cell types [15]. In vivo experiments demonstrated that PPy presented no significant acute systemic toxicity [92] or induced only a minimal tissue response [90]. Besides, chemically polymerized PPy particles neither showed any toxic or allergic response in mice,

nor affected the spleen, liver and kidney indexes [93]. Thanks to the good biocompatibility, PPy has been extensively studied in various biomedical applications as shown in Fig 1.7.

1.2.1.1 Tissue engineering and regenerative medicine

Since multiple types of cells such as neurons, myocytes, fibroblasts and osteoblasts are responsive to electrical stimuli in nature, PPy has been used to prepare conductive scaffold to regenerate functional tissues with the help of electrical stimulation [94]. Numerous research has mainly focused on applying conducting PPy scaffolds for neural repair and wound healing. After providing electric field to neuroblastoma cells on PPy [90], Schmidt demonstrated enhanced attachment and neurite extension of rat PC-12 cells [95]. Thereafter, her group prepared PPy scaffolds that supported the attachment and proliferation of human neuroblastoma cells in vitro and exhibited non-immunogenicity in vivo [96]. In addition, the incorporation of the nerve growth factor (NGF) in PPy scaffold further promoted neurite formation and elongation [97]. Zhang's research group pioneered and conducted a great deal of research about using PPy scaffold and electrical stimulation for wound healing [98-103]. They found that the migration, growth, differentiation and secretion of growth factors were modulated by both constant and pulsed electrical stimulations. Moreover, the electrically simulated fibroblasts maintain their myofibroblast phenotype after 15 days implantation in nude mice [99], showing that the electrically activated features may be transferred to new generations Besides that, PPy-based conducting scaffolds have also been used to electrically simulate cardiomyocytes [104], skeletal muscle cells [105], osteoblasts [106], and stem cells [107]. However, because of the poor processability and biodegradability, PPy is often compounded with other polymers to construct a conductive scaffold, such as with poly(ethylene terephthalate) (PET) [108], polylactide (PLA) [109], poly(lactic-co-glycolic acid) (PLGA) [52], and collagen (Col) [110]. To further improve the bioactivity, various biomolecules were incorporated into PPy by doping during synthesis, by covalent grafting, or by physical blending. Using heparin (HE) as a dopant, Zhang's group prepared the PLA/PPy/HE membrane that demonstrated simultaneously improved electrical stability and cell adhesion [109]. Further, fibronectin and bovine serum albumin (BSA) were also used to bioactivate the PPy/PLA membrane [111].

1.2.1.2 Neural prostheses

Neural prostheses are the medical implants consisting of multiple electrodes to electrically stimulate neurological activities in neural tissue and to perform the recording functions [5]. Implantable microelectrodes typically are fabricated from metal and silicon. Despite the clinical success of neural prostheses, their recording and therapeutic ability deteriorate resulting from the capsulation of fibrotic connective tissue during chronic implantation[112]. To resolve this adverse host response and the consequent poor interaction between electrode and target tissue, a desirable approach is to modify the surface of electrodes. Martin's research group electropolymerized PPy on micromachined neural probes [113], together with fibronectin fragments (SLPF) and nonapeptide CDPGYIGSR incorporated into PPy to improve neural cell attachment and growth on the PPy-coated neural probes [114]. In addition, they tried to increase the surface area of PPy on neural probes by coating PPy onto a hydrogel or fabricating PPy nanotubes, which reduced the impedance at electrode-tissue interface [115, 116]. He et al. grafted an anti-inflammatory drug onto the surface of the electrode to reduce the formation of fibrotic capsule by controlling inflammation and host response [117]. Similarly, Cui's group also used an anti-inflammatory drug, dexamethasone, in PPy-based micromachined neural electrode arrays [118]. Richardson [119] otherwise incorporated neurotrophin-3 onto neural probes to enhance neuron migration towards electrodes and to reduce the formation of capsule. PPy supports neuron growth and has been widely investigated as a coating layer on electrodes to improve the biocompatibility of neural prostheses [5, 120]. Modification of neural electrodes with PPy will not only maintain the electrical communication between neurons and probe, but also contribute to probe sensitivity, durability and biocompatibility. Especially considering the feasibility of modifying PPy with biomolecules, PPy has attracted significant attention in neural prostheses. Liu introduced chondroitin sulphate (CS) to act as dopant in a PPy/CS/Col membrane, which increased rat nerve cell attachment, differentiation and neurite outgrowth [121]. By using covalent bonds, NGFs were immobilized in PPy matrix and significantly increased neurite extension [122]. The capability to attach different neurotrophic biomolecules, particularly through various surface functional groups on PPy, makes PPy potentially useful in neural interfacing.

1.2.1.3 Biosensors

PPy has been widely studied in chemical sensing thanks to its sensitive physicochemical response (conductivity) to environmental stimuli such as pH, chemical gas, and humidity [3]. In particular, because of the feasibility to couple with biomolecules, PPy has been extensively investigated in biosensing. A biosensor is an analytical device, combining a biological component with a physicochemical detector, to detect an analyte. A biosensor can be decomposed into three parts: a biological sensing element, a transducer or detector, and associated electronics or signal processors (shown as Fig. 1.8). When a target analyte interacts with the sensing element, a signal will be generated and measured quantitatively and qualitatively via the transduction of optical, electrochemical or thermal signals[88].

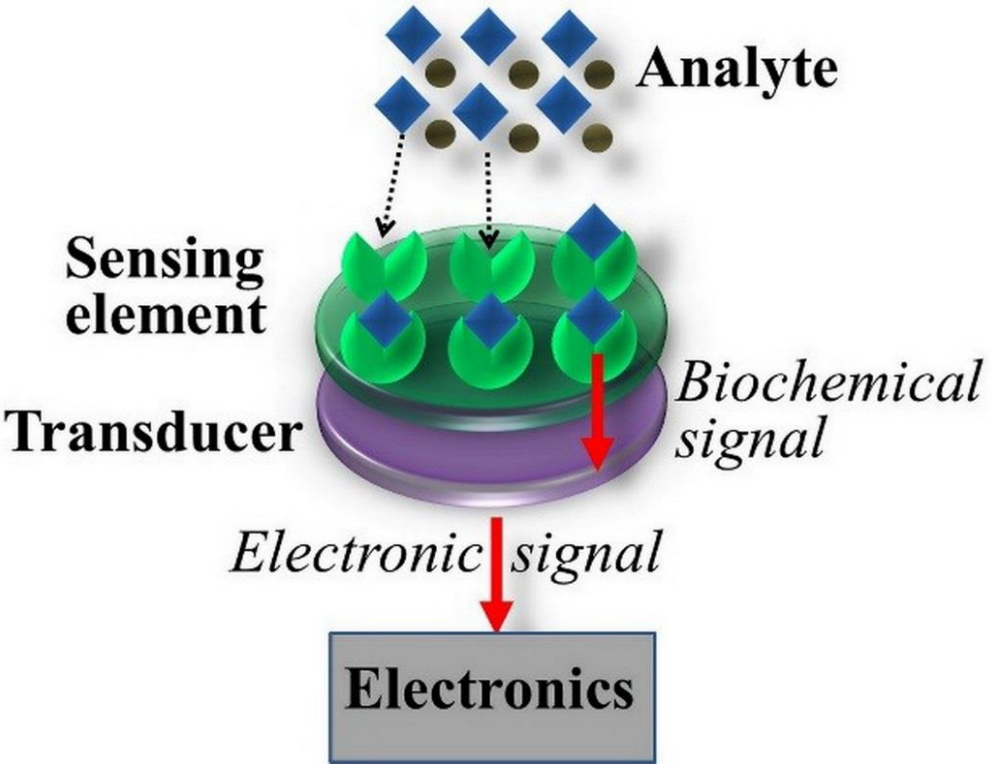

Figure 1.8 Schematic of a biosensor. The sensing element (e.g., biomacromolecule) detects the analyte, and then a series of signal will be produced and monitored by electronic device.

The sensing element, which is the core of the device, is made of biologically active molecules, such as enzymes, microorganisms, nucleic acids, antibodies, or multi-components. In PPy based biosensors, the conductive PPy is used as a carrier to incorporate the sensing molecules, and to integrate with electrical transducers to form the recognition element. Once the analytes

couple with the recognition center, there will be electrochemical or physical changes in the conducting polymer layer due to biochemical reactions, and such changes are subsequently detected through a amperometric, potentiometric, conductometric, optical, calorimetric or piezoelectric process [123, 124]. Based on the nature of the sensing element, biosensors mainly include the following three main groups.

1.2.1.3.1 Enzyme biosensors

Enzyme biosensors take the advantages of the biospecificity of enzymatic reactions, often a redox reaction, between the enzymes immobilized on PPy electrode and the substrate in analyte. The reaction generates detectable signals such as the change in electric current or potential that can be quantified [125]. Taking common clinical indices as examples, a portable device for fast and accurate measurement of glucose or urea concentration in blood is convenient for patients. Fang designed a glucose biosensor by embedding glucose oxidase (GOD) in chitosan/PPy nanocomposites, which exhibited a fast response (5s) to glucose and a linear current-time correlation over a wide range of concentration [126]. Soares constructed a urea sensor by immobilizing urease onto a PPy film, which exhibited selectivity and efficiency at urea concentrations below 3.0 mmol L^{-1} [127]. In order to increase the sensitivity, several problems should be overcome, such as the loss of enzyme and enzyme activity due to desorption and the process of synthesis. These issues could be effectively solved through covalent grafting of the enzymes. In fact, GOD was covalently grafted onto PPy composite nanowires to increase the sensitivity, detection limit and stability of glucose biosensors [128].

1.2.1.3.2 DNA biosensors

DNA biosensors are getting more attention because of enormous applications in clinical examination of genetic diseases and rapid diagnosis of pathogenic infections [123]. Typically, single stranded DNA (ssDNA) [129] or double stranded DNA (dsDNA) [130] are immobilized onto PPy electrodes to constitute the sensing element. In the early stage of research, DNA biosensors had also been prepared by adsorbing DNA related biomolecules to PPy probe surfaces [131]. After that, Ko et al. fabricated PPy nanotubes and grafted ssDNA to the nanotubes by covalent crosslink [132]. Both DNA and RNA have been confirmed to produce reduction and oxidation signals upon [133]. Theoretically, DNA can be electrochemically

detected based on the natural electroactivity of the nucleotide residues present in DNA. However, for a long time, signals were absent with dsDNA biosensor, which otherwise was observed on the oscillopolarograms of ssDNA. Labels, for example, redox-active molecules or enzymes, have been used in DNA sensors to act as the source of signals. As research continues, redox-active guanine was identified as the culprit inhibiting readable signals [134]. Various label-free DNA biosensors have recently been fabricated by the immobilization of guanine-free probes [132, 135].

1.2.1.3.3 Immunosensors

Immunosensors, normally antibody based, are also widely investigated in pharmaceutical research, food safety, and environmental monitoring due to their excellent specificity, sensitivity and convenience [136]. It is generally known that the antibody-antigen layer on electrode significantly disturbs ion diffusion and also changes electrical capacitance; and these changes can be converted into electrical signals that are easily monitored by electrochemical impedance spectroscopy (EIS) [137] and surface plasmon resonance (SPR) [138]. To effectively immobilize antibody onto a PPy biosensor probe, some strategies have been selected, including adsorption, doping, and covalent binding. Li pioneered the immobilization of protein onto PPy probes [138-140]. The functionalized PPy was investigated by BSA [140] absorption, covalent binding of goat IgG [138], and immobilizing anti-leptin IgG [139] via protein G grafting. Undoubtedly covalent binding can remarkably increase the stability and density of protein immobilization. Furthermore, Kausaite-Minkstimiene [137] prepared a sensitive probe through oriented antibody immobilization by using protein G, which significantly improved the antibody immobilization density and the antigen binding capacity. To achieve oriented antibody immobilization, there are three conventional strategies, including binding at the Fc region of immunoglobulins, direct immobilization of antibody fragments, and via oxidized oligosaccharide moieties [141]. In comparison, Fc binding shows predominance due to its high sensitivity and without any complex process of modification on antibodies. However, although a suitable immobilization method, labeled or label-free, can improve the efficacy of immunosensors, the performance of an immunosensor is closely related and even dependent on the nature of the selected antibody-antigen complex.

Selectively fastening appropriate antibody enables immunosensors to have the ability to detect various antigens. Accurate and rapid detection of biomarkers provides important diagnostic information, to which PPy immunosensors may provide a solution. Human chorionic gonadotropin (HCG), as a tumor marker in gestational trophoblastic disease and germ cell tumors, can be sensitively detected by a PPy-based HCG-immunosensor [142]. Similarly, other biomarkers such as hormone (human growth hormone) [136], growth factor (vascular endothelial growth factor) [143] and cancer marker protein (CA 125) [144] were detected with PPy-based immuosensors. Pathogens are the essential detection targets in food safety and environmental monitoring. Anti-Listeria [145] and a plant pathogen specific antibody [146] were covalently conjugated on the surface of PPy to fabricate a recognition system to detect Listeria and cucumber mosaic virus. Shirale immobilized Anti-T7 and anti-MS2 antibodies onto single PPy nanowire using NHS-EDC chemistry to selectively detect bacteriophages T7 and MS2 [147].

1.2.1.4 Drug delivery

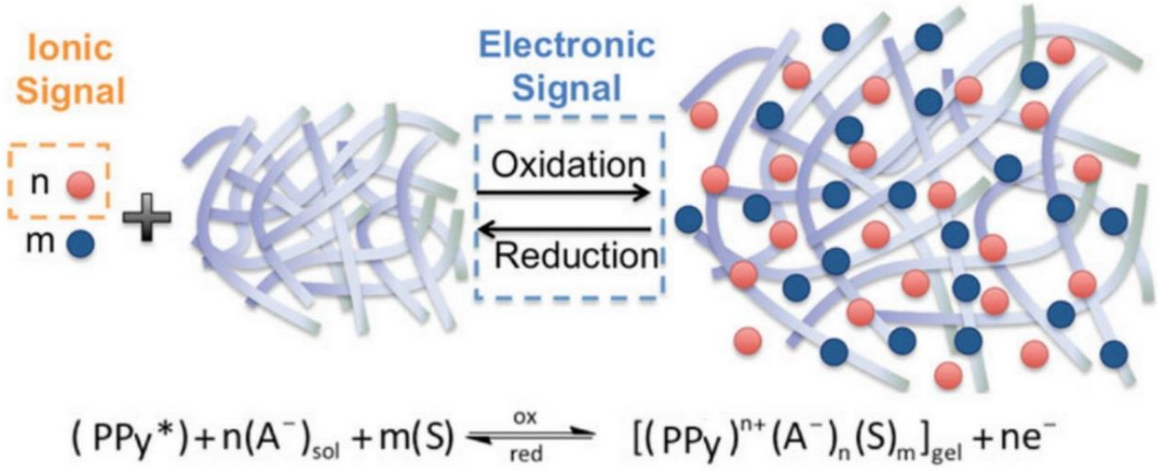

Figure 1.9 The oxidation-reduction reaction of PPy in solution [87]. A^- : an anionic dopant (red dots); S: solvent molecule (blue dots).

As shown in Fig. 1.5, anions are automatically incorporated into the oxidized PPy molecules to balance the positive charges during polymerization. And a controllable release of those anions can be accomplished during the reduction procedure of PPy via electrical stimulation as illustrated in Fig. 1.9. Thus the anionic drugs such as glutamate [148], dexamethasone [118], HE [109], and anthraquinone-2,6-disulfonic acid [149] were entrapped into PPy matrix as anionic

dopants to form controlled drug delivery systems. Some cationic and neutral drugs can also be incorporated into PPy during synthesis owing to physical entrapment and the combination of electrostatic and hydrophobic interactions among drugs, anionic dopants and polymer backbone [150, 151]. Svirskis summarized the construction of controlled drug delivery systems based on PPy matrix, and illustrated the factors affecting drug release, including the thickness and density of PPy, nature of the media, and electrochemical parameters [152]. However, the activity and stability of the drugs still limit the application of PPy for drug release. The drugs are usually incorporated into PPy through polymerization, a procedure that may lead to the deactivation of the drugs. And the drugs loaded in PPy usually tend to leach out through diffusion, resulting in the loss and uncontrollable release of drugs. Thus, biotin was introduced as dopants to offer covalent binding points for bioactive molecules, and then to realize uniform release kinetics with electrical stimulation [153].

1.2.1.5 Artificial muscle

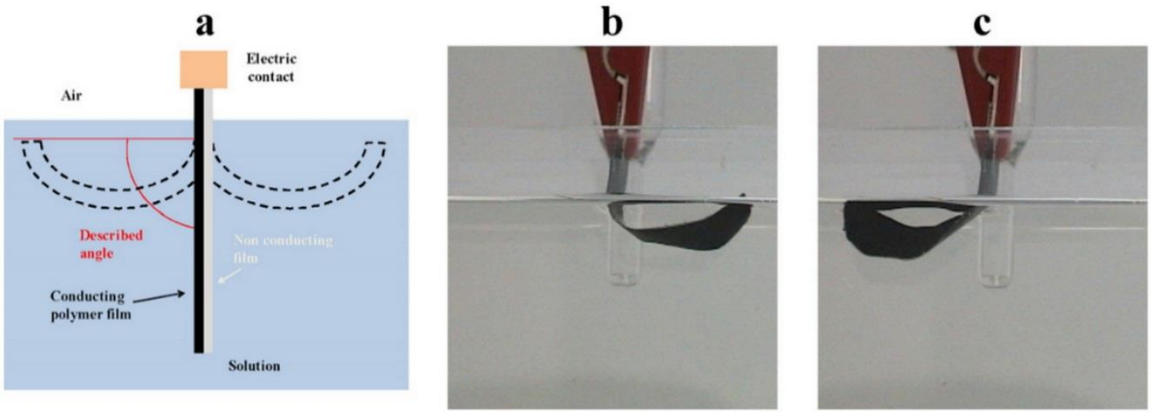

Figure 1.10 Scheme of a bilayer device: (a) conducting polymer film adhered to a non-conductive tape; (b) Anticlockwise movements during oxidation; and (c) clockwise movements during reduction [154].

As illustrated in Fig. 1.9, the volume of PPy will change through the inflow and outflow of ions or electrolytes during the switch of oxidation-reduction reactions (doping and dedoping processes), making PPy materials good candidates to make actuators such as artificial muscle [87]. As shown in Fig. 1.10 a, the simplest PPy-based bilayer artificial muscle is constructed by two components, i.e., a PPy layer and a non-conducting layer (plastic tape). During oxidation, volume of the PPy film increases due to the inflow of ions or electrolytes, resulting in an anticlockwise deformation. Conversely, a clockwise deformation occurs during reduction. In

a bilayer device, a metal counter electrode is required to facilitate current flow. To avoid the metallic electrode, sandwich-like three-layer (PPy/tape/PPy) device was designed [155]. In this three-layer system, one PPy layer acts as a working electrode, and the other conducting layer plays the role of a counter electrode. The three-layer design remarkably raises efficiency due to the opposite volume changes in the two PPy films that experience oxidation and reduction respectively at the same time. To generate linear movements, a freestanding and flexible PPy film capable of retaining large anionic dopants is highly recommended [156, 157]. But, for now, it is still challenging to fabricate truly freestanding and flexible PPy film.

1.2.2 Energy storage

Increasing demand for renewable energy storage devices is putting the two most promising candidates, i.e. batteries and supercapacitors, in the spotlight [45, 158]. The properties of the electrode or anode materials, such as the electrochemically active surface area, nanostructure and porosity, determine the performance of the energy storage devices [159]. PPy is considered especially promising as electrode materials owing to its electrochemical activity, controllable morphology (from 1D to 3D), feasible to compound with other materials, low cost and good environmental stability. Moreover, PPy is one of the few types of CPs that can be used in lithium batteries [160].

1.2.2.1 Supercapacitors

Supercapacitor, as an emergent technology, has been extensively studied worldwide as the next generation energy storage device due to its high power density, fast charge-discharge characteristics, long cycle life and stability [161, 162]. According to the charge storage mechanisms, supercapacitors can be divided into two types: electric double layer supercapacitors (EDLCs) and pseudocapacitors. EDLCs are also termed as non-Faradaic or true capacitors, in which ions are adsorbed onto the electrochemically non-active electrode. That is, the charge storage in EDLCs is achieved by a non-Faradaic process rather than electrochemical reactions. So carbon materials with high specific surface area are selected to construct the electrodes, such as activated carbon, porous carbon, carbon nanotubes (CNTs), and graphene [163]. Whereas, pseudocapacitors are assembled by electrochemically active electrode materials allowing a fast and reversible redox reaction (Faradaic reaction) during

the charge-discharge process. The Faradaic current is generated by the movement of charges across the double layer. Because pseudocapacitors exhibit a greater capacitance 10-100 times higher than that of EDLCs, as well as the energy density [164], pseudocapacitors have gained extensive attention and research in the past decade. As aforementioned, the performance of supercapacitors depends mostly on the nature of the electrode materials used. In case of pseudocapacitors, transition metal oxides/nitrides/sulfides and CPs are frequently adopted as electrode materials [158]. Owing to the superior intrinsic physical and chemical properties, PPy has been regarded as a promising candidate for the electrode of supercapacitors.

Past studies have found that the specific capacitance of supercapacitors is inextricably linked with the microstructure and morphology of CPs [71]. For the capacitance of the systems containing PANI, the order is film < microparticle < microtube < nanowire [71]. Similarly, PPys with different morphologies exhibit varied specific capacitance as shown in Table 1.1. The specific capacitance of PPy electrodes varies according to their the nanostructure and morphology. This is due mainly to the variations in contact surface area and charge transfer rate of the PPy-based electrodes with different nanoscale designs. Normally, low dimensional structures, especially the 1D nanostructures, are recommended because of high efficiency in charge transport. Moreover, the preparation method of PPy also affects the performance of the final supercapacitor. For example, a specific capacitance of ~220 F g^{-1} at a scan rate of 5 mV s^{-1} was obtained for the PPy thin films synthesized by anodic EP deposition [165]. Whereas, for PPy film polymerized via chemical oxidation, the maximum specific capacitance can be achieved at 329 F g^{-1} at the same scan rate [166]. Hence, through a combination of different template polymerizations, PPy with various morphologies from 0D to 3D can be fabricated to accomodate different types of electrode, such as linear, planar, and 3D spongy electrodes.

However, two properties have impeded the application of single-component PPy-based electrode in high performance supercapacitors, i.e., insufficient specific capacitance and poor stability in long-term charge-discharge cycling. Sharma demonstrated that the initial capacitance of a PPy electrode (120 F g^{-1}) dropped dramatically (~50%) after 1000 cycles [167]. To improve both the capacitance and cycle stability, besides a nanoscale structure design to increase specific area, another effective strategy is to prepare composites of PPy with other electrode materials including carbon materials, metal oxides, and other conducting polymers.

A PPy/carbon fiber composite prepared through in situ chemical polymerization revealed a high specific capacitance of 588 F g^{-1} at 30 mV s^{-1} and maintained it at 200 mV s^{-1} [168]. As metal oxides are superior faradaic capacitor but low in conductivity, the combinations of PPy with metal oxides has been developed. Various metal oxides were coated with PPy to construct core-shell electrodes, such as V_2O_5, MnO_2, $NiCo_2O_4$, WO_3, Co_3O_4, and SnO_2, as summarized in Table 1.1. Among them, V_2O_5 and MnO_2 are the most widely investigated by taking advantage of a reactive template system. In addition, other polymers were also combined with PPy to improve the performance of electrode. Insulating polymers with nanostructures such as bacterial cellulose (BC) were used as template for PPy polymerization resulting in high surface area [169]. PANI nanofibril seeds was also used as template to form a PANI@PPy composite with a maximum specific capacitance of 346 F g^{-1}, which is higher than that of PANI nanofibers (100 F g^{-1}) and pure PPy (149 F g^{-1}). The suggested reason is that the strong π-π interaction between PPy shell and PANI core promotes more planar conformation of PPy and so contributes to more efficient charge transport. More recently, composites formed by three constituents, i.e., carbon nanomaterials, metal oxides, and PPy nanomaterials, were designed to make best use of the advantages and to bypass the disadvantages of each component. Combining MnO_2/PPy with carbon nanotubes or graphene can improve both the specific capacitance and cycling stability [170, 171]. It is well known that the poor cycling stability of single-component electrodes made of conducting polymers is predominantly due to the cracks and break resulting from the volumetric swelling and shrinking during the redox process (Fig. 1.9). To solve this problem, attempts were made to coat non-faradaic electrode materials onto PPy nanostructures. For example, layered double hydroxides (LDH), a class of 2D structure anionic clays, were covered onto PPy as a protection layer to reduce cracks in long-term charge/discharge cycling [172]. Thanks to the protection of LDH, the PPy@CoNi-LDH electrode showed an excellent capacitance retention (115.4 %) after 20,000 cycles. Along with the popularity of portable electronic devices, study about high performance flexible and wearable energy storage devices rose rapidly, propelling the design and investigation of flexible solid-state supercapacitors [158, 173]. Flexible electrode materials, as the core component of supercapacitors, are highly desirable.

Table 1.1 Performance of PPy-based elecrodes for supercapacitors

Electrode material	Morphology	Electrolyte	Specific capacitance	Current density	Cycle stability	Ref.
PPy	hydrogel	1.0 M H_2SO_4	~300 F g^{-1}	0.2 A g^{-1}	93% (2000)	174
	film	0.5 M Na_2SO_4	~250 F g^{-1}	2.0 mA cm^{-2}	~50% (1000)	167
		0.5 M Na_2SO_4	329 F g^{-1}	1.0 mA cm^{-2}	78% (3000)	166
	hollow microspheres	1.0 M $NaNO_3$	146 F g^{-1}	5.0 mA cm^{-2}	38% (500)	175
		0.5 M H_2SO_4	566 F g^{-1}	1.1 A g^{-1}	70% (300)	176
	nanowires	1.0 M KCl	305 F g^{-1}	0.5 A g^{-1}	87.5% (1000)	177
		1.0 M H_2SO_4	179 F g^{-1}	1.0 A g^{-1}	75.7% (600)	178
	nanotubes	1.0 M Na_2SO_4	420 F g^{-1}	1.5 A g^{-1}	97.9% (800)	179
	nanofibers	1.0 M KCl	284 F g^{-1}	1.0 A g^{-1}	76% (600)	180
	nanoparticles	1.0 M $NaNO_3$	120 F g^{-1}	5.0 mA cm^{-2}	80% (100)	181
PPy/carbon black	nanoparticles	1.0 M $NaNO_3$	366 F g^{-1}	5.0 mA cm^{-2}	88-95% (100)	181
PPy/carbon fiber	fibers	1.0 M KCl	14.8 F cm^{-3}	0.4 mA cm^{-1}	85% (5000)	182
PPy/carbon nanotubes	nanotubes	2.0 M KCl	300 F g^{-1}	0.5 A g^{-1}	90% (1000)	183
	nanotubes	1.0 M H_2SO_4	264 F g^{-1}	5.0 mA cm^{-2}	89% (1000)	184
	nanotubes array	0.1 M $NaClO_4$	587 F g^{-1}	3.0 A g^{-1}	>90% (1000)	185
	film	1.0 M KCl	660 F g^{-1}	0.5 mA cm^{-2}	90% (1000)	186
	nanowires	1.0 M KCl	696 F g^{-1}	1.0 A g^{-1}	93% (1000)	187
PPy/graphene	nanotubes	1.0 M H_2SO_4	512 mF cm^{-2}	1.0 mA cm^{-2}	82.7% (10000)	188
	nanotubes	1.0 M $HClO_4$	509 F g^{-1}	0.15 A g^{-1}	93% (1500)	189
	nanoparticles	1.0 M KOH	418 F g^{-1}	0.5 A g^{-1}	74% (2000)	190

MnO_2@PPy	nanoparticles	0.5 M Na_2SO_4	~376 F g^{-1}	3.0 mA cm^{-2}	90% (500)	191
	nanofilms	1.0 M Na_2SO_4	320 F g^{-1}	0.5 A g^{-1}	91.4% (5000)	192
	nanotubes	1.0 M KCl	328 F g^{-1}	3.0 mA cm^{-2}	>95% (500)	193
	nanograins	0.5M Na_2SO_4	620 F g^{-1}	2.0 mA cm^{-2}	85% (4000)	167
	3D network	1.0 M Na_2SO_4	502 F g^{-1}	0.25 A g^{-1}	74% (10000)	194
V_2O_5@PPy	nanoparticles	5.0 M LiNO3	559 F g^{-1}	3.0 A g^{-1}	70% (100)	195
	nanoparticles	5.0 M LiCl	412 F g^{-1}	4.5 mA cm^{-2}	80% (5000)	196
$NiCo_2O_4$@PPy	nanowires	6.0 M KOH	1876 F g^{-1}	5.0 mA cm^{-2}	95% (5000)	197
Co_3O_4@PPy	nanosheets	1.0 M KOH	211 mF cm^{-2}	2.0 mA cm^{-2}	85.5% (5000)	198
	nanowires	3.0 M KOH	2017 F g^{-1}	1.0 mA cm^{-2}	60% (1000)	199
CoO@PPy	nanowires	3.0 M NaOH	2223 F g^{-1}	20 mA cm^{-2}	99.8% (2000)	200
WO_3@PPy	nanowires	3.0 M NaOH	253 mF cm^{-2}	0.67 mA cm^{-2}	85% (5000)	201
PPy/PANI	nanotubes	1.0 M H_2SO_4	416 F g^{-1}	5.0 mA cm^{-2}	-	202
	nanofibers	1.0 M Na_2SO_4	346 F g^{-1}	2.0 A g^{-1}	~65% (500)	203
	nanoarrays	1.0 M H_2SO_4	209.5 F g^{-1}	2.0 A g^{-1}	79.5% (500)	204
PPy/BC	nanofibers	0.5 M KCl	316 F g^{-1}	0.2 A g^{-1}	88.2% (1000)	169
PPy/MnO_2/CNTs	nanotubes	1.0 Na_2SO_4	402.7 F g^{-1}	1.0 A g^{-1}	96.2% (1000)	170
PPy/MnO_2/graphene	nanoparticles	1.0 M Na_2SO_4	600 F g^{-1}	1.0 A g^{-1}	92% (5000)	171
$NiCo_2O_4$/PPy/hemp-derived carbon	nanotubes	3.0 M NaOH	2055 F g^{-1}	1.0 A g^{-1}	90% (5000)	205

1.2.2.2 Lithium batteries

In the early 1990s, the first lithium-ion battery (LIB) was announced by Sony Corporation, showing a high voltage (~3.7), high energy, lightweight and good environmental

compatibility. This makes LIB, although costly, widely used in portable electronic devices such as mobile phone, laptop, and medical devices [161, 206, 207]. Lithium is the lightest metal and has the highest oxidation potential. Therefore, LIBs have a great potential to satisfy the requirements of high performance energy storage devices. As shown in Fig. 1.11, the materials with high lithium storage capacity are used as the positive and negative electrodes. During the charge-discharge cycles, lithium ions (Li^+) shuttle between anode and cathode, accompanied by the concomitant oxidation and reduction of two electrodes. Similar to supercapacitors, the electrodes with microstructures or appropriate architectures are the heart of LIBs and determine battery long-term performance.

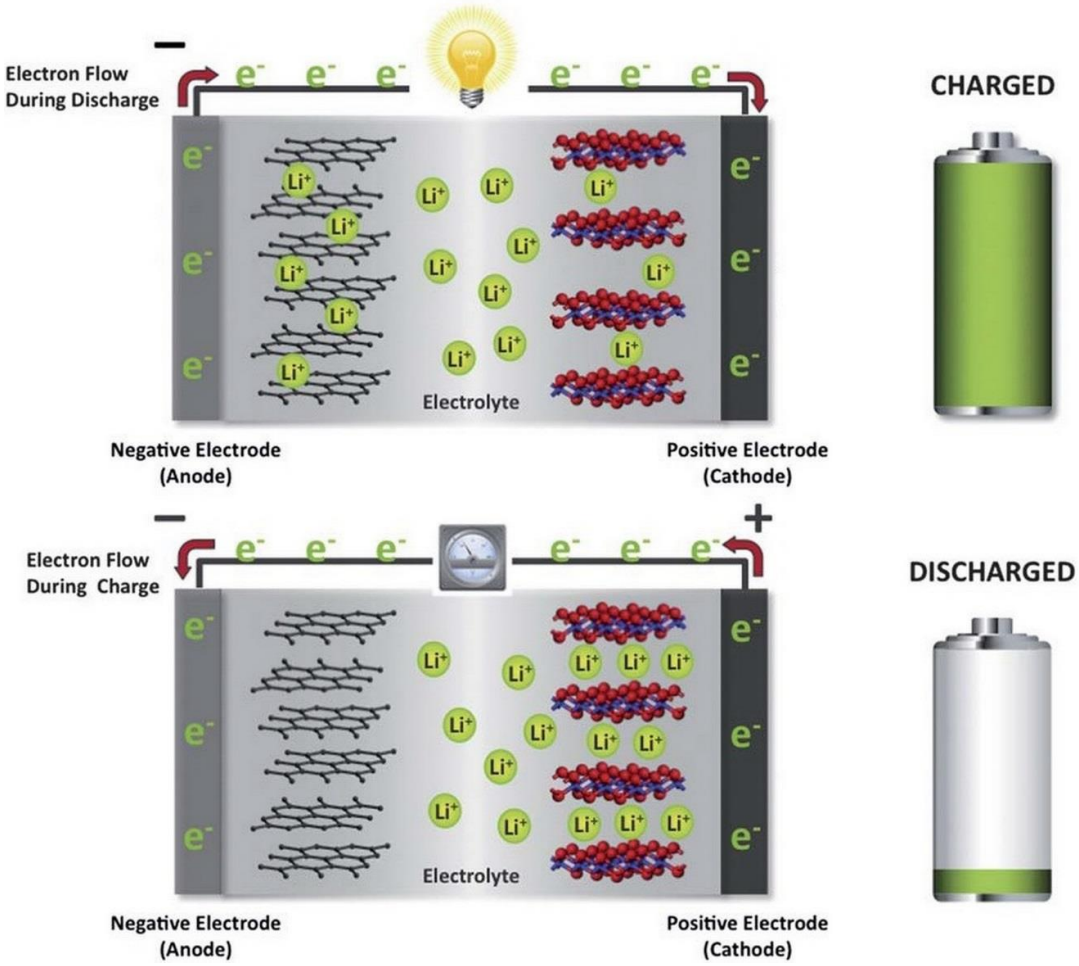

Figure 1.11 A schematic illustration of the working principles of lithium-ion battery [206].

The reasons why PPy has gained a broad interest in LIBs include [160, 208-210]: a). After an anionic doping, PPy shows an increased conductivity and offers an easy insertion and

extraction of anions to enhance the battery capacity; b). PPy can incorporate metal oxides and other oxide compounds to form a composite electrode with improved electrochemical performance. When used in a composite electrode, PPy not only can act as a host matrix for Li^+ to protect the microstructure framework from collapse during the charge/discharge cycling, but also can connect metal oxide particles and deliver an additional capacity to the composite electrode; c). Through a template method, a PPy-based electrode can be fabricated into designed micro/nanostructures contributing more surface area for Li^+ and so a further increased capacity. Li et al. prepared PPy nanofibers by template polymerization and illustrated a high discharge capacity of 98 mA h g^{-1} [160]. Based on the V_2O_5@PPy nanowires, a V_2O_5@PPy//$LiMn_2O_4$ rechargeable lithium battery was prepared showing an initial discharge capacity of 95.2 mA h g^{-1} and a capacity retention of 85.6% after 100 cycles [211]. Recently, PPy coated NiS-carbon nanofiber (CNF) films were tested as free-standing cathode reporting a high discharge capacity of 635 mA h g^{-1} at 0.1 A g^{-1} and an exceptional areal capacity and cycling life [212]. Moreover, in some cases, PPy-based ternary composites have also been investigated as anode of LIBs. Through in situ chemical polymerization of PPy, a core-shell structured hollow SnO_2/reduced graphene oxide (rGO)/PPy ternary composite anode was obtained and demonstrated a capacity of about 647.8 mA h g^{-1} after 100 cycles at 3.9 A g^{-1} [213]. A binder-free 3D hierarchical MoS_2-PPy-rGO ternary electrode presented a long-term stability after 400 cycles at a capacity of 1070 mA h g^{-1} and a current density of 200 mA g^{-1} [214]. Flexible paper-like LIBs are considered as the next generation batteries especially for wearable and portable electronic devices. Thus, currently, many efforts are made to enhance the mechanical properties and stability of PPy film electrodes.

1.2.3 Electric heating elements

An electric heating element converts electricity into heat through the process of Joule heating, also called resistive heating. Electric heating elements or appliances are commonly required in industry and daily life, such as in water heating, thermal induced deicing device, heated clothing or flexible deicing units, heated clothing or equipment for extremely cold environment, and heated medical devices [10, 215, 216]. For now, metal wires and fibers are the most popular and commercially used electric heating materials. In order to replace those heavy, vulnerable to corrosion and less flexible fibers, various alternatives have been

proposed including carbon nanomaterials, metal nanofibers/nanowires, and CPs [11, 215, 217]. Among these conducting materials, CPs have gained more attentions due to their low cost, lightweight, environmental stability, and the feasibility of compounding with other polymers to achieve long-term durability, 3D structure and proper mechanical properties. In 2003, Lee et al. firstly coated PPy onto woven nylon fabrics to prepare a flexible heating element; and this PPy coated fabric was able to reach 55 ℃ from room temperature in two min using a 3.6 V powder source [11]. After that, many polymer fabrics were tested as the support substrate, such as PET [218-220], cotton [221], polyacrylonitrile (PAN) fibers [222], poly(vinyl alcohol-co-ethylene) nanofibers on PET [10], to name a few. Although these PPy coated composite fabrics reveal good electrothermal properties in short-term, the electrical heating efficiency was found to deteriorate due to the delamination and cracking of the PPy layer from the substrate resulting from their different thermal expansion coefficents. Furthermore, because the mechanical properties of the compostie mainly dependant on the substrate, the heating temperature can't be above the melt point of the substrate polymer. Similarly, the composite will become inflexible and stiff if the using temperature is lower than the glass transition temperature of the substrate. To solve this problem, some research groups have attempted to fabricate the heating elements made of the pure conducting polymers. For instance, Zhou et al. prepared poly(3,4-ethylenedioxythiophene)/poly(styrenesulfonate) (PEDOT/PSS) microfibers without any supporting material [223]. However, for now, it is still difficult to obtain large sized and flexible PPy membrane.

1.2.4 The challenges facing PPy in practical applications

Despite the early discovery of PPy and the intensive studies, there are only a few commercial products of PPy available in the market. The main limitations lie in its poor processability, deficient mechanical property and inadequate functionality that is important for biomaterials. As shown in Fig. 1.1, PPy is formed by repeated pyrrole rings without any functional groups. Biofunctionalization has great importance in biomedical applications because various bioactive molecules can be incorporated into a material through such functional groups. For example, HE, an important glycosaminoglycan on cell membrane and in extracellular matrix (ECM), was integrated into PPy to improve cell adhesion [109]. NGF such as neurotrophin-3 was immobilized onto PPy-coated neuroelectrode to enhance neuron migration towards the

electrode thus reducing gliosis [119, 224]. Especially for biosensors, it is imperative to biofunctionalize PPy by biomolecules to form the recognition center. In immunosensors, for instance, the specific detection of target antigen molecules can only be achieved after immobilization of the active antibodies onto PPy substrate [140]. Also, owing to its extended and conjugated rigid π-system backbone, PPy always displays infusibility, insolubility and inferior mechanical properties (stiff and brittle), which has severely limited its application. When come to the flexible electronics and energy storage devices, as well as artificial muscles, PPy is often restricted by the insufficient processability and mechanical properties. Therefore, more attentions should be paid to improve the biofunctionalization and mechanical properties of PPy-based conducting materials.

1.3 Biofunctionalization of PPy

Biofunctionalization refers combining bioactive molecules with otherwise bio-inert materials, to make these materials bioactive or having specific biofunctions. To biofunctionalize PPy, there are mainly three strategies including physical adsorption and entrapment, doping, and covalent binding as shown in Fig. 1.12.

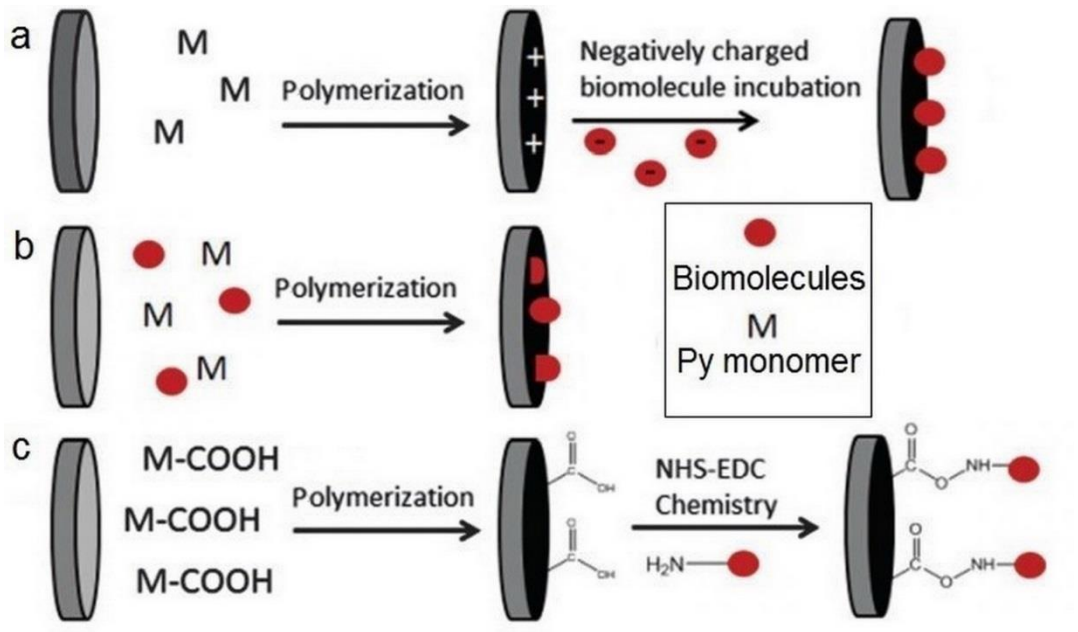

Figure 1.12 A schematic illustration of functionalization of PPy by biomolecules via (a) physical adsorption; (b) doping; (c) covalent binding [88].

1.3.1 Physical adsorption

Physical adsorption depends on the physical interactions on surface between biomolecules and PPy, including electrostatic force, hydrophobic force, and van der Waals force. Dicks et al. firstly reported an adsorption-based PPy biosensor via simple adsorption of glucose oxidase on PPy electrode surface [225]. Schmidt modified PPy with a 12 amino acid peptide (T59) by electrostatic adsorption, in order to increase neuron adhesion and neurite extension [226, 227]. Langmuir-Blodgett technique was also employed to produce a glucose biosensor by embedding glucose oxidase (GOx) into PPy film [228]. Additionally, a nanostructure is helpful for PPy to adsorb biomolecules. Glucose biosensors constructed using PPy nanotubes reportedly increased both enzyme loading efficiency and sensing area [229]. Noticeably, physical adsorption is affected by factors such as temperature, pH, solvent, and the net charge of the PPy-based probe. However, physical adsorption is rarely used now due to the weak binding of physical adsorption leading to the loss of biomolecules.

1.3.2 Doping

Doping is an essential process to introduce charge carriers (polarons and bipolarons) into PPy chains to render it conductive as shown in Fig. 1.2. The electrochemical performance of PPy is largely dependent on the nature of dopants and doping level. As a classic p-doping polymer PPy has positive charges that are counterbalanced by the negatively charged molecules from dopants. This provides the often negatively charged biomolecules a possibility to be "doped" into PPy matrix. The doping process occurs automatically during polymerization no matter chemical or electrochemical. And the doping process is reversible allowing the dopants to move out and re-enter PPy during redox. Generally, dopants can be classified into to two types based on their size, i.e., small dopants and large dopants. Cl^- is the most common small dopant that easily dopes conductive polymers when $FeCl_3$ is used as the oxidant [34]. Although Cl^- is biocompatible, it is easy to leach out in aqueous environment causing a decrease in conductivity, particularly compared to large dopants such as biomolecules [15]. Negatively charged biomolecules, for example proteins (enzymes and antibodies) at pH higher than their isoelectric points, can be doped into PPy during oxidation. Doping as a strategy of protein immobilization is a straightforward and provides a more prolonged immobilization stability of stable biomolecules than physical absorption does [88].

A variety of biomolecules (ECM components, proteins, and peptides) have been selected as dopants to improve the affinity and specific interactions of PPy with different cell types [230]. HE was used as dopant for PPy scaffolds because it is an important cell adhesion molecule and an anticoagulant [106, 231-233]. Other biomolecules such as dextran sulphate (DS), hyaluronic acid (HA), chitosan, Col, growth factors, laminin fragments, chondroitin sulfate A (CS), oligodeoxyguanylic acids and adenosine triphosphate (ATP) have been investigated as dopants to form bioactive PPy scaffolds [15, 230, 234]. Noticeably, these bio-dopants not only can introduce specific bioactivity but also can affect the physical and chemical properties of the PPy scaffolds, depending on the nature of the dopants. For example, the CS doped PPy showed an increased surface roughness at high doping level [235]. Wallace's group compared the influence of different dopants including para-toluenesulfonic acid (pTS), HA, DS, CS, and poly(2-methoxyaniline-5-sulfonic acid) (PMAS) on the physical properties of PPy films. It was demonstrated that both PPy/PMAS and PPy/CS films had lower surface roughness and Young's modulus than that of the films used other dopants [236]. Surface morphology is a critical factor affecting cell behaviors. To construct the recognition center of biosensors, ligands and receptor proteins were also incorporated in PPy electrode via doping [237-239]. The doping-dedoping strategy has been found particularly useful in drug delivery, shown as Fig. 1.9. As previously described, many anionic drugs such as glutamate [148], dexamethasone [118], HE [109], and anthraquinone-2,6-disulfonic acid [149] can be entrapped into PPy as anionic dopants for drug delivery. Moreover, Konturri et al. designed a two-step method to construct the drug delivery system [240]. In this design, pTS was used to dope PPy firstly and then replaced by either salicylate, naproxen or nicoside anions via a redox process. A post-synthesis incorporation was proposed to entrap cationic drugs, such as dopamine [241] and chlorpromazine [242]. For neutral drugs, such as N-methylphenothiazine (NMP), PPy was polymerized using anionic β-cyclodextrins as dopants, which allowed consequent incorporation of NMP [151]. However, there are some limitations for the incorporation of biomolecules by doping, including low loading, decrease in conductivity, uncontrollable loss of biomolecules due to diffusion, and decline in biomolecule activity during polymerization. In addition, while biomolecules, either as dopants or physically entrapped, are present throughout the PPy substrates, only a small amount on the surface is available for the reactions.

1.3.3 Covalent binding immobilization

With respect to the limitations of physical adsorption and doping, surface covalent immobilization of biomolecules clearly has some advantages. Copolymerization of pyrrole with functional pyrrole derivatives is probably the most promising approach to functionalize PPy because of the availability of various functional monomers, the flexibility in further modification, high surface activity, and the structural stability of the immobilized molecules. As shown in Fig. 1.12 c, Py derivatives with functional groups such as carboxyl (-COOH), amine ($-NH_2$), hydroxyl (-OH), hydroxyl succinimidyl ester (-NHS), cyano (-CN), and epoxy (C_2H_2O) groups can be homopolymerized or compolymerized with Py to introduce functional groups on PPy surface prior to covalent grafting of biomolecules using cross-linker. The superiority of covalent binding immobilization mainly manifests in [8]: a). Tight control over grafting; b). High accessibility of analytes; c). Minimal loss of biomolecules over time, d). Possibility to control biomolecule orientation. Thus, covalent grafting of biomolecules to PPy is considered the most efficient and stable immobilization [3]. According to the substituted position, functionalized Py monomers fall into three types: N-substitution, α- substitution and β- substitution. Taking carboxylic acid-substituted Py as an example, Fig. 1.13 indicates the chemical structures of Py carboxylic acid substituted at the three positions.

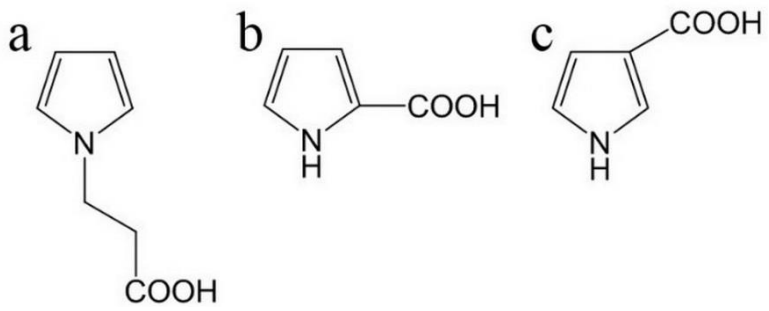

Figure 1.13 Chemical structures of carboxylic acid-functionalized Py monomers: (a) N-position substituted 1-(2-carboxyethyl)pyrrole; (b) α-position substituted pyrrole-2-carboxylic acid; (c) β-position substituted pyrrole-3-carboxylic acid.

According to the polymerization mechanism (Fig. 1.4), α-position is the important reactive site for molecular chain growth of PPy. So functionalized PPy based on the α-substituted Py has only been explored by a few researchers. Lee et al. synthesized poly(pyrrole-co-pyrrole-2-carboxylic acid) by modification of PPy surface using pyrrole-2-carboxylic acid, which

was further grafted with cell adhesive peptide Arg-Gly-Asp (RGD) to improve the adhesion and spreading of human umbilical vein endothelial cells [243]. In comparison, more researchers used β-substituted and N-substituted Py. Roy et al. used EP to copolymerize Py and pyrrole3-carboxylic acid to prepare films and nanotubes for covalent grafting of PEG chains in order to enhance their antifouling property [244]. Similarly, poly(pyrrole-3-carboxylic acid) homopolymer film was synthesized by EP, to which antihuman IgG was immobilized to construct a biosensor [245, 246]. Chemical polymerization was also employed to obtain poly(pyrrole-3-carboxylic acid) homopolymer on alumina membrane allowing lysine grafting for affinity adsorption of bilirubin [247]. However, the available β-substituted Py derivatives are rare due to the difficulty in modifying the β position in pyrrole ring. So, that is why N-substituted Py has gained more interest, because pyrroles can be easily substituted at N position through alkylation and further modified into various Py derivatives with different groups.

1.3.3.1 N-functionalized PPys

In order to obtain N-functionalized PPys, many N-substituted Py monomers were synthesized. N-(2-cyanoethyl)pyrrole (PyCN) is the main commercial product of Py derivative due to the easy synthesized through direct cyanoethylation of Py [248]. From PyCN, a variety of N-functionalized Pys can be obtained. 1-(2-carboxyethyl)pyrrole is the product of the nitrile hydrolyzation of PyCN in strongly alkaline solution (6.7 M KOH) [249]. N-3-aminopropyl pyrrole can be obtained via the reduction of PyCN using lithium aluminium hydride in ester solvent [250]. By direct alkylation reaction between Py and epichlorohydrin, N-glycidylpyrrole monomer was prepared to introduce the reactive epoxy group allowing binding protein molecules via their amine, thiol, hydroxyl and carboxyl groups [251]. And the carboxyl groups can be modified to hydroxyl succinimidyl ester groups using N-hydroxysuccinimide (NHS)/1-ethyl-3-(3-dimethylaminopropyl)carbodiimide (EDC) chemistry [252]. In fact, N-functionalized PPy homopolymers and copolymers with Py have been successively synthesized and extensively investigated, such as poly(pyrrole-co-1-(2-carboxyethyl) (PPyCOOH) [28], poly(pyrrole-co-N-3-aminopropylpyrrole) (PPy-NH_2) [250], poly(pyrrole-co-succinimidyl pyrrole) (PPy-NHS) [253], and poly(pyrrole-co-N-glycidylpyrrole) (PPy-PO) [251]. Yet most of such copolymers are obtained through EP, with the pitfalls inherently associated

with EP. Rajesh et al., for the first time, electrochemically polymerized Py and Py-NH_2 to prepare a PPy-NH_2 copolymer film for the covalent immobilization of urease [250]. The urease enzyme biosensor exhibited a fast response time (25-50s), a linear response to urea from 6.3×10^{-3} to 4.1×10^{-1} mM, and a stability for about 2 months. Same enzyme, urease, was also grafted to a conducting PPy-PO film prepared by EP to construct the urease enzyme biosensor [251]. A faster response time (4s) was achieved by this biosensor as well as a linear response to urea from 0.1 to 0.7 mM with a sensitivity of 4.5 mA mM^{-1}. Neither PPy-NH_2 nor PPy-PO catched further research interest due to the complex synthesis procedures, low productivity and high protein feeding concentration (10.0 mg mL^{-1}) that is not practical because of the high cost of proteins such as antibodies.

As shown in Fig. 1.14 and Fig. 1.15, PPy-NHS is in fact the reactive intermediate of PPy-COOH. Therefore, all the PPy-NHS molecules can be considered the downstream products, that is, PPy-NHS is the final state of PPyCOOH before reacting with biomolecules. Two strategies were developed to prepare PPy-NHS: homo/copolymerization of Py and Py-NHS (Fig.1.14) and modification of PPyCOOH by NHS-EDC (Fig.1.15). In order to improve the biocompatibility of stainless steel, Py-NHS was polymerized onto the metal substrate by EP, followed by BSA immobilization [252]. However, this method was gradually abandoned due to the instability of Py-NHS especially during the chemical polymerization of PPy-NHS. Now more researchers choose the latter method. In this method, a PPyCOOH copolymer is synthesized first, and then the carboxyl groups are activated by NHS-EDC to form PPy-NHS. In addition, via simple chemical reactions, the carboxyl groups in PPyCOOH can be converted to primary and secondary amines [254]. Therefore, PPyCOOH has become the most extensively investigated intermediate in the functionalization of conducting PPy for biomedical applications.

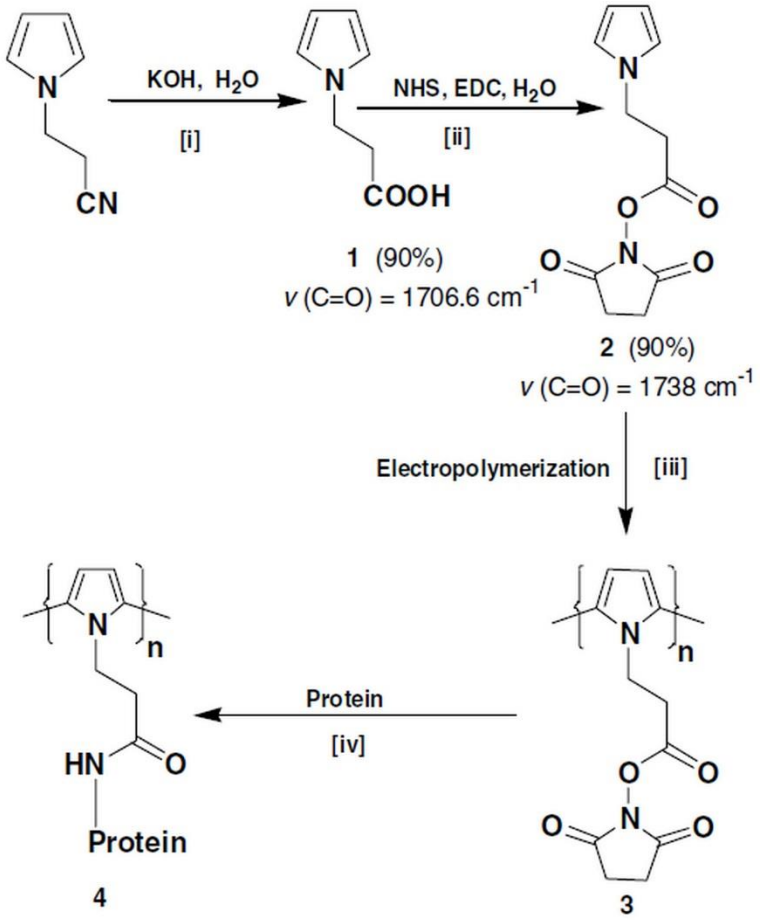

Figure 1.14 Schematic representation of grafting biomolecules onto PPy-NHS [252], showing the yield and the characteristic absorptions of carboxyl groups.

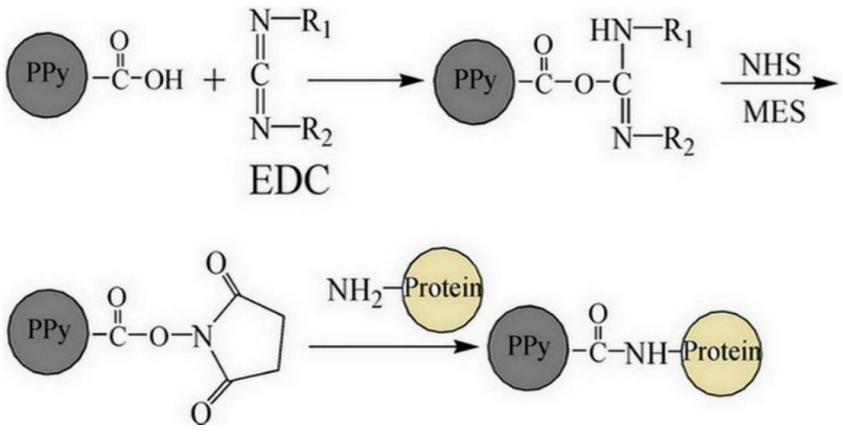

Figure 1.15 Schematic representation of grafting biomolecules onto PPyCOOH based PPy-NHS using NHS-EDC coupling

1.3.3.2 Poly(pyrrole-co-(1-(2-carboxyethyl)pyrrole))

PPyCOOH homopolymers (made by PyCOOH) and copolymers (made of Py and PyCOOH) are widely used in biomedical investigations especially in tissue engineering and biosensing, as summarized in Table 1.2. By using NHS-EDC chemistry, various biomolecules were grafted onto PPyCOOH and showed a good stability and activity. Conductivity of the PPyCOOH homopolymers is lower than that of the PPyCOOH copolymers and this decrease in conductivity is proportional to the increase in the feeding ratio of PyCOOH [255]. Noticeably, most PPy-COOH polymers reported in literature were polymerized through EP and so were inevitably associated with the pitfalls of EP such as small size, low productivity, high cost, and the requirement of specialized equipment. Chemical polymerization has also been attempted to obtain PPyCOOH polymers in larger-scale. PPyCOOH was copolymerized onto silica microparticles to produce stable colloidal dispersions 20 years ago [249]. Also, polystyrene (PS)-PPyCOOH core-shell particles were prepared using $FeCl_3$ as oxidant [256, 257]. In both work, silica and PS particles were just used as the templates. Meanwhile, due to the incompatibility between the core particles and the PPy shell, modification of particle surface is required to improve the core-shell adhesion strength. An ideal core-shell structure would be PPy as the core to provide high conductivity and PPyCOOH homopolymer as the shell to offer surface reactivity. To our best knowledge, such core-shell structured particles have not been reported. The contradiction between conductivity and surface reactivity of the PPyCOOH particles is a problem to be solved imperatively.

Table 1.2 Biomedical applications of PPyCOOH

Synthesis method[a]	Ratio of PyCOOH	Grafted molecules	Conductivity	Performance	Suggested applications	Ref.
CP	100%	RGD	2.83×10^{-4} S cm^{-1}	-	tissue engineering	258
CP	50%	NGF	64±50 kΩ/square	improve neuron development and neurite length	tissue engineering	97
CP	100%	copper ions	-	high adsorption capacity and good selectivity to bovine hemoglobin	protein purification	259
EP	100%	RGD	4.65×10^{-4} S cm^{-1}	promoting cell adhesion and proliferation	tissue engineering	258

EP	100%	GOx	-	1.7μA cm^{-2} at 1 mM glucose up to 80 mM	enzyme biosensor	260
EP	0-100%	GOx	10^{-8}-10^{-3} S cm^{-1}	amperometric response to glucose	enzyme biosensor	255
EP	100%	GOx	-	linear range of 1 -18 mM, sensitivity of 0.42 mA mM^{-1}	enzyme biosensor	261
EP	100%	alcohol dehydrogenase	10^{-4}-10^{-3} S cm^{-1}	amperometric response to ethanol	enzyme biosensor	262
EP	5%	alcohol dehydrogenase	6.6×10^{-4} S cm^{-1}	10 μA cm^{-2} at a concentration of 14 mM	enzyme biosensor	263
EP	100%	anti-mouse IgG	-	sensitivity of ~20 pg mL^{-1}	immunosensor	264
EP	0-30%	goat IgG	-	sensitivity of 1μg mL^{-1}	immunosensor	138
EP	20%	protein G/anti-leptin IgG	-	linear range of 10^{1} -10^{5} ng mL^{-1} with sensitivity of 3.1 Ω mg^{-1} mL^{-1}	immunosensor	139
EP	100%	anti-rabbit IgG	-	linear range of 119 pg mL^{-1} - 5.95 ng mL^{-1}	immunosensor	265
EP	100%	anti-hormone prolactin	-	linear range of 10^{-2} -10^{4} ng mL^{-1}	immunosensor	266

a: CP - chemical polymerization; EP - electrochemical polymerization.

1.4 Manufacture of polypyrrole-based conducting materials

As previously stated, due to its unique molecular structure, PPy is rigid, infusible and insoluble, resulting in a great difficulty in processing once synthesized. For now, due to the poor mechanical properties and processability, it is difficult to use PPy alone in any application. To solve this problem, a common method is to integrate PPy with other materials that have good mechanical performance and processability. Recently, the mechanical properties of single-component PPy were reportedly enhanced via micro/nanostructure design [53, 267, 268].

1.4.1 Polypyrrole composites

A composite is a material made from at least two constituents and possesses an integrated performance of the individual components. To benefit from its electrical conductivity, PPy is always compounded with other polymers (synthesis or natural polymers) and carbon nanomaterials via coating or blending.

1.4.1.1 Surface coating

Chemical or electrochemical deposition is the principal and effective route to coat a thin PPy layer on the supporting substrate surface. The thin PPy coating formed on a substrate surface renders a desired conductivity, while the substrate plays the role of not only a hard-template to guide the growth of PPy on its surface, but also a scaffold to provide mechanical strength. Electrochemical deposition is only applicable to conductive substrates such as carbon fibers [269], carbon nanotubes [270], graphene [271], carbon paper [272], as well as metals [273]. In contrast, chemical deposition offers an opportunity for both conductive and insulating substrates. In order to increase the adhesion between PPy and substrates, a two-step chemical deposition is typically utilized to obtain PPy-coated fiber or fabrics. To do so, Py monomers are firstly adsorbed onto the surface of the substrates, followed by a polymerization in an oxidant solution. For example, in Zhang's research group, PPy was coated to PET fabric through this method [101, 103]. After washing, the PET fabric was incubated in a Py/methanol/water solution to enrich monomer absorption on the fabric. The fabric was then put into an aqueous solution of $FeCl_3$ to complete polymerization. The surface electrical resistivity of the PPy/PET fabric was measured to be 63.4 $k\Omega\ \square^{-1}$ and retained ~80% of original conductivity after 24 incubation in cell culture medium. Similarly, PPy coating was formed on various fabrics including paper [274], cotton [275], and nylon [276].

And nanostructured substrates were also used to prepare PPy-based composites because of various reasons such as that a nanofibrous structure can mimic the features of ECM that is the ideal tissue engineering scaffold, and also can provide high specific surface area that is useful for energy storage. Thus, recently, more investigations are focusing on the nanostructured PPy composites. For example, bacterial nanocellulose was coated with PPy to form a core-shell structured composite for potential application in tissue engineering and

supercapacitors [169, 277]. PPy coating was found to improve PC12 cell adhesion and proliferation in the absence of electrical field. With electrical stimulation, this conductive nanofibrous scaffold could be used to regulate cell activity through electrical field delivered through the interface between PPy and cells. The PPy coated bacterial nanocellulose has a high specific surface area (56 m^2 g^{-1}) and the highest mass specific capacitance up to 316 F g^{-1} at 0.2 A g^{-1} current density. Thanks to the electrospinning techniques, numerous synthetic and natural polymers can now be fabricated into nanofibers, providing a firm foundation for the preparation of PPy-based nanofibrous composites. By using the aqueous solution of $FeCl_3$ as the oxidation system, the fine nanostructures of electrospun nanofibers can be well preserved after PPy polymerization. Thus, PPy has been easily introduced onto various template nanofibers (e.g., fibroin [278], PLLA [279], PCL [280], PLGA [52]) by chemical polymerization. In addition, as an alternative, vapor-phase polymerization is also effective in obtaining a fine PPy coating on nanofibers[281]. The conductivity of those PPy composites largely depends on the amount of PPy on substrate surface, which is affected by reaction time, feeding of monomer and oxidant, and also by dopants [52]. Although the mechanical properties of the PPy composites are improved by using flexible polymer fibers or fabrics, the eventual separation of PPy from the substrate is still a crucial issue due to the weak bonding between PPy and the substrates [108].

1.4.1.2 Particle filling

Another strategy to obtain PPy-based composite is blending PPy particles with other polymers, in which PPy is used as a conductive filler. Though carbon black may be more competitive than "pyrrole black" in commercial market, PPy particles as a conductive filling material has received much more attention in biomedical area due to its biocompatibility. The conductivity of such PPy composites arises owing to the conductive paths formed by the PPy fillers in the matrix, which is regulated by the state of dispersion, the geometry, the ratio of fillers, and the properties of the PPy particles [282]. Among them, the filling ratio or the percentage of PPy particles in the composite is considered the critical factor for conductivity. As shown in Fig 1.16, the critical loading of conductive fillers is known as the percolation threshold, after which the conductivity increases dramatically (orders of magnitude) with the increase of the conductive fillers following a percolation theory [283]. The

loading of PPy particles at percolation zone is enough to form continuous conductive paths within the composites. The preparation methods of the PPy particle filled composites generally include mechanical blending, solution mixing and in situ polymerization. In the solution mixing method, PPy particles are prepared by chemical polymerization first, and then mixed with a solution of the polymer to be composed, followed by removing the solvent by, for example, membrane casting and evaporation. Zhang's group prepared PPy/PLLA composite membranes (10^2 -10^3 Ω □$^{-1}$) by mixing PPy particles (5%) synthesized via emulsion polymerization with a PLLA/$CHCl_3$ solution and has been extensively studied how to use this composite for biomedical applications, especially for electrically stimulated cell culture and wound healing [43, 98, 102, 106, 109]. PPy/chitosan composite membrane (2.5% w/w PPy) was also fabricated showing a conductivity of 10^{-3} S cm^{-1} [284]. An enormous amount of research effort goes into the in situ polymerization method to prepare PPy particle filled composite membranes. By adding poly(D,L-lactide) (PDLLA) into the emulsion polymerization system, the synthesized PPy nanoparticles were automatically dispersed in PDLLA matrix [285]. Finally, PPy/PDLLA composite membranes with different PPy contents (1-17%) and surface resistivity from 2×10^7 to 15 Ω □$^{-1}$ were easily obtained by diluting the as-prepared PPy-PDLLA solution (20% PPy) with PDLLA solution [286].

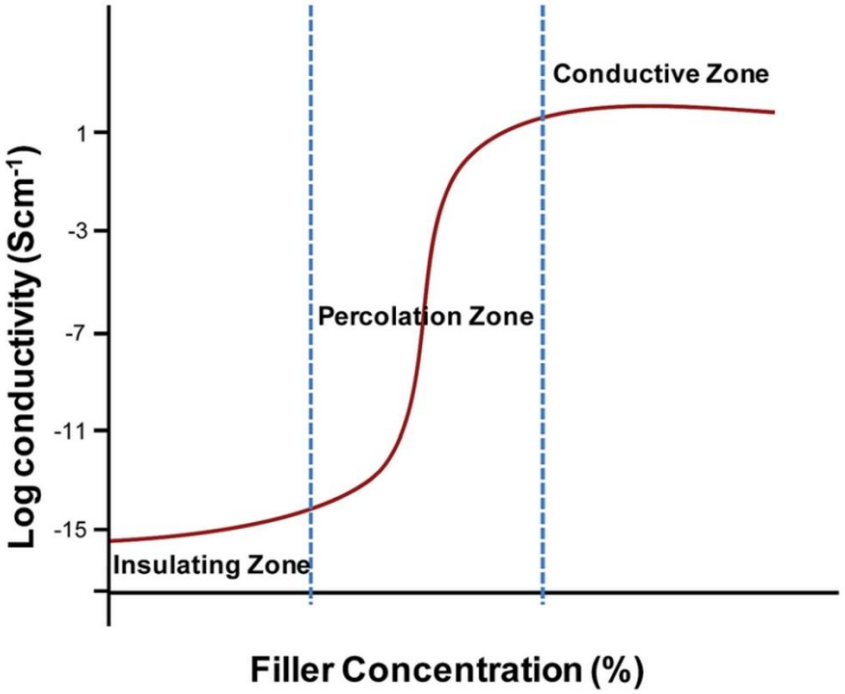

Figure 1.16 Conductivity of polymer composites as function of PPy filler concentration [282].

A PPy/cellulose acetate film was fabricated by in situ polymerization, showing maximum electrical conductivity of 3.6×10 S cm^{-1} with only 4.7 wt% loading of PPy [287]. Similarly, a PPy/hyaluronic acid membrane was prepared for tissue engineering [288]. As these composite membranes are more brittle than flexible, an elastomeric material, polyurethane (PU), was composed with PPy nanoparticles via an in situ polymerization of Py using $FeCl_3$ as oxidant in a PU emulsion [289].

However, due to the low affinity or compatibility between PPy and base polymers, those composites may suffer from the issues of delamination, agglomeration, and loss of conductivity [290, 291]. Meanwhile, aging and degradation of the substrates will lead to the weakening of the performance, or even destroy the composite structure during heating. The physicochemical stability of the composites depends on the temperature, pH, humanity, and environmental radiation. Considering the high thermal and environmental stability of PPy, single-component PPy materials that can be manipulated and have certain mechanical properties are highly desirable.

1.4.2 Micro/nanostructure design

Many attempts have been made to fabricate a pure PPy material having considerable mechanical properties via a nano/microstructural design without adding any supporting component [53, 267, 268]. Wang et al. constructed a free-standing 3D PPy framework by using a porous nickel foam as a removable template [268]. Thanks to the unique microstructure of the 3D PPy foam and the combination with graphene oxide, a high flexibility and meaningful mechanical strength (~180 kPa) were achieved. Through a multiphase synthesis technique at low temperature, an interconnected hollow-sphere PPy network was prepared [267]. And it was demonstrated that the hollow-sphere structure enabled the PPy film to deform elastically. That is, a spherical shell geometry could render a tunable elastic modulus to the inherently brittle materials. Recently, a free-standing PPy membrane with a certain degree of flexibility was constructed using PPy nanotubes synthesized via chemical polymerization with a reactive self-degraded template [53, 292]. However, such a film exhibits more fragile performance rather than an incommensurable flexibility compared with the PPy composite membranes. Although, for now, a highly flexible pure PPy membrane has not been reported, these significant attempts mentioned above provide new thoughts about improving the

mechanical strength of single-component PPy membrane through nano/microstructure designs.

1.5 Aims of study

1.5.1 Background

PPy has been widely investigated for biomedical applications, energy storage and heating elements for decades. The principal limitations on its application are the lack of functionality, poor mechanical properties, and very limited processability. In literature, PPyCOOH polymers have been reported to immobilize biomolecules. However, most PPyCOOH polymers were synthesized by EP that is inherently associated with small size, low productivity, high cost, and the requirement for special equipment. In addition, the incorporation of PyCOOH units decreased the conductivity of the copolymer. A high quantity of carboxyl groups on the surface of PPyCOOH polymers is necessary to provide sufficient reactive sites for biomolecule grafting. A core-shell structured PPyCOOH copolymer with PPy as the core and PPyCOOH homopolymer as the shell may solve this issue. However, this structure cannot be prepared through EP. For now, it is still difficult to chemically synthesize PPyCOOH polymers due to the low reactivity of PyCOOH monomers.

The extended conjugated π-system of PPy leads to the insolubility, infusibility and inferior mechanical properties (stiff and brittle) that have greatly limited the application of PPy. PPy-based composites have been widely prepared to improve the mechanical properties and processability. However, these composites suffer the issues of delamination, agglomeration, and loss of conductivity because of the low affinity between PPy and the base polymers. Attempts have been conducted to increase the mechanical performance of pure PPy materials via nano/microstructural designs without adding other supporting components. To the best of our knowledge, large-sized and highly flexible single-component PPy membrane has not been fabricated either by EP or through chemical polymerization.

1.5.2 Objectives

To develop functionalized and mechanically amenable polypyrrole for biomedical applications.

Four specific aims are:

1. Synthesis of core-shell structured functional PPy particles.
2. Grafting bioactive proteins to functionalized PPy particles and characterizations.
3. Preparation and characterization of flexible PPy membranes.
4. Combination of functional PPy particles and flexible PPy membrane.

1.5.3 Hypotheses

1. Functionalized core-shell PPy particles can be chemically polymerized based on the difference in comonomer reactivity.
2. The mechanical properties of pure PPy can be improved via nano/microstructural design.

1.5.4 Research design

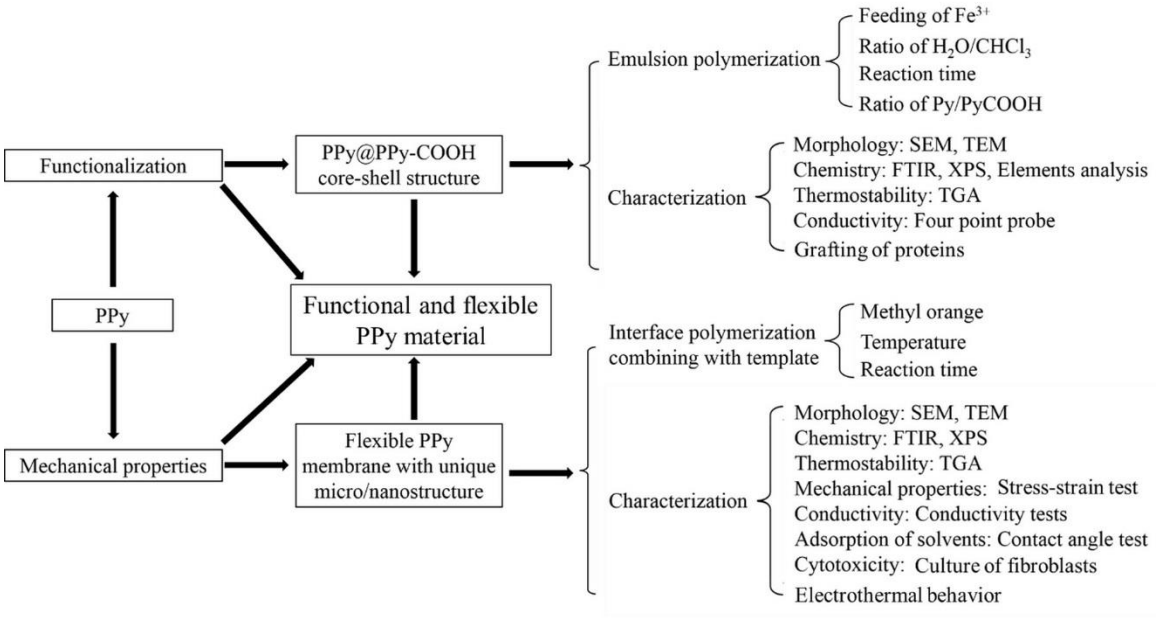

Figure 1.17 The schematic of research design.

CHAPTER II

SYNTHESIS AND CHARACTERIZATION OF CORE-SHELL POLY(PYRROLE-CO-(1-(2-CARBOXYETHYL)PYRROLE)) PARTICLES BASED ON A REACTIVITY-DRIVEN MECHANISM

One-Step Reactivity-Driven Synthesis of Core-Shell Structured Electrically Conducting Particles for Biomedical application

Jifu Mao and Ze Zhang*

a. Centre de recherche du CHU de Québec, Département de chirurgie, Faculté de médecine, Université Laval, Québec (QC), Canada.

b. Centre de recherche Hôpital Saint-François d'Assise, CHU, 10 rue de l'Espinay, Local E00-177, Québec (QC), G1L 3L5, Canada.

E-mail: Ze.Zhang@chg.ulaval.ca

J. Mater. Chem. B, 2016, 4, 5429-5436 DOI: 10.1039/c6tb00642f

Electronic supplementary information (ESI) available. See DOI: 10.1039/c6tb00642f

2.1 Résumé

Cet article rapporte une polymérisation en émulsion en une étape pour la synthèse des particules de polymère conducteur à structure cœur-coquille, basée sur la différence de réactivité des comonomères. La morphologie et la chimie de surface et de masse des poly (pyrrole-co-(1-(2- carboxyéthyl pyrrole)) (PPy-co-PPyCOOH) formés dans différents temps de réaction ont été analysées. Les particules étaient constituées d'une coquille d'homopolymère PPyCOOH, et d'un noyau du copolymère PPy-co-PPyCOOH composé principalement de PPy. L'anticorps anti-albumine de sérum humain (anti-HSA) immobilisé de manière covalente sur la surface de la particule s'est révélé réactif à HSA. Un schéma en cinq étapes a été proposé pour expliquer la formation de la structure cœur-coquille. Il s'agit d'une méthode simple et générale pour fabriquer des particules conductrices ayant une structure de cœur-coquille et une surface fonctionnelle.

2.2 Abstract

Electrically conductive and functional polymeric nanoparticles have significant potential in biomedical applications such as in sensing and stimulation. Polymeric core-shell particles are usually prepared either through a multiple-step process or by the design of amphiphilic macromolecules. Here we report a simple one-step and one-pot emulsion polymerization method to synthesize the core-shell structured electrically conducting polymer particles based on the difference in comonomer reactivity. The morphology and the surface and bulk chemistry of poly(pyrrole-co-(1-(2-carboxyethyl)pyrrole)) (PPy-co-PPyCOOH) particles formed in different reaction times were analyzed with scanning electron microscopy (SEM), transmission electron microscopy (TEM), X-ray photoelectron spectroscopy (XPS), Fourier transform infrared spectroscopy (FTIR), thermal gravity analysis (TGA) and total element analysis. The particles were found formed by a shell composed of the less conductive but functional PPyCOOH homopolymer, and a core made of the PPy dominated PPy-co-PPyCOOH copolymer of high conductivity. Human serum albumin antibody (anti-HSA) as a model molecule was covalently immobilized onto the particle surface and proven reactive to HSA. A five-step schema based on a novel reactivity-driven mechanism was proposed to explain the formation of the core-shell structure. This new strategy therefore provides a simple and general route to prepare core-shell conductive particles with functional surface, based on the reactivity of comonomers.

2.3 Introduction

Core-shell structures are among the most fascinating material architectures with enormous potential in biomedical applications [1-3]. Many efforts have been devoted to the development of new strategies to form polymeric particles with core-shell structures [1, 4]. The four commonly used methods include two-step polymerization, emulsion polymerization with reactive surfactant, step-wise hetero-coagulation of small cationic polymer particles onto large anionic polymer particles, and self-assembly of block amphiphilic polymers [5]. Among them, emulsion polymerization is the most widely adopted process to prepare core-shell polymer particles. Recently, controlled/living radical polymerization has been investigated to introduce polymer brush onto the particles through a "grafting from" design [6]. Discontinuous, semi-continuous and pre-swelling processes have also been reported to introduce shell-forming monomers [7]. Noticeably, among the above mentioned methods, at least two steps are required to form a core-shell structure. At meantime, it is very useful to study multifunctional core-shell polymer particles with distinct properties such as conductivity, magnetism and surface functionality [8]. Accordingly, electrically conducting polymers with functional groups have been investigated for biomedical applications such as biosensor and bioelectrical interface.

Among intrinsically conducting polymers, functional polypyrrole (PPy) has gained new momentum in biomedical research [9-11] and in studies related to energy sectors [12]. For example, PPy nanowires with carboxyl groups on surface were electrochemically synthesized from 1H-pyrrole-1-propionic acid and then decorated with Ag nanoparticles to increase the opto-electronic property [13]. Similarly, surface functionalized PPy was conjugated with bioactive proteins to form biosensors [14] or with palladium to form hydrogen sensor with high sensitivity [15]. In such applications, electrical conductivity, high surface area and surface functionality are required. These requirements can be met with the core-shell structured functional PPy micro- or nanoparticles. The shell should be made of pyrrole derivative with functional group, which usually has low electrical conductivity; and the core should be made of pyrrole to achieve sufficient conductivity. A number of studies have reported the core-shell

PPy particles. Silica core-PPy shell composite particles have been prepared since 1990's [16], with recent advance in silica surface modifications to improve the compatibility between PPy and silica [17]. Similarly, polymeric particles were also investigated to produce the core-shell structures with PPy [18, 19]. The surface functionality of the PPy core-shell particles is often achieved through N-functionalized pyrrole derivatives.

Poly(pyrrole-co-(1-(2-carboxyethyl)pyrrole)) (PPy-co-PPyCOOH), a typical N-functionalized PPy copolymer, has been studied due to its functional carboxyl groups, electrical conductivity and easy preparation [20, 21]. PPy-co-PPyCOOH was polymerized onto silica microparticles to produce stable colloidal dispersions 20 years ago [22]. Polystyrene (PS)/PPy-co-PPyCOOH core-shell particles were also reported [23, 24]. Through simple chemical reactions, the carboxyl groups in PPy-co-PPyCOOH can be further modified into active ester [25] and amine [26], having immense potential in biomedical field due to it conductivity and reactivity. However, all reported approaches require a template such as silica or PS particles; and the template particles need surface activation to strengthen the attachment of PPy-co-PPyCOOH to the template.

We report in this work a one-pot and one-step emulsion polymerization of functional conductive particles, with the PPy dominated PPy-co-PPyCOOH copolymer as the core and PPyCOOH homopolymer as the shell. This core-shell architecture was achieved because of the difference in reactivity between pyrrole and its derivative (e.g., 1-(2-carboxyethyl)pyrrole). The dynamic growth of the particles and the percentage of PPyCOOH in the particles and on particle surface were studied, as well as the effect of reaction time on the yield, morphology, structure and conductivity of the particles. A plausible mechanism of polymerization was proposed. Through simple and mild chemical reactions, anti-HSA was readily immobilized onto particle surface and showed reactivity towards HSA. The controlled conductivity and the biofunctionality make such core-shell PPy-co-PPyCOOH particles useful in biomedicine especially for biosensor. Meanwhile, because the difference in reactivity

between a monomer and its derivative is a common phenomenon, the reactivity-driven formation of core-shell structures could be applied to other chemical reactions.

2.4 Results and discussion

2.4.1 Preparation of PPy-co-PPyCOOH core-shell particles

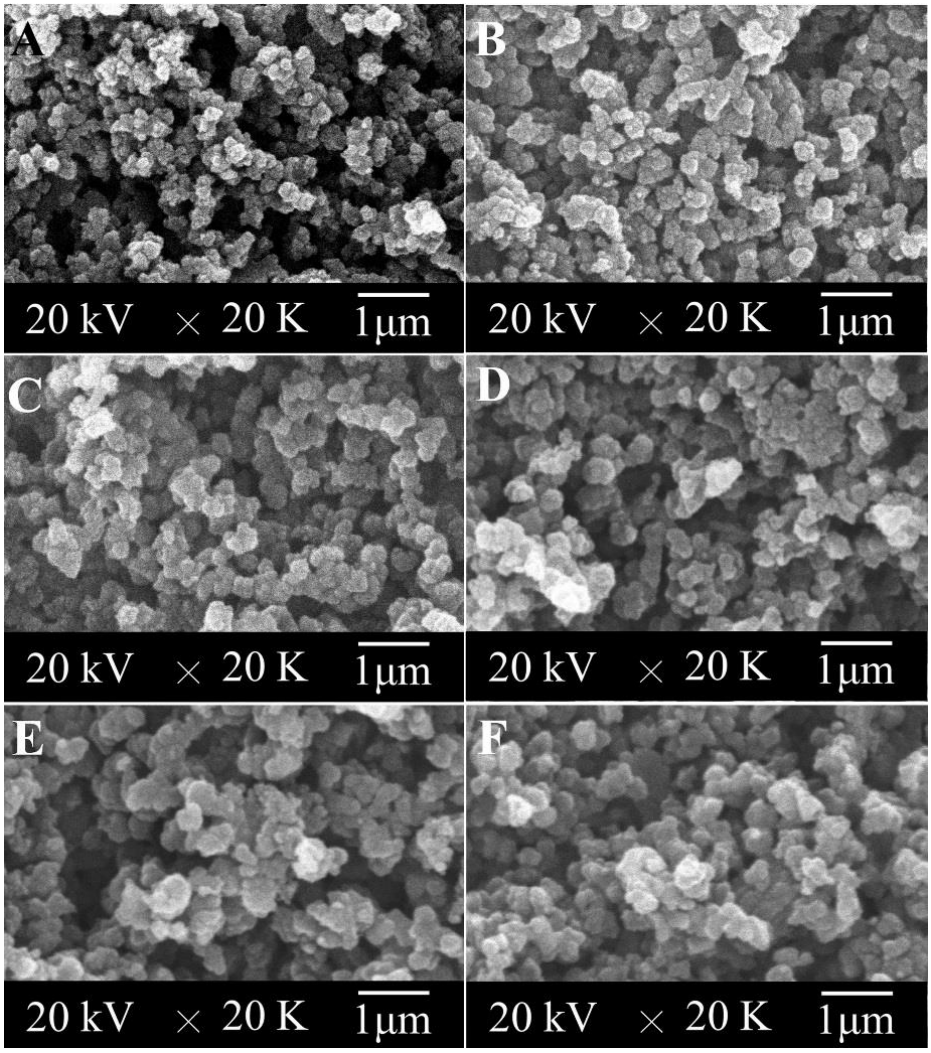

Figure 2.1 SEM photomicrographs of PPy-co-PPyCOOH particles prepared in different reaction times from 10 min to 24 hours: (A) 10 min, (B) 40 min, (C) 1.5 h, (D) 6 h, (E) 12 h, and (F) 24 h.

Compared with literature [22], a high feeding of alkali and a long reaction and extraction time were selected to improve the overall yield of the PyCOOH monomer. After purification and drying, high-purity white crystals were obtained with an overall yield of 96%, compared to 51% in literature [22]. The chemical structure was confirmed by

^{1}H NMR (Fig. S2.1), ^{13}C NMR (Fig. S2.2) as well as FTIR (Fig. S2.3), which were identical with that in literature [14].

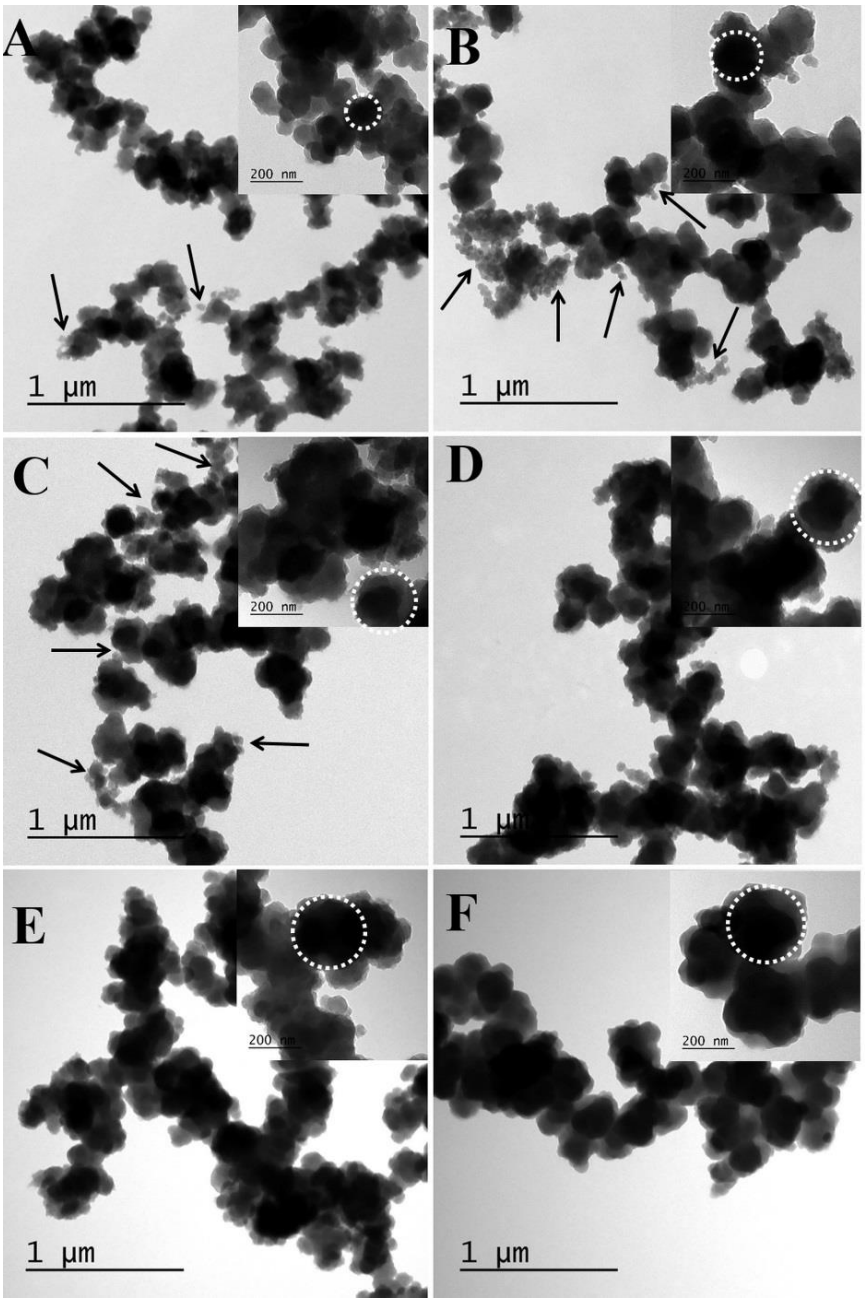

Figure 2.2 TEM photomicrographs of PPy-co-PPyCOOH particles prepared in different reaction times from 10 min to 24 hours: (A) 10 min, (B) 40 min, (C) 1.5 h, (D) 6 h, (E) 12 h, and (F) 24 h.

The copolymerization of Py and PyCOOH took place in the water phase of the emulsion. In addition to the feed of Fe^{3+} and ratio of monomers, the solvent system,

reaction temperature and time, and monomer reactivity are all the controlling factors to the formation of copolymer [27, 28]. Due to the lower reactivity of PyCOOH (oxidation potential +1.2 V) relative to Py (+0.75 V) [14, 20], a high feeding of oxidant and low ratio of aqueous phase were designed to increase the oxidative capacity of the system and consequently the incorporation of PyCOOH. As showed in Figure 2.1, the size of the particles increased only in the first 1.5 hour and then remained unchanged at about 200-300 nm, which was in good agreement with the TEM observation (Fig. 2.2, dotted circle). At the same time, the changes in particle structure with reaction time were readily discovered by TEM. An architecture aggregated by the nanoparticles was formed within the first 10 minutes of polymerization. What appeared most interesting was that, from the very beginning, there were smaller particles of about 50 nm progressively appeared around the initial larger particles and then attached to them (Fig. 2.2, arrows). At the end of polymerization, the initial structures appeared completely covered by these small particles.

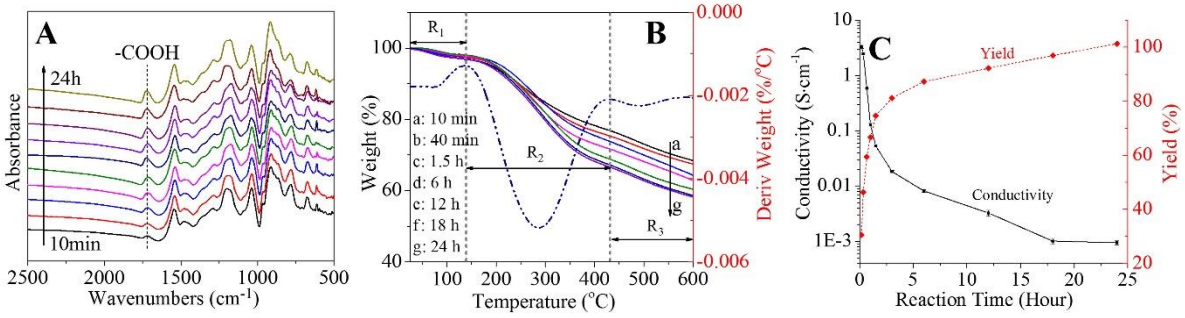

Figure 2.3 The FTIR spectra (A), TG and DTG analyses (B), and the yield and conductivity (C) of the PPy-co-PPyCOOH particles synthesized at different reaction times from 10 min to 24 h.

The FTIR spectra of the particles (Fig. 2.3A) revealed the characteristic C=O stretching vibration in PPyCOOH at 1715 cm^{-1}, the C=C double bond stretching in aromatic ring at 1545cm^{-1}, the C-N stretching at 1454 cm^{-1}, the two peaks of the =CH- in-plane vibration at 1295 cm^{-1} and the vibration of pyrrole ring at 1190 cm^{-1}. The growth of the absorption intensity at 1715 cm^{-1} indicated the increasing carboxyl groups in the particles with reaction time, which was further supported by the similar increase in oxygen element on surface of the particles (Table 2.1). As shown in Figure 2.3B, the thermogravimetric analysis displayed three regions according to the deriv.

weight loss curve (dash line) of the sample obtained at 18h: the first region corresponds to the loss of the absorbed water in temperature range of 40˚C - 140˚C; the second region of 140˚C - 430˚C is supposed to be the loss of propionic acid groups in the copolymer [29]; and the weight loss after 430 ˚C results from the removal of the DBS dopants and the thermal decomposition of the copolymer backbone. The TGA results clearly indicate that the increase in PyCOOH component has caused the decline of the thermostability of the copolymer. Moreover, the increase in weight loss in the second region correlates well with the FTIR and XPS data, suggesting a growing number of PyCOOH units in copolymer with reaction time. What also increased with the reaction time was the yield that raised gradually from 30.5% to 101.3% (Fig. 2.3C). Conversely, the conductivity of the copolymer particles reduced significantly with reaction time, from 3.3 $S \cdot cm^{-1}$ to 9.4×10^{-4} $S \cdot cm^{-1}$, which was in agreement with the increasing amount of the less conductive PyCOOH units. All these results suggest that the copolymer particles were initially formed by the PPy dominated copolymer and then gradually covered by PPyCOOH, meaning a core-shell structure of the particles. To further prove the core-shell structure, the particles were subjected to systematic element analysis to investigate the difference between the core and the shell.

2.4.2 Different chemical compositions between core and shell

Considering the size of the particles (200 - 300 nm) and the sampling depth of XPS (ca. 10 nm), XPS is the only reliable tool to analyze the surface composition of the particles. Table 2.1 summarizes the surface elemental composition of the particles harvested at different polymerization times. The theoretical ratio of carbon to nitrogen in pyrrole and 1-(2-carboxyethyl)pyrrole is 4:1 and 7:1, respectively. The value of C/N in Table 2.1 demonstrates a gradual increase from 5.4 to 6.9 in the first 3 h of polymerization and then becomes constant at about 7.1 that is almost the theoretical ratio of carbon to nitrogen in PPyCOOH homopolymer. The initial ratio of 5.4 at 10 min is close to the theoretical C/N ratio of the ideal copolymer that is 5.5 (Py/ PyCOOH = 1:1). However, the total element analysis at 10 min recorded 4.7 for C/N (Table 2.2), which is in between the pure pyrrole and the ideal copolymer. This difference in XPS and total elemental analyses (5.4 vs. 4.7) is likely because of the

difference in surface and bulk compositions. The ratio of C/N measured with total elemental analysis for the particles of long polymerization time (18 h to 24 h) is about 5.6, which corresponds very well with the theoretical C/N ratio of the ideal copolymer. Based on the C/N ratios at different reaction times, the molar ratios of Py and PyCOOH were calculated and listed in Table 2.2. The particles revealed a high Py content (Py/PyCOOH = 3.2) at 10 min, meaning a Py-dominated copolymer, and almost equal amount of Py and PyCOOH (Py/Py-COOH = 0.9) at long polymerization time. What deserves to be noticed is that calculations based on the ratio of Py/PyCOOH and the overall yield indicate the depletion of Py at 40 min. To conclude, XPS and total element analysis demonstrated that the particle was formed initially as a Py-dominated copolymer core and then covered by a shell of PPyCOOH homopolymer.

Table 2.1 Surface elements analysis by XPS (Atomic %)

Reaction time	C_{1s}	O_{1s}	N_{1s}	Cl_{2p}	$\underline{C}=O/C_{1s}$	N^+/N_{1s}[a]	C/N
10 min	74.7±2.3	8.2±1.2	13.9±1.4	3.2±0.4	9.9±1.3	19.6±1.4	5.37±0.34
20 min	73.7±1.8	9.8±1.0	13.5±1.0	3.0±0.1	11.7±1.0	17.5±1.9	5.46±0.29
40 min	72.4±2.1	13.9±1.1	12.7±0.8	1.0±0.1	13.0±1.3	16.0±1.3	5.70±0.22
1 h	70.1±2.5	17.3±1.3	11.6±1.0	1.0±0.1	15.3±0.9	12.7±0.8	6.04±0.35
1.5 h	70.4±2.3	17.7±1.2	11.2±1.1	0.8±0.2	16.1±1.5	11.6±1.4	6.28±0.32
3 h	69.6±1.9	19.3±1.6	10.1±1.1	1.0±0.1	16.6±1.1	10.8±1.8	6.89±0.27
6 h	69.3±1.9	19.9±1.2	9.8±1.3	1.0±0.1	16.9±2.4	10.7±0.9	7.07±0.30
12 h	69.0±3.0	19.9±1.3	9.7±1.6	1.4±0.2	17.4±1.7	10.7±1.7	7.11±0.29
18 h	69.1±1.5	19.9±1.4	9.6±0.6	1.4±0.3	17.3±1.2	9.8±1.4	7.19±0.19
24 h	69.2±2.4	19.8±1.7	9.7±1.5	1.3±0.2	17.6±2.2	9.5±1.0	7.13±0.33

a: Ratio between deprotonated nitrogen and total nitrogen based on curve fitting of N_{1s}.

Table 2.2 Total elements analysis (mass %)

Reaction time	C	N	H	S	C/N[a]	Py/PyCOOH[b]
10 min	57.2	13.8	3.6	0.2	4.71	3.24
20 min	56.5	13.1	3.8	0.4	4.77	2.91
40 min	58.1	13.4	3.7	0.2	4.93	2.24
1 h	58.6	13.0	3.9	0.2	5.11	1.71
1.5 h	58.8	12.9	3.7	0.3	5.14	1.63
3 h	58.4	12.4	4.0	0.3	5.33	1.25
6 h	57.9	12.1	4.0	0.3	5.40	1.14
12 h	56.5	11.6	3.8	0.2	5.49	1.01
18 h	58.3	11.9	3.8	0.3	5.56	0.93
24 h	55.8	11.4	3.7	0.2	5.57	0.92

a: The mole ratio between carbon and nitrogen calculated by total elements analysis.
b: The mole ratio between Py and PyCOOH in PPy-co-PPyCOOH copolymers calculated based on the mole ratio of carbon and nitrogen.

This core-shell structure is also supported by the changes in oxygen content on particle surface. In the first 1.5 h, oxygen content increased from 8.2% at 10 min to 17.7%, corresponding to the increase of PyCOOH. When the reaction time reached 3 h, surface oxygen reached about 20% and did not change further, which correlated very well with the theoretical oxygen content in PyCOOH (2 oxygen in a total of 10 atoms, noting that hydrogen is not detectable by XPS). Furthermore, the high resolution spectra of carbon (C_{1s}), nitrogen (N_{1s}) and oxygen (O_{1s}) of the specimens obtained at different reaction times are presented in Figures 2.4A to 2.4C, with the curve fitting results summarized in Table 2.1. Figures 2.4D to 2.4F represent the curve fitting for the PPy-co-PPyCOOH copolymer harvested at 18 h. The spectrum of C_{1s} was fitted with three components[27], including the first peak at 284.6 eV assigned to the β-carbons (C-C-C-N-C) in pyrrole unit and the saturated carbons in PyCOOH unit, the second peak at 285.9 eV assigned to the α-carbons (C-C-C-N-C) in pyrrole and -C-O- in

PyCOOH, and the third peak at 288.9 eV assigned to the O<u>C</u>=O in PyCOOH plus the minor contributions from chain termination and over-oxidation. Therefore, for the copolymer, the increase at 288.9 eV in C_{1s} (Fig. 2.4A) clearly indicated the quantity of carboxyl groups on particle surface. Since the principal source of O_{1s} in copolymer is the carboxyl groups, the increase in O_{1s} and O<u>C</u>=O in the first 3 h, as showed in Figure 2.4C and Table 2.1, also supports the core-shell structure. As a further proof, the values of <u>C</u>=O/C_{1s} and O_{1s} became little changed after 3 h (Table 2.1), meaning that the quantity of PyCOOH on particle surface was almost constant.

As previously mentioned, the oxidation potential of PyCOOH is much higher than that of Py, meaning that Py is much easier to be polymerized than PyCOOH would be. The consequence was that more Py was polymerized during the initial period of reaction to form the PPy dominated core. With the depletion of the Py monomers, the PyCOOH monomers became dominated and were polymerized and deposited as a shell onto the core. It is therefore reasonable to believe that the small nanoparticles attached to the initial particulate frameworks are made of the PPyCOOH homopolymer.

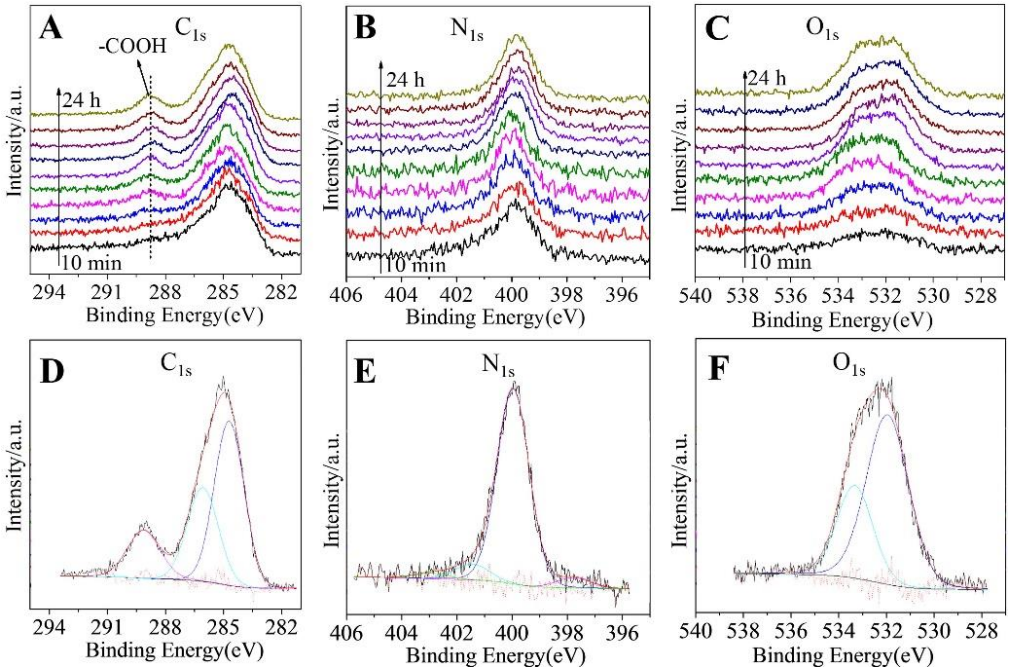

Figure 2.4 High resolution XPS spectra of C_{1s} (A), N_{1s} (B) and O_{1s} (C) of the PPy-co-PPyCOOH particles synthesized at different reaction times ranging from 10 min to 24 h. D to F are the representative curve fittings for the particles harvested at 18 h.

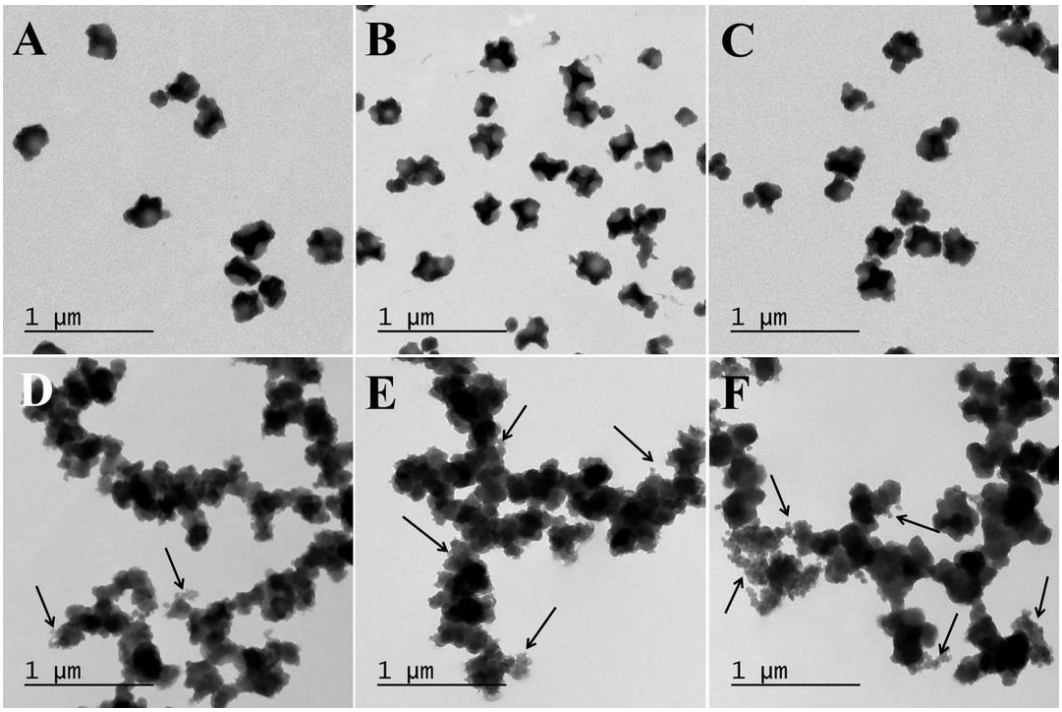

Figure 2.5 TEM photomicrographs of PPy homopolymer (upper panel) and PPy-co-PPyCOOH copolymer (lower panel) synthesized at different reaction times from 10 min to 40 min: (A) and (D) 10 min, (B) and (E) 20 min, (C) and (F) 40 min.

PPy homopolymer synthesized in the same reaction system showed different morphology and high yield in much shorter time (110% yield in 40 min), which is well in line with the previous calculation. As presented in Figure 2.5, the small nanoparticles observed in copolymer (arrows, Fig. 2.5D-2.5E) were absent in PPy homopolymer (Fig. 2.5A-2.5C). This further suggests that the small nanoparticles formed on the surface of the large particulate frameworks are likely composed of the PPyCOOH homopolymer. In addition, black polymer particles were still formed from the filtrate after harvesting the copolymer particles at 12 h. The morphology and XPS full scan of these particles harvested from the filtrate are showed in Figure S2.4. Due to the fact that Py monomers were already completely consumed during first 40 min, and also due to the fact that the XPS spectrum of these later-formed particles is similar to that of the copolymer particles formed at 24 h, these particles formed in filtrate were considered made of the PPyCOOH homopolymer. The large and round particles were presumably formed by self-assembly of small particles.

2.4.3 Conductivity of PPy-co-PPyCOOH core-shell particles

It was reported that the conductivity of PPy-co-PPyCOOH copolymer was significantly lower than that of PPy, with a tendency to decrease with the increase of the PyCOOH component in the copolymer, no matter via chemical or electrochemical synthesis [22, 30]. The similar tendency in Figure 2.3C therefore also supports the core-shell structure. Disruption of the planarity and inhibition of the π-π electron conjugation due to PyCOOH units were believed to be the primary causes of conductivity decline in PPy-co-PPyCOOH copolymer [31]. In addition, the doping process was also suppressed by PyCOOH units. The doping level of pyrrole units is typically estimated by the ratio of the areas of the positively charged nitrogen and total nitrogen (denoted as N^+/N), with a higher ratio indicating a higher doping level. As shown in Table 2.1, the ratio of N^+/N records a remarkable decrease with the polymerization time, meaning that the doping level of the copolymer continuously declines with the incorporation of PyCOOH units. It was believed that the low doping level in PPy-co-PPyCOOH copolymer was inextricably linked with the carboxyethyl groups substituted at the N-position of pyrrole [31]. Therefore, it is understandable that with the increase in PyCOOH units the conductivity of the copolymer has declined accordingly. Nevertheless, the conductivity of the PPy-co-PPyCOOH copolymers in this work, i.e., ca. 10^0-10^{-4} $S \cdot cm^{-1}$, is among the highest reported in literature, no matter synthesized by chemical or electrochemical polymerization. This is probably because of the PPy dominated core. A different way to prepare such a core-shell structure might be achieved by a semi-batch reaction, in which PPy is formed first then followed by the addition of PyCOOH to form a shell on PPy particles [24].

2.4.4 Grafting and activity of model antibody

Biomolecules are incorporated into PPy commonly through physical adsorption, doping, or covalent grafting [21]. Covalent bond provides stable immobilization but requires sufficient functional groups on surface and also mild chemical reactions [32]. The shell made of PyCOOH guaranteed the possibly highest amount of carboxyl groups on particle surface, providing abundant binding sites for biomolecules. In order to prove the ability to immobilize functional biomolecules, FITC conjugated human

serum albumin antibody (Anti-HSA, as a model molecule) and bovine serum albumin (BSA, as a control) were grafted onto the surface of the PPy-co-PPyCOOH particles using NHS-EDC coupling. The structure of the PPy-co-PPyCOOH coated membrane is shown in Figure 2.6A. The particulate layer, with around 100 μm thickness, is a porous network structure offering high surface area for protein grafting. The results of protein grafting (Fig. 2.6, B&C) showed that Anti-HSA was successfully grafted onto the particulate surface (Fig. 2.6, B1) and remained active to its antigen HSA (Fig. 2.6, B2). The immobilization was observed over the entire surface with fairly uniform fluorescent intensity. Control experiment showed negligible autofluorescence of the grafted BSA (Fig. 2.6, C1), and negligible non-specific absorption of Anti-HAS to the albumin grafted surface (Fig. 2.6, C2). Consequently, it was demonstrated that active anti-HSA had been uniformly immobilized onto the PPy-co-PPyCOOH particles.

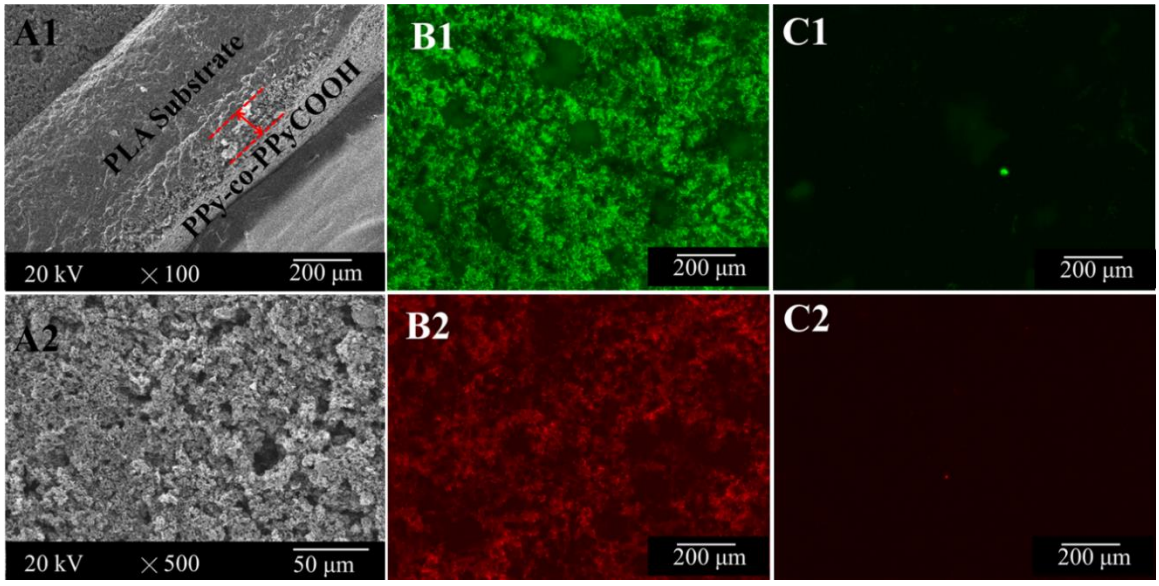

Figure 2.6 SEM photomicrographs of the PPy-co-PPyCOOH coated membrane (A) and fluorescence photomicrographs of protein immobilization (B, C). A1: cross-section showing a layer of particles on a PLA substrate; A2: morphology of the particulate surface; B1: Anti-HSA (FITC, green) grafted surface showing successful immobilization of the antibodies; B2: B1 incubated in HSA (rhodamine, red) showing the functionality of the immobilized antibodies; C1: BSA grafted surface showing no fluorescence; and C2: C1 incubated in HSA (rhodamine) showing little nonspecific absorption of HSA (rhodamine).

2.4.5 A suggested schema for the formation of the core-shell structure

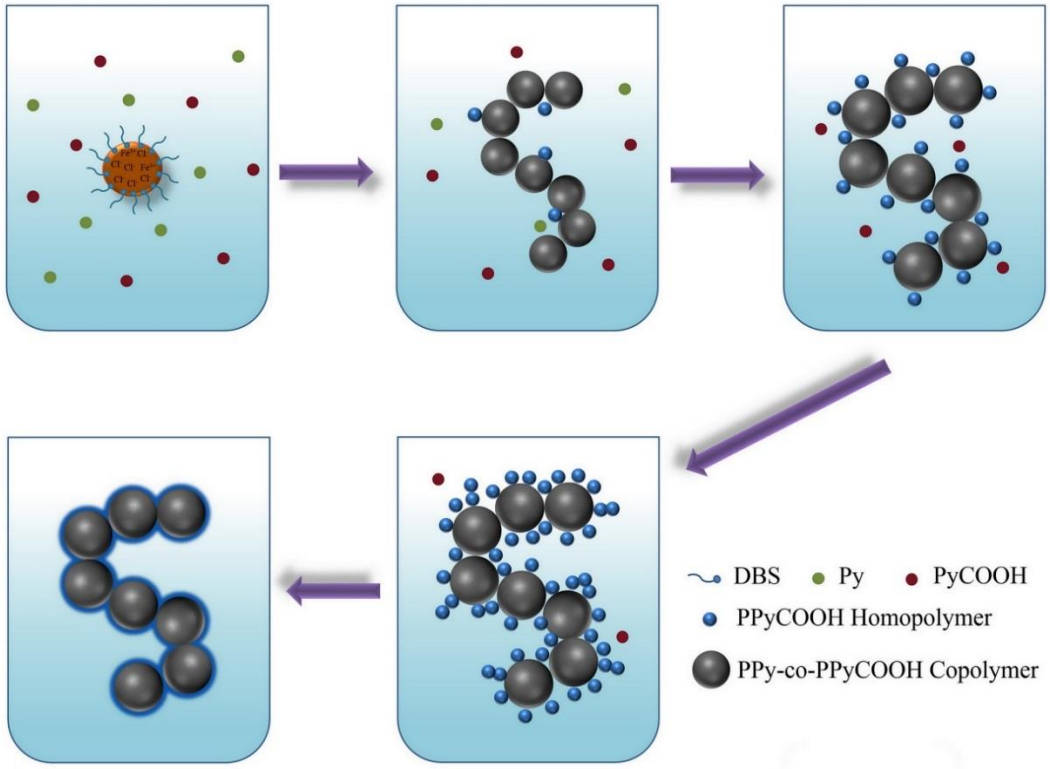

Figure 2.7 A five-step schema to explain the formation of the core-shell structured PPy-co-PPyCOOH particles. The quickly formed framework is made of the aggregation of the PPy dominated copolymer cores, which are gradually surrounded and finally wrapped by a shell made of the PPyCOOH homopolymer nanoparticles.

To explain how the core-shell structure is formed, a five-step schema has been proposed in Figure 2.7. In the first step, DBS (surfactant) and $FeCl_3$ (oxidant) are added into the $CHCl_3/H_2O$ system with vigorous stirring to form an emulsion consisting of a continuous oil phase and the DBS micelles that contain the aqueous solution of $FeCl_3$. Then Py and PyCOOH are added. The second step begins when the monomers start to diffuse into the micelles and quickly form the Py dominated copolymer particles in about 10 min. These particles form the initial framework to which very few PyCOOH nanoparticles attach. In the third step that takes place between 20 to 40 min, with the gradual depletion of Py and the increase in size of the initial framework, more PPyCOOH nanoparticles appear and attach to the copolymer framework. The next step is between 1.5 to 3 h that is featured with the appearance of large amount of PPyCOOH nanoparticles around the initial cores. In the final step or

from 3 to 24 h, with the accumulation and fusion of the PPyCOOH nanoparticles, the core-shell structure finally form.

Compared with the conventional methods to prepare core-shell structures, the unique strategy demonstrated in this paper is based on the different reactivity of the comonomers and the drift in comonomer feed. According to copolymerization equation, the mechanism suggested above (Fig. 2.7) would only occur when reactivity ratio $r_1 > 1$ ($r_1 = k_{11}/k_{12}$, Py = M1, PyCOOH = M2) and $r_2 < 1$ ($r_2 = k_{22}/k_{21}$). This is in fact the case of this work, i.e., the propagation of PPy homopolymer (k_{11}) is much faster than that of the copolymer (k_{12}) and PPyCOOH homopolymer (k_{22}). The only assumption we made is $k_{12} = k_{21} > k_{22}$. Considering that the particles formed in the late stage are basically made of PPyCOOH homopolymer, we believe that this assumption is valid. The main advantage of this reactivity driven strategy lies in its simplicity, requiring no tedious processes and complicate molecule design. Moreover, core-shell particles with a variety of functional groups could be fabricated by this method via selecting suitable comonomers. For example, functional conductive particles may be obtained by replacing PyCOOH with other functional monomers such as PyCN, N-3-aminopropylpyrrole ($PyNH_2$), N-glycidylpyrrole (PyPO) and 2-(1H-Pyrrol-1-yl)ethanol (PyOH). Conspicuously, it is unnecessary to excessively increase the feeding of M2 to gain more functional groups on particle surface because M2 would eventually form the shell that offers the highest amount of functional groups on particle surface. Moreover, the composition of the shell does not depend on the hydrophilicity or hydrophobicity of the monomers, completely different from the commonly recognized theory of controlling surface property by using amphiphilic monomers[7]. In this work, the more hydrophilic PyCOOH failed to compete in polymerization with the less hydrophilic Py in water phase. Instead, the PPyCOOH homopolymer or the shell was formed near the oil phase. Therefore, under the reactivity driven mechanism, the reactivity ratio is the key to decide which monomer plays the role of the core or shell of the particles.

2.5 Conclusions

Core-shell structured polymeric particles with controlled conductivity and surface chemistry were prepared via a simple emulsion polymerization based on a novel reactivity driven mechanism. These particles were formed by a core made of the PPy dominated and therefore more conductive PPy-co-PPyCOOH copolymer, and a shell composed by the PPyCOOH homopolymer that is less conductive but rich in carboxyl groups. The conductivity and surface carboxyl groups can be regulated through reaction time. To explain the formation of the core-shell structure, a five-step schema has been proposed based on the reactivity driven mechanism. The particles were readily immobilized with functional antibodies. Such functional and conductive polymeric particles could be used for biosensor or other biomedical applications.

2.6 Experimental section

2.6.1 Materials

Pyrrole (Py, 98%, Alfa Aesar-A Johnson Matthey Company, Ward Hill, MA, USA) was distilled twice under reduced pressure and stored in a refrigerator at 4°C prior to use. 1-(2-Cyanoethyl)pyrrole (PyCN, 98%, Sigma-Aldrich , Oakville, Ontario, Canada), dodecylbenzenesulfoinc acid sodium (DBS, Sigma-Aldrich), ferric chloride hexahydrate ($FeCl_3 \cdot 6H_2O$, 97%, Laboratoire Mat, Quebec, QC, Canada), N-Hydroxysuccinimide (NHS, 98%, Sigma-Aldrich), N-(3-Dimethylaminopropyl)-N′-ethylcarbodiimide hydrochloride (EDC, 98%, Sigma-Aldrich), anti-human serum albumin antibody (FITC) (anti-HSA, Abcam Inc, Toronto, ON, Canada), human serum albumin (rhodamine) (HSA, Abcam Inc), bovine serum albumin (BSA, 98%, Sigma-Aldrich), Triton 100-X (Sigma-Aldrich), polylactide (PLA η=1.3 dL/g, Hycail B.V., Noordhorn, Netherlands) and all other chemicals (Analytical Grade) were used as received.

2.6.2 Synthesis of functional monomer

1-(2-Carboxyethyl)pyrrole (PyCOOH) was synthesized according to the procedure described by Maeda et al. [22]. Briefly, 24 ml of PyCN was added into 120 ml of 6.7 M

KOH solution; and this mixture was heated to boiling and refluxed with N_2 protection until no more NH_3 generated. After cooling to room temperature, the reddish solution was acidified to pH 5.0 using 8 M HCl and then extracted with ether (5 × 6 hours). After removing ether with a rotary evaporator, the crude product in light yellow was recrystallized twice in n-heptane. After evaporation of the solvent and drying under vacuum for 24h, the white crystal of PyCOOH was obtained.

2.6.3 Polymerization of PPy-co-PPyCOOH particles

The PPy-co-PPyCOOH particles were synthesized through water-in-oil (chloroform) emulsion polymerization using DBS (1%, w/v) as emulsifier, as we previously reported [33]. The feeding ratio of reactants has been optimized previously by considering the surface carboxyl groups, conductivity and particle morphology. Therefore, following parameters were used in all polymerization experiments: 0.8 M $FeCl_3$, 100 ml solution of H_2O in $CHCl_3$ (25:75, v/v), and 1:1 mole ratio of Py to PyCOOH. Typically, 16.5 ml of aqueous solution of $FeCl_3 \cdot 6H_2O$ was added into 60 ml $CHCl_3$ containing 1g DBS. After stirring under N_2 protection for 30 minutes to form emulsion, 15 ml $CHCl_3$ containing 15 mmol Py/PyCOOH mixture was added dropwise. The reaction was maintained at room temperature for a period from 10 min to 24 h, with the N_2 protection for the first 3 h. The reaction was terminated by demulsification with methanol. The product was harvested through vacuum filtration and washed in methanol, methanol/water (50/50, v/v) mixture, 1M HCl, and finally in deionized water, 3 times in each solution. The product was dried under vacuum for at least 48 h before characterization.

2.6.4 Characterization

2.6.4.1 Model biomolecule grafting and detection

Before antibody grafting, the PPy-co-PPyCOOH particles were coated onto a PLA substrate. The PLA substrate was prepared by casting a PLA/$CHCl_3$ solution (10%, w/w) followed by solvent evaporation. Then PPy-co-PPyCOOH particles in $CHCl_3$ (30%, w/w) were dropped with pipette to cover the PLA membrane. After evaporation of $CHCI_3$, the particle coated membrane was washed in ethanol, 1M HCl and finally

in deionized water, 3 times in each solution treated with ultrasound to remove the unfastened particles. Through NHS-EDC chemistry, either FITC conjugated Anti-HSA or BSA (as control) were grafted onto the surface of the PPy-co-PPyCOOH particles. Briefly, the membranes were incubated in the solution containing 0.4M EDC and 0.1M NHS for 45 min to activate the carboxyl groups on PPy-co-PPyCOOH particles. Then the activated membranes were washed in PBS and incubated in either BSA (200 µg/ml) or Anti-HSA (200 µg/ml) solution for 1 h at room temperature. After, the protein grafted membranes were washed with PBS, 0.1% Triton 100-X, and PBS again, to remove the non-specifically absorbed proteins. After pre-treated in BSA (10 mg/ml) solution for 30 min, the protein grafted membranes were incubated in rhodamine conjugated HSA (20 µg/ml) solution for 1 h, washed and dried. The membranes were observed and photographed with an epifluorescence microscope (Axiophot, Zeiss, Oberkochen, Germany).

2.6.4.2 Morphology observation

The morphology of the particles and the particles coated membrane were observed with a scanning electron microscope (SEM, Model JSM-6360LV, JEOL, Japan) at an accelerating voltage of 20 kV. Prior to observation, the specimens were spatter-coated with gold in a sputter coater (Fisons Instruments Polaron SC500, UK). A transmission electron microscope (TEM, Model JEM-1230, JEOL) was further employed to identify the structure of the particles at 45 µA and an accelerating voltage of 80 kV. To prepare TEM specimens, diluted particle suspensions were treated with ultrasound for 10 min before being dropped on a sample grid and dried in air.

2.6.4.3 Chemical composition

The infrared spectra were recorded with a Nicolet Magna-IR 550 spectrophotometer (Nicolet Instrument, Madison, USA) in the ATR mode. The specimens were pressed against a silicon hemispherical ATR crystal and scanned 64 times between 500-4500 cm^{-1} at a resolution of 4 cm^{-1}. Spectrum processing was completed by using the software provided by the manufacturer.

The surface elemental composition of the particles was analyzed by using a Perkin Elmer PHI Model 5600 X-ray photoelectron spectrometer (XPS, Eden Prairie, USA). The high-resolution spectra were obtained via a standard magnesium source (1253.6 eV) and the surface elemental content was measured through survey scan using a monochromatic aluminum source at 1486.6 eV. The take-off angle was at 45°, with pass energy at 187.9 eV and 5.85 eV for the survey and high resolution scans respectively. Curve fitting of the high-resolution spectra was accomplished using the software provided by the manufacturer.

The total element analysis was performed using an element analyzer (Flash 2000, Thermo Scientific, USA). The mass of sample feeding was around 1 mg. The molar ratio of carbon to nitrogen (C/N) was calculated to display the percentage of the functional monomer units in the copolymer. Cystine was used as the reference.

2.6.4.4 Thermostability

The thermal degradation of the particles was measured with a TGA/SDTA 851e thermogravimetric analyzer (Mettler-Toledo, Mississauga, Ontario, Canada). Approximately 5 mg of samples was loaded into an alumina crucible pan and heated from 25 to 600 °C at a heating rate of 10 °C/min in the atmosphere of nitrogen flowing at 40 ml/min. The data were analyzed with the software provided by the manufacturer.

2.6.4.5 Conductivity measurement

The particles were mechanically pressed into pellets of 10 mm in diameter and approximately 1 mm in thickness. The surface resistance *R*s (Ω/□) of the specimens was measured with the Jandel Multi Height Four-Point Probe (Jandel Engineering Ltd., Linslade, Beds, UK) at room temperature. The radius of the needles of the probe was 100 μm and the space between the bordering needles was 1 mm. The surface electrical resistivity (ρ, Ω·cm) was calculated based on the formula (2.1) [27, 34] where Rs is the surface resistance, t is the sample thickness, f1 is the finite thickness correction and f2 is the finite width correction. Conductivity (σ, S/cm) was calculated as formula (2.2). The surface resistance of each pellet was measured 10 times; and

three pellets were fabricated for each sample. The thickness correction and width correction were obtained from the report of Smits [34].

$$\rho = Rs \times t = 4.5324 \times Rs \times t \times f1 \times f2 \quad (2.1)$$

$$\sigma = {}^{1}/_{\rho} \quad (2.2)$$

2.6.4.6 Statistical analysis

Data were reported as means ± standard deviations ($n \geqq 3$). A Student's t-test was adopted to analyze the statistical differences of the results with $p < 0.05$ considered statistically significant.

2.7 Acknowledgments

This work was supported by the Natural Sciences and Engineering Research Council of Canada (262258-2011), the Canadian Institutes of Health Research (MOP106555) and Le Centre de recherche du CHU de Québec. The first author acknowledges Les Bourses de la Fondation du CHU de Québec aux Étudiants. The technical assistance of Stéphane Turgeon, Pascale Chevalierare and Andrée-Anne Guay-Bégin is greatly appreciated.

Notes and references

1. Ramli RA, Laftah WA, Hashim S, Core–shell polymers: a review. *RSC Advances*. 2013, 3, (36): 15543-15565.

2. Chatterjee K, Sarkar S, Rao KJ, Paria S, Core/shell nanoparticles in biomedical applications. *Adv. Colloid Interface Sci.* 2014, 209: 8-39.

3. Xiong X-B, Falamarzian A, Garg SM, Lavasanifar A, Engineering of amphiphilic block copolymers for polymeric micellar drug and gene delivery. *J. Control. Release*. 2011, 155, (2): 248-261.

4. Ho KM, Li WY, Wong CH, Li P, Amphiphilic polymeric particles with core–shell nanostructures: emulsion-based syntheses and potential applications. *Colloid. Polym. Sci.* 2010, 288, (16-17): 1503-1523.

5. Li W-H, Stöver HD, Monodisperse cross-linked core-shell polymer microspheres by precipitation polymerization. *Macromolecules*. 2000, 33, (12): 4354-4360.

6. Li GL, Möhwald H, Shchukin DG, Precipitation polymerization for fabrication of complex core–shell hybrid particles and hollow structures. *Chem. Soc. Rev.* 2013, 42, (8): 3628-3646.

7. Ma J-Z, Liu Y-H, Bao Y, Liu J-L, Zhang J, Research advances in polymer emulsion based on "core–shell" structure particle design. *Adv. Colloid Interface Sci.* 2013, 197: 118-131.

8. Wei SY, Wang Q, Zhu JH, Sun LY, Lin HF, Guo ZH, Multifunctional composite core–shell nanoparticles. *Nanoscale*. 2011, 3, (11): 4474-4502.

9. Ravichandran R, Sundarrajan S, Venugopal JR, Mukherjee S, Ramakrishna S, Applications of conducting polymers and their issues in biomedical engineering. *J. Royal Soc. Interface.* 2010: S559–S579.

10. Guimard NK, Gomez N, Schmidt CE, Conducting polymers in biomedical engineering. *Prog. Polym. Sci.* 2007, 32, (8): 876-921.

11. Thompson DM, Koppes AN, Hardy JG, Schmidt CE, Electrical stimuli in the central nervous system microenvironment. *Annu. Rev. Biomed. Eng.* 2014, 16: 397-430.

12. Shi Y, Peng L, Ding Y, Zhao Y, Yu G, Nanostructured conductive polymers for advanced energy storage. *Chem. Soc. Rev.* 2015, 44, (19): 6684-6696.

13. Lee S-H, Bae J, Lee S, Jang J-W, Improvement of polypyrrole nanowire devices by plasmonic space charge generation: high photocurrent and wide spectral response by Ag nanoparticle decoration. *Nanoscale*. 2015, 7, (41): 17328-17337.

14. Jiang H, Zhang A, Sun Y, Ru X, Ge D, Shi W, Poly (1-(2-carboxyethyl) pyrrole)/polypyrrole composite nanowires for glucose biosensor. *Electrochim. Acta*. 2012, 70: 278-285.

15. Lee JS, Kim SG, Cho S, Jang J, Porous palladium coated conducting polymer nanoparticles for ultrasensitive hydrogen sensors. *Nanoscale*. 2015, 7, (48): 20665-20673.

16. Maeda S, Armes SP, Preparation and characterisation of novel polypyrrole–silica colloidal nanocomposites. *J. Mater. Chem.* 1994, 4, (6): 935-942.

17. Marini M, Pilati F, Pourabbas B, Smooth Surface Polypyrrole-Silica Core-Shell Nanoparticles: Preparation, Characterization and Properties. *Macromol. Chem. Phys.* 2008, 209, (13): 1374-1380.

18. Jang J, Oh JH, Fabrication of a highly transparent conductive thin film from polypyrrole/poly (methyl methacrylate) core/shell nanospheres. *Adv. Funct. Mater.* 2005, 15, (3): 494-502.

19. Huijs F, Lang J, Morphology and film formation of poly (butyl methacrylate)–polypyrrole core–shell latex particles. *Colloid. Polym. Sci.* 2000, 278, (8): 746-756.

20. Okner R, Domb AJ, Mandler D, Electrochemical formation and characterization of copolymers based on N-pyrrole derivatives. *Biomacromolecules*. 2007, 8, (9): 2928-2935.

21. Ahuja T, Mir IA, Kumar D, Biomolecular immobilization on conducting polymers for biosensing applications. *Biomaterials*. 2007, 28, (5): 791-805.

22. Maeda S, Corradi R, Armes SP, Synthesis and characterization of carboxylic acid-functionalized polypyrrole-silica microparticles. *Macromolecules*. 1995, 28, (8): 2905-2911.

23. Madani A, Nessark B, Brayner R, Elaissari H, Jouini M, Mangeney C, Chehimi MM, Carboxylic acid-functionalized, core–shell polystyrene@polypyrrole microspheres as platforms for the attachment of CdS nanoparticles. *Polymer*. 2010, 51, (13): 2825-2835.

24. Li W, Qiu T, Wang L, Ren S, Zhang J, He L, Li X, Preparation and electromagnetic properties of core/shell polystyrene@ polypyrrole@ nickel composite microspheres. *ACS Appl. Mater. Interfaces.* 2013, 5, (3): 883-891.

25. Azioune A, Ben Slimane A, Ait Hamou L, Pleuvy A, Chehimi MM, Perruchot C, Armes SP, Synthesis and characterization of active ester-functionalized polypyrrole-silica nanoparticles: application to the covalent attachment of proteins. *Langmuir*. 2004, 20, (8): 3350-3356.

26. Ko S, Jang J, Controlled amine functionalization on conducting polypyrrole nanotubes as effective transducers for volatile acetic acid. *Biomacromolecules*. 2007, 8, (1): 182-187.

27. Meng S, Zhang Z, Rouabhia M, Surfactant-templated crystalline polygon nanoparticles of heterocyclic polypyrrole prepared with Fenton's reagent. *Synth. Met.* 2010, 160, (1): 116-122.

28. Machida S, Miyata S, Techagumpuch A, Chemical synthesis of highly electrically conductive polypyrrole. *Synth. Met.* 1989, 31, (3): 311-318.

29. Chen S, Shen W, Wu G, Chen D, Jiang M, A new approach to the functionalization of single-walled carbon nanotubes with both alkyl and carboxyl groups. *Chem. Phys. Lett.* 2005, 402, (4): 312-317.

30. Shimomura M, Miyata R, Kuwahara T, Oshima K, Miyauchi S, Immobilization of glucose oxidase on the films prepared by electrochemical copolymerization of pyrrole and 1-(2-carboxyethyl) pyrrole for glucose sensing. *Eur. Polym. J.* 2007, 43, (2): 388-394.

31. Lee J-W, Serna F, Nickels J, Schmidt CE, Carboxylic acid-functionalized conductive polypyrrole as a bioactive platform for cell adhesion. *Biomacromolecules*. 2006, 7, (6): 1692-1695.

32. Truong LT, Chikae M, Ukita Y, Takamura Y, Labelless impedance immunosensor based on polypyrrole–pyrolecarboxylic acid copolymer for hCG detection. *Talanta*. 2011, 85, (5): 2576-2580.

33. Shi G, Rouabhia M, Meng S, Zhang Z, Electrical stimulation enhances viability of human cutaneous fibroblasts on conductive biodegradable substrates. *J. Biomed. Mater. Res. A.* 2008, 84, (4): 1026-1037.

34. Smits F, Measurement of sheet resistivities with the four-point probe. *Bell Syst. Tech. J.* 1958, 37, (3): 711-718.

Supporting information for

One-Step Reactivity-Driven Synthesis of Core-Shell Structured Electrically Conducting Particles for Biomedical application

Jifu Mao and Ze Zhang*

a. Centre de recherche du CHU de Québec, Département de chirurgie, Faculté de médecine, Université Laval, Québec (QC), CanadaAddress here.

b. Centre de recherche Hôpital Saint-François d'Assise, CHU, 10 rue de l'Espinay, Local E00-177, Québec (QC), G1L 3L5, Canada.

E-mail: Ze.Zhang@chg.ulaval.ca

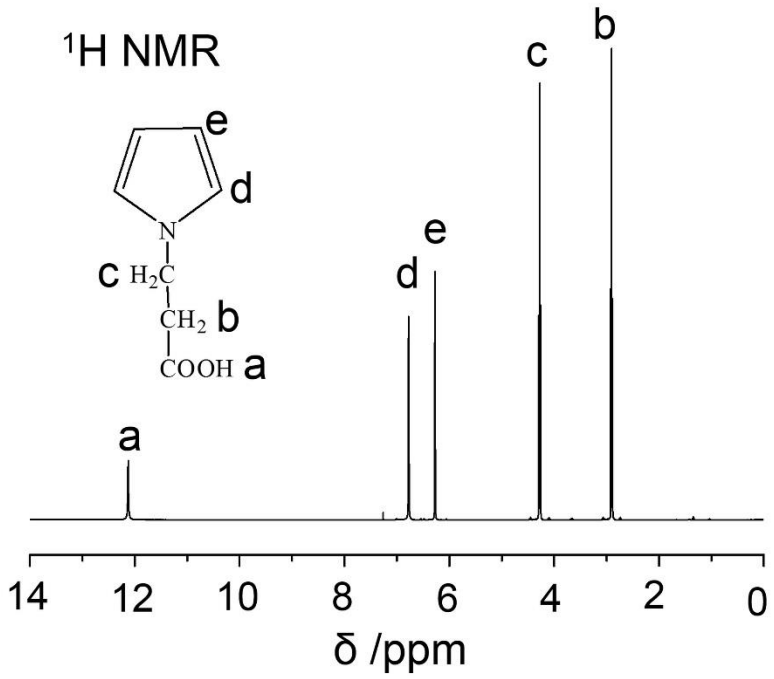

Figure S2.1 ^{1}H NMR (400 MHz, CDCl3) result of 1-(2-Carboxyethyl)pyrrole.

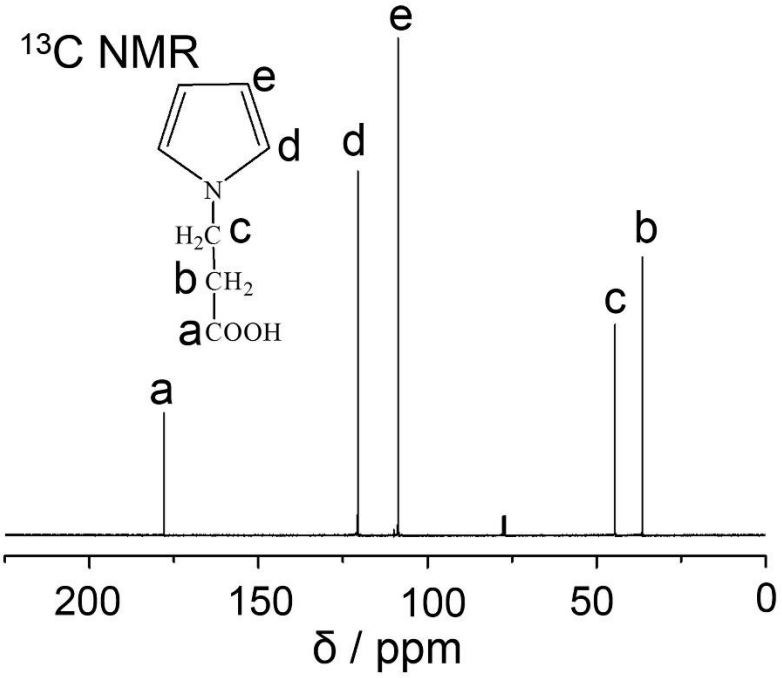

Figure S2.2 ^{13}C NMR (100 MHz, CDCl3) result of 1-(2-Carboxyethyl)pyrrole.

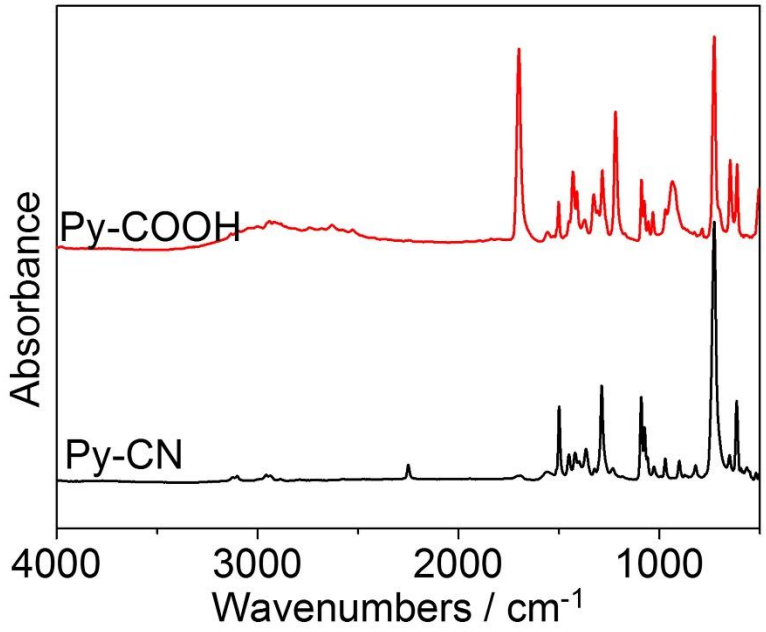

Figure S2.3 FTIR spectra of 1-(2-Carboxyethyl)pyrrole and 1-(2-cyanoethyl)pyrrole.

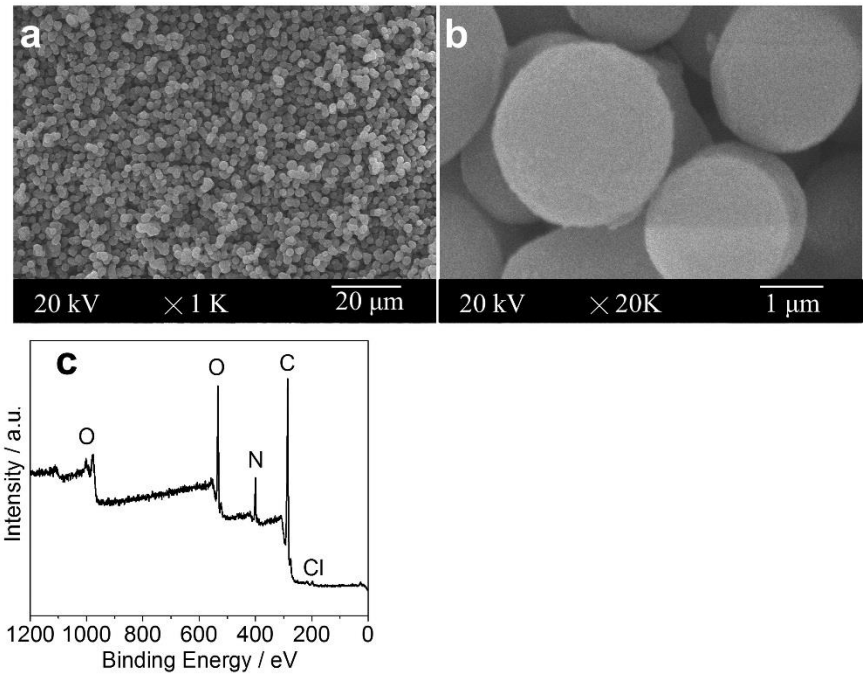

Figure S2.4 SEM photomicrographs and XPS spectra of PPy-COOH polymer obtained from filtrate of reaction for 12h: (A-B) SEM photos, (C) Full XPS spectra.

CHAPTER III

OPTIMIZATION OF PARAMETERS FOR SYNTHESIS OF POLY(PYRROLE-CO-(1-(2-CARBOXYETHYL) PYRROLE)) CORE-SHELL PARTICLES

Conductive Poly(pyrrole-co-(1-(2-carboxyethyl)pyrrole)) Core-shell Particles：Synthesis, Characterization, and Optimization

Jifu Mao and Ze Zhang*

a. Département de chirurgie, Faculté de médecine, Université Laval, Québec (QC), G1V 0A6, Canada.
b. L'Axe médecine régénératrice, Centre de recherche du CHU de Québec (QC), G1L 3L5, Canada.

jeff.mao.33@gmail.com；Ze.Zhang@chg.ulaval.ca

Correspondence: Ze.Zhang@chg.ulaval.ca；Tel. : (418) 525-4416；Fax. : (418) 525-4372

Keywords: poly(pyrrole-co-(1-(2-carboxyethyl)pyrrole)); core-shell structure; conductive particles; emulsion polymerization; synthesis parameters.

Polymer 2016,105,113-123 DOI: 10.1016/j.polymer.2016.10.022

3.1 Résumé

Le copolymère de poly (pyrrole-co-(1-(2-carboxyéthyl) pyrrole)) (P(Py-PyCOOH)) a suscité de très grands intérêts de recherche dans le domaine biomédical. Cependant, la plupart des P(Py-PyCOOH) sont synthétisés par électropolymérisation avec de faibles rendements. Dans ce travail, les particules en P(Py-PyCOOH) ont été synthétisées par polymérisation en émulsion en une étape. Les paramètres expérimentaux incluant le rapport eau/huile, l'alimentation en FeCl3 et les monomères fonctionnels, et le temps de réaction ont été évalués pour définir les conditions expérimentales optimales. Les particules présentent une structure cœur-coquille comprenant le copolymère P(Py-PyCOOH) dominé par le pyrrole (Py) comme noyau et le PPyCOOH comme coquille. Les particules possèdent une bonne conductivité ($>10^{-3}$ S cm^{-1}), une fonctionnalité de surface maximisée, une grande surface, une excellente dispersibilité dans l'eau et un rendement global élevé. De telles particules conductrices peuvent permettre d'anticiper des applications de détection et des applications biomédicales.

3.2 Abstract

Functional conductive polymers such as poly(pyrrole-co-(1-(2-carboxyethyl)pyrrole)) (P(Py-PyCOOH)) copolymer has raised significant research interests in biomedical field for their electrical conductivity, biocompatibility, and functionality that facilitates further biological modifications. However, most P(Py-PyCOOH) polymers are synthesized through electropolymerization with small sample size and low productivity. In this work, the core-shell P(Py-PyCOOH) particles were synthesized through a simple one step emulsion polymerization. Experimental parameters including the ratio of water/oil, feeding of $FeCl_3$ and functional monomers, as well as reaction time were evaluated to define the balanced optimal conditions. The obtained P(Py-PyCOOH) particles were characterized by scanning electron microscopy (SEM), transmission electron microscopy (TEM), X-ray photoelectron spectroscopy (XPS), Fourier transform infrared spectroscopy (FTIR), thermogravimetric analysis (TGA) and total elements analysis. The particles present a core-shell structure comprising the pyrrole (Py) dominated P(Py-PyCOOH) copolymer as the core and PPyCOOH homopolymer as the shell. Given the composition of the shell, the quantity of carboxyl groups on particle surface already reached maximum; further polymerization of excessive functional monomers would not increase any surface functionality but decrease conductivity of the particles. To conclude, the core-shell P(Py-PyCOOH) particles possess a good conductivity ($>10^{-3}$ S cm^{-1}), maximized surface functionality, large surface area, excellent dispersibility in water, and high overall yield. Such conductive particles can be good candidate for sensing and biomedical applications.

3.3 Introduction

Polypyrrole (PPy) has been extensively investigated for biomedical applications such as in tissue engineering, neural prostheses and biosensors, due to the combination of its properties of low cost, easy synthesis, inherent electrical conductivity and ionic activity, chemical and environmental stability, and biocompatibility [1-4]. However, the lack of functional site as well as the low bioactivity have seriously limited its applications. In order to functionalize PPy, various methods have been adopted including physical adsorption of biomolecules [5], doping of biomolecules [6], and copolymerization of pyrrole with its derivatives [7-11]. The copolymerization with pyrrole derivatives is probably the most promising approach thanks to the availability of various functional monomers. These functional monomers ensure a high reactivity and further modifiability of the polymer. Among the functional pyrrole monomers, N-functionalization provides a variety of functional groups and so has been widely used in biomedical research.

Specialized biomolecules had been immobilized onto PPy via physical adsorption, doping, or covalent grafting to construct the recognition centre of biosensors [12]. Understandably, covalent immobilization is the most reliable method to attach stable and active biomolecules to construct sensor recognition centre. 1-(2-carboxyethyl) pyrrole ($C_7H_9NO_2$, PyCOOH), the most prevalent N-substituted pyrrole monomer, was widely used to prepare P(Py-PyCOOH) to act as the substrate for biomolecule immobilization [13-15]. In particular, the carboxyl groups in P(Py-PyCOOH) can be further modified into active ester [11] and primary and secondary amine [9], showing great modifiability. Through covalent linkage, glucose oxidase was grafted onto PPy-COOH/PPy composite nanowires to increase the sensitivity and stability of the glucose sensors [13]. Similarly, an ethanol biosensor was constructed by grafting the alcohol dehydrogenase through amide linkages onto the surface of P(Py-PyCOOH) [16]. In addition, DNA and antibodies were also introduced to fabricate DNA biosensors [17] and immunosensors [18]. For such applications both high density of functional groups on surface and favourable conductivity are required. However, conductivity of the N-functionalized PPy is low. Thus, ideally, core-shell P(Py-PyCOOH) particles with pure PPy as the core and PyCOOH as the shell may solve this dilemma between reactivity and conductivity. The PPy

internal core would guarantee particle conductivity and the PPyCOOH shell would ensure surface functionality.

Noticeably, the morphology and property of a P(Py-PyCOOH) copolymer are inextricably linked to the method of synthesis. Though electropolymerization, the most commonly utilized approach for the synthesis of P(Py-PyCOOH) copolymers, has many advantages such as high conductivity, auto-doping, and controllable mass and thickness, it is also often associated with small size, low yield, high cost and the need for special equipment [3]. On the other hand, chemical polymerization has been frequently used to coat P(Py-PyCOOH) copolymer on template. For example, P(Py-PyCOOH) was coated onto silica microparticles to increase the stability of colloidal dispersions [19]. Similarly, polystyrene@P(Py-PyCOOH) [20] and polystyrene@P(Py-PyCOOH)@nickel [21] core-shell particles were fabricated to introduce functional groups on surface of the polystyrene particles. Moreover, P(Py-PyCOOH) was also coated onto the electrospun poly(lactide-co-glycolide) nanofibers to immobilize nerve growth factors for neural engineering applications [22]. Among these methods, a high feeding of PyCOOH in comonomers was normally attempted to increase the quantity of the carboxyl groups on surface, leading to the decline of conductivity. Although there are a few reports indicating that PPyCOOH homopolymer powder and microtubes could be obtained by chemical polymerization [23, 24], the conversion of monomers and the core-shell P(Py-PyCOOH) particles were seldom mentioned. In our previous work, core-shell P(Py-PyCOOH) particles without template were synthesized by a facile emulsion polymerization method, with a plausible mechanism proposed [25]. According to the proposed mechanism, it is inferred that the quantity of the carboxyl groups on particle surface will become saturated when the shell becomes formed by PyCOOH; that is, there exists an optimal limit of PyCOOH feeding above that any higher feeding of PyCOOH becomes meaningless. However, in that report the P(Py-PyCOOH) particles were synthesized using a single set of parameters except polymerization time. Whether the core-shell particles can be formed under other experimental conditions and how such conditions could be used to define particle properties remain unanswered. To answer those questions and to verify the hypothesis that there exists an optimal limit of PyCOOH feeding in terms of maximum surface

functional groups, this work systematically evaluated the impact of water/oil ratio, reaction time, and feeding of oxidant and functional monomer, on the property of the copolymer particles. The results demonstrate that it is unnecessary to excessively increase the feeding of functional monomers to maximize surface functional groups. It is also demonstrated that core-shell P(Py-PyCOOH) particles with tunable properties, e.g., surface chemistry and conductivity, can be obtained by selecting well defined experimental parameters. Preparation of functional polymers through copolymerization is a common approach widely used in polymer chemistry, polymer engineering and synthetic biomaterials. This work may help readers in these fields to appreciate how functional polymer particles could be synthesized in one step by considering the difference in monomer reactivity and carefully controlling experimental parameters.

3.4 Results and discussion

3.4.1 The feeding of oxidant

Pyrrole is vulnerable to oxidation and therefore can be easily polymerized owing to its low oxidation potential that is less than 0.8 V [26]. It was reported that when the mole ratio between Fe^{3+} and Py was 2.33 and in a short reaction time and at low temperature, the highest conductivity of PPy could reach 220 S cm^{-1} [27]. Fe^{3+} was also utilized to synthesize P(Py-PyCOOH) copolymers; however no study reported about how the ratio of Fe^{3+}/PyCOOH would affect product property and yield. Due to the lower reactivity of PyCOOH (oxidation potential +1.2 V) compared to Py (+0.8 V) [13, 14], an elevated feeding of Fe^{3+} is naturally expected to initiate PyCOOH polymerization. In literature, the mole ratio of Fe^{3+}/PyCOOH was reportedly ranging from 1.4 to 4.0 without considering monomer conversion rate [20, 23, 24]. In this work, when Fe^{3+} increased from 35 mmol to 130 mmol (100 mL solution; $H_2O/CHCl_3$=30/70; Py/PyCOOH=50/50, 15 mmol; 24 h), morphology of the particles (around 300 nm in diameter) had not shown any appreciable change until Fe^{3+} reached 90 mmol and higher, when the flak-like structures formed by the aggregated nanoparticles as indicated by the arrows (Fig. 3.1E, 3.1F). The aggregation could be the result of emulsion instability as the consequence of a high Fe^{3+} concentration in the water

phase. Moreover, the particles formed at 130 mmol ferric salt were found smaller, i.e., ca. 200 nm (Fig. 3.1F, insert).

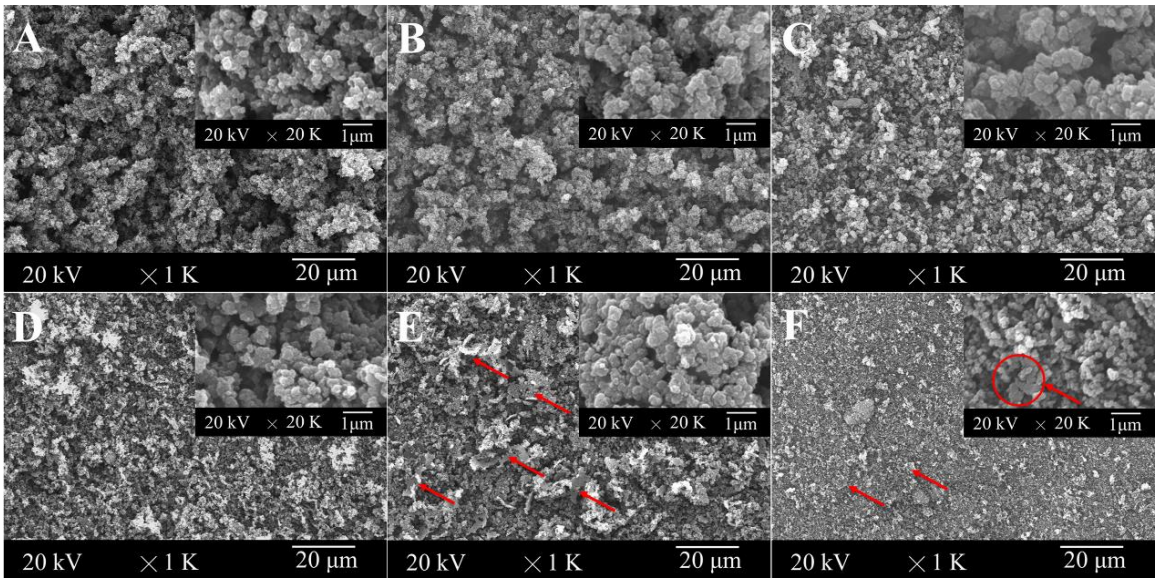

Figure 3.1 SEM photomicrographs of P(Py-PyCOOH$_{50}$) copolymers synthesized with different feedings of Fe^{3+} (100 mL solution; Py/PyCOOH=50/50, 15 mmol; $H_2O/CHCl_3$= 30/70; reaction for 24 h): (A) 35 mmol; (B) 50 mmol; (C) 70 mmol; (D)80 mmol; (E) 90 mmol ; (F) 130 mmol.

Pyrrole is vulnerable to oxidation and therefore can be easily polymerized owing to its low oxidation potential that is less than 0.8 V [26]. It was reported that when the mole ratio between Fe^{3+} and Py was 2.33 and in a short reaction time and at low temperature, the highest conductivity of PPy could reach 220 S cm^{-1} [27]. Fe^{3+} was also utilized to synthesize P(Py-PyCOOH) copolymers; however no study reported about how the ratio of Fe^{3+}/PyCOOH would affect product property and yield. Due to the lower reactivity of PyCOOH (oxidation potential +1.2 V) compared to Py (+0.8 V) [13, 14], an elevated feeding of Fe^{3+} is naturally expected to initiate PyCOOH polymerization. In literature, the mole ratio of Fe^{3+}/PyCOOH was reportedly ranging from 1.4 to 4.0 without considering monomer conversion rate [20, 23, 24]. In this work, when Fe^{3+} increased from 35 mmol to 130 mmol (100 mL solution; $H_2O/CHCl_3$=30/70; Py/PyCOOH=50/50, 15 mmol; 24 h), morphology of the particles (around 300 nm in diameter) had not shown any appreciable change until Fe^{3+} reached 90 mmol and higher, when the flak-like structures formed by the aggregated nanoparticles as indicated by the arrows (Fig. 3.1E, 3.1F). The aggregation could be the result of

emulsion instability as the consequence of a high Fe^{3+} concentration in the water phase. Moreover, the particles formed at 130 mmol ferric salt were found smaller, i.e., ca. 200 nm (Fig. 3.1F, insert).

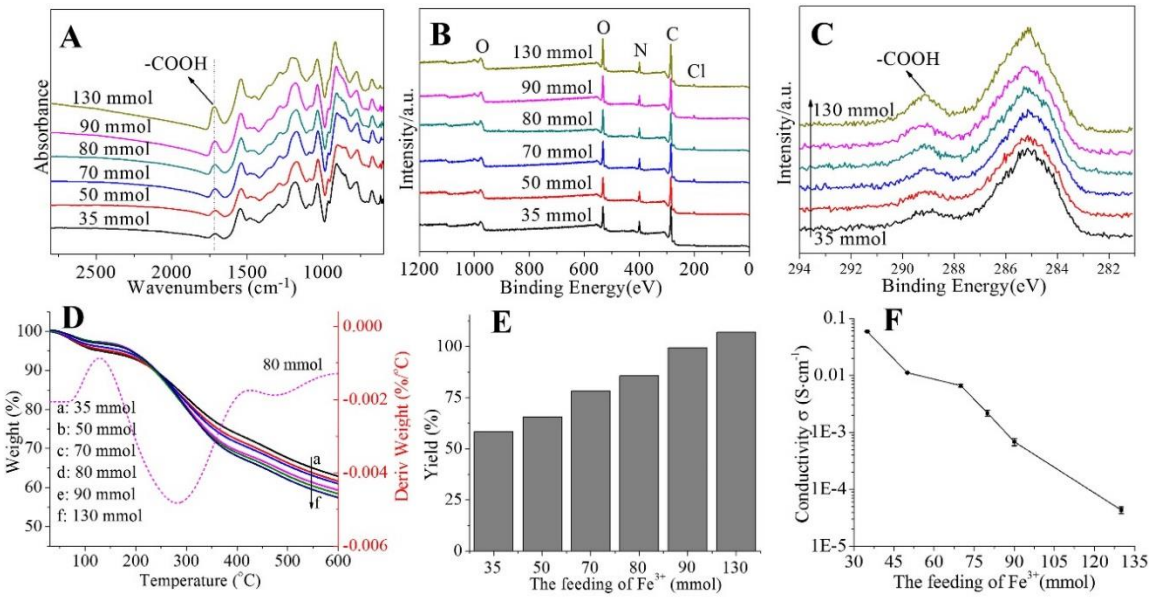

Figure 3.2 Properties of the P(Py-PyCOOH$_{50}$) copolymers synthesized with different feedings of Fe^{3+} (100 mL solution; Py/PyCOOH=50/50, 15 mmol; $H_2O/CHCl_3$= 30/70; reaction for 24 h). (A): FTIR spectra; (B): Full XPS spectra; (C): C_{1S} core level spectra; (D): TGA thermograms; (E): The overall yield; and (I): Surface conductivity.

Though no significant morphological difference was observed with respect to the different feedings of Fe^{3+} except for the smaller size at 130 mmol, both FTIR and XPS spectra revealed remarkable distinction on surface chemistry of the particles. The FTIR spectra of the polymers (Fig. 3.2A) show the characteristic C=O stretching vibration at 1715 cm^{-1}, of which the growing intensity demonstrates the increasing quantity of carboxyl groups in the particles. The bands at 1545 cm^{-1}, 1454 cm^{-1}, 1295 cm^{-1} and 1190 cm^{-1} are ascribed to the C=C double bond stretching in aromatic ring, C-N stretching, =CH- in-plane vibration and vibration of the pyrrole ring, respectively [28]. The full spectra of XPS show that oxygen element increased from 17.8% to 21.3% (Fig. 3.2B). In further analyses of the high resolution spectra of carbons (C_{1s}), a distinct peak (288.9 eV) appeared at the high binding energy side of the C-C-C, ascribed to OC=O. Both the increase in O_{1s} content and the peak area at 288.9 eV (Fig.

3.2C) indicate the increasing quantity of carboxyl groups on particle surface, confirming the results of FTIR.

Fig. 3.2D shows three regions in thermograms: the first stage between 40 and140 ˚C corresponding to the loss of absorbed water, the second region between 140 and 430 ˚C revealing the loss of the propionic acid groups [29], and the weight loss after 430 ˚C designated to the thermal degradation of the polymeric backbone and the removal of the DBS dopants. The steeper slop of the thermograms of higher oxidant feeding in the second region also suggests the growing PyCOOH units in copolymers along with the increasing dose of Fe^{3+}. Fig. 3.2E show that the overall yield raised from 58.4% to 104.5% corresponding with the increase of oxidant. The increase of carboxyl groups in the particles reflected the growing number of PyCOOH units according to the FTIR, XPS and TGA results, demonstrating that a high oxidant concentration is needed to incorporate more PyCOOH monomers.

Conductivity of the P(Py-PyCOOH) particles was found decrease exponentially with Fe^{3+} feeding, ranging from 0.06 S cm^{-1} to 4.34×10^{-5} S cm^{-1}, as showed in Fig. 3.2F. The conductivity of the P(Py-PyCOOH) copolymers synthesized by electropolymerization with different ratios of PyCOOH was in the range of 10^{-8}-10^{-3} S cm^{-1}, 10^5 times lower than that of PPy [30]. In literature, the PPyCOOH powder prepared by chemical polymerization reported a conductivity of about 10^{-4} S cm^{-1} [24]; and the P(Py-PyCOOH) coated silica microparticles presented an even lower conductivity (<10^{-6} S cm^{-1}) [19]. The low conductivity of P(Py-PyCOOH) has been attributed to the PyCOOH component that disrupts the planarity and π-π electron conjugation [24]. Again, in these literatures the percentage and surface distribution of PyCOOH in the copolymers were not reported. In this work we found that a high feeding of Fe^{3+} is one of the effective means to polymerize PyCOOH; this however also leads to the exponential decline of conductivity. Taking into account the conductivity (> 10^{-3} S cm^{-1}), yield (> 85%) and particle morphology (no flak), a feeding of Fe^{3+} at 80 mmol (Fe^{3+}/monomers= 5.3) is considered the most appropriate in this work.

3.4.2 The solvent systems

Emulsion polymerization, a common chemical synthesis method of PPy, comprises two phases, i.e., water phase and oil phase. According to the ratio of water and oil, the solvent system can be generally divided into W/O (water in oil, oil forms the continuous phase and water is the dispersed phase) emulsion system and O/W (oil-in-water) emulsion system. The W/O (water/chloroform; 3:7; v/v) emulsion system using DBS as emulsifier is a typical design to synthesize PPy powder [31]. However, in literature there is very few report about preparing P(Py-PyCOOH) copolymer by emulsion polymerization [25]. Since the optimal ratio of W/O for P(Py-PyCOOH) synthesis had been unknown, a solvent system similar to that used for PPy synthesis was employed in this work, with variations in W/O ratio. Figs. 3.3A-3.3D show the effect of W/O ratio on the morphology of the P(Py-$PyCOOH_{50}$) (100 mL solution, 80 mmol Fe^{3+}, Py/Py-COOH=50/50, 24 h) particles. The particle size appeared increasing with the addition of water. When water phase reached 40% the dispersion of the nanoparticles became significantly deteriorated. At same time the overall yield fell from 109.1% to 76.0% (Fig. 3.3I) and conductivity increased from 10^{-4} to 10^{-2} S cm^{-1} (Fig. 3.3H). There are two main reasons to explain these phenomena: the size of the droplets and the concentration of oxidant. At the same stirring speed the size of the water droplets became smaller when the ratio of water was lower, together with a higher oxidant concentration in the droplets. On the other hand, with a constant feeding of $FeCl_3$, the concentration of Fe^{3+} in water droplets was diluted correspondingly from 4.0 M to 2.0 M when the amount of water increased from 20% to 40%. A high Fe^{3+} concentration was expected and indeed promoted the formation of cation radical monomers, PyCOOH radicals in particular, and accelerated polymerization, which agrees with the analyses of FTIR, XPS and four point probe. The peak intensity at 1715 cm^{-1}, characteristic of C=O stretching, recorded the increasing carboxyl groups in the particles along with the decrease of water (Fig. 3.3E). At same time, no significant change could be observed concerning either the oxygen content (Fig. 3.3F) or the percentage of COOH (O<u>C</u>=O) on particle surface (Fig. 3.3G). These results confirm the increase of PyCOOH in the particles with the decrease of water phase. As mentioned above, PyCOOH units tend to reduce

copolymer conductivity. So the falling conductivity also supports the high degree of PyCOOH incorporation as consequence of the raise in oxidant concentration in water droplets. A 25% water system should be recommended because of the preferable morphology, dispersion and conductivity.

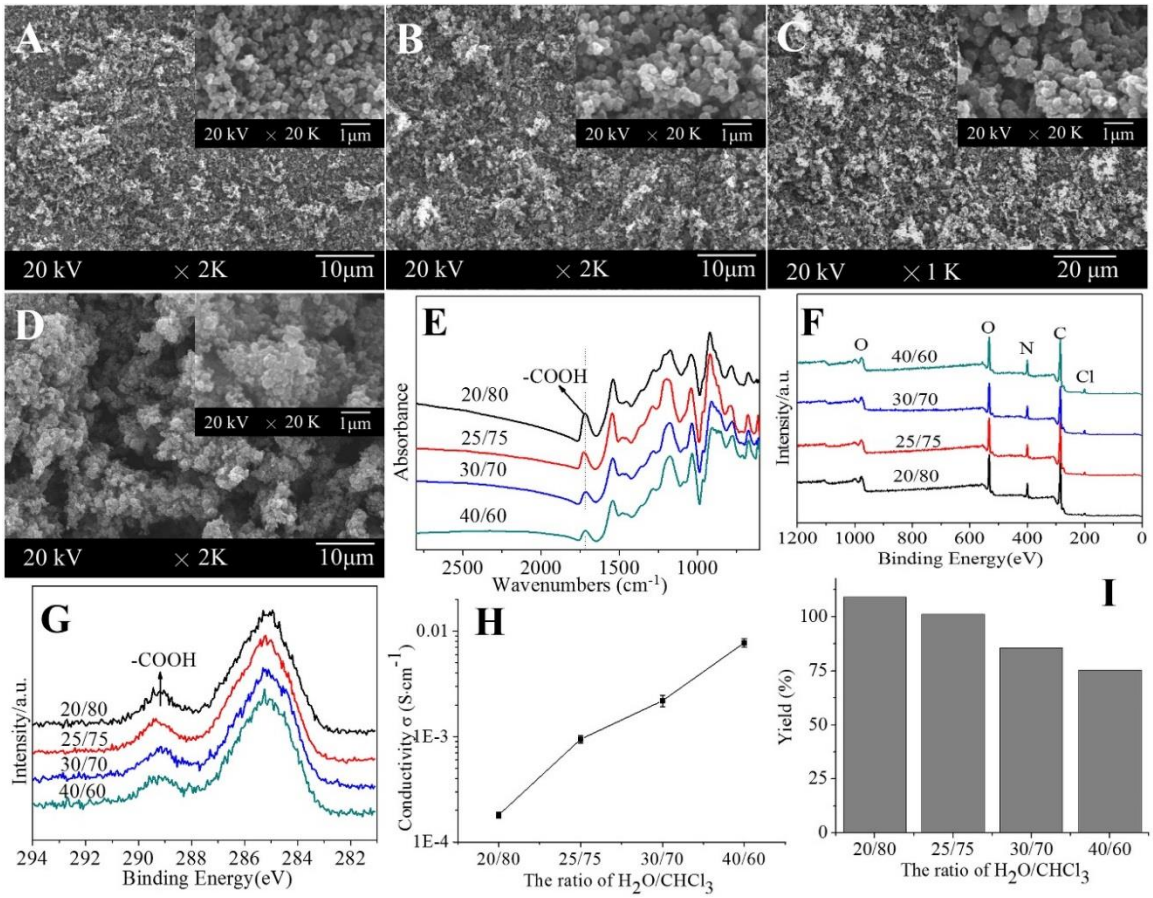

Figure 3.3 Effect of W/O ratio on copolymer properties (100 mL solution; 80 mmol Fe^{3+}; Py/PyCOOH=50/50, 15 mmol; reaction for 24 h): (A-D) SEM photos: (A) 20/80; (B) 25/75; (C) 30/70; (D) 40/60; (E) FTIR spectra; (F) Full XPS spectra; (G) C_{1S} core level spectra; (H) Conductivity; and (I) Overall yield.

3.4.3 The reaction time

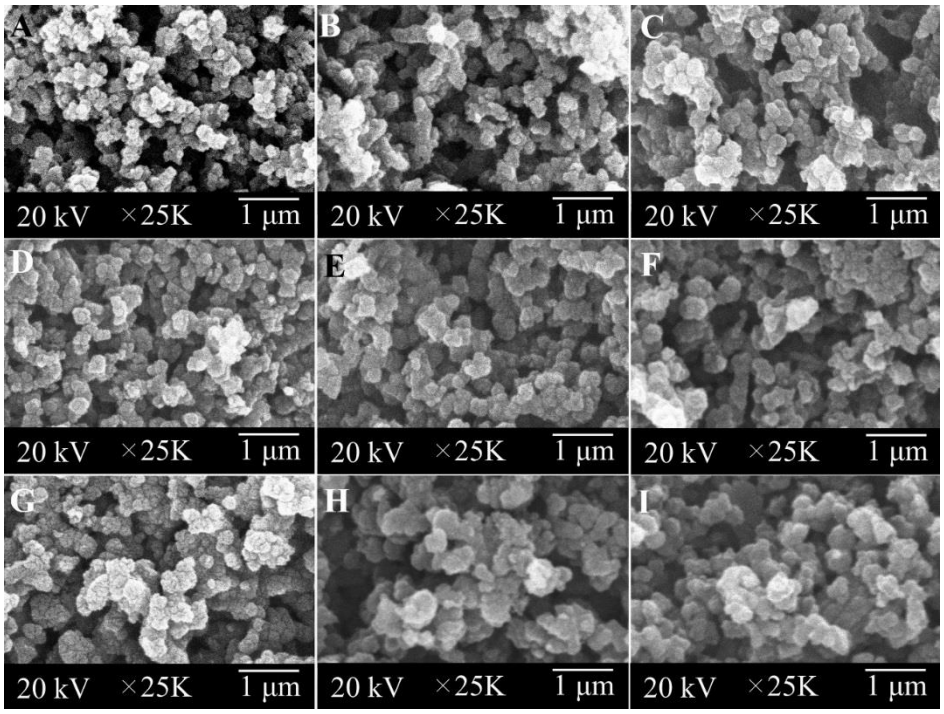

Figure 3.4 SEM photomicrographs of P(Py-PyCOOH$_{50}$) particles synthesized in different reaction times from 10 min to 24 h (100 mL solution; 80 mmol Fe^{3+}; Py/PyCOOH=50/50, 15 mmol; $H_2O/CHCl_3$= 25/75): (A) 10 min, (B) 20 min, (C) 40 min, (D)1 h, (E) 1.5 h , (F)6 h, (G) 12 h, (H) 18 h, and (I) 24 h.

In our previous report, the dynamic growth of the PPy molecules was investigated, as well as the formation of the core-shell P(Py-PyCOOH$_{50}$) particles [25, 32]. In this work, the morphology and properties of the P(Py-PyCOOH50) particles related to reaction times were studied in detail to define the optimum parameters. As shown in Fig. 3.4, all particles were 200-300 nm in diameter, showing a remarkable increase in the first 1.5 hour. After that, no further appreciable morphological alteration observed. The FTIR results however recorded a continuous increase in carboxyl groups from 10 min to 24 h (Fig. 3.5A). In comparison, the content of oxygen on polymer surface remarkably increased from 8.2% to 19.3% in the first 3 h, along with the reduction of C, N and Cl elements (Fig. 3.5B). Thereafter, however, all the elements on surface, as well as the high resolution spectra of carbon (C_{1s}) and oxygen (O_{1s}), remained unchanged with reaction time, as summarized in Table 3.1. The spectra of C_{1s} were curve-fitted into three components [32]: the first peak at 284.6 eV assigned to the β-carbons in pyrrole ring (C-C-N) and the saturated carbons in PyCOOH unit, the second

peak at 285.9 eV belonged to the α-carbons (C-C-N) and the carbons with single oxygen bond (-C-O-), and the third peak at 288.9 eV ascribed to OC=O. Therefore, the ratio of OC=O in C1s and the percentage of O_{1s} can be used to evaluate the quantity of carboxyl groups on surface, which increased dramatically in the first hour and then was ever-increasing but insignificant until the reaction time reached to 3 hours. Yet, the yield and conductivity offer strong support to the FTIR results. With the reaction time increased from 10 min to 24 h, the yield rose from 30.5% to 101.3%; and the conductivity declined from 10^0 to 10^{-4} S·cm^{-1} (Table 3.1), indicating that the PyCOOH units were incorporated continuously. Considering the size of the particles (200 - 300 nm) and the sampling depth of XPS (ca. 10 nm), only XPS is reliable to characterize the particle surface chemical composition, while FTIR and conductivity are more inclined toreflect the bulk properties. Therefore, the little changed XPS data after 3 h and the ever evolving other properties reflect the chemically inhomogeneous bulk and surface of the P(Py-PyCOOH) particles.

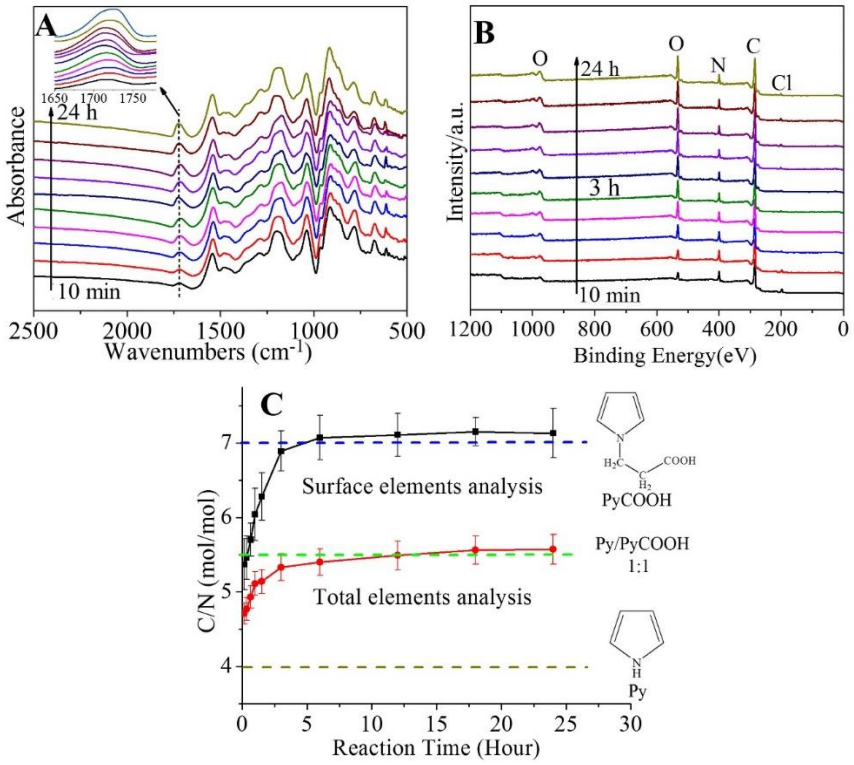

Figure 3.5 FTIR spectra (A), XPS spectra (B), and elements analyses (C) of the P(Py-$PyCOOH_{50}$) copolymers synthesized in different reaction times from 10 min to 24 h (100 mL solution; 80 mmol Fe^{3+}; Py/PyCOOH=50/50, 15 mmol; $H_2O/CHCl_3$= 25/75). The dash lines in C represent the theoretical values of the corresponding structures.

Table 3.1 Surface chemical composition, conductivity, and the yield of the P(Py-PyCOOH$_{50}$) particles in different reaction time

Reaction time	C=O/C$_{1s}$ %	Conductivity S·cm^{-1}	Yield %
10 min	9.9 ± 1.3	3.3 ± 0.3	30.5
20 min	11.7 ± 1.0	2.5 ± 0.1	46.3
40 min	13.0 ± 1.3	(5.9 ± 0.2)×10^{-1}	59.4
1 h	15.3 ± 0.9	(1.3 ± 0.1)×10^{-1}	66.6
1.5 h	16.1 ± 1.5	(5.3 ± 0.3)×10^{-2}	74.7
3 h	16.6 ± 1.1	(1.8 ± 0.1)×10^{-2}	81.2
6 h	16.9 ± 2.4	(8.1 ± 0.5)×10^{-3}	87.3
12 h	17.4 ± 1.7	(3.3 ± 0.4)×10^{-3}	92.2
18 h	17.3 ± 1.2	(1.0 ± 0.1)×10^{-3}	96.9
24 h	17.6 ± 2.2	(9.4 ± 0.7)×10^{-4}	101.3

The ratio of C/N based on XPS survey scan and total elemental analysis was employed to evaluate the dynamic incorporation of PyCOOH into the P(Py-PyCOOH$_{50}$) copolymers. XPS results indicate that the ratio of C/N was around 7.1 when the reaction time was longer than 3 h, similar to that of the PyCOOH monomers (Fig. 3.5C); alternatively, the total elemental analysis demonstrated that with the increasing reaction time the ratio of C/N gradually increased from 4.7 to 5.6, and finally approached to 5.5, i.e., the theoretical value of P(Py-PyCOOH$_{50}$), as shown in Fig. 3.5C. It means that it was the P(Py-PyCOOH) copolymer rich in Py segments rather than the PPy homopolymer that was formed in the initial stage of the polymerization. Afterwards, more PyCOOH was incorporated and finally the PPy-COOH homopolymer formed on particle surface. TEM revealed more details on the structure of the particles, as shown in Fig. 3.6. The images show that a framework or core was formed by the aggregation of the copolymer nanoparticles at the very beginning. Then

small nanoparticles (50 nm, arrows) progressively appeared at the edge of the framework, leading to an increase in the size of the framework, which confirmed the results of SEM. Ultimately, the framework was completely enclosed by the small nanoparticles to form the core-shell structure. Combining the results of chemical analyses, it is concluded that the small nanoparticles are made of the PPy-COOH homopolymer. We previously reported that Py monomers copolymerized with PyCOOH monomers and became completely consumed in 40 min [25]. Thereafter, PPy-COOH homopolymer was continuously generated by the remaining PyCOOH monomers and attached as a shell onto the existing particles. This work shows that reaction time is an effective controlling factor to regulate the surface and bulk chemistry, conductivity and the overall yield of P(Py-$PyCOOH_{50}$). By selecting reaction time, the core-shell P(Py-PyCOOH) particles with desired conductivity (from 10^{-3} S cm^{-1} to 3 S cm^{-1}) and chemical composition can be synthesized. Importantly, because it is the PPy-COOH homopolymer that is finally formed on particle surface, it is ineffective and unnecessary to further increase the feeding of functional monomers to raise surface functionality.

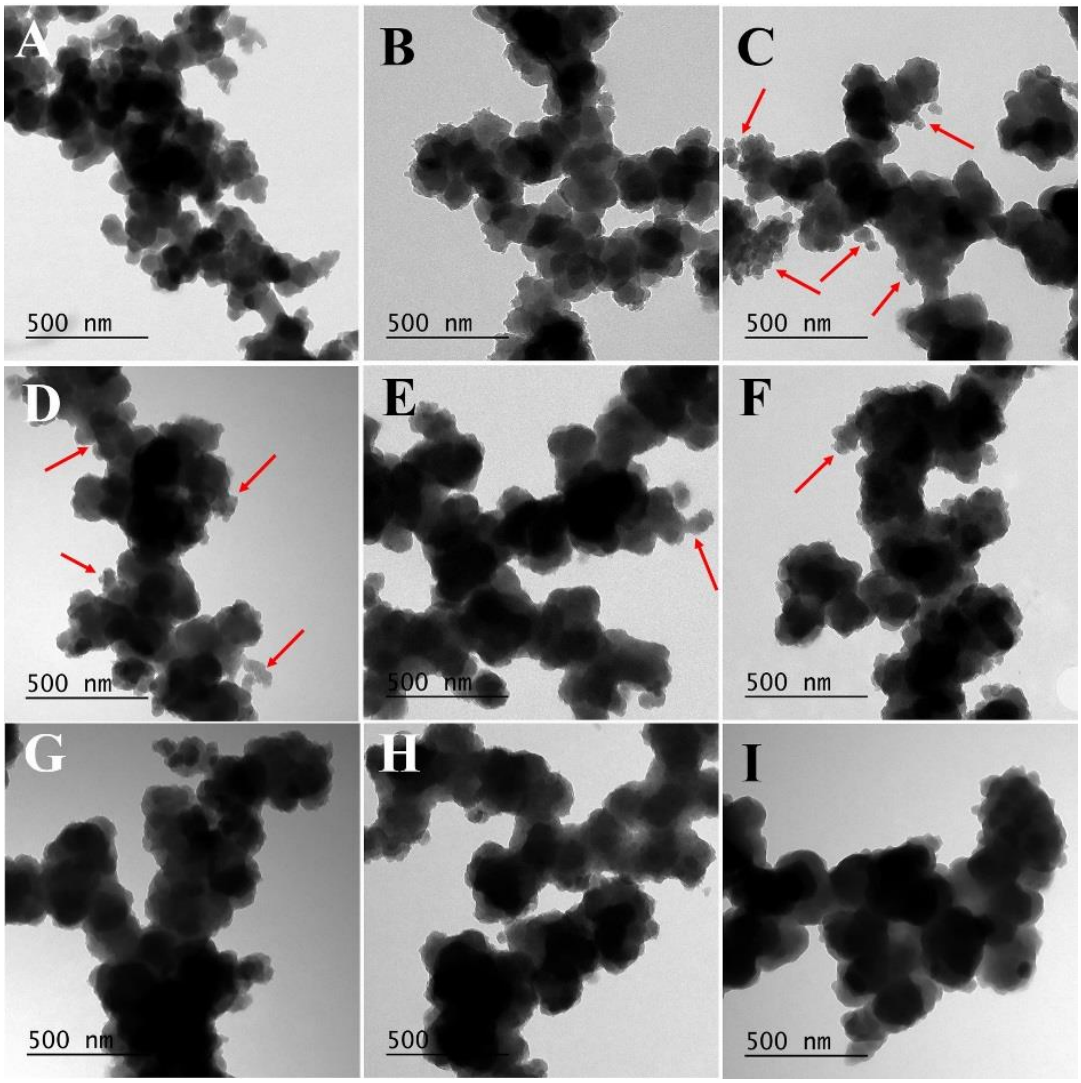

Figure 3.6 TEM photomicrographs of P(Py-PyCOOH$_{50}$) copolymers synthesized in different reaction times from 10 min to 24 h (100 mL solution; 80 mmol Fe^{3+}; Py/PyCOOH=50, 15 mmol; $H_2O/CHCl_3$= 25/75): (A) 10 min, (B) 20 min, (C) 40 min, (D)1 h, (E) 1.5 h , (F) 6 h, (G) 12 h, (H) 18 h, and (I) 24 h.

3.4.4 The ratio of Py/PyCOOH

The feeding of PyCOOH has been used as the single most important and an apparently very rational parameter to modulate the quantity of carboxyl groups on surface of the copolymer particles [33]. Madani attempted to copolymerize P(Py-PyCOOH) with different Py/PyCOOH feeding ratios onto polystyrene particles [20]. It was illustrated that the thickness and mass of the coating layer decreased with the increasing feeding ratio of PyCOOH. In particular, the ratio of Fe^{3+}/(Py+PyCOOH) in their work was 1.4, much lower than what we used. We found that the ratio of Fe^{3+}/(50%Py+50%PyCOOH) should be higher than 8.0 to achieve 100%

conversion of PyCOOH. Therefore the reduction in thickness and mass in Madani's work was likely the result of the low conversion of the PyCOOH monomers rather than the steric hindrance of carboxyl groups. As in previous discussion (Table 3.1, Fig. 3.5C), the COOH groups on particle surface will reach saturation at the moment when the PPyCOOH homopolymer forms, even if the PyCOOH feeding ratio is only 50%. After that point the density of the carboxyl groups on particle surface will not supposed to increase any more via raising the feeding of PyCOOH. To verify that, different feeding ratios of Py/PyCOOH were selected to synthesize the copolymers in the optimized emulsion system (100 mL; 80 mmol Fe^{3+}; $H_2O/CHCl_3$=25/75; 18 h).

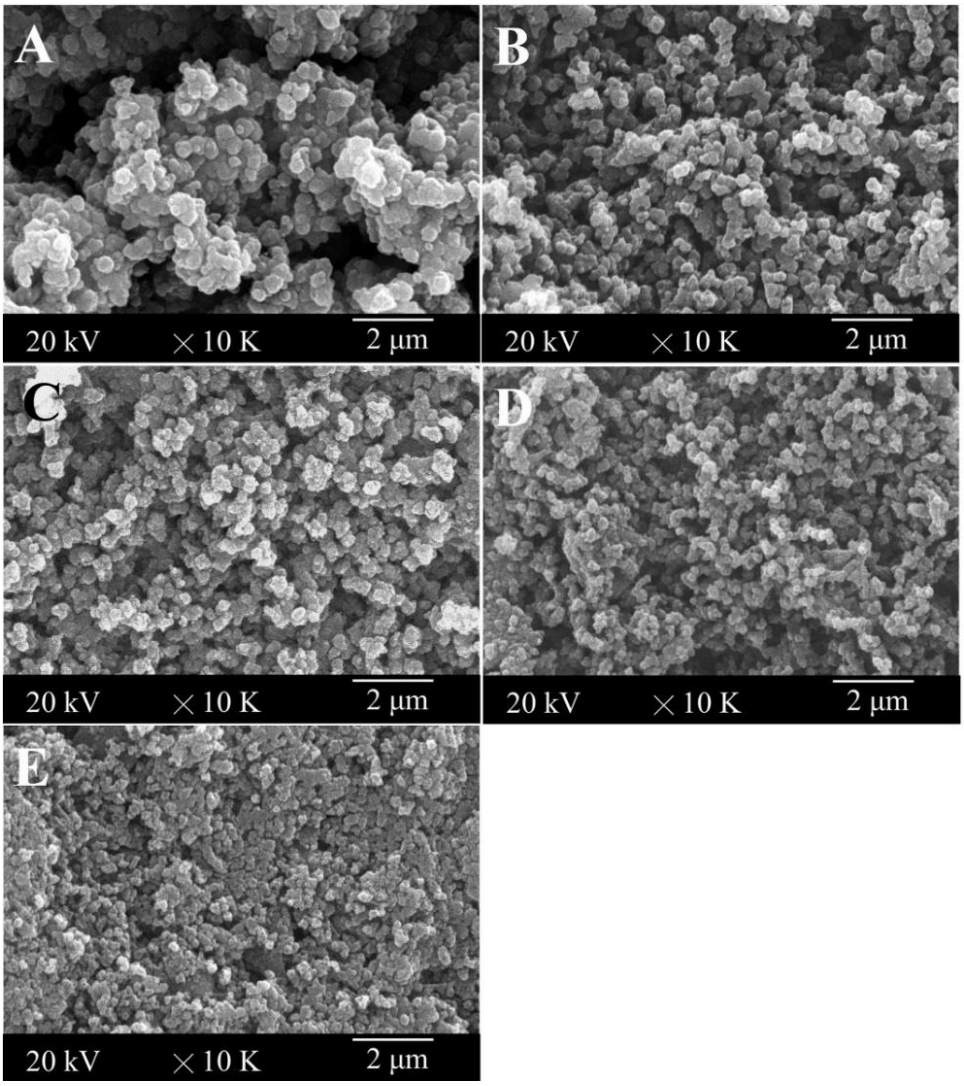

Figure 3.7 SEM photomicrographs of the P(Py-PyCOOH) polymers synthesized with different ratios of Py/PyCOOH (100 mL solution; 80 mmol Fe^{3+}; $H_2O/CHCl_3$= 25/75; 18 h): (A) 100:0, (B) 75:25, (C) 50:50, (D) 25:75, (E) 0:100.

Fig. 3.7 showed the morphology of the P(Py-PyCOOH) particles with different ratios of Py/PyCOOH from 100:0 to 0:100. All the particles are in nano-size, with the mean diameter decreased from 300 nm to 150 nm as the feeding of PyCOOH increased from 0 to 100%. The increasing polar COOH groups in water phase may have contributed to micelles stability, so smaller particle size. In FTIR spectra (Fig. 3.8A), the strength of C=O absorption at 1715 cm^{-1} sharply elevated with the increase of the PyCOOH monomer, showing the incorporation of PyCOOH into the particles. This is confirmed by TGA. The TGA results effectively showed a progressive deterioration in thermostability of the copolymers proportional to PyCOOH incorporation (Fig. 3.8B). In particular, DTGA analysis clearly showed the maximum weight loss at around 300˚C, originated from the decomposition of the propionic acid groups. In combination FTIR and TGA demonstrated the harmony between PyCOOH feeding and incorporation. Thus, increasing functional monomer feeding ratio will raise the percentage of PyCOOH in the product. Again, this is on the basis that the oxidant is sufficient enough to convert them. As expected, the survey scans of XPS (Fig. 3.8C) recorded a remarkable increase in oxygen content from 5.4% for the pure PPy to 19.9% for the P(Py-PyCOOH50), correlated very well with the theoretical content of oxygen in PyCOOH (2 oxygen in a total of 10 atoms, noting that hydrogen is not detectable by XPS). When the ratio of PyCOOH exceeded 50%, no more increase in oxygen and other elements was observed. The high resolution C_{1s} spectra of the P(Py-PyCOOH) polymers are shown in Fig. 3.8D. The percentage of O<u>C</u>=O in C_{1s} exhibited a similar tendency as the oxygen content, increasing from 6.2% in PPy to 13.8% in P(Py-$PyCOOH_{25}$) and finally stabilized around 17.5% in other copolymers. This directly confirms that it is impracticable to increase the quantity of carboxyl groups on copolymer particle surface through a feeding ratio higher than 50%. Therefore, taking into account the high cost of the PyCOOH, we consider 50% PyCOOH the most appropriate to prepare the P(Py-PyCOOH) particles.

Fig. 3.8F shows the relation between the conductivity of P(Py-PyCOOH) copolymers and the feeding ratio of Py/PyCOOH. The conductivity of PPy (100/0) is more than 10^5 times higher than that of the PPyCOOH homopolymers, which fairly accords with the P(Py-PyCOOH) copolymers synthesized through electropolymerization [30]. Also, the conductivity of the copolymers declines exponentially with the increase of PyCOOH. For intrinsically conductive polymers, the conductivity varies significantly depending on the nature of the

dopant and doping level [3]. Randomly oriented PPy chains are often planar; and the dopants are inserted in the interplane space [34]. Hence, the nature of the dopant, such as chemical properties and size, affects both the conductivity and the structure of the conductive polymers. Chlorine anions (Cl^-) are the most common dopant due to their auto-doping capability during synthesis [3]. Large molecules such as DBS, biomolecules and even polyanions are also incorporated as dopants because of their low diffusion coefficient and strong physical entanglement with conductive polymer chains [35]. It was reported that the introduction of PyCOOH component led to a decrease in the doping level of Cl^- because that the deprotonated carboxyl groups acted as co-dopant [20]. A similar decline of chlorine was also indicated in this work by the surface elemental analysis of XPS. The atomic percentage of Cl was: 4.1% for PPy, 1.4% for P(Py-PyCOOH50) and 1.0% for P(Py-PyCOOH$_{100}$). Lee et al. adopted the ratio of Cl/N to evaluate the doping degree, and reported a lower doping level of P(Py-PyCOOH) compared with PPy (4.9% vs. 23.9%) [24], which is in agreement with our results (9.6% for P(Py-PyCOOH$_{100}$), 14.6% for P(Py-PyCOOH$_{50}$), and 24.2% for PPy). TGA data shows that a certain amount of DBS was integrated into PPy and P(Py-PyCOOH) copolymers. As shown in Fig. 3.8B, the thermal decomposition temperature of DBS is around 450 ˚C in the atmosphere of nitrogen. A weight loss in this temperature range was found for PPy via DTGA analysis. In addition, the total elemental analysis also revealed the presence of sulfur that decrease from 1.1% in PPy to 0.3% in P(Py-PyCOOH$_{50}$). These data suggest that both the PPy and the P(Py-PyCOOH) copolymers were co-doped by Cl^- and DBS. The ratio of Cl/N therefore cannot reflect correctly the true doping level. Accordingly, in this paper, the ratio of the positively charged nitrogen (N_{1s}^+/N_{1s}) was used to evaluate the doping level. As shown in Fig. 3.8E, with the increase of the PyCOOH, the ratio of N_{1s}^+/N_{1s} decreased correspondingly. That is, the introduction of the PyCOOH component has adverse effect on the doping process in P(Py-PyCOOH) copolymers, which also explains the decrease of conductivity. At meantime, we suggest that the electrostatic repulsion between carboxylic ion and sulphonic acid ion may have reduced the integration of DBS in the P(Py-PyCOOH) copolymers. Consequently, for the P(Py-PyCOOH) copolymers, the effects of PyCOOH component on conductivity may include the disruption of the planarity and the π-π electron conjugation, low deprotonation of the N-derived pyrrole unites and the electrostatic repulsion between deprotonated hydroxyl groups and dopants.

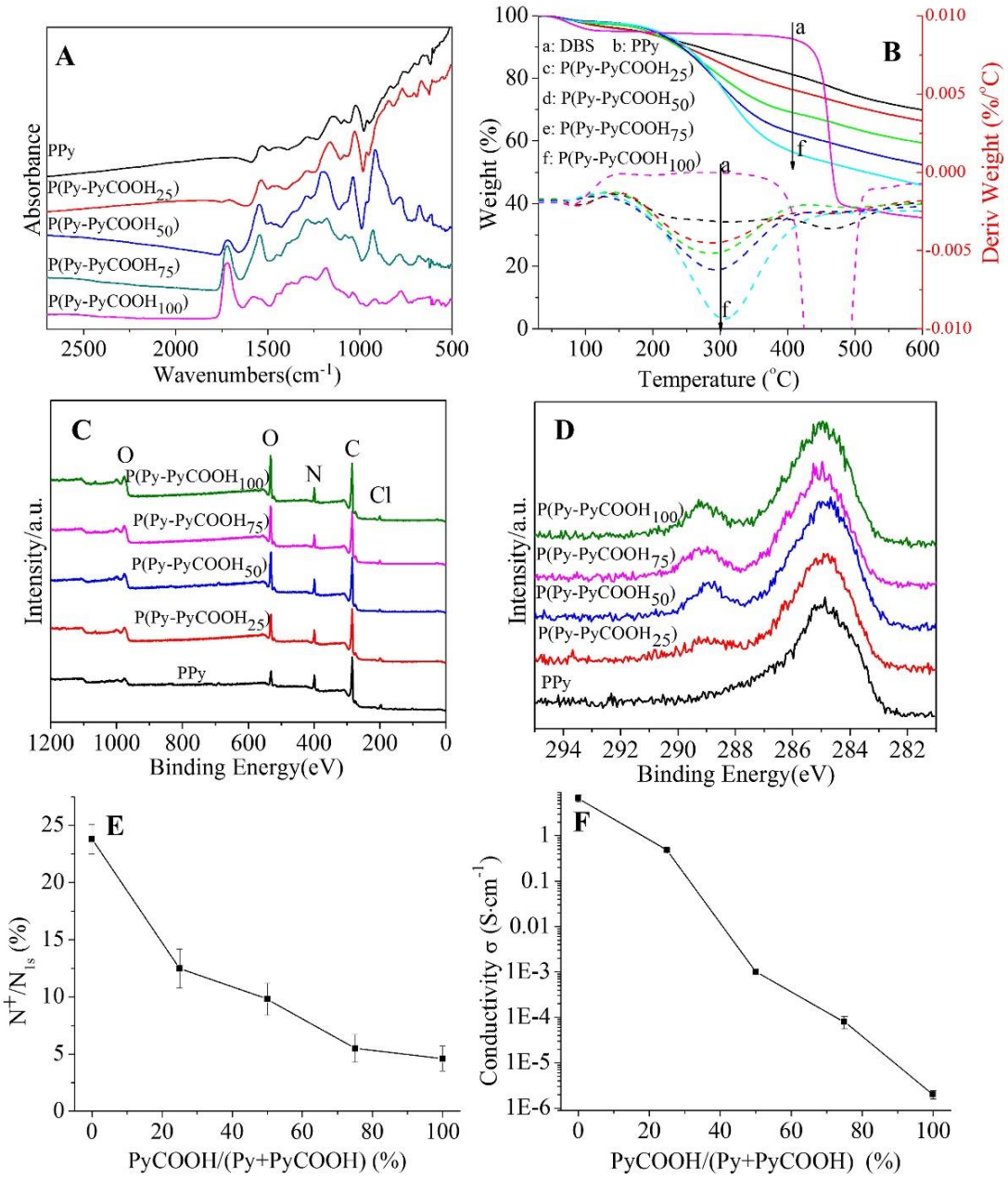

Figure 3.8 Properties of the P(Py-PyCOOH) particles synthesized with different ratios of Py/PyCOOH (100 mL solution; 80 mmol Fe^{3+}; $H_2O/CHCl_3$= 25/75; 18 h): (A) FTIR spectra, (B) TGA thermograms, (C) conductivity, (D) XPS survey scans, (E) C_{1s} core level spectra, and (F) ratio of N_{1s}^{+}/N_{1s} based on curve fitting of the N_{1s} core level spectra.

3.5 Experimental

3.5.1 Materials

Pyrrole (Py, 98%, Alfa Aesar, Ward Hill, MA, USA) was purified twice by reduced pressure distillation and was stored at 4 °C before use. 1-(2-cyanoethyl)pyrrole (PyCN, 98%, Sigma-

Aldrich， Oakville, Ontario, Canada), Iron (III) chloride hydrated ($FeCl_3 \cdot 6H_2O$, 97%, Laboratoire Mat, Quebec, QC, Canada), dodecylbenzenesulfonic acid sodium salt (DBS; Sigma-Aldrich) and other reagents (analytically grade) were used as purchased.

3.4.2 Synthesis of functional monomer

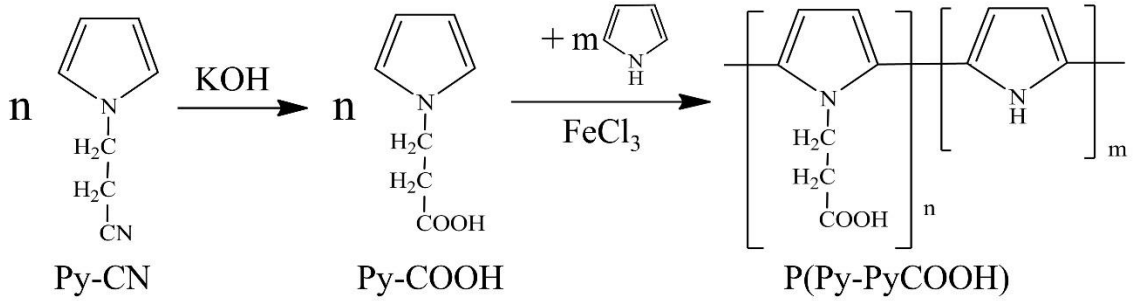

Figure 3.9 Chemical reaction scheme of the synthesis of P(Py-PyCOOH) copolymers.

1-(2-carboxyethyl)pyrrole (PyCOOH) was synthesized following the procedure described in literature showing in Fig. 3.9 [19]. Briefly, PyCN (24 mL) was slowly added into 120 mL of 6.7 M KOH and refluxed under N_2 protection until no more NH_3 generated. After cooling and acidification, the obtained solution was extracted with ether for 5 times, 6 hours each time. After vacuum-rotary evaporation of ether, the crude yellow product was purified twice by recrystallization using n-heptane. The white crystal product (overall yield 96%) was obtained after removing the solvent and drying under vacuum for 24 h. The chemical structure and purity of the product were confirmed by Fourier transform infrared spectroscopy (ATR-FTIR) and nuclear magnetic resonance (NMR) according to the literatures [13, 19].

3.5.3 Polymerization of PPy-COOH particles

A classic emulsion polymerization system was employed to synthesize the P(Py-PyCOOH) copolymer particles as we previously reported [25], with the chemical reaction scheme showed in Fig 3.9. To optimize experimental parameters to achieve the maximum surface carboxyl groups, desired conductivity and suitable morphology, the feeding of oxidant (from 35 mmol to 130 mmol in 100 mL solution), ratio of H_2O to $CHCl_3$ (20/80, 25/75, 30/70, 40/60; v/v), and ratio of Py to PyCOOH (100/0, 75/25, 50/50, 25/75, 0/100; mol/mol) were experimented. Typically, an aqueous solution $FeCl_3 \cdot 6H_2O$ was added into 60 mL $CHCl_3$ solution containing

1.0 g DBS. The above solution was stirred under N_2 protection for 30 minutes prior to adding 10 mL $CHCl_3$ solution containing 15 mmol Py/PyCOOH. The reaction was maintained at room temperature for periods from 10 min to 24 h with N_2 protection for the first 3 h. After demulsification using methanol, the product was harvested by vacuum filtration and washed in series in methanol, methanol/water (50/50) mixture, 1M HCl, and deionized water, repeated for 3 times. The final product was obtained after drying under vacuum for at least 48 h.

3.5.4 Characterization

3.5.4.1 Particle morphology

The P(Py-PyCOOH) particles were observed with scanning electron microscopy (SEM, JEOL JSM-6360LV, Japan) at an accelerating voltage of 20 kV after spatter-coating with gold for 120 s by a sputter coater (Fison Instruments Polaron SC500, UK). Furthermore, the morphology and structure of the particles were also analyzed by transmission electron microscopy (TEM, JEOL JEM-1230, Japan) at an accelerating voltage of 80 kV. To prepare TEM samples, a diluted P(Py-PyCOOH) suspension after 10 min ultrasonic treatment was dropped on a sample grid and air dried.

3.5.4.2 Chemical composition

A Nicolet Magna-IR 550 spectrophotometer (Nicolet Instrument, Madison, USA) was employed at ATR mode to obtain the infrared absorption spectra to identify the surface chemistry of the particles. The surface elemental composition and high-resolution spectra of the P(Py-PyCOOH) particles was analyzed using a 5600 X-ray photoelectron spectrometer (XPS, Eden Prairie, USA). Meanwhile, the total elemental analysis of the particles (ca. 1 mg) was performed using an element analyzer (Flash 2000, Thermo Scientific, USA), with cystine as reference.

3.5.4.3 Thermostability

The thermal degradation of the particles under a nitrogen atmosphere was investigated with a TGA/SDTA 851e thermogravimetric analyzer (Mettler-Toledo, Mississauga, Ontario,

Canada). Approximately 5 mg of the sample was heated from 25 °C to 600 °C at a heating rate of 10 °C/min under the protection of N_2 that flew at 40 mL/min.

3.5.4.4 Electrical conductivity

P(Py-PyCOOH) pellets of 10 mm in diameter and approximately 1 mm in thickness were fabricated by mechanical compression. Afterwards, the surface resistance Rs (Ω/□) of the specimens was measured by the four-point probe (Jandel Engineering Ltd., Linslade, Beds, UK). The surface electrical resistivity (ρ, Ω·cm) was calculated according to the formula (3.1) [25, 32, 36], where Rs refers to surface resistance, t the sample thickness, f1 the finite thickness correction factor, and f2 the finite width correction factor. Finally, the conductivity (σ, s/cm) was defined as formula (3.2) thereupon. The Rs of each sample was determined by averaging the measurements of 3 pellets, with 10 measurements for each pellet. The thickness and width correction factors were obtained from Smits' report [36].

$$\rho = 4.5324 \times Rs \times t \times f1 \times f2 \qquad (3.1)$$

$$\sigma = 1/\rho \qquad (3.2)$$

3.5.4.5 Statistical analysis

Data were presented as means ± standard deviations ($n \geqq 3$). Student's t-test was adopted to analyse the statistical differences. A statistically significant result is attained when a value of $P < 0.05$.

3.6 Conclusions

The conductive P(Py-PyCOOH) copolymer core-shell particles with tunable surface chemistry and conductivity were studied and optimized with a wide range of experimental parameters. The properties of the copolymers were found inextricably linked with the dosage of Fe^{3+}, solvent system, feeding ratio of PyCOOH and reaction time. No more than 50% PyCOOH in comonomers is sufficient to form a PPy-COOH homopolymer surface, ensuring the maximum surface functionality. The content of PyCOOH strongly affects the doping level of the copolymer and reduces copolymer conductivity. Taking into account the yield, conductivity and surface chemical

reactivity of the particles, a feeding of 80 mmol Fe^{3+} in 100 mL solution and a 25/75 water/chloroform emulsion system are considered optimal. In the presence of sufficient oxidant, it is not feasible to further increase surface carboxyl groups using a feeding ratio of PyCOOH higher than 50%. These functional conductive P(Py-PyCOOH) particles can be easily grafted with biomolecules for sensing and biomedical applications.

3.7 Acknowledgements

This work was supported by the Natural Sciences and Engineering Research Council of Canada (262258-2011) and the Canadian Institutes of Health Research (MOP106555). The first author acknowledges the Bourse de la Fondation du CHU de Québec aux étudiants. The technical assistance of Stéphane Turgeon, Pascale Chevalierare and Andrée-Anne Guay-Bégin are greatly appreciated.

Reference

1. Bendrea A-D, Cianga L, Cianga I, Review paper: progress in the field of conducting polymers for tissue engineering applications. *J. Biomater. Appl.* 2011, 26, (1): 3-84.

2. Ravichandran R, Sundarrajan S, Venugopal JR, Mukherjee S, Ramakrishna S, Applications of conducting polymers and their issues in biomedical engineering. *J. Royal Soc. Interface*. 2010, 7: S559-S579.

3. Guimard NK, Gomez N, Schmidt CE, Conducting polymers in biomedical engineering. *Prog. Polym. Sci.* 2007, 32, (8): 876-921.

4. Geetha S, Rao CR, Vijayan M, Trivedi D, Biosensing and drug delivery by polypyrrole. *Anal. Chim. Acta.* 2006, 568, (1): 119-125.

5. Nickels JD, Schmidt CE, Surface modification of the conducting polymer, polypyrrole, via affinity peptide. *J. Biomed. Mater. Res., Part A*. 2013, 101, (5): 1464-1471.

6. Cho Y, Borgens RB, Biotin-doped porous polypyrrole films for electrically controlled nanoparticle release. *Langmuir*. 2011, 27, (10): 6316-6322.

7. Zhang LL, Zhang Z, Electrical field directed electropolymerization of free-standing film of polypyrrole and poly (1-(2-carboxyethyl) pyrrole at the air/liquid interface. *Synth. Met.* 2011, 161, (9): 724-730.

8. Bozgeyik İ, Şenel M, Çevik E, Abasıyanık MF, A novel thin film amperometric urea biosensor based on urease-immobilized on poly (N-glycidylpyrrole-co-pyrrole). *Curr. Appl. Phys.* 2011, 11, (4): 1083-1088.

9. Ko S, Jang J, Controlled amine functionalization on conducting polypyrrole nanotubes as effective transducers for volatile acetic acid. *Biomacromolecules*. 2007, 8, (1): 182-187.

10. Bisht V, Takashima W, Kaneto K, A novel thin film urea biosensor based on copolymer poly (N-3-aminopropylpyrrole-co-pyrrole) film. *Surf. Coat. Technol.* 2005, 198, (1): 231-236.

11. Azioune A, Ben Slimane A, Ait Hamou L, Pleuvy A, Chehimi MM, Perruchot C, Armes SP, Synthesis and characterization of active ester-functionalized polypyrrole-silica nanoparticles: application to the covalent attachment of proteins. *Langmuir*. 2004, 20, (8): 3350-3356.

12. Ahuja T, Mir IA, Kumar D, Biomolecular immobilization on conducting polymers for biosensing applications. *Biomaterials*. 2007, 28, (5): 791-805.

13. Jiang H, Zhang A, Sun Y, Ru X, Ge D, Shi W, Poly (1-(2-carboxyethyl) pyrrole)/polypyrrole composite nanowires for glucose biosensor. *Electrochim. Acta*. 2012, 70: 278-285.

14. Okner R, Domb AJ, Mandler D, Electrochemical formation and characterization of copolymers based on N-pyrrole derivatives. *Biomacromolecules*. 2007, 8, (9): 2928-2935.

15. Oshima K, Nakamura T, Matsuoka R, Kuwahara T, Shimomura M, Miyauchi S, Immobilization of alcohol dehydrogenase on poly [1-(2-carboxyethyl) pyrrole] film for fabrication of ethanol-responding electrode. *Synth. Met.* 2005, 152, (1): 33-36.

16. Shimomura M, Kuwahara T, Iizuka K, Kinoshita T, Immobilization of alcohol dehydrogenase on films prepared by the electrochemical copolymerization of pyrrole and 1-(2-carboxyethyl) pyrrole for ethanol sensing. *J. Appl. Polym. Sci.* 2010, 116, (5): 2651-2657.

17. Ko S, Jang J, Label-free target DNA recognition using oligonucleotide-functionalized polypyrrole nanotubes. *Ultramicroscopy*. 2008, 108, (10): 1328-1333.

18. Hu WH, Li CM, Dong H, Poly (pyrrole- co-pyrrole propylic acid) film and its application in label-free surface plasmon resonance immunosensors. *Anal. Chim. Acta.* 2008, 630, (1): 67-74.

19. Maeda S, Corradi R, Armes SP, Synthesis and characterization of carboxylic acid-functionalized polypyrrole-silica microparticles. *Macromolecules*. 1995, 28, (8): 2905-2911.

20. Madani A, Nessark B, Brayner R, Elaissari H, Jouini M, Mangeney C, Chehimi MM, Carboxylic acid-functionalized, core–shell polystyrene@ polypyrrole microspheres as platforms for the attachment of CdS nanoparticles. *Polymer*. 2010, 51, (13): 2825-2835.

21. Li W, Qiu T, Wang L, Ren S, Zhang J, He L, Li X, Preparation and electromagnetic properties of core/shell polystyrene@ polypyrrole@ nickel composite microspheres. *ACS Appl. Mater. Interfaces.* 2013, 5, (3): 883-891.

22. Lee JY, Bashur CA, Milroy CA, Forciniti L, Goldstein AS, Schmidt CE, Nerve growth factor-immobilized electrically conducting fibrous scaffolds for potential use in neural engineering applications. *IEEE T. NanoBiosci.* . 2012, 11, (1): 15-21.

23. Shi W, Cao HH, Shen YQ, Song CF, Li DH, Zhang Y, Ge DT, Chemically modified PPyCOOH microtubes as an affinity matrix for protein purification. *Macromol. Chem. Phys.* 2009, 210, (17): 1379-1386.

24. Lee J-W, Serna F, Nickels J, Schmidt CE, Carboxylic acid-functionalized conductive polypyrrole as a bioactive platform for cell adhesion. *Biomacromolecules*. 2006, 7, (6): 1692-1695.

25. Mao J, Zhang Z, One-step reactivity-driven synthesis of core–shell structured electrically conducting particles for biomedical applications. *J. Mater. Chem. B.* 2016, 4, (32): 5429-5436.

26. Ansari R, Polypyrrole conducting electroactive polymers: synthesis and stability studies. *J. Chem.* 2006, 3, (4): 186-201.

27. Machida S, Miyata S, Techagumpuch A, Chemical synthesis of highly electrically conductive polypyrrole. *Synth. Met.* 1989, 31, (3): 311-318.

28. López-García F, Canché-Escamilla G, Ocampo-Flores A, Roquero-Tejeda P, Ordóñez L, Controlled size nano-polypyrrole synthetized in micro-emulsions as PT support for the ethanol electro-oxidation reaction. *Int. J. Electrochem. Sci*. 2013, 8: 3794-3813.

29. Chen S, Shen W, Wu G, Chen D, Jiang M, A new approach to the functionalization of single-walled carbon nanotubes with both alkyl and carboxyl groups. *Chem. Phys. Lett.* 2005, 402, (4): 312-317.

30. Shimomura M, Miyata R, Kuwahara T, Oshima K, Miyauchi S, Immobilization of glucose oxidase on the films prepared by electrochemical copolymerization of pyrrole and 1-(2-carboxyethyl) pyrrole for glucose sensing. *Eur. Polym. J.* 2007, 43, (2): 388-394.

31. Shi G, Rouabhia M, Wang Z, Dao LH, Zhang Z, A novel electrically conductive and biodegradable composite made of polypyrrole nanoparticles and polylactide. *Biomaterials*. 2004, 25, (13): 2477-2488.

32. Meng S, Zhang Z, Rouabhia M, Surfactant-templated crystalline polygon nanoparticles of heterocyclic polypyrrole prepared with Fenton's reagent. *Synth. Met.* 2010, 160, (1): 116-122.

33. Mangeney C, Bousalem S, Connan C, Vaulay M-J, Bernard S, Chehimi MM, Latex and hollow particles of reactive polypyrrole: Preparation, properties, and decoration by gold nanospheres. *Langmuir*. 2006, 22, (24): 10163-10169.

34. McCarthy G, Armes S, Greaves S, Watts J, Synthesis and characterization of carboxylic acid-functionalized polypyrrole-silica microparticles using a 3-substituted pyrrole comonomer. *Langmuir*. 1997, 13, (14): 3686-3692.

35. Vernitskaya TyV, Efimov ON, Polypyrrole: a conducting polymer; its synthesis, properties and applications. *Russ. Chem. Rev.* 1997, 66, (5): 443-457.

36. Smits F, Measurement of sheet resistivities with the four-point probe. *Bell Syst. Tech. J.* 1958, 37, (3): 711-718.

CHAPTER IV

PREPARATION AND CHARACTERIZATION OF HIGHLY FLEXIBLE POLYPYRROLE MEMBRANE

Conductive Polymer Waving in Liquid Nitrogen

Jifu Mao,[†,‡] Chaojing Li,[†,‡,§] Hyun Jin Park,[†,‡,∥] Mahmoud Rouabhia,[∥] Ze Zhang[*,†,‡]

†Département de chirurgie, Faculté de médecine, Université Laval, Québec (QC), G1V 0A6, Canada.

‡L'Axe médecine régénératrice, Centre de recherche du CHU de Québec (QC), G1L 3L5, Canada.

§Key Laboratory of Textile Science and Technology of Ministry of Education and College of Textiles, Donghua University, 2999 North Renmin Road, Shanghai 201620, China.

∥Groupe de Recherche en Écologie Buccale, Faculté de Médecine Dentaire, Université Laval, Québec (QC), Canada.

ACS Nano. 2017 (in press) DOI : 10.1021/acsnano.7b05546

Electronic supplementary information (ESI) available. See DOI : 10.1021/acsnano.7b05546

4.1 Résumé

Les propriétés mécaniques insuffisantes et le manque de capacité de traitement des polymères conducteurs hétérocycliques vierges réduisent considérablement les applications possibles de ces polymères. Nous rapportons une membrane souple et mécaniquement modulable en polypyrrole vierge (PPy-N), qui est synthétisée par polymérisation interfaciale assistée dans un gabarit. Le PPy-N est aussi doux dans l'azote liquide (-196 ^{o}C) qu'à température ambiante. Ce PPy-N présente également une combinaison de propriétés très séduisante, y compris la processabilité mécanique, légère (9 g m^{-2}), la grande surface (14,5 m^2 g^{-1}), le comportement électrothermique stable, l'amphiphilicité et l'excellente cytocompatibilité. Ces résultats démontrent la capacité de modifier les propriétés mécaniques du polymère conducteur hétérocyclique sans modification chimique ou de composition, ce qui permet d'améliorer le développement de polymères conducteurs intrinsèques pour des applications telles que le stockage de l'énergie et la biomédecine ou encore comme matériaux conducteurs légers et matériaux de chauffage.

4.2 Abstract

The poor mechanical properties and processability of pristine heterocyclic conductive polymers represent the most notable scientific and technological challenges that have greatly limited the application of these polymers. We report on a soft and mechanically processable free-standing pristine polypyrrole (PPy) membrane (PPy-N) that is as soft in liquid nitrogen (-196 ^{o}C) as it is at room temperature, despite a glass transition temperature (Tg) above 100 ^{o}C. This PPy membrane also displays a highly attractive combination of properties, including mechanical processability, light weight (9 g m^{-2}), large surface area (14.5 m^2 g^{-1}), stable electrothermal behavior, amphiphilicity, excellent cytocompatibility, and easy synthesis, in virtually any size. This discovery demonstrates an approach to changing the mechanical property of heterocyclic conductive polymer with no chemical alterations or compounding, and may enhance the development of inherently conducting polymers for applications in energy storage and biomedicine, and as lightweight conducting and heating materials.

Keywords: polypyrrole, flexibility, processability, ultralow temperature resistant, porous.

4.3 Introduction

Poor mechanical property and processability remain the two significant limitations of heterocyclic inherently conductive polymers. These obstacles are considered intrinsic to conductive polymers because of the extensive conjugation in the polymer chains and the aggregation state resulting in very high surface tension and lattice energy.[1] While this extended conjugation is the foundation of charge transfer and therefore electrical conductivity, it also restrains the rotation and bending of polymer molecules, resulting in high material rigidity.

Since the development of highly conductive synthetic polymers in the 1970s and despite the initial enthusiasm and the 2000 Nobel Prize in Chemistry, large-scale industrial use of inherently conductive polymers remains very limited. Efforts deployed to prepare soluble pristine conductive polymers have largely failed and those appearing "soluble" are often in suspension.[1] Introducing polar side groups to monomers was shown to increase solubility at the expense of conductivity.[2] Water-soluble polyaniline (PANI) was reported, however it used a significant amount of polyelectrolyte such as polystyrene sulfonate (PSS) to stabilize the PANI.[3] Similarly, high molecular weight PPy was reported to be soluble in organic solvents with the help of di(2-ethylhexyl) sulfosuccinate (DEHS) as the dopant.[4] The bulky DEHS separates PPy molecules and reduces intramolecular interactions, leading to a low solubility (2-9%) of DEHS-doped PPy in organic solvent. The most successful commercial products are probably the PEDOT:PSS water suspension, now commercially available from AGFA (Orgacon™ Electronic Materials), and Heraeus (Clevios ™ Conductive Polymers), made of poly(3,4-ethylenedioxythiophene) (PEDOT) gel particles doped and stabilized by PSS.

Because of their poor mechanical properties, conductive polymers are almost always compounded with other insulating ductile materials to gain mechanical or processing advantages. For example, Orgacon™ and Clevios™ are used as a coating to provide an antistatic property and to form a transparent conducting film. Conductive polymer powder can be mixed with other materials to form a conductive composite.[5] When conductive polymers as the only component material is not an option because of their poor processability and mechanical property, compounding with other materials provides an excellent solution.

It must be understood, however, that when used in any type of composites, some important properties of the conductive polymers become useless, such as thermal stability, resistivity to organic solvent and to hydrolysis, and bulk electrical properties. These properties are determined by the composing polymer. In addition, issues regarding delamination, agglomeration, and loss of conductivity cannot be ignored for conductive polymer-based composites.[6, 7] For these reasons, a flexible and processable pristine conductive polymer material is highly desirable.

Efforts to achieve truly flexible pristine conductive polymer membranes that can be scaled up for industrial applications have been unsuccessful until now. The interfacial oxidative polymerization of PPy was first mentioned in a short communication in 1986, reporting that free-standing PPy was formed between a $FeCl_3$ aqueous solution and a pyrrole benzene or toluene solution.[8] The authors obtained a small piece of thin, flexible, and transparent film. Another group followed the same route and reported PPy membranes of 1 to 10 microns in thickness, which was flexible only in the early phase of polymerization and became less conductive and brittle as the polymerization progressed.[9] A thin PPy film electrochemically formed on an electrode and then separated was also found to be flexible, again very small, and only 4 to 7 μm in thickness.[10] To conclude, although flexible PPy films have been synthesized through interfacial and electrochemical polymerization, these films remain very small in size and extremely thin (10 to 100 μm), with no impact as to solving the two aforementioned major limitations. A PPy membrane with a certain degree of flexibility and meaningful size has been made by casting a PPy nanotube suspension;[11, 12] however, this membrane shows little mechanical strength, easily breaks under large bending, and disintegrates back to nanotubes when, for example, it is washed in ultrasonic bath. A flexible PPy foam was also prepared electrochemically, using nickel foam as a template (working electrode).[13] This approach however is difficult to scale up; and the membrane showed a relatively large radium of curvature. To the best of our knowledge, a truly flexible membrane of pristine heterocyclic conductive polymers has not been reported.

This work presents a truly flexible and mechanically processable pristine PPy membrane achieved through a simple approach which we have called template-assisted interfacial polymerization (TIP). The extraordinary mechanical property stems from the structure of the

membrane. Understanding this phenomenon may provide an interesting opportunity to make flexible structures out of other rigid materials.

4.4 Results and discussion

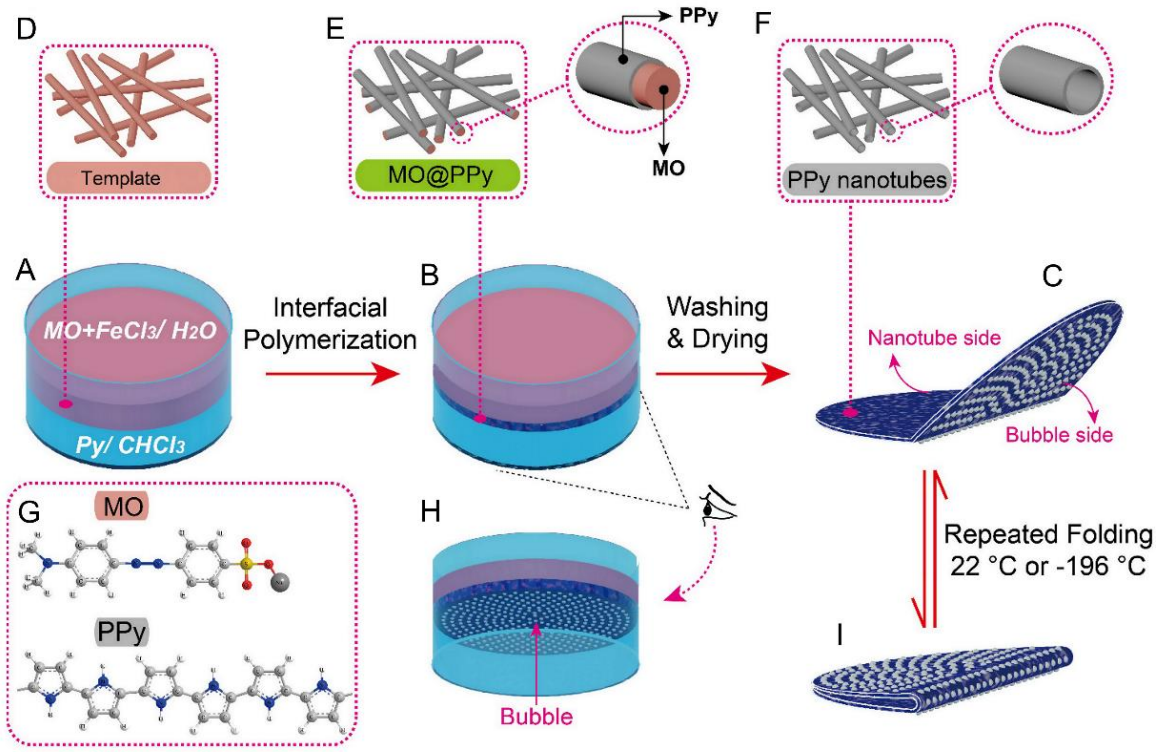

Figure 4.1 Diagram of the template-assisted interfacial polymerization (TIP) of a flexible PPy membrane (PPy-N). (A) Beginning of TIP, showing the enrichment of the nanorod templates. (B) End of TIP, showing a black product near the interface. (C) Final PPy-N membrane obtained after washing and drying. (D) Nanorod template structure formed by FeCl3 and MO. (E) MO@PPy nanorod structure on the water side of the membrane. (F) PPy nanotube structure following removal of templates. (G) MO and PPy molecular structure. (H) Bubbles on the chloroform side. (I) Final PPy-N membrane is flexible both at room temperature and in liquid nitrogen, showing PPy bubbles.

Figure 4.1 illustrates how PPy-N was synthesized via TIP (see Experiment). The $FeCl_3$ and methyl orange (MO) complex precipitated to the bottom of the water phase because of density, resulting in a high oxidant concentration near the chloroform/water interface. The polymerization was therefore confined to a narrow zone in the water phase, near the water/chloroform interface where PPy-N was formed. Without MO, however, polymerization not only took place at the water/chloroform interface forming a particulate PPy membrane (PPy-P) but also occurred throughout the water phase to form a PPy particle

suspension (Figure S4.1 and S4.2). Figure S4.1 and S4.2 show the beginning and the end of the TIP, respectively. Many noticeable bubbles formed under the membrane throughout the TIP process (Figure S4.2B). In contrast, bubbles were hardly visible in the system without the template (Figure S4.2A).

The formation of the $FeCl_3$/MO complex template and its role in guiding PPy nanotube polymerization were previously reported by Yang et al.[14] Briefly, due to the flocculation and complexation of Fe^{3+}, the negatively charged MO aggregates into a Fe^{3+}/MO rod-like complex, providing the reactive surface for PPy polymerization. The PPy nanotubes are form after removal of the template.

The PPy-N presented an asymmetrical morphology on two sides, i.e., a bubble side formed in the chloroform phase and a nanotube side formed in the water phase (Figure 4.2). The bubble side was entirely covered by the overlapped PPy bubbles of relatively uniform size (ca. 300 to 500 μm in diameter and 200 nm in wall thickness), of which some appear to be either broken or collapsed (Figure 4.2A). The surface of the unbroken bubbles was dense (Figure 4.2A, insert). A cross section shows the bubbles settled on a thin membrane that in fact separated the two sides or two phases (Figure 4.2B). Initially, this membrane was approximately 300 nm in thickness and gradually became 1 μm at the end of the polymerization. The water phase of the membrane was topped with a thick layer of PPy nanotubes (Figure 4.2B, insert). These PPy nanotubes were approximately 300 nm in diameter and 30 nm in wall thickness, and were to some extent longitudinally assembled into randomly oriented bundles, as shown in Figure 4.2G and 4.2H. In the absence of MO templates, PPy particles close to 700 nm in size instead of PPy nanotubes were formed in the water phase, while small compact PPy bubbles of non-uniform size formed in the chloroform phase (Figure 4.2, D to F), separated by a solid membrane approximately 700 nm in thickness (similar to PPy particle size) (Figure 4.2E, insert).

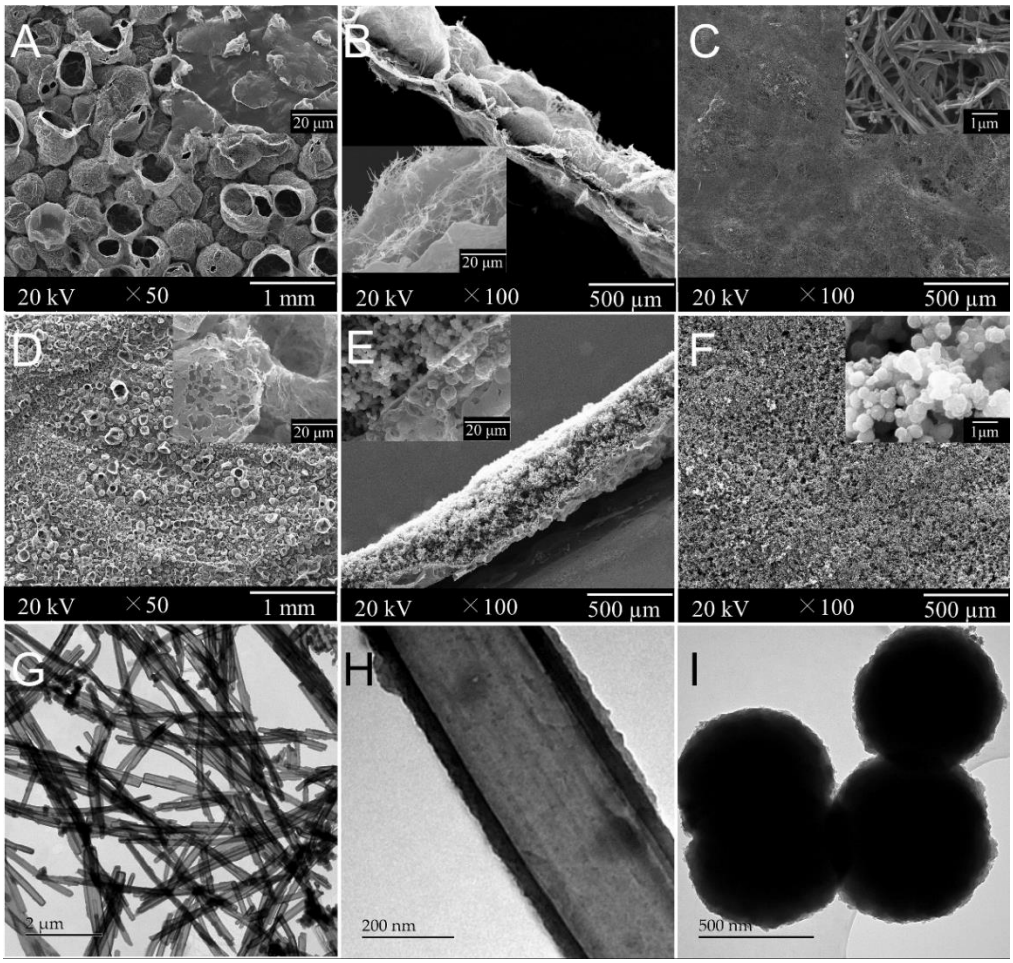

Figure 4.2 Morphology of PPy-N and PPy-P synthesized at 4 °C. (A-C) Scanning electron microscopy (SEM) photos of PPy-N. (A) Large intact and burst bubbles formed in the chloroform phase; insert shows their dense surface. (B) Cross section at low and high (insert) magnifications, showing the multilayer structure and thin solid membrane. (C) Nanotube side formed in the water phase. (D-F) SEM photos of PPy-P. (D) Small intact and burst bubbles formed in the chloroform phase; insert shows the porous bubble surface. (E) Cross section at low and high (insert) magnifications, showing the thick layer of PPy particles and thin solid membrane. (F) Particle side formed in the water phase. (G-I) Transmission electron microscopy (TEM) photos of PPy nanotubes and particles. (G) PPy nanotubes removed from PPy-N. (H) High magnification of (G). (I) PPy particles removed from the PPy-P.

PPy-N and PPy-P were both asymmetric in terms of structure, yet their characteristics were somehow inversed, i.e., a thin layer of nanotubes vs. a thick layer of sub-micron particles, and large thin-walled bubbles vs. small thick-walled bubbles. It is clear that the presence of MO dictated the yield and morphology of the PPy in the two phases. While it is obvious that we understand the different shapes of PPy precipitated in the water phase because of the presence or not of the MO/$FeCl_3$ complex, we were initially frustrated by the presence of

bubbles instead of particles in the chloroform. We now believe that this was due to the exothermic nature of pyrrole polymerization[15] which produced chloroform vapor upon polymerization. Only under such circumstances could PPy form symmetric bubbles because of the equal internal pressure of the chloroform vapor in all directions. In fact, the bubbles appeared shortly after the formation of the thin membrane at the chloroform/water interface and remained present throughout the entire period of polymerization (Figure S4.3). Upon the forming of the bubbles, new interfacial polymerization (liquid chloroform/chloroform vapor) began from where the bubbles attached to the membrane, and developed throughout the entire bubble surface. While oxidant is not soluble in chloroform, it can diffuse through the PPy membrane and make it available at the chloroform/bubble interface. With the progress of polymerization, the bubbles either solidified or collapsed, on which new bubbles formed. Figure 4.3 illustrates how the PPy-N and PPy-P membranes formed. This mechanism was supported by the polymerization at -20 ^{o}C, where almost all of the bubbles collapsed as a result of a too slow bubble solidification (Figure S4.4) and by the polymerization at 22 ^{o}C, where large thick bubbles flourished (Figure S4.5).

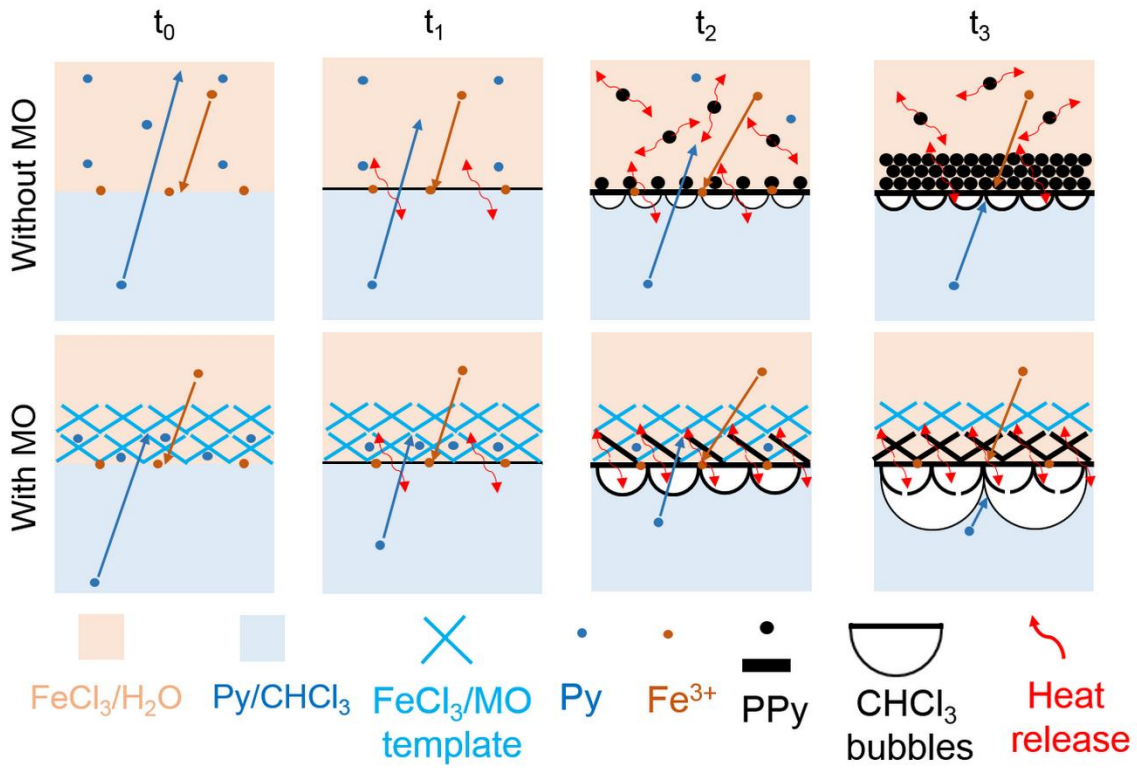

Figure 4.3 Formation of the flexible PPy-N and PPy-P membranes.

At time zero (t_0), monomers and oxidants made contact at the interface and began to diffuse to other phases. Because ferric chloride is insoluble in chloroform but pyrrole monomers are partially soluble in water, polymerization took place only at the interface and in the water phase, resulting in the almost instant formation of a thin PPy film at the interface (t_1). In the presence of MO, the Fe^{3+}/MO complex precipitated to the bottom of the water phase because of density to form an oxidant-rich layer above the chloroform. Without MO, the Fe^{3+} ions were uniformly distributed in the water phase. Therefore, PPy nanotubes formed only at the bottom of the water phase, while PPy particles formed at the interface and throughout the water phase. This localized heat of reaction vaporized the chloroform to form bubbles, which supported further interfacial polymerization on the bubble surface. Ferric chloride was able to diffuse through the amphiphilic membrane to oxidize pyrrole monomers at the interface of the chloroform vapor and liquid chloroform (chloroform bubble surface). (t_2). This process continued and eventually led to the formation of a multilayer of bubbles and nanotubes/particles (t_3).

The PPy-N membrane had a nominal thickness of approximately 0.45 mm, dominated by the multilayer of bubbles (SEM observation). This thickness was reduced to approximately 0.17 mm when measured under 22 kPa using a thickness gauge (see Supplementary Materials) due to the deformation of the bubbles upon pressure. In comparison, the PPy-P membrane, with a thickness dominated by the particle layer, was much thicker under the same pressure because the compact particles were more resistant to compression (Table S4.1). The PPy-N membrane displayed an unexpected light weight of only 8.9 g m^{-2} in areal density, which was one-sixth that of the PPy-P membrane (350 μm thick, 54 g m^{-2}), one-ninth that of ordinary print paper (130 μm thick, 80 g m^{-2}), and close to 3-folds lighter than that of steel foil (3 μm thick, 24 g m^{-2}).[16] The PPy-N membrane also had a higher BET specific surface area (14.5 ± 0.2 m^2 g^{-1}) than that of the PPy-P (6.38 ± 0.06 m^2 g^{-1}), and both were lower than that of the PPy nanotube membrane (74.3 ± 0.3 m^2 g^{-1}).

Despite the huge morphological difference, attenuated total reflectance Fourier transform infrared spectroscopy (ATR-FTIR) and X-ray photoelectron spectroscopy (XPS) recorded almost identical chemical structures of the PPy-N and PPy-P membranes on both sides (Figure S4.6). A slight difference observed on the water side recorded a small peak at 1715

cm^{-1} in the FTIR spectrum and more oxygen element in the XPS results (Table S4.2), confirming the generation of –C=O due to over-oxidation[17] and the termination of PPy chains by oxygen and water molecules.[18] The level of oxidation was measured by XPS and is presented as the ratio of the positively charged nitrogen to total nitrogen (denoted as N^+/N) (Table S4.2).

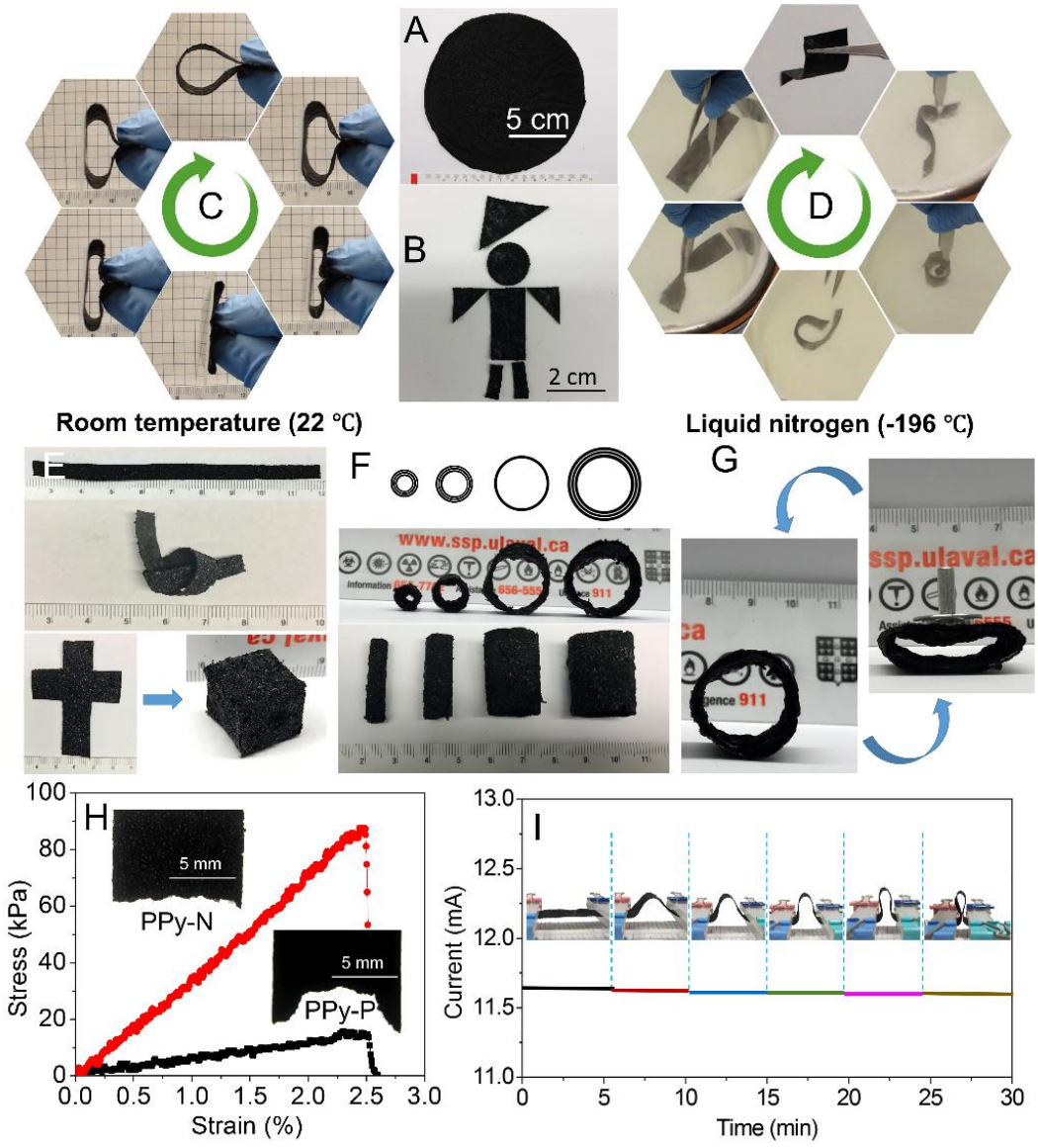

Figure 4.4 Physical properties and processability of PPy-N. (A) An as-prepared membrane 15 cm in diameter. (B) Cutout. (C) Cyclic bending at room temperature (7.5 cm × 2.5 cm). (D) Waving in liquid nitrogen (7.5 cm × 1.0 cm). (E) Tie and cube. (F) Rolling and laminating. (G) Radial elasticity of a triple-layer tube. (H) Stress-strain curves of PPy-N vs. PPy-P (5.0 cm × 1.0 cm). Insert: Section following tensile fracture. (I) Current-time curve of a 7.5 cm × 2.5 cm strip bent to different curvatures under 2.0 V.

Our findings show that despite the high Tg of the pristine PPy (ca. > 100 ºC), the free-standing PPy-N membrane (Figure 4.4A, ϕ 15 cm) presented fascinatingly remarkable softness and flexibility. It could easily be cut into any shape (Figure 4.4B) and exhibited incredible capacity under repeated bending at room temperature (Figure 4.4C). In comparison, the PPy-P membrane showed only a limited flexibility and broke under large curvature, comparable to that observed with the PPy nanotube-cast membrane (Movies S4.1 to S4.3, video file has been filed separately). What is more surprising is that this outstanding softness and flexibility remained practically unchanged in liquid nitrogen, as shown in Figure 4.4D and Movie S4.4 (video file has been filed separately), compared to that of the PPy nanotube-cast membrane (Movie S4.5, video file has been filed separately). This degree of flexibility is far superior to that of any type of pure PPy membrane in the literature,[11, 12, 19, 20] in addition to reaching or exceeding that of PPy composite membranes.[21-23]

Furthermore, this innovative PPy-N membrane was found to be mechanically processable, as demonstrated by the fact that it could be tied or folded into a cubic box (Figure 4.4E), and be laminated and rolled into tubes displaying both radial strength and elasticity (Figure 4.4F to 4.4G). Moreover, the PPy-N membrane showed a tensile strength of 90 kPa at 2.5% elongation at break, which was much higher than that recorded by the PPy-P (15 kPa at 2.5% elongation) (Figure 4.4H) and of 3D PPy foam (18 kPa at 3.3% elongation).[13] The elastic moduli at 1% strain were 3.4 MPa for the PPy-N, 0.6 MPa for the PPy-P, and 0.5 MPa for the PPy foam[13] (Table S4.1). The mechanical feature of the PPy nanotube-cast membrane could not be measured due to its weak mechanical integrity. The superior structural stability of the PPy-N membrane was also confirmed when treating it in an ultrasound bath with respect to the PPy-P and PPy nanotube-cast membranes (Figure S4.7 and Movie S4.6, video file has been filed separately). The structure also rendered the PPy-N and PPy-P amphiphilic, with an excellent capacity in both water and heptane adsorptions (Movie S4.7 and S4.8 and Table S4.1, video file has been filed separately).

To explain the flexibility of the PPy-N membrane, two aspects were considered, namely, structure and thickness. It is well known that material properties including mechanical properties change significantly at nanoscale. The stiffness and brittleness of dense PPy due

to its rigid conjugated-ring backbone can be largely reduced through interconnections based on micro/nanostructure design.[13, 24]

When looking at the cross section, the PPy-N membrane displayed a layer of nanotubes, a continuous membrane in the middle, and finally a multilayer of thin-walled bubbles, of which at least one dimension was in nano or submicron range. Among these, the nanotube layer was not considered as a determinant of flexibility because the nanotubes were only physically compacted and could be physically removed without affecting membrane flexibility. The continuous membrane displayed a thickness of approximately 1 micron with bubble wall thickness close to 200 nm. As illustrated in Figure S4.8 and explained in Supplementary Materials, bending radius is proportional to membrane thickness and inversely proportional to strain, which is why a thin stainless steel sheet can present excellent flexibility. According to the formula for the PPy-N, the minimum bending radius of the 1-μm-thick PPy membrane at 2.5% strain was as small as 20 μm. Bubbles with a wall thickness as small as 200 nm only ensured an even smaller bending radius.

It was recently demonstrated that microfolds constructed by single or multilayer graphene sheets greatly improved the flexibility of graphene films.[25] We believe that the superior flexibility of our PPy-N at room temperature was mainly due to its thin-walled structure. The bubble deformation modes upon membrane bending are obviously extremely complex and cannot be fully explained by the simple illustration shown in Figure S4.8. Nevertheless, the principle described above should apply. The thin-walled theory may not explain low temperature flexibility. The mechanism governing low temperature flexibility will require further investigations.

Polymer crystallinity influences many polymer characteristics including strength and rigidity. However, PPy is generally regarded as an amorphous material. Our work on the crystallinity of electrochemically synthesized PPy films also confirms the broad and weak X-ray diffractions.[26] Similarly, PPy films prepared by interfacial polymerization are typically amorphous, as are PPy-MO nanotubes.[14, 20, 27] On the other hand, a high crystallinity only renders PPy more rigid and brittle. Therefore, crystallinity was not considered playing any significant role in membrane flexibility.

The conductivity of the as-synthesized PPy-N measured 1.5 S cm^{-1} by the four-point probe method, which is normal for chemically polymerized PPy and slightly higher than that of PPy-P (0.3 S cm^{-1}) and PPy-Ag films formed at the CH_2Cl_2/water interface (0.1 S cm^{-1}),[19] and lower than that of PPy nanotube membranes (3.4-9.8 S cm^{-1}).[12, 28] In this study, chloride anions from ferric chloride were the only dopant, as confirmed by XPS (Figure S4.3B and Table S4.2). This was to ensure material cytocompatibility. When PPy is used as biomaterials in an aqueous environment, dopants may diffuse out. Chlorine anions exist in body fluid and cell culture medium. A small amount of chlorine anions leaching into culture medium or tissue normally does not cause cytotoxicity.

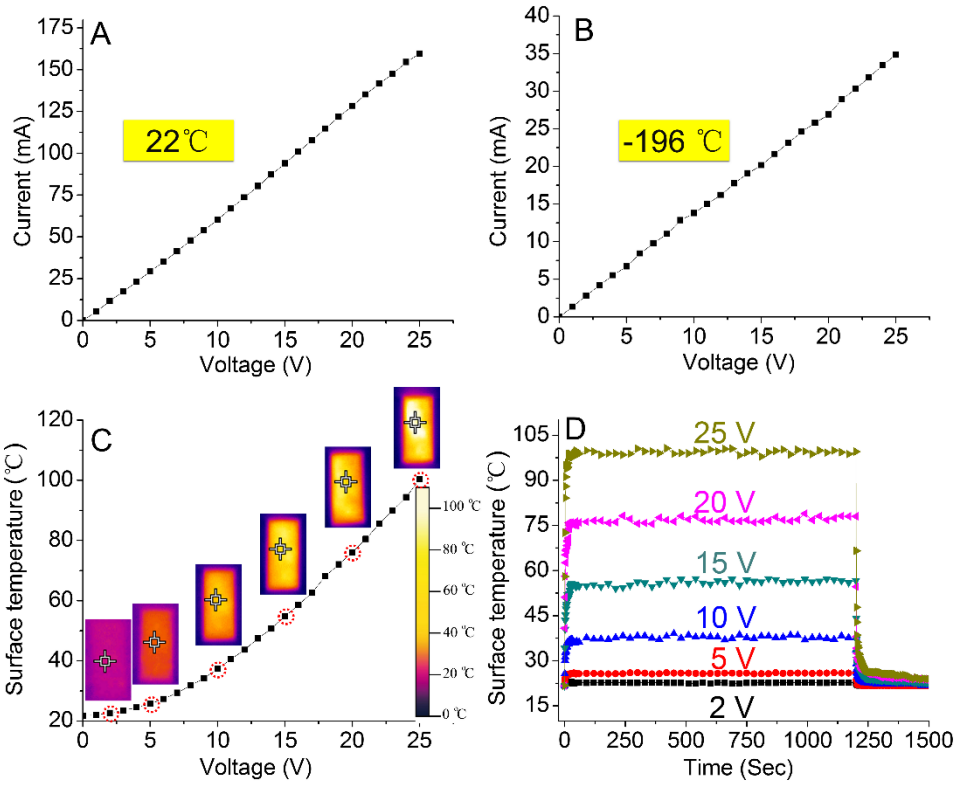

Figure 4.5 Ohmic and electrothermal behavior of PPy-N. (A) Current-voltage (I-V) curves at room temperature. (B) Current-voltage (I-V) curves in liquid nitrogen. (C) Membrane surface temperature (Tmax) vs. voltage. Insert: Infrared thermal images of the membrane surface at specific voltages (red dot circles). (D) Time-dependent surface temperature changes at various voltages.

Figure 4.4I shows a stable conductance of the PPy-N during bending, meaning no microscopic damage to the membrane under large deformation. Meanwhile, a linear I/V relationship observed at both 22 °C and - 196 °C (Figure 4.5A and 4.5B) indicates that the

material obeyed Ohm's law in a wide range of temperatures. The conductivity of PPy-N at room temperature and at -196 °C was calculated at 1.15 S cm^{-1} and 0.24 S cm^{-1}, respectively, based on the I/V curves (described in Supplementary Materials). For conducting polymers, the temperature dependence of conductivity is interpreted by the Mott 3D variable range hopping conduction model,[19, 29] following a positive correlation. Thus, the conductivity of PPy-N at -196 °C was found to be lower than that at 22 °C. These results thus demonstrate the potential of using PPy-N in flexible and lightweight electronics, even under extremely cold conditions.

The soft and compliant nature of the PPy-N membrane inspired us to test it as a heating pad. Prior to the heating experiment, the thermal stability of PPy-N was evaluated. A slight weight loss was observed between 30 and 150 °C (loss of moisture), followed by significant thermal degradation (Figure S4.3C). Hence, 150 °C was deemed as the maximum heating temperature. The electrothermal behavior of PPy-N was monitored by measuring membrane surface temperature between 1 and 25 V. Figure 4.5C shows a nonlinear increase in maximum temperature (T_{max}) that reached above 100 °C at 25 V. Figure 4.5D shows the time-dependence of the temperature for a period of 1200 s. The T-t curves were divided into three regions: temperature growth (0-20 s), steady-state temperature region (20-1200 s), and temperature decay region (1200-1300 s). Three important characteristics were calculated from these regions: growth time constant (τ_g), heat transfer by radiation and convection (h_{r+c}), and decay time constant (τ_d),[30, 31] with τ_g and τ_d measuring temperature response to voltage and cooling behavior. The PPy-N exhibited far lower τ_g and τ_d (12.5 and 40.5 s, respectively) than those of the PPy composite membranes,[30] demonstrating a rapid temperature response to voltage as well as an efficient cooling behavior. The h_{r+c} of the PPy-N was 42.6 mW $°C^{-1}$, showing electric heating efficiency comparable to that of the PPy composite membrane (28-126 mW $°C^{-1}$)[30] and of carbon nanotube composite (2-22 mW $°C^{-1}$).[31, 32] Compared to conductive composites, the advantages of PPy-N are clearly evidenced in its light weight, low-temperature flexibility and stable electrothermal behavior.

When used as biomaterials, PPy can mediate electrical signals to activate cells.[33, 34] Similar to most synthetic polymers, PPy is usually not an ideal substrate for cell adhesion and growth. In this study, however, the surface structure of the PPy-N membrane supported the excellent

adhesion and growth of human skin fibroblasts (Figure S4.9). Furthermore, both the number and distribution of cells on the membranes were significantly superior to what was observed on the cell culture glass coverslips (controls), probably owing to the nano-sized features resembling extracellular matrix.

Given the combination of properties and its numerous advantages, this novel PPy membrane shows enormous potential for use in a wide range of applications. For example, because of its light weight, low temperature flexibility, and conductivity, it can be optimally used as antistatic materials and heating elements in both the aviation industry and space technology. With its high surface area and electroactivity, it may be used in flexible supercapacitors.[35, 36] Furthermore, its attractive weight, electroactivity, and stability in acid may be useful in new types of batteries. Its flexibility at low temperature and electrothermal property may be worthwhile in lightweight heated clothing or equipment for outdoor activities. In biomedical research, this new PPy membrane can be easily custom-tailored to fit culture plates for electrically stimulated cell cultures. Moreover, conductive polymers can be readily made into electrical stimulation skin patches and even used as patches to rewire/repair infarcted heart tissue.[37, 38] Finally, our methodology demonstrates many notable advantages, including simplicity, low cost, and high reproducibility, thus ensuring the fabrication of PPy-N in large scale.

4.5 Conclusion

In conclusion, we present a solution to the two major issues significantly hindering conductive polymer applications, namely, poor mechanical property and processability. With no chemical modification to the monomers and with no need to compound with any other materials, the proposed unique physical structure renders the otherwise brittle PPy extremely flexible in a wide range of temperatures. Capable of being synthesized in virtually any size, this PPy membrane can be easily manipulated through various processes such as cutting, rolling, laminating, and adhesion. Due to its attractive processability, lightweight, high-surface area, electrical and electrothermal properties, cytocompatibility, and low fabrication cost, this versatile material shows potential for a wide range of applications such as energy storage, anti-static uses, heating, and biomedical engineering. Finally, the principle of this approach may also be applied to other conductive polymers.

4.6 Methods

4.6.1 Materials

Pyrrole (Py, 98%, Alfa Aesar, Ward Hill, MA, USA) was distilled twice under reduced pressure and stored in a refrigerator at 4 °C prior to use. Ferric chloride hexahydrate ($FeCl_3 \cdot 6H_2O$, 98%, Sigma-Aldrich, Oakville, ON, Canada), methyl orange (MO, ACS reagent, dye content 85 %, Sigma-Aldrich), and all other chemicals (Analytical Grade) were used as received.

4.6.2 Preparation of PPy membranes

PPy-N membranes were synthesized through a template-assisted interfacial polymerization (TIP) technique using MO as the template, while PPy-P was synthesized in the same manner without MO. The template and oxidant complex were prepared following a modified formula based on the study by Peng:[12] 18.2 g of $FeCl_3 \cdot 6H_2O$ was added to 320 mL of deionized water containing 5 mM of MO. Following vigorous stirring for 30 min, the mixture was transferred onto the top of 150 mL of chloroform containing 3 mL of pyrrole monomers, with the reaction maintained for 48 h at either -20 °C, 4 °C, or room temperature (22 °C). After 48 h, the membrane was collected, washed sequentially with ethanol, 1 M of HCl in 70% ethanol solution, and deionized water until the solution became colorless and neutral. The PPy membrane was then moved to a Teflon plate for drying at ambient temperature. To prepare PPy nanotube membranes as the references, PPy nanotubes were synthesized and cast into membranes as reported.[11]

4.6.3 Characterizations

4.6.3.1 Morphology

The morphology of the membranes was observed under a scanning electron microscope (SEM, Model JSM-6360LV, JEOL, Tokyo, Japan) at an accelerating voltage of 20 kV. Prior to SEM observation, the specimens were sputter-coated with gold in a sputter coater (Fison Instruments, Polaron SC500, Uckfield, UK). A transmission electron microscope (TEM, Model JEM-1230, JEOL) was further employed to identify the structure of the PPy nanotubes and particles at 45 μA and an accelerating voltage of 80 kV. To prepare the TEM specimens,

the nanotubes and particles were harvested from the membranes and prepared as a diluted suspension to drop onto a sample grid that was dried in air.

4.6.3.2 Chemical composition

The infrared spectra were recorded by means of a Nicolet Magna-IR 550 spectrophotometer (Nicolet Instrument, Inc., Madison, WI, USA) in the ATR mode. Specimens were pressed against a silicon hemispherical ATR crystal and scanned 64 times between 500 and 4500 cm^{-1} at a resolution of 4 cm^{-1}. The surface elemental composition of the membranes was analyzed using a Perkin Elmer PHI Model 5600 X-ray photoelectron spectrometer (XPS, Eden Prairie, MN, USA).

4.6.3.3 Tensile property

The tensile properties of the membranes were tested using an YG-B026H Universal Mechanical Tester (Wenzhou Darong Textile Instrument Co., Wenzhou, Zhejiang, China). The gauge length was 20.0 mm. A pre-tension of 0.01 N was applied to the sample, and a constant strain rate of 10.0 mm/min was used to stretch the sample until failure. Failure stress was calculated according to ISO 527-3:1995. Membrane thickness was measured using a digital thickness gauge under a pressure of 22 kPa (CH-12.7-BTSX, Shanghai Liuling Instrument Factory, Shanghai, China).

4.6.3.4 Electrical properties

Conductivity: The surface resistance Rs ($\Omega\ \square^{-1}$) of the specimens was measured as we previously reported using the Jandel Multi-Height Four-Point Probe (Jandel Engineering Ltd., Linslade, Beds, UK) at room temperature.[39] The surface electrical resistivity (ρ, Ω cm) was calculated based on formula (1),[39, 40] where Rs denotes the surface resistance, t represents sample thickness, f1 is the finite thickness correction, and f2 the finite width correction. Conductivity (σ, S cm^{-1}) was calculated according to formula (2). The surface resistance of each membrane was measured 10 times. The thickness and width corrections were from Smits.[40]

$$\rho = 4.5324 \times Rs \times t \times f1 \times f2 \qquad (4.1)$$

$$\sigma = 1/\rho \quad (4.2)$$

Current-time Curves: Specimens 7.5 cm × 2.5 cm in size were clamped between two flat electrodes 60 mm apart. Electrical current was measured by means of a Keithley 2700 Digital Multimeter/Data Acquisition System (Keithley Instruments, Cleveland, OH, USA) when the voltage changed from 1 to 25 V from a DC power supply (Topward 3303A, Topward Electric Instruments Co., Taipei, China). For low temperature tests the specimens were immersed in liquid nitrogen.

4.6.3.5 Thermostability

The thermostability of the membranes was measured using a TGA/SDTA 851e thermogravimetric analyzer (Mettler-Toledo, Mississauga, ON, Canada). Approximately 3 mg of samples were heated from 30 to 800 °C at a heating rate of 10 °C min^{-1} under nitrogen protection.

4.6.3.6 Electrothermal behavior

Using the same setup as in the current-time dependence test, the surface temperature of the PPy-N membranes when voltage changed from 1 to 25 V was measured using an infrared camera (TG165, FLIR Systems, Burlington, ON, Canada). The distance between the membrane and the infrared camera was maintained at 20 cm. The sample membranes measured 2.5 cm in width and 7.5 cm in length.

4.6.3.7 Liquid adsorption

The adsorption speed of deionized water and heptane was recorded using a VCA 2500 XE video contact angle system (AST, Billerica, MA, USA) in air at 25.0 °C ± 0.1 °C and 15% humidity. Drops of the probe liquid (3 μL) were placed on each side of the membranes and recorded. Each test was performed in triplicate. To determine the liquid sorption capacity (q, cm^3 g^{-1}), PPy membranes of 2.5 cm in width and 7.5 cm in length were weighed (m0, g), immersed in either water or heptane for 5 min, and weighed again after removing the visible surface liquid with a filter paper (m1, g). Five specimens were used for each membrane. The liquid sorption capacity was calculated according to the following equation:[41]

$$q = \frac{(m_1 - m_0)/_D}{m_0} \quad (4.3)$$

where D is the liquid density at 25 °C (g cm^{-3}).

4.6.3.8 Specific surface area

The specific surface area of the PPy membranes was evaluated by a nitrogen adsorption-desorption measurement with a Micromeritics ASAP 3020 analyzer (Micromeritics, Norcross, GA, USA) at -196 °C. The samples were degassed in a vacuum at 120 °C for at least 6 h prior to measurement. The specific surface area was calculated according to the Brunauer-Emmett-Teller (BET) method using the software supplied by Micromeritics.

4.6.3.9 Cytotoxicity

The PPy-N membrane was cut into circular specimens to cover the entire bottom of the wells of standard 24-well cell culture plates. The assembly was then sterilized with ethylene oxide (EO) gas at 37 °C according to standard industrial procedures. Prior to cell seeding, the specimens were pre-incubated in Dulbecco's modified Eagle's medium (DMEM, M-0268, Sigma Chemical, St. Louis, MO, USA) for 24 h under cell culture conditions. After refreshing the culture medium, human skin fibroblasts (Clonetics, San Diego, CA, USA) were seeded (1 × 105 cells per well) onto the PPy-N and cultured for 8, 24, and 48 h, after which time the cells on the PPy-N were fixed with 4% paraformaldehyde at 4 °C for 30 min and subsequently washed three times with phosphate buffered saline (PBS). For fluorescent staining, fixed samples were incubated in a solution of 50 µg mL^{-1} Hoechst 33342 (ThermoFisher Scientific, Burlington, ON, Canada) in PBS for 15 min at room temperature. After three washings with PBS, the specimens were observed under an epifluorescence microscope (Axiophot, Zeiss, Oberkochen, Germany) and photographed. Because of the membrane surface structure, it was difficult to detach all of the cells from the specimens. A total protein assay was then performed to correlate protein content with cell numbers. Following PBS washing, 100 µL of cell lysis buffer (Cell Signaling Technology, Whitby, ON, Canada) was added to each well and incubated thereafter in an ice bath for 45 min (pipetting every 5 min). A Bradford protein assay kit (ThermoFisher Scientific) was used to measure the protein concentration in the supernatant obtained after centrifuging at 14000 g for 10 min.

4.6.3.10 Statistical analysis

All of the data are presented as means ± standard deviations ($n \geq 3$). A Student t-test was performed to analyze the statistical difference of the results, with $p < 0.05$ considered statistically significant.

4.7 Author information

Corresponding author

*Correspondence to: Ze.Zhang@chg.ulaval.ca

Address: Hôpital Saint-François d'Assise, 10 rue de l'Espinay, Local E00-177, Québec (QC) G1L 3L5, Canada.

Tel: (418) 525-4416； Fax: (418) 525-4372.

4.8 Acknowledgment

This work was supported by the Natural Sciences and Engineering Research Council of Canada (262258-2011), the Canadian Institutes of Health Research (MOP106555) and Le Centre de recherche du CHU de Québec. The first author acknowledges Les Bourses de la Fondation du CHU de Québec aux étudiants. The technical assistance of Stéphane Turgeon, Pascale Chevallier, Andrée-Anne Guay-Bégin and Ying Mao is greatly appreciated.

4.9 Associated content

Supporting Information. The Supporting Information is available free of charge on the

ACS Publications website:

Additional data and text (PDF);

Movies (AVI), Video file has been filed separately:

Movie S1. Flexibility of PPy-N at room temperature

Movie S2. Flexibility of PPy-P at room temperature

Movie S3. Flexibility of PPy nanotube membrane at room temperature

Movie S4. Flexibility of PPy-N at -196 ^{o}C

Movie S5. Flexibility of PPy nanotube membrane at -196 ^{o}C

Movie S6. Flexibility of PPy membranes under ultrasound

Movie S7. Solvent absorption of PPy-N

Movie S8. Solvent absorption of PPy-P

References

1. Dyer A, Reynolds J, Skotheim T, Reynolds J, *Handbook of conducting polymers. Conjugated polymers: theory, synthesis, properties, and characterization*. 3rd ed.; CRC Press: Boca Raton, 2007; p 3-75.

2. Zhang S, Wang G, Lv G, Yu D, Ding Y, Synthesis and fluorescence properties of a soluble polypyrrole derivative based on a dipyrrole monomer. *Synth. Met.* 2014, 195: 185-192.

3. Detsri E, Dubas ST, Interfacial polymerization of water-soluble polyaniline and its assembly using the layer-by-layer technique. *J. Met., Mater. Miner.* 2009, 19, (1): 39-44.

4. Oh EJ, Jang KS, MacDiarmid AG, High molecular weight soluble polypyrrole. *Synth. Met.* 2001, 125, (3): 267-272.

5. Shi G, Rouabhia M, Wang Z, Dao LH, Zhang Z, A novel electrically conductive and biodegradable composite made of polypyrrole nanoparticles and polylactide. *Biomaterials*. 2004, 25, (13): 2477-2488.

6. Guo B, Glavas L, Albertsson A-C, Biodegradable and electrically conducting polymers for biomedical applications. *Prog. Polym. Sci.* 2013, 38, (9): 1263-1286.

7. Severt SY, Ostrovsky-Snider NA, Leger JM, Murphy AR, Versatile Method for Producing 2D and 3D Conductive Biomaterial Composites Using Sequential Chemical and Electrochemical Polymerization. *ACS Appl. Mater. Interfaces.* 2015, 7, (45): 25281-25288.

8. Bocchi V, Gardini GP, Chemical synthesis of conducting polypyrrole and some composites. *J. Chem. Soc., Chem. Commun.* 1986, (2): 148a-148a.

9. Nakata M, Shiraishi Y, Taga M, Kise H, Synthesis of electrically conductive polypyrrole films by interphase oxidative polymerization. *Die Makromolekulare Chemie*. 1992, 193, (3): 765-771.

10. Sultana I, Rahman MM, Wang J, Wang C, Wallace GG, Liu H-K, All-polymer battery system based on polypyrrole (PPy)/para (toluene sulfonic acid)(pTS) and polypyrrole (PPy)/indigo carmine (IC) free standing films. *Electrochim. Acta*. 2012, 83: 209-215.

11. Zhao C-e, Wu J, Kjelleberg S, Loo JSC, Zhang Q, Employing a flexible and low-cost polypyrrole nanotube membrane as an anode to enhance current generation in microbial fuel cells. *Small*. 2015, 11, (28): 3440-3443.

12. Peng T, Sun W, Huang C, Yu W, Sebo B, Dai Z, Guo S, Zhao X-Z, Self-assembled free-standing polypyrrole nanotube membrane as an efficient FTO-and Pt-free counter electrode for dye-sensitized solar cells. *ACS Appl. Mater. Interfaces.* 2013, 6, (1): 14-17.

13. Wang C, Ding Y, Yuan Y, Cao A, He X, Peng Q, Li Y, Multifunctional, highly flexible, free-standing 3D polypyrrole foam. *Small*. 2016, 12, (30): 4070-4076.

14. Yang X, Zhu Z, Dai T, Lu Y, Facile fabrication of functional polypyrrole nanotubes via a reactive self-degraded template. *Macromol. Rapid Commun.* 2005, 26, (21): 1736-1740.

15. Blinova NV, Stejskal J, Trchová M, Prokeš J, Omastová M, Polyaniline and polypyrrole: A comparative study of the preparation. *Eur. Polym. J.* 2007, 43, (6): 2331-2341.

16. Kaltenbrunner M, Sekitani T, Reeder J, Yokota T, Kuribara K, Tokuhara T, Drack M, Schwödiauer R, Graz I, Bauer-Gogonea S, An ultra-lightweight design for imperceptible plastic electronics. *Nature*. 2013, 499, (7459): 458-463.

17. Ge H, Qi G, Kang E-T, Neoh KG, Study of overoxidized polypyrrole using X-ray photoelectron spectroscopy. *Polymer*. 1994, 35, (3): 504-508.

18. Dong S, Ding J, Study on polypyrrole film by electrochemical polymerization in aqueous solution. *Synth. Met.* 1987, 20, (1): 119-124.

19. Singh A, Salmi Z, Jha P, Joshi N, Kumar A, Decorse P, Lecoq H, Lau-Truong S, Aswal DK, Gupta SK, One step synthesis of highly ordered free standing flexible polypyrrole-silver nanocomposite films at air–water interface by photopolymerization. *RSC Advances*. 2013, 3, (32): 13329-13336.

20. Qi G, Wu Z, Wang H, Highly conductive and semitransparent free-standing polypyrrole films prepared by chemical interfacial polymerization. *J. Mater. Chem. C.* 2013, 1, (42): 7102-7110.

21. Yuan L, Yao B, Hu B, Huo K, Chen W, Zhou J, Polypyrrole-coated paper for flexible solid-state energy storage. *Energy Environ. Sci.* 2013, 6, (2): 470-476.

22. Xu J, Li M, Wu L, Sun Y, Zhu L, Gu S, Liu L, Bai Z, Fang D, Xu W, A flexible polypyrrole-coated fabric counter electrode for dye-sensitized solar cells. *J. Power Sources*. 2014, 257: 230-236.

23. Wang Z, Tammela P, Strømme M, Nyholm L, Nanocellulose coupled flexible polypyrrole@ graphene oxide composite paper electrodes with high volumetric capacitance. *Nanoscale*. 2015, 7, (8): 3418-3423.

24. Pan L, Chortos A, Yu G, Wang Y, Isaacson S, Allen R, Shi Y, Dauskardt R, Bao Z, An ultra-sensitive resistive pressure sensor based on hollow-sphere microstructure induced elasticity in conducting polymer film. *Nat. Commun.* 2014, 5: 3002

25. Peng L, Xu Z, Liu Z, Guo Y, Li P, Gao C, Ultrahigh thermal conductive yet superflexible graphene films. *Adv. Mater.* 2017.

26. Zhang L, Zhang Z, Electrical field directed electropolymerization of free-standing film of polypyrrole and poly (1-(2-carboxyethyl) pyrrole at the air/liquid interface. *Synth. Met.* 2011, 161, (9): 724-730.

27. Qi G, Huang L, Wang H, Highly conductive free standing polypyrrole films prepared by freezing interfacial polymerization. *Chem. Commun.* 2012, 48, (66): 8246-8248.

28. Wu J, Sun Y, Pei W-B, Huang L, Xu W, Zhang Q, Polypyrrole nanotube film for flexible thermoelectric application. *Synth. Met.* 2014, 196: 173-177.

29. Mott N, Davis E, Electronic processes in non-crystalline solids. *Clarendon, Oxford*. 1979: 465.

30. Wang Y, Jiang H, Tao Y, Mei T, Liu Q, Liu K, Li M, Wang W, Wang D, Polypyrrole/poly (vinyl alcohol-co-ethylene) nanofiber composites on polyethylene terephthalate substrate as flexible electric heating elements. *Composites Part A.* 2016, 81: 234-242.

31. Jeong YG, Jeon GW, Microstructure and performance of multiwalled carbon nanotube/m-aramid composite films as electric heating elements. *ACS Appl. Mater. Interfaces.* 2013, 5, (14): 6527-6534.

32. Isaji S, Bin Y, Matsuo M, Electrical conductivity and self-temperature-control heating properties of carbon nanotubes filled polyethylene films. *Polymer*. 2009, 50, (4): 1046-1053.

33. Rouabhia M, Park HJ, Zhang Z, Electrically activated primary human fibroblasts improve in vitro and in vivo skin regeneration. *J. Cell. Physiol.* 2016, 231, (8): 1814-1821.

34. Wei Y, Mo X, Zhang P, Li Y, Liao J, Li Y, Zhang J, Ning C, Wang S, Deng X, Jiang L, Directing Stem Cell Differentiation via Electrochemical Reversible Switching between Nanotubes and Nanotips of Polypyrrole Array. *ACS Nano*. 2017, 11, (6): 5915-5924.

35. Shinde SS, Gund GS, Kumbhar VS, Patil BH, Lokhande CD, Novel chemical synthesis of polypyrrole thin film electrodes for supercapacitor application. *Eur. Polym. J.* 2013, 49, (11): 3734-3739.

36. Wang Z, Carlsson DO, Tammela P, Hua K, Zhang P, Nyholm L, Strømme M, Surface Modified Nanocellulose Fibers Yield Conducting Polymer-Based Flexible Supercapacitors with Enhanced Capacitances. *ACS Nano*. 2015, 9, (7): 7563-7571.

37. Mihic A, Cui Z, Wu J, Vlacic G, Miyagi Y, Li S-H, Lu S, Sung H-W, Weisel RD, Li R-K, A conductive polymer hydrogel supports cell electrical signaling and improves cardiac function after implantation into myocardial infarct. *Circulation*. 2015, 132, (8): 772-784.

38. Wu Y, Wang L, Guo B, Ma PX, Interwoven Aligned Conductive Nanofiber Yarn/Hydrogel Composite Scaffolds for Engineered 3D Cardiac Anisotropy. *ACS Nano*. 2017, 11, (6): 5646-5659.

39. Mao J, Zhang Z, One-step reactivity-driven synthesis of core–shell structured electrically conducting particles for biomedical applications. *J. Mater. Chem. B.* 2016, 4, (32): 5429-5436.

40. Smits F, Measurement of sheet resistivities with the four-point probe. *Bell Syst. Tech. J.* 1958, 37, (3): 711-718.

41. Wu J, Wang N, Wang L, Dong H, Zhao Y, Jiang L, Electrospun porous structure fibrous film with high oil adsorption capacity. *ACS Appl. Mater. Interfaces.* 2012, 4, (6): 3207-3212.

Supplementary materials for

Conductive Polymer Waving in Liquid Nitrogen

Jifu Mao,[†,‡] Chaojing Li,[†,‡,§] Hyun Jin Park,[†,‡,‖] Mahmoud Rouabhia,[‖] Ze Zhang[*,†,‡]

†Département de chirurgie, Faculté de médecine, Université Laval, Québec (QC), G1V 0A6, Canada.

‡L'Axe médecine régénératrice, Centre de recherche du CHU de Québec (QC), G1L 3L5, Canada.

§Key Laboratory of Textile Science and Technology of Ministry of Education and College of Textiles, Donghua University, 2999 North Renmin Road, Shanghai 201620, China.

‖Groupe de Recherche en Écologie Buccale, Faculté de Médecine Dentaire, Université Laval, Québec (QC), Canada.

4.10 Supplementary text

4.10.1 Thickness

Based on SEM observations, the thickness of the PPy-N was between 0.30 and 0.48 mm, and that of the PPy-P membranes was between 0.25 and 0.40 mm. PPy-N thickness decreased to 0.17 mm when measured with a thickness gauge under 22 kPa (Table S4.1); the reason is that the PPy bubbles on the PPy-N were soft and easily compressed. In the PPy-P, the bubbles were much smaller and the particle layer was thick and compact, resulting in no significant change in thickness upon pressure.

4.10.2 Absorption capacity

Both PPy-N and PPy-P displayed a superwetting behavior to nonpolar solvent (i.e., heptane) compared to water (Movies S4.7 and S4.8, video file has been filed separately). Nevertheless, both types of membrane showed a similar adsorption capacity to water and heptane. For example, the PPy-N absorbed 2230% of water and 1440% of heptane in weight gain, which is comparable to that of the cryptomelane nanowire membrane.[1]

4.10.3 A plausible mechanism of bubbles formation

To investigate the mechanism of bubble formation, polymerizations were also performed at -20 ℃ and 22 ℃ to compare with that at 4 ℃. As shown in Figure S4.1, a thin transparent film formed at the interface in the first few minutes in the system without MO (Figure S4.1A2), while the film formed in the TIP system was opaque with micro-structures. After 48 h, the entire aqueous phase of the system without MO turned black because of the homogeneous polymerization (Figure S4.2). In the TIP system, the black product was only found near the water/chloroform interface, proving that the polymerization was inhomogeneous in the presence of the MO template. A noticeably thin PPy film also formed at the air/water interface (Figure S4.2A1); this film was absent in the TIP system, showing that no Py monomers diffused to the entire water phase. Macroscopically, the bottom side of the films (facing the chloroform) had a very different appearance, i.e., smooth vs. bubbly (Figure S4.2, A2 vs. B2). The morphology of the PPy-N and PPy-P membranes polymerized at -20 ℃ and 22 ℃ is shown in Figs. S4.4 and S4.5. With the increase in temperature, a

thicker, heavier PPy membrane was formed with larger bubbles, showing an increasing conversion of Py. The PPy bubbles were approximately 400 and 150 μm in diameter for the PPy-N and PPy-P membranes synthesized at 4 ℃, respectively. At -20 ℃, the membranes became much thinner (Figure S4.4, B and E) and the bubbles collapsed (Figure S4.4, A and D). The PPy nanotubes appeared dense and fused (Figure 4.4C) and the PPy particles were discrete (Figure 4.4F). When the reaction took place at 22 ℃, large, millimeter range-sized multilayered bubbles formed no matter with or without the MO template (Figure S4.5). This positive relationship between bubble size and reaction temperature supports our theory that the formation of the bubbles was due to chloroform evaporation. The reaction localized near the water/chloroform interface resulted in more heat being released at the interface and consequently more bubbles in the TIP system. The larger bubbles were likely from the fusion of small bubbles, as demonstrated by the dynamic bubble-forming process (Figure S4.3).

4.10.4 Conductivity

The conductivity of PPy-N was calculated using the following formula (4.4):

$$\sigma=1/\rho=L/(R\times S)=(I\times L)/(V\times S) \qquad (4.4)$$

where ρ is the surface electrical resistivity (Ω cm), R the resistance (Ω), L the length of the membrane (cm), S the cross-section (cm^2), I the current (ampere), and V the voltage (volt).

The calculated conductivity was 1.15 S cm^{-1} which was comparable to the value obtained by the four-point probe (1.5 S cm^{-1}).

Contrary to metals, the conductivity of conducting polymers decreases with the decrease in temperature, as described by the Mott 3-dimensional variable-range hopping conduction model (4.5):[2, 3]

$$ln\sigma = A - (T_0/T)^{-1/4} \qquad (4.5)$$

where A is a constant and T_0 denotes to the characteristic Mott temperature.

4.10.5 Three characteristics of electric heating

The T-t curves at various voltages can be divided into three regions, and three important characteristics can be calculated for each region using certain formulas.[4-7] The temperature growth region can be empirically described as (4.6):

$$\frac{T_t - T_0}{T_m - T_0} = 1 - e^{-t/\tau_g} \quad (4.6)$$

where T_0, T_m and T_t are the initial temperature, maximum temperature, and temperature at time t, respectively. τ_g is the characteristic growth time constant, which can be calculated from the first region in Figure 4.4D.

In the steady-state temperature region, the heat transferred by radiation and convection (h_{r+c}) was obtained by the following equation (4.7):

$$h_{r+c} = \frac{I_c \times V_0}{T_m - T_0} \quad (4.7)$$

where I_c is the steady-state current and V_0 is the applied voltage.

In the decay region, the PPy-N was cooled down by radiation and convection, with the decrease in temperature *vs* time described by the following empirical formula (4.8):

$$\frac{T_t - T_0}{T_m - T_0} = e^{-t/\tau_d} \quad (4.8)$$

where τ_d is the decay time constant. The τ_d values were calculated by fitting the experimental data of temperature decay as a function of time.

4.10.6 Bending of a thin-walled sheet

Figure S4.8 illustrates the bending of a thin-walled sheet. Bending causes tension at the top and compression at the bottom. At the neutral surface (red line), there is no tension or compression representing the original length.

The strain of the top layer is therefore (4.9-4.10):

$$\varepsilon = \frac{\Delta L}{L} = \frac{\left(R + \frac{a}{2}\right)\theta - R\theta}{R\theta} \quad (4.9)$$

$$R = \frac{a}{2\varepsilon} \quad (4.10)$$

where, ε is the strain, ΔL is the change of the length of the outer layer, L is the original length, R is the radius of curvature, a is plate thickness, and θ is the angle in radians.

This novel PPy-N membrane consists of three layers: the nanotube layer, a thin membrane in the middle, and a bubble layer. We found that a membrane made of PPy nanotubes did not have high flexibility (Movie S4.3, video file has been filed separately), that the nanotubes on the PPy-N membrane could be physically removed, and that it was possible for the nanotube-free PPy-N membrane to remain flexible.

We thus conclude that PPy nanotubes on the membrane were not required to maintain the flexibility of the membrane. Consequently, only the membrane in the middle and the bubbles were calculated according to the above-stated formula. The middle layer displayed a maximum thickness of approximately 1 μm and the bubbles had a wall thickness of approximately 200 nm. For a plate 1 μm in thickness and a maximum strain of 2.5%, the minimum radius was calculated to be 20 μm, meaning that the middle membrane could withstand a very large bending without being broken. Because the wall thickness of the bubbles was much smaller, the wall of the PPy bubbles could deform even further (4 μm in radius of curvature).

Table S4.1 Properties of PPy membranes prepared by interfacial polymerization.

	Thickness[a)] (mm)	Areal density (g m^{-2})	Conductivity[b)] (S cm^{-1})	Specific surface area[c)] (m^2 g^{-1})	Break stress (KPa)	Break strain (%)	Elastic modulus (MPa)	Liquid adsorption (cm^3 g^{-1})	
								water	heptane
PPy-P	0.35±0.03	54.3±7.8	0.30±0.06	6.38±0.06	15.4±1.8	2.4±0.2	0.6±0.1	5.5±1.1	5.3±1.2
PPy-N	0.17±0.01	8.9±0.5	1.54±0.12	14.52±0.24	82.5±9.7	2.3±0.3	3.9±0.7	22.3±2.0	21.2±2.6

[a)]Measured with a digital thickness gauge under 22 kPa; [b)]Measured with the Jandel Multi Height Four-Point Probe; [c)]BET surface area.

Table S4.2 Surface elemental analysis by XPS (Atomic %).

		C_{1s}	N_{1s}	O_{1s}	Cl_{2p}	N_{1s}^{+}/N_{1s}
PPy-P	water phase	73.8±0.3	16.2±0.3	6.6±0.2	3.4±0.2	18.0±0.9
	chloroform phase	75.4±0.6	16.3±0.6	4.4±0.7	3.7±0.2	18.5±0.3
PPy-N	water phase	72.3±0.7	15.2±0.5	10.4±0.4	2.1±0.3	15.6±0.5
	chloroform phase	76.4±0.6	15.1±0.6	5.0±0.2	3.5±0.3	19.4±0.2

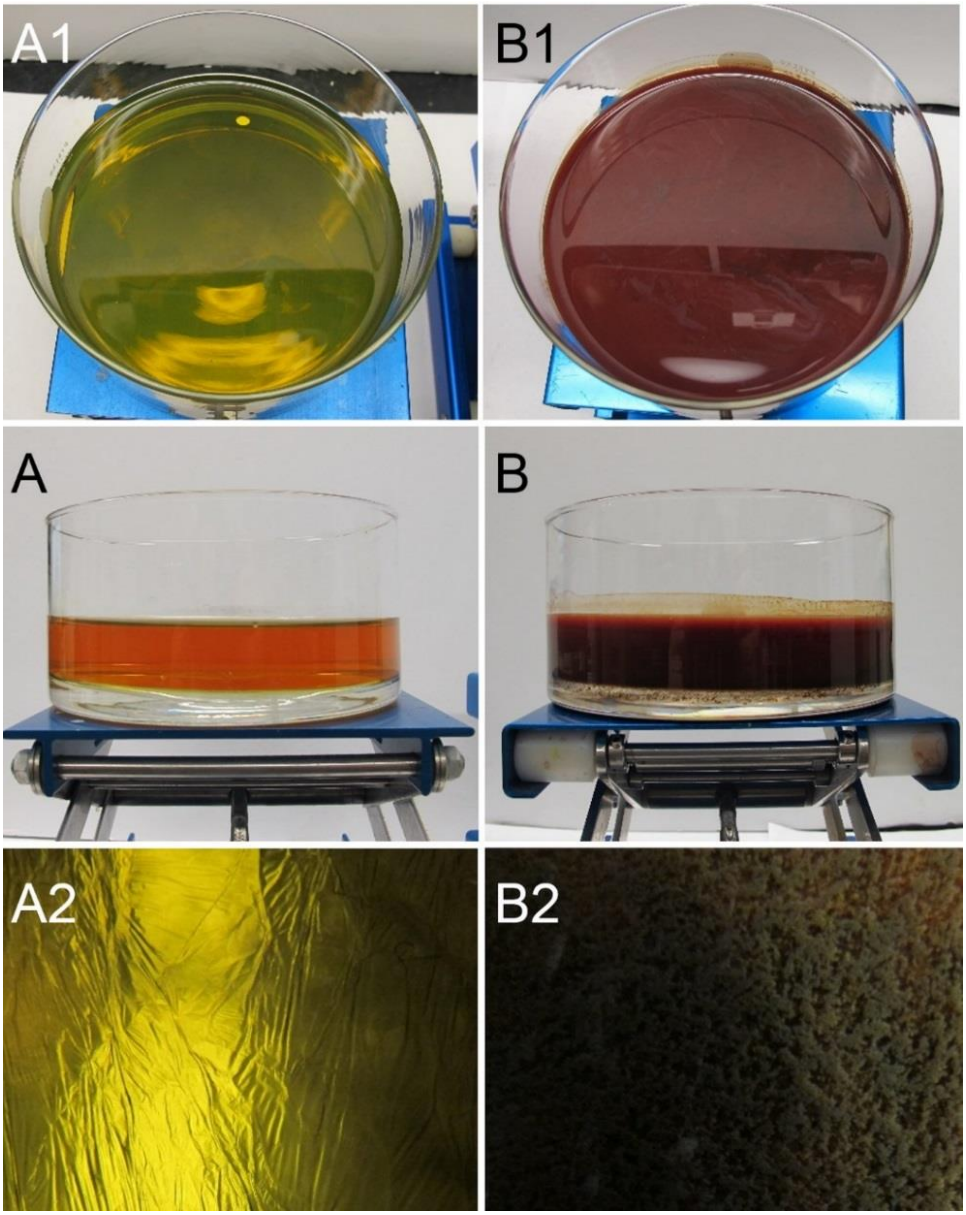

Figure S4.1 Photographs taken at 10 minutes after polymerization. (A) Without the MO template. (B) With the MO template (TIP). (A and B) Side view. (A1 and B1) Top view. (A2 and B2) Bottom view.

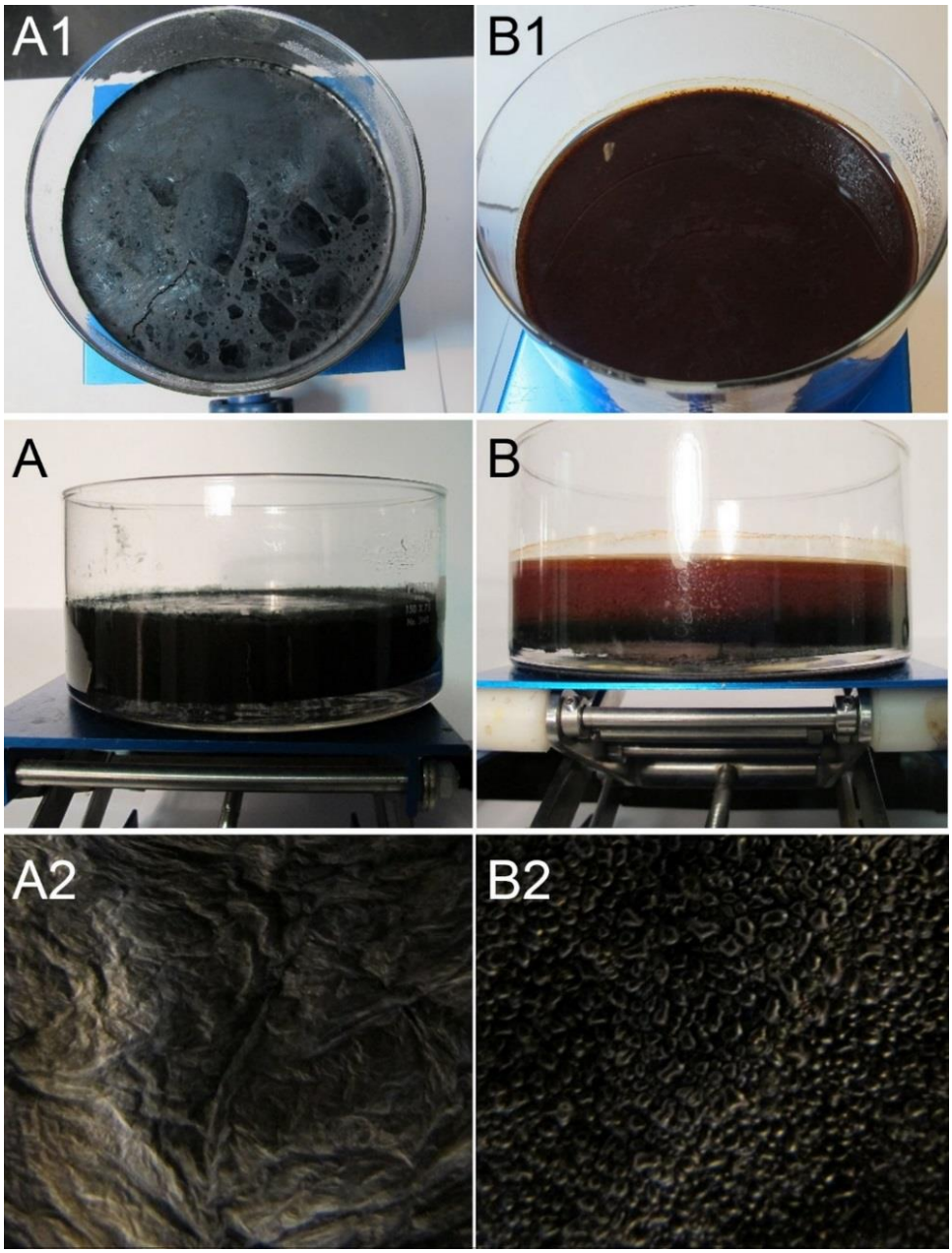

Figure S4.2 Photographs taken after polymerization. (A) Without the MO template. (b) With the MO template (TIP). (A and B) Side view. (A1 and B1) Top view. (A2 and B2) Bottom view.

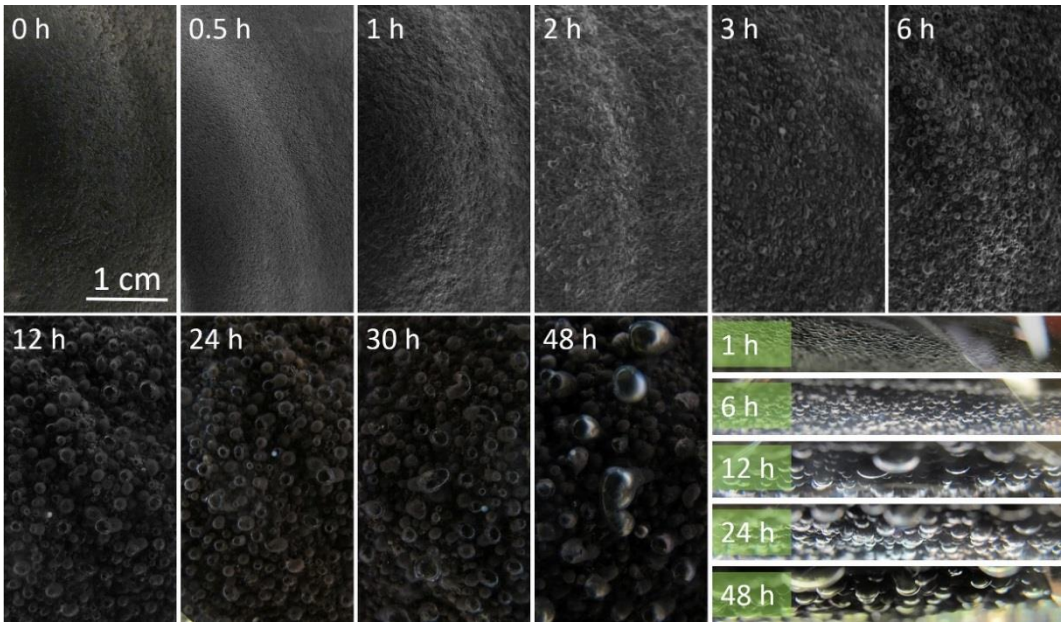

Figure S4.3 Appearance and growth of the bubbles at the chloroform side of the PPy-N membrane synthesized at 22˚C.

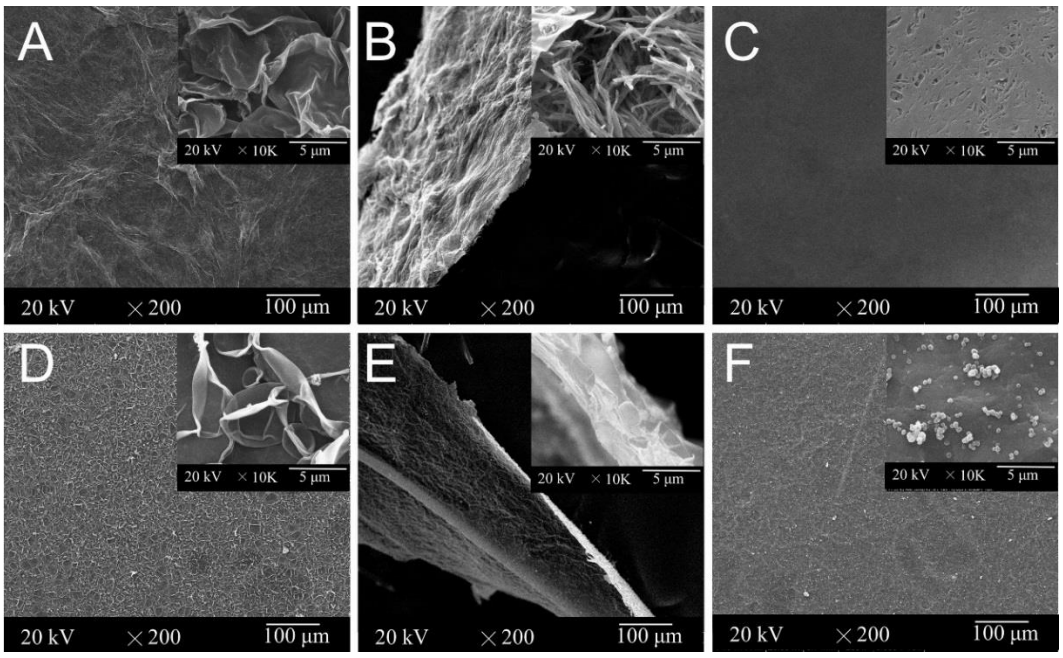

Figure S4.4 Scanning electron microscopy photomicrographs of PPy-N and PPy-P membrane synthesis at -20 ˚C. (A-C) PPy-N. (A) Bubble side. (B) Cross section. (C) Nanotube side. (D-F) PPy-P. (D) Bubble side. (E) Cross section. (F) Particle side. (A-F) Inset: High magnification.

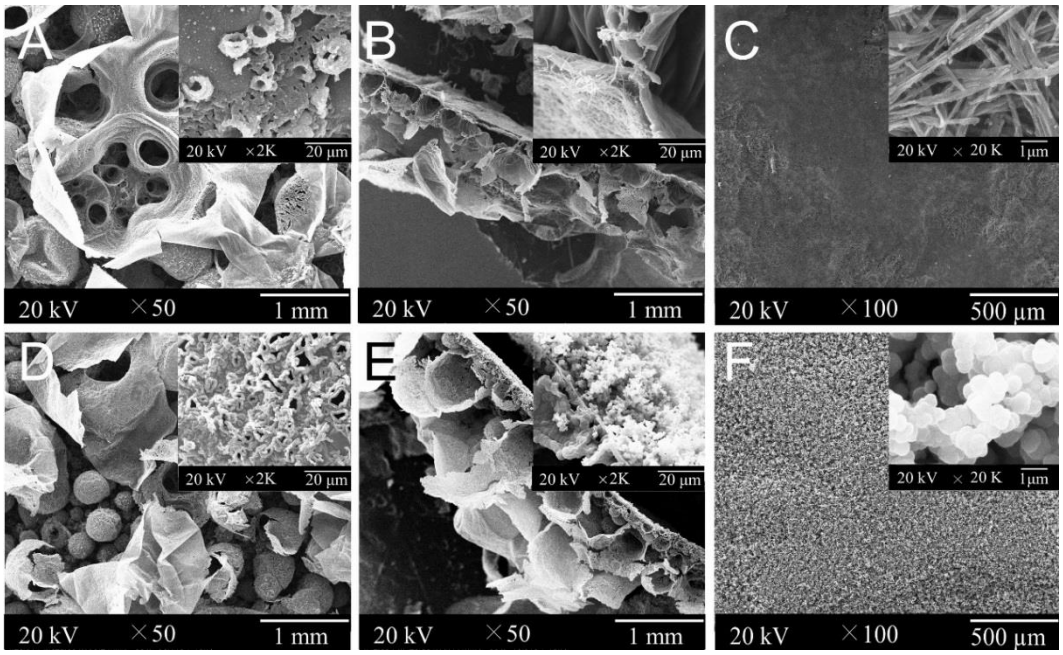

Figure S4.5 Scanning electron microscopy photomicrographs of PPy-N and PPy-P membrane synthesis at 22 ˚C. (A-C) PPy-N. (A) Bubble side. (B) Cross section. (C) Nanotube side. (D-F) PPy-P. (D) Bubble side. (E) Cross section. (F) Particle side. (A-F) Inset: High magnification.

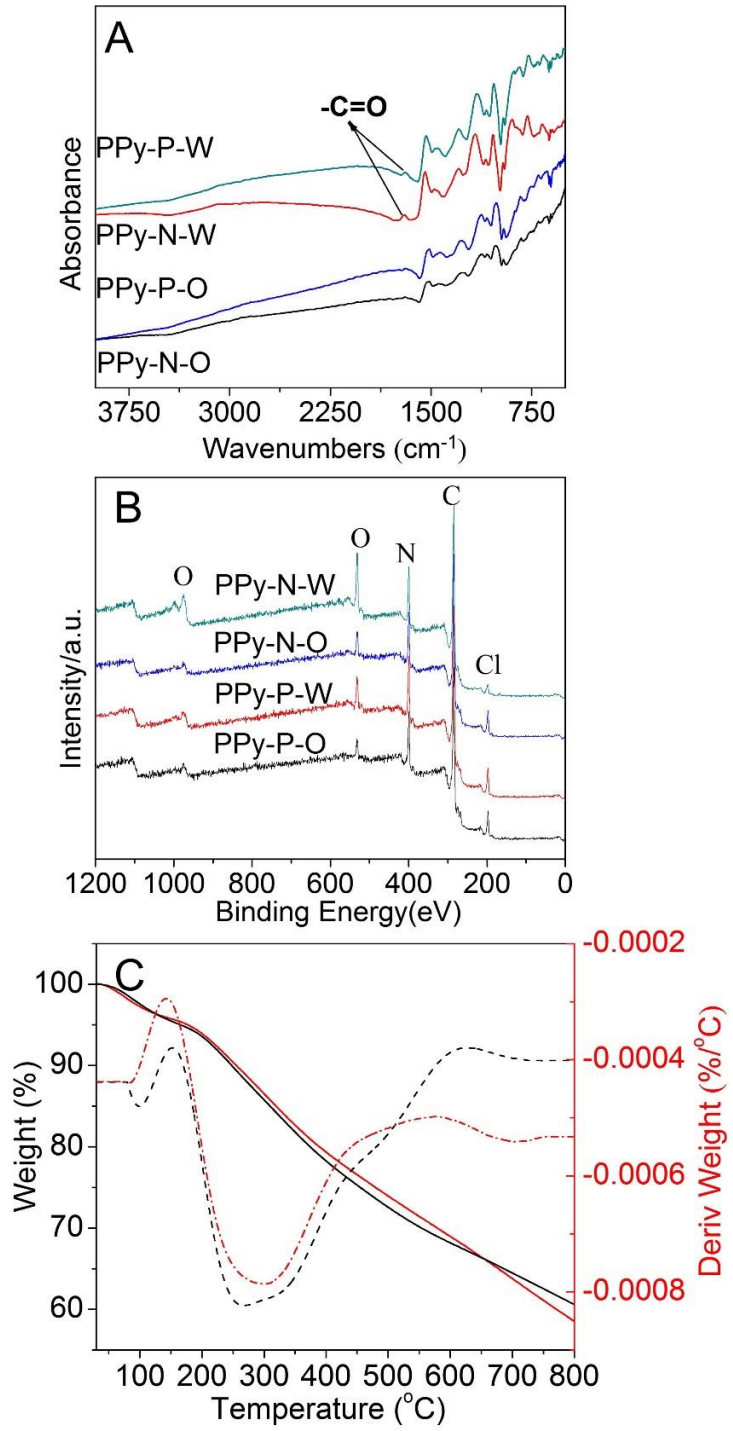

Figure S4.6 Chemical and thermal properties of PPy-N and PPy-P. (A) Attenuated total reflectance Fourier transform infrared spectroscopy (ATR-FTIR) spectra. (B) Full scans of X-ray photoelectron spectroscopy (XPS). (C) Thermograms of thermogravimetric analysis (TGA). PPy-N-O: side of PPy-N facing the chloroform; PPy-P-O: side of PPy-P facing the chloroform; PPy-N-W: side of PPy-N facing the water; PPy-P-W: side of PPy-P facing the water.

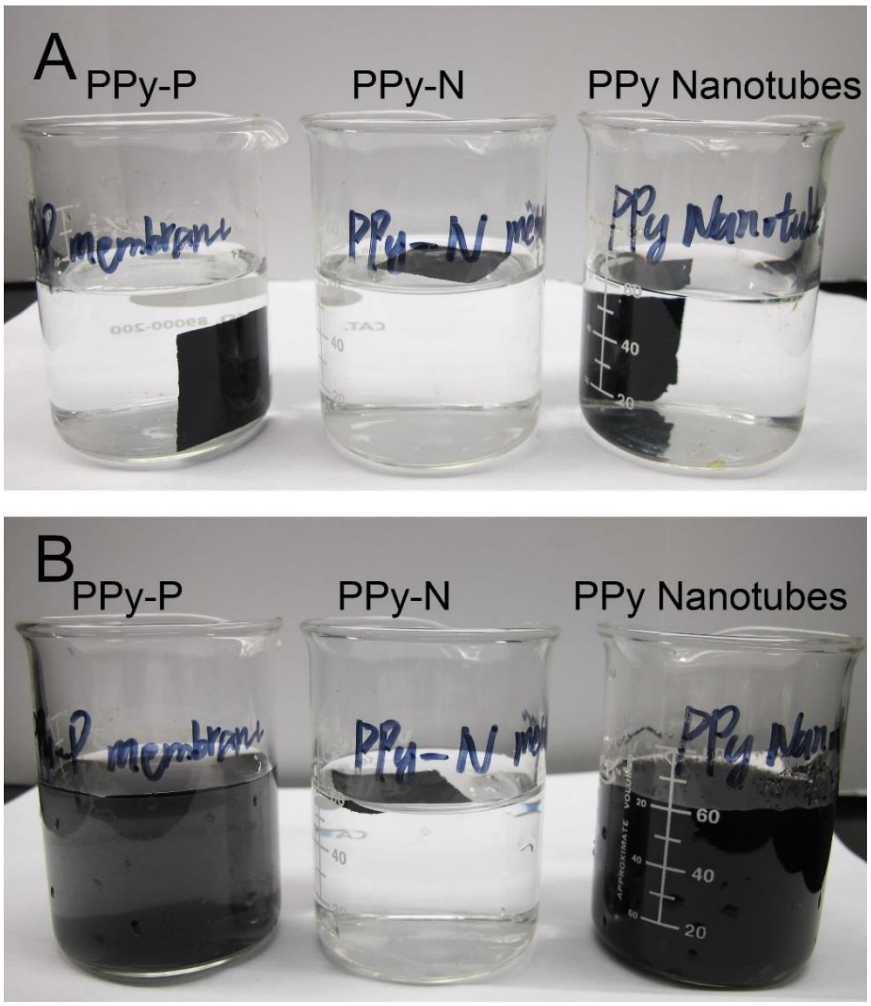

Figure S4.7 Stability of the PPy-N, PPy-P, and PPy nanotube-cast membranes under ultrasound treatment. (A) Before ultrasound treatment. (B) After 30 min of ultrasound treatment.

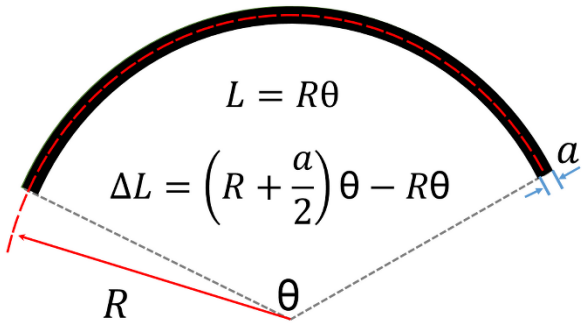

Figure S4.8 Illustration of the bending of a thin-walled plate. R: radius of curvature; θ: radian of curvature; L: length of neutral line; ΔL: change in length of the external layer; a: thickness of the plate.

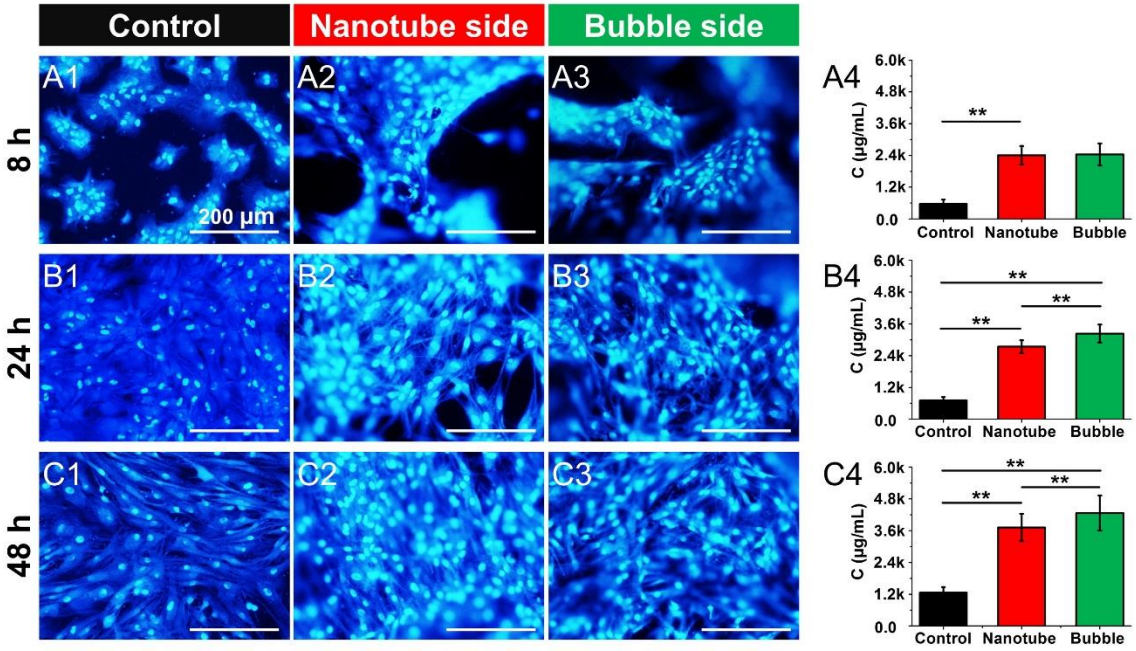

Figure S4.9 Attachment and growth of human skin fibroblasts on PPy-N. Left panel (1-3): Cell nuclei stained with Hoechst fluorescent dye. Right panel (4): Quantification of cell membrane proteins (Bradford assay) as an indication of cell numbers. ** $p < 0.01$, $n \geqslant 4$.

Movie S4.1 Flexibility of PPy-N at room temperature

Movie S4.2 Flexibility of PPy-P at room temperature

Movie S4.3 Flexibility of PPy nanotube membrane at room temperature

Movie S4.4 Flexibility of PPy-N at -196 ^{o}C

Movie S4.5 Flexibility of PPy nanotube membrane at -196 ^{o}C

Movie S4.6 Flexibility of PPy membranes under ultrasound

Movie S4.7 Solvent absorption of PPy-N

Movie S4.8 Solvent absorption of PPy-P

Reference

1. Yuan J, Liu X, Akbulut O, Hu J, Suib SL, Kong J, Stellacci F, Superwetting nanowire membranes for selective absorption. *Nat. Nanotechnol.* 2008, 3, (6): 332-336.

2. Singh A, Salmi Z, Jha P, Joshi N, Kumar A, Decorse P, Lecoq H, Lau-Truong S, Aswal DK, Gupta SK, One step synthesis of highly ordered free standing flexible polypyrrole-silver nanocomposite films at air–water interface by photopolymerization. *RSC Advances*. 2013, 3, (32): 13329-13336.

3. Mott N, Davis E, Electronic processes in non-crystalline solids. *Clarendon, Oxford*. 1979: 465.

4. Wang Y, Jiang H, Tao Y, Mei T, Liu Q, Liu K, Li M, Wang W, Wang D, Polypyrrole/poly (vinyl alcohol-co-ethylene) nanofiber composites on polyethylene terephthalate substrate as flexible electric heating elements. *Composites Part A*. 2016, 81: 234-242.

5. Jeong YG, Jeon GW, Microstructure and performance of multiwalled carbon nanotube/m-aramid composite films as electric heating elements. *ACS Appl. Mater. Interfaces*. 2013, 5, (14): 6527-6534.

6. Isaji S, Bin Y, Matsuo M, Electrical conductivity and self-temperature-control heating properties of carbon nanotubes filled polyethylene films. *Polymer*. 2009, 50, (4): 1046-1053.

7. Yoon YH, Song JW, Kim D, Kim J, Park JK, Oh SK, Han CS, Transparent Film Heater Using Single-Walled Carbon Nanotubes. *Adv. Mater*. 2007, 19, (23): 4284-4287.

CHAPTER V

PREPARATION AND CHARACTERIZATION OF FUNCTIONAL AND FLEXIBLE POLYPYRROLE MEMBRANE

A Novel Modular Approach to Prepare a Multi-Biofunctional Surface by Using Flexible and Electrically Conducting Polypyrrole Membranes and Functional Particles

(To be submitted)

Jifu Mao and Ze Zhang*

Département de chirurgie, Faculté de médecine, Université Laval, Québec (QC), Canada.

L'Axe médecine régénératrice, Centre de recherche du CHU de Québec, Québec, Canada

E-mail: Ze.Zhang@chg.ulaval.ca

Keywords: poly(pyrrole-co-(1-(2-carboxyethyl)pyrrole)); functional particles; flexible membrane; biofunctionalization; polypyrrole

5.1 Résumé

L'immobilisation de protéines bioactives à la surface des dispositifs médicaux, des échafaudages de tissus ou des implants médicaux requiert fréquentent des techniques sophistiquées, en particulier lorsque plusieurs types de protéines sont essentiels. Dans ce travail, une stratégie modulaire a été proposée pour former un échafaudage à membrane électriquement conducteur et flexible avec double fonctionnalité, en utilisant la membrane de polypyrrole flexible (PPy) et le poly(pyrrole-co-(1-(2-carboxyéthyl) pyrrole) (P(Py-PyCOOH)) en tant que modules à assembler. L'albumine de sérum bovine (HSA) et de sérum humain (HSA) comme molécules modèles ont été immobilisées de manière covalente sur la surface de la particule, séparément, et les particules greffées de protéines ont été mélangées dans un ratio de 1:1 et assemblées sur la membrane souple pour construire un échafaudage avec coexistence de deux types de biomolécules. Cette stratégie modulaire offre une solution simple pour immobiliser de multiples biomolécules en quantités bien définies sur un substrat.

5.2 Abstract

Immobilization of bioactive proteins to the surface of medical devices, tissue engineering scaffolds or medical implants often requires sophisticated techniques, particularly, when multiple types of proteins are essential. Recently, a soft and flexible PPy membrane and the functional poly(pyrrole-co-(1-(2-carboxyethyl)pyrrole)) (P(Py-PyCOOH)) copolymer particles were synthesized through a template-assisted interfacial polymerization (TIP) and a simple one step emulsion polymerization, respectively. In this work, a modular strategy was proposed, which used the flexible PPy membrane and functional particles as modules and assembled them together. In such a way, a thin layer of (P(Py-PyCOOH)) particles with more than one bioactivity was integrated onto the nanotube side of the flexible PPy membrane, forming a dual biofunctionalized flexible and electrically conducting membrane scaffold. The PPy membranes with varying quantity of functional particles were characterized by scanning electron microscopy (SEM), Fourier transform infrared spectroscopy (FTIR) and four-point probe to investigate the optimal particle feeding that was found to be 0.27 mg cm^{-2}. Bovine serum albumin (BSA) and human serum albumin (HSA) as model molecules were covalently immobilized onto the particle surface, separately; and the protein grafted particles were mixed at 1:1 ratio and assembled onto the flexible membranes to construct a conducting scaffold with the coexistence of two types of biomolecules. This modular strategy provides an easy solution to immobilize multiple biomolecules at a well-defined quantity onto a substrate. The electrically conductive and multi-biofunctional flexible PPy membrane can be an excellent material platform for biomedical applications such as multi-target biosensing and multifunctional electrical stimulation.

5.3 Introduction

Polypyrrole (PPy), one of the p-type semiconducting polymers, has shown considerable potential in biomedical applications such as in tissue engineering, neural prostheses, artificial muscle, and biosensors, owing to its inherent electrical conductivity, ease synthesis, potential of chemical modification, and biocompatibility [1-5]. However, two critical shortcomings of PPy have greatly restricted its application in biomedicine, i.e., the inferior mechanical properties and the lack of biofunctionality. PPy is a π-conjugated polymer formed by a number of pyrrole rings repeatedly connected through not only α sites but also β sites, which allows different spatial arrangements of pyrrole rings and forms a cross-linked chain network [6]. Thus, there is not any functional group on PPy that may permit further biofunctionalization. Meanwhile, due to its unique extensively conjugated and cross-linked molecular structure, PPy is rigid, brittle, insoluble and infusible, resulting in a great difficulty in processing once synthesized.

In order to biofunctionalize PPy, various methods have been proposed to incorporate biomolecules, including physical adsorption and entrapment [7], doping [8], and copolymerization of pyrrole with its functional derivatives to obtain functional PPy that can be further used for covalent immobilization [9-13]. Covalent bonding on surface is the most reliable method to immobilize biomolecules compared with physical adsorption and doping that suffer low loading, decrease in conductivity, uncontrollable diffusion of biomolecules, and decline in biomolecule activity during polymerization. Poly(pyrrole-co-(1-(2-carboxyethyl)pyrrole)) (P(Py-PyCOOH)), a typical N-functionalized PPy copolymer, has been widely studied as a substrate for biomolecule immobilization [14-16]. Through covalent linkages, enzymes, DNA and antibodies were introduced to P(Py-PyCOOH) to construct enzyme biosensors [17], DNA biosensors [18] and immunosensors [19]. For such applications, a high density of functional groups on the surface and a sufficient electrical conductivity are both required. However, the conductivity of PPyCOOH homopolymers is lower than that of the P(Py-PyCOOH) copolymers. Even for the copolymer, the conductivity will decrease with increasing ratio of PyCOOH [20]. Therefore the requirements for more surface functional groups and high conductivity contradict each other. In our previous study, core-shell P(Py-PyCOOH) particles were synthesized through a simple one step emulsion polymerization

based on the difference in comonomer reactivity [21, 22]. These particles featured pure PPy as the core and PPyCOOH as the shell, which ideally solved the dilemma between reactivity and conductivity.

Meanwhile, attempts have been made to improve the mechanical performance of PPy via nano/microstructural design without using supporting components [23-25]. For example, a free-standing PPy membrane with a certain degree of flexibility was constructed by casting a PPy nanotube solution [24, 26]. However, such a film exhibits more fragile performance rather than an incommensurable flexibility compared with the PPy composite membranes. Through interfacial polymerization, highly conductive and semitransparent free-standing PPy films were reported, which however were very small in size and were only several hundred nanometers in thickness [27, 28]. Such extremely thin films are very fragile and not suitable for applications. To address the above problems, our research group succeeded in the synthesis of a first-ever, large-sized, flexible and mechanically processable PPy membrane through a template assisted interfacial polymerization (TIP) [29]. This PPy membrane exhibited incredible capability to bend and fold repeatedly at room temperature and in liquid nitrogen. However, for now, it is still a challenge to prepare a functional and flexible PPy-COOH membrane because of the low reactivity of PyCOOH.

In this paper, we used the functional core-shell P(Py-PyCOOH) particles and the flexible PPy membranes as modules and assembled them together to form a functional and flexible conductive scaffold membrane. By this strategy, different proteins such as antibodies and growth factors can be separately immobilized onto the functional particles, which will then be integrated into the flexible PPy membrane according to desired ratio. Such a bioactive and electrically conductive flexible membrane may find applications in sensing and electrical stimulation in medicine.

5.4 Experiment

5.4.1 Materials

Pyrrole (Py, 98%, Alfa Aesar-A Johnson Matthey Company, Ward Hill, MA, USA) was distilled twice under reduced pressure and stored in a refrigerator at 4 °C prior to use. 1-(2-

Cyanoethyl)pyrrole (PyCN, 98%, Sigma-Aldrich, Oakville, Ontario, Canada), dodecylbenzenesulfonic acid sodium (DBS, Sigma-Aldrich), ferric chloride hexahydrate ($FeCl_3 \cdot 6H_2O$, 97%, Laboratoire Mat, Quebec, QC, Canada), methyl orange (MO, ACS reagent, dye content 85 %, Sigma-Aldrich), N-hydroxysuccinimide (NHS, 98%, Sigma-Aldrich), N-(3-dimethylaminopropyl)-N'-ethylcarbodiimide hydrochloride (EDC, 98%, Sigma-Aldrich), FITC conjugated bovine serum albumin (BSA, Sigma-Aldrich), rhodamine conjugated human serum albumin (HSA, Abcam Inc), Triton X-100 (Sigma-Aldrich) and all other chemicals (Analytical Grade) were used as received.

5.4.2 Preparation of PPy membranes

The flexible PPy membranes were synthesized through TIP, a process described in detail in our previous work [29]. In brief, 18.2 g $FeCl_3 \cdot 6H_2O$ was added to 320 mL water solution containing 5 mM methyl orange (MO) with vigorous stirring for 30 min to form a suspension of the $FeCl_3$/MO complex templates. And then, the above suspension was transferred to the top of 150 mL chloroform containing 3 mL pyrrole monomer, followed by a polymerization at 4 °C for 48 hours. The membrane formed at the water/chloroform interface was carefully collected and washed in ethanol, 70% ethanol with 1 M HCl, and in deionized water until the washing solution turned to colorless and neutral. Finally the PPy membrane was placed on a Teflon plate and dried at room temperature.

5.4.3 Polymerization of P(Py-PyCOOH) particles

Firstly, the functional monomer PyCOOH was prepared via hydrolysis of PyCN, according to Maeda et al. [30]. Then the P(Py-PyCOOH) core-shell particles were prepared using a simple water-in-oil emulsion polymerization according to our previous report[21, 22]. Typically, 16.5 mL of aqueous solution of $FeCl_3 \cdot 6H_2O$ (20.9 g) was added into 60 mL $CHCl_3$ containing 1 g DBS with mechanical stirring (30 min) and N_2 protection to form an emulsion. After that, 15 mL of $CHCl_3$ containing 15 mmol Py/PyCOOH (1:1, mol/mol) mixture was added dropwise into the above emulsion. The reaction was maintained at room temperature for 3 h with N_2 protection, and then terminated by demulsification with methanol. The product was harvested and purified through vacuum filtration (polyvinylidene fluoride filter membrane, 0.45 μm of pore size, Sigma-Aldrich) and washing in a series of solutions including methanol,

methanol/water (50/50, v/v) mixture, 1M HCl, and deionized water, 3 times in each solution. The final product was obtained after drying under vacuum for at least 48 h.

5.4.4 Preparation of flexible and functional PPy membranes

A varying quantity of P(Py-PyCOOH) particles (1 to 20 mg) was ultrasonically dispersed in 5 mL of ethanol (30 min). And then, 1 mL particle suspension was dropped with pipette to cover a wet rectangular PPy membrane (7.5 cm × 2.5 cm), a process that was repeated for 5 times. The particle coated PPy membranes were moved to a Teflon plate for evaporation of ethanol at room temperature (24 hours). In order to remove the loosely attached particles, the membranes were washed in ethanol in an ultrasound bath (B2500A-DTH, VWR Scientific, Alberta, CA) for at least 30 min, with the ethanol changed five times until the solution became colorless. Finally, the membranes were dried again as described above. The changes in sample weight were used to evaluate the residual percentage of feeding particles after wash (P_R), and the weight ratio of immobilized particles (P_F) following the equations (5.1-5.2):

$$\boldsymbol{P_R = \frac{m_1 - m_0}{m_p}} \qquad (5.1)$$

$$\boldsymbol{P_F = \frac{m_1 - m_0}{m_0}} \qquad (5.2)$$

where m_1 is the mass of the functionalized PPy membrane after wash; m_0 is the mass of the PPy membrane before adding particles; m_p is the feeding of functional particles.

5.4.5 Grafting of model molecules

Figure 5.1 illustrates the process of grafting model proteins onto the flexible PPy membrane. To do so, 20 mg particles were dispersed in 10 mL aqueous solution containing 0.4M EDC and 0.1M NHS and incubated for 45 min. The activated particles were collected by vacuum filtration and washed in PBS 3 times. After washing, 10 mg activated particles were incubated in 3 mL of FITC conjugated BSA or rhodamine conjugated HAS (200 µg/mL) PBS solution at 4 °C overnight. After, the protein grafted particles were filtered and washed sequentially with PBS, 0.1% Triton X-100 and PBS, to remove the non-specifically absorbed proteins. The BSA and HSA grafted particles (each 2.5 mg) were mixed and dispersed in 5 mL of

water, and coated onto the freshly prepared wet PPy membrane, followed by drying, wash in ultrasound bath, and drying again, as described in previous text. The protein immobilized membranes were observed and photographed with an epifluorescence microscope (Axiophot, Zeiss, Oberkochen, Germany).

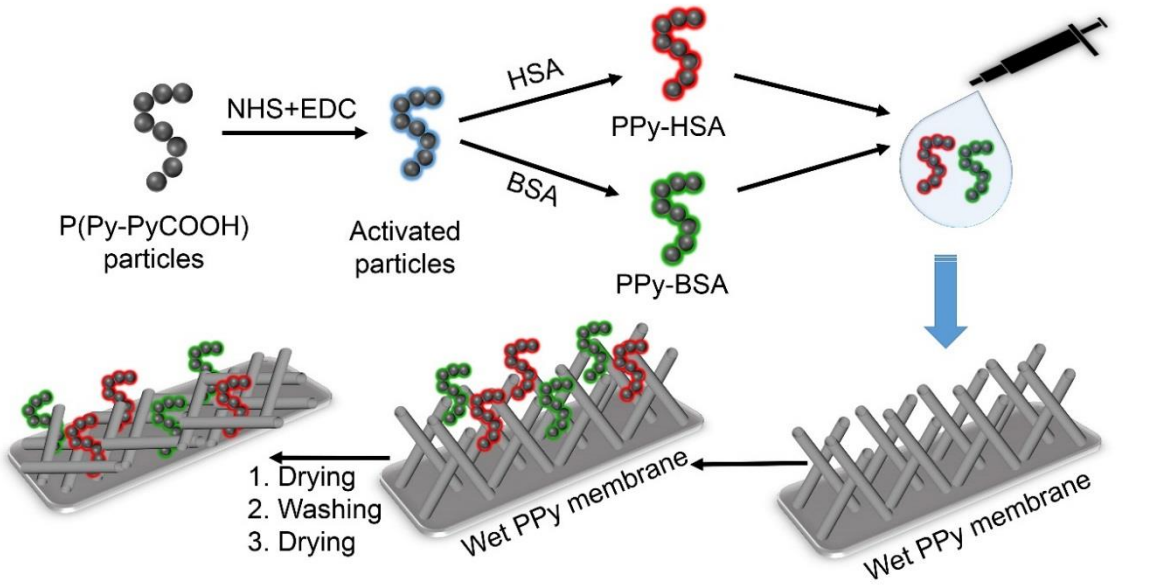

Figure 5.1 Diagram of entrapping the model protein grafted P(Py-PyCOOH) particles onto the nanotube side of the flexible PPy membrane.

5.4.6 Characterization

5.4.6.1 Morphology observation

The morphology of the particles, PPy membranes and the particles coated membranes were observed with a scanning electron microscope (SEM, Model JSM-6360LV, JEOL, Japan) at an accelerating voltage of 20 kV. Prior to SEM observation, the specimens were spatter-coated with gold in a sputter coater (Fisons Instruments Polaron SC500, UK). A transmission electron microscope (TEM, Model JEM-1230, JEOL) was further employed to identify the structure of the P(Py-PyCOOH) particles and nanotubes of the PPy membrane at 45 μA and an accelerating voltage of 80 kV. To prepare TEM specimens, diluted particle suspensions were treated with ultrasound for 10 min before being dropped on a sample grid and dried in air.

5.4.6.2 Chemical composition

Infrared spectra were recorded with a Nicolet Magna-IR 550 spectrophotometer (Nicolet Instrument, Madison, USA) in the ATR mode. The specimens were pressed against a silicon hemispherical ATR crystal and scanned 64 times between 500-4500 cm^{-1} at a resolution of 4 cm^{-1}. Spectrum analysis was performed using the software provided by the manufacturer.

5.4.6.3 Conductivity measurement

The particles were mechanically pressed into pellets of 10 mm in diameter and approximately 1 mm in thickness. The surface resistance *R*s ($\Omega\ \square^{-1}$) of the particles, PPy membrane (7.5 cm × 2.5 cm), and protein immobilized PPy membranes (7.5 cm × 2.5 cm) was measured with a Jandel Multi Height Four-Point Probe (Jandel Engineering Ltd., Linslade, Beds, UK) at room temperature. The radius of the probe needles was 100 μm and the space between the bordering needles was 1 mm. The surface electrical resistivity (ρ, Ω cm) was calculated based on equation (5.3)[31, 32]. Conductivity (σ, S cm^{-1}) was calculated according to equation (5.4). The surface resistance of each sample was measured 10 times. The thickness and width corrections were obtained from the report of Smits [31].

$$\rho = Rs \times t = 4.5324 \times Rs \times t \times f1 \times f2 \qquad (5.3)$$

$$\sigma = {}^{1}/_{\rho} \qquad (5.4)$$

where Rs is the surface resistance, t is the sample thickness, f1 is the finite thickness correction and f2 is the finite width correction.

5.4.6.4 Statistical analysis

Data were reported as means ± standard deviations ($n \geqq 3$). A Student's t-test was adopted to analyze the statistical difference of the results with $p < 0.05$ considered statistically significant.

5.5 Results and discussion

5.5.1 Flexible PPy membane and P(Py-PyCOOH) core-shell particles

Through the TIP method, highly flexible and free-standing PPy membranes (ϕ 15 cm) were obtained after washing and drying. An asymmetrical surface morphology of the membrane was confirmed, showing densely packed nanotubes on the water-facing side, and multiple bubbles side on the chloroform-facing side (Fig. 5.2a - 5.2c). The PPy nanotubes formed randomly oriented bundles. Under TEM, these PPy nanotubes were found about 300 nm in diameter and 30 nm in wall thickness as shown in Figure 5.1e. The other side of the membrane is formed entirely by overlapped PPy bubbles, some of which are either broken or collapsed (Fig. 5.2c). Figure 5.2b represents the cross-section of the PPy membrane, from which a nominal thickness about 0.3 mm was measured. The mechanism of how such an asymmetrical PPy membrane was formed has been discussed in our previous report [29]. Chloroform vapor produced by pyrrole reaction heat [33] was considered causing the formation of chloroform bubbles that in turn supported multiple interfacial polymerization on their surface. Noticeably, during the drying of the membrane, the PPy nanotubes became compactly stacked similar to the drying of aquatic plants, leading to a decreased membrane thickness and a microporous network as shown in the insert of Figure 5.2a. Thanks to the nano- and micro-structures, this PPy membrane can be cut, tied, folded, laminated and rolled into tubes. In addition, after drying, the PPy nanotube network cannot be rehydrated or damaged under ultrasonic treatment.

However, it is difficult to synthesize a similar P(Py-PyCOOH) copolymer membrane by TIP due to the lower reactivity of PyCOOH (oxidation potential +1.2 V) compared to Py (+0.8 V) [14, 15]. For P(Py-PyCOOH50) (Py/PyCOOH=1/1), the most appropriate ratio of Fe^{3+}/monomer is 5.3, taking into account the conductivity and yield [21], which is much higher than that used in TIP (1.6). And the mole ratio between Fe^{3+} and Py was always selected at 2.3 for the chemical polymerization of PPy [34]. However, the Fe^{3+}/MO complex will be destroyed at high feeding of ferric chloride. At such a low feeding of ferric chloride as in TIP, the yield of the PPy membrane synthesized by TIP was only around 6%.

Understandably, the conversion of PyCOOH, which is much less reactive than Py, in the TIP system is too low to form a copolymer membrane.

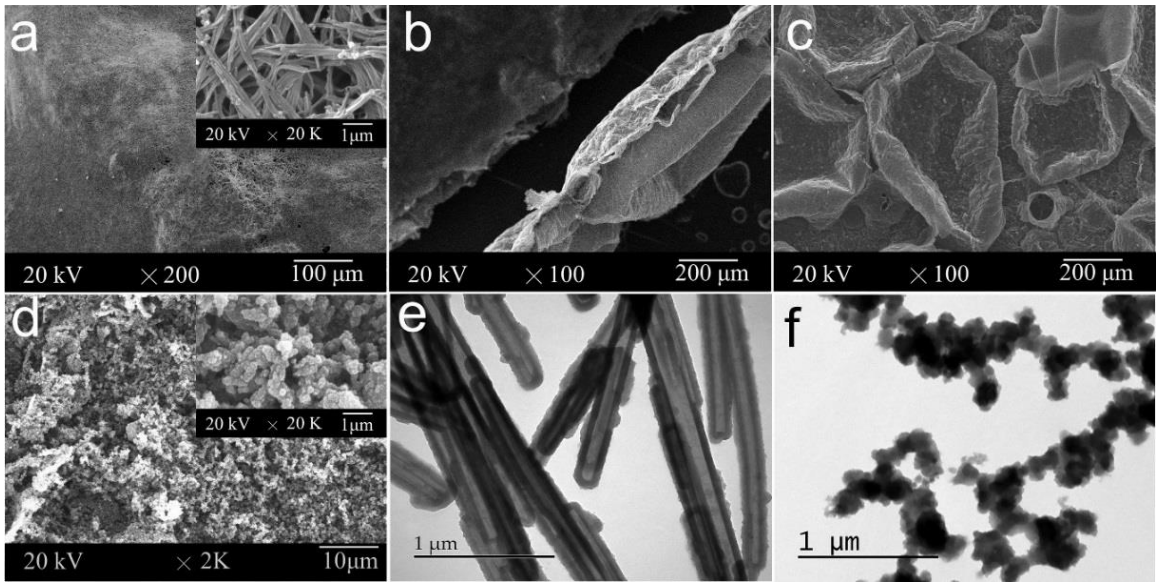

Figure 5.2 Morphology of flexible PPy membrane and core-shell P(Py-PyCOOH) particles: (a-c), SEM photos of PPy membrane: (a), Nanotube side formed in water phase at low and high (insert) magnifications; (b), Cross-section of the membrane; (c), Intact and burst large bubbles formed in oil phase. (d), SEM photos of P(Py-PyCOOH) particles at low and high (insert) magnifications. (e-f), TEM photos of PPy membrane and particles: (e), PPy nanotubes removed from the PPy membrane; (f), P(Py-PyCOOH) particles.

As we previously reported [21, 22], the core-shell structured P(Py-PyCOOH) particles were synthesized by simple one-step and one-pot emulsion polymerization, comprising the pyrrole (Py) dominated P(Py-PyCOOH) copolymer as the core and PPyCOOH homopolymer as the shell. Particles morphology is illustrated in Figure 5.2d, showing a size of around 300 nm in diameter. TEM observation reveals the structure of particles in detail. It was demonstrated that the framework or core was initially formed by the aggregation of the Py dominated copolymer nanoparticles, which was gradually enclosed by the smaller PPyCOOH homopolymer nanoparticles [22]. According to our previous study, the surface and bulk chemistry, conductivity and the overall yield of the particles can be regulated by reaction time [21]. In this work, the particles synthesized in 3 h were used, which present balanced surface carboxyl groups and conductivity. The P(Py-PyCOOH) particles showed in Figure 5.2f appeared threaded together rather than individual particles due to aggregation and the growth of

PPyCOOH homopolymer surrounding them. Such pea-like structure is advantageous for the P(Py-PyCOOH) particles to anchor themselves into the microporous nanotube network of the flexible PPy membrane. When the nanotube network became compact after drying, the embedded pea-like P(Py-PyCOOH) particles were securely immobilized to the membrane surface (Fig. 5.1).

5.5.2 Flexible and functional PPy membrane and its properties

With the increase of feeding particles, the color of the washed PPy membrane changed from luster to dark black as shown by the inserts of Figure 5.3a, suggesting more P(Py-PyCOOH) particles immobilized at the PPy membrane. During this time, the conductivity of the functionalized membrane did not change significantly (Fig. 5.3a), despite the fact that the conductivity of the particles (1.8×10^{-2} S cm^{-1}) is lower than that of the membrane (0.8 S cm^{-1}). This means that the membrane surface conductivity is mainly decided by the nanotubes. Figure 5.3b shows the residual percentage of particles (P_R) and the weight ratio of particles (P_F). P_R first increased and then decreased as the feeding particles increased from 0.05 mg cm^{-2} to 1.07 mg cm^{-2}, with a maximum P_R at 0.27 mg cm^{-2}. This suggests that more particles were washed away at high feeding ratio. In comparison, P_F showed a continuous growth from 3.6% to 36.4%, meaning that even more particles were washed away at high feeding ratio, there was still an increasing amount of particles being immobilized. The increase in immobilized particles was supported by the FTIR results (Fig. 5.3c). The characteristic peaks of PPy observed at 1545 cm^{-1}, 1454 cm^{-1}, 1295 cm^{-1} and 1190 cm^{-1} were ascribed to the C=C double bond stretching in aromatic ring, C-N stretching, =CH- in-plane and the pyrrole ring vibration, respectively [35]. A small peak appeared at 1715 cm^{-1} of the pure PPy membrane is from -C=O due to over-oxidation [36] and termination of the PPy chains by oxygen and water molecules [37]. Nevertheless, the functionalized membranes recorded the characteristic -C=O stretching vibration in P(Py-PyCOOH) at 1715 cm^{-1}, of which the growth of the absorption intensity demonstrates an increasing quantity of the particles on membrane surface. Remarkably, when the feeding of particles reached 1.07 mg cm^{-2}, the FTIR spectrum of the functionalized membrane became the

same as that of the functional particles, meaning that the nanotubes on membrane surface was completely covered by the particles.

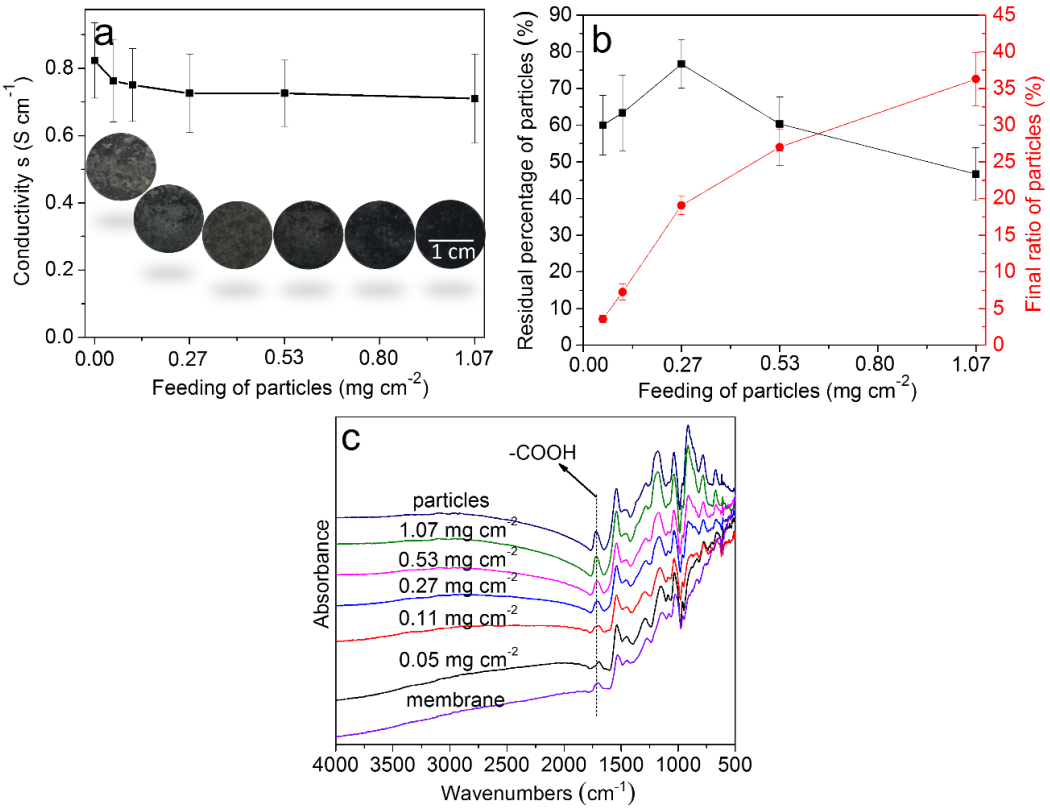

Figure 5. 3 The conductivity and gross observation (a), the residual percentage (P_R) and weight ratio of particles (P_F) (b), and the FTIR spectra of the P(Py-PyCOOH) particles and the PPy membranes immobilized with varying amount of particles.

The morphology of the functionalized PPy membranes is showed in Figure 5.4, which correlated very well with the FTIR results. The quantity of the P(Py-PyCOOH) particles on the surface increased when the feeding of particles increased from 0.05 mg cm^{-2} to 1.07 mg cm^{-2} (Fig. 5.4a - 5.4e). The PPy nanotubes appeared completely covered by the particles when the feeding was higher than 0.53 mg cm^{-2} (insets of Fig. 5.4f and 5.4e). As expected, a considerable amount of the functional particles were trapped in nanotube network and these trapped particles increased gradually with the feeding of particles (insets of Fig. 5.4a to 5.4c). On the bubble side of the membrane, only very few particles attached even at a high feeding ratio (1.07 mg cm^{-2}) (Fig. 5.4f). Factors contributing to the anchoring of particles include physical entanglement and a variety of non-covalent interactions such as hydrogen bonding, hydrophilic and

hydrophobic interactions. Among them, physical entanglement between the particles and the nanotubes network is considered as the primary force as most particles on the bubble side were removed by ultrasonic wash. The characteristics 2D structure of the aggregated particles helped them to penetrate into the nanotube network that had openings as large as one micron even after drying. The affinity between particles and nanotubes likely also contributed to the immobilization but to a much less extent. During drying, under the action of gravity and capillary effect, the particles migrate down and finally rooted themselves inside the nanotube network, forming a layer on top of the membrane (Fig. 5.1). There were some individual nanoparticles that could not firmly attach to the nanotubes and were washed away. In addition, some particles could have been separated from the particle threads owing to the ultrasonic treatment. This may explain why P_R decreased when feeding was higher than 0.27 mg cm^{-2}. At high feeding a high percentage of the particles were not in contact with nanotube network and became more vulnerable to ultrasonic treatment. Therefore, under the conditions of this experiment, 0.27 mg cm^{-2} is recommended as the optimal feeding.

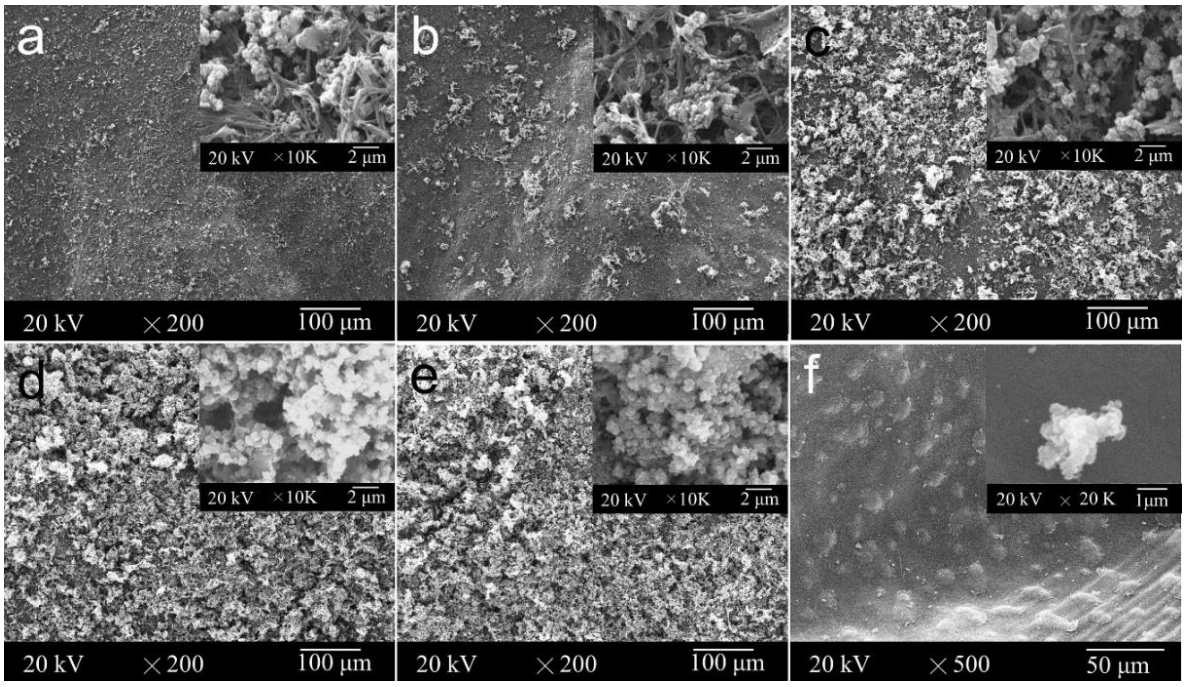

Figure 5.4 SEM photomicrographs of the P(Py-PyCOOH) particle immobilized flexible PPy membranes at different particle feeding ratios: (a) 0.05 mg cm^{-2}, (b) 0.11 mg cm^{-2}, (c) 0.27mg cm^{-2}, (d) 0.53 mg cm^{-2}, (e) 1.07 mg cm^{-2}, (f) the bubble side of the membrane loaded with 1.07 mg cm^{-2} particles.

Since the discovery of conductive polymers, their applications have been severely hindered by the poor mechanical property and processability rooted in their chemical structures. Mechanically, pristine PPy is stiff and brittle due to the extensive conjugation in polymer chains and the aggregation state resulting in very high surface tension and lattice energy [38]. And the glass transition temperature (Tg) of PPy is above 100 ^{o}C [39], meaning that pristine PPy stays in a glassy state well above room temperature. However, the PPy membrane prepared via TIP presents a remarkable flexibility and processability. This demonstrates that the stiff and brittle nature of PPy can be significantly improved through micro and nano structure designs [23, 25]. The unique interconnected topological structures of the PPy membrane also have contributed to the incredible mechanical properties.

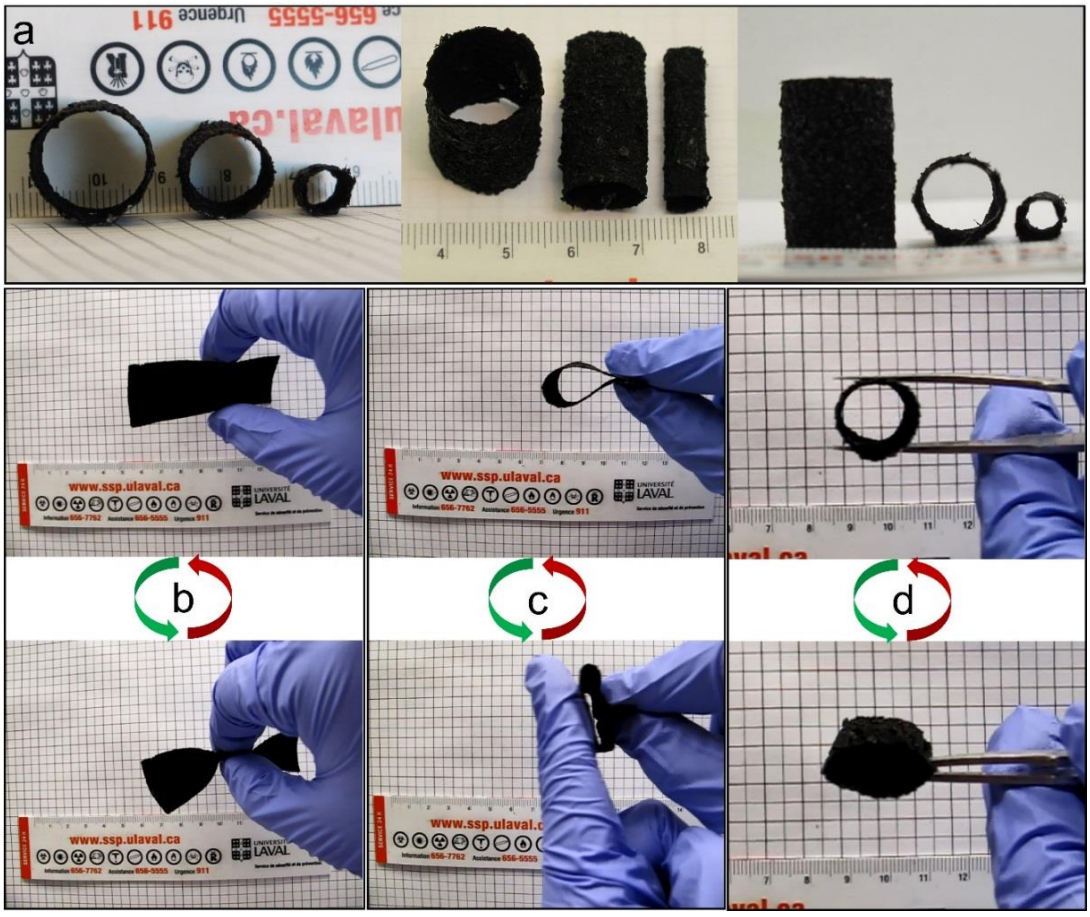

Figure 5.5 The processability and flexibility of the P(Py-PyCOOH) particle immobilized flexible membranes: (a) functionalized PPy tubes, (b) cyclic fold in longitudinal direction, (c) cyclic fold in latitudinal direction, (d) radial compression recovery of PPy tube.

As shown in Figure 5.5, after the loading of 0.27 mg cm^{-2} of P(Py-PyCOOH) particles, which accounts for about 20% of the original weight of the membrane (Fig. 5.3b), the functionalized PPy membrane retained its outstanding processability and flexibility. This functionalized conductive membrane can be easily rolled and glued into tubes of different diameters (16 mm, 10 mm, 5 mm, Fig. 5.5a), or cut into different shapes as a paper. Figures 5.5b and 5.5c also illustrate that the membrane can stand repeated large deformation without any damage in both longitudinal (Fig. 5.5b) and latitudinal directions (Supplementary movie S5.1 and S5.2, video file has been filed separately). Such a flexibility is far superior to any type of known pure PPy membranes [24, 26, 27, 40] and is comparable to PPy composite membranes [41-43]. A complete radial compression recovery of the functionalized PPy tube (ϕ 10 mm) is showed in Figure 5.5d and supplementary movie 5.3 (video file has been filed separately). Similar radial compression recovery was found in all functionalized PPy tubes of different diameters.

PPy based composite tubes have been investigated as nerve guidance conduits (NGCs) with the capacity to electrically stimulate axonal regeneration [44]. Xu mixed PPy particles with poly(D,L-lactic acid) (PDLLA) to prepare a NGC (12 mm in length, 1.6 mm in inner diameter, and 2 mm in outer diameter) for the reparation of a rat sciatic nerve defect, reportedly achieving a similar result as the gold standard autologous never graft [45]. NGCs of 1 mm or 6 mm in inner diameter were also fabricated with a polypyrrole-block-polycaprolactone (PPy-PCL) copolymer coated with poly(lactic-co-glycolic acid) (PLGA), and an increased axon growth was observed under a direct current electric field [46]. Moreover, nerve growth factor (NGF) was chemically immobilized onto the surface of the PPyCOOH coated PLGA scaffold to further improve neurite development and extension [47]. All the PPy-based NGCs mentioned above are constructed with other polymers by either surface coating or particles filling, because it is difficult to use PPy alone as a conducting substrate. Noticeably, the Tgs of PLA and its copolymers are higher than 40 °C [48, 49] leading to stiff NGCs in a physiological environment. In contrast, the functionalized conductive PPy tube possesses not only softness and flexibility but also a functional surface for chemical immobilization of biomolecules, showing a great potential for NGCs.

5.5.3 Grafting of model biomolecules

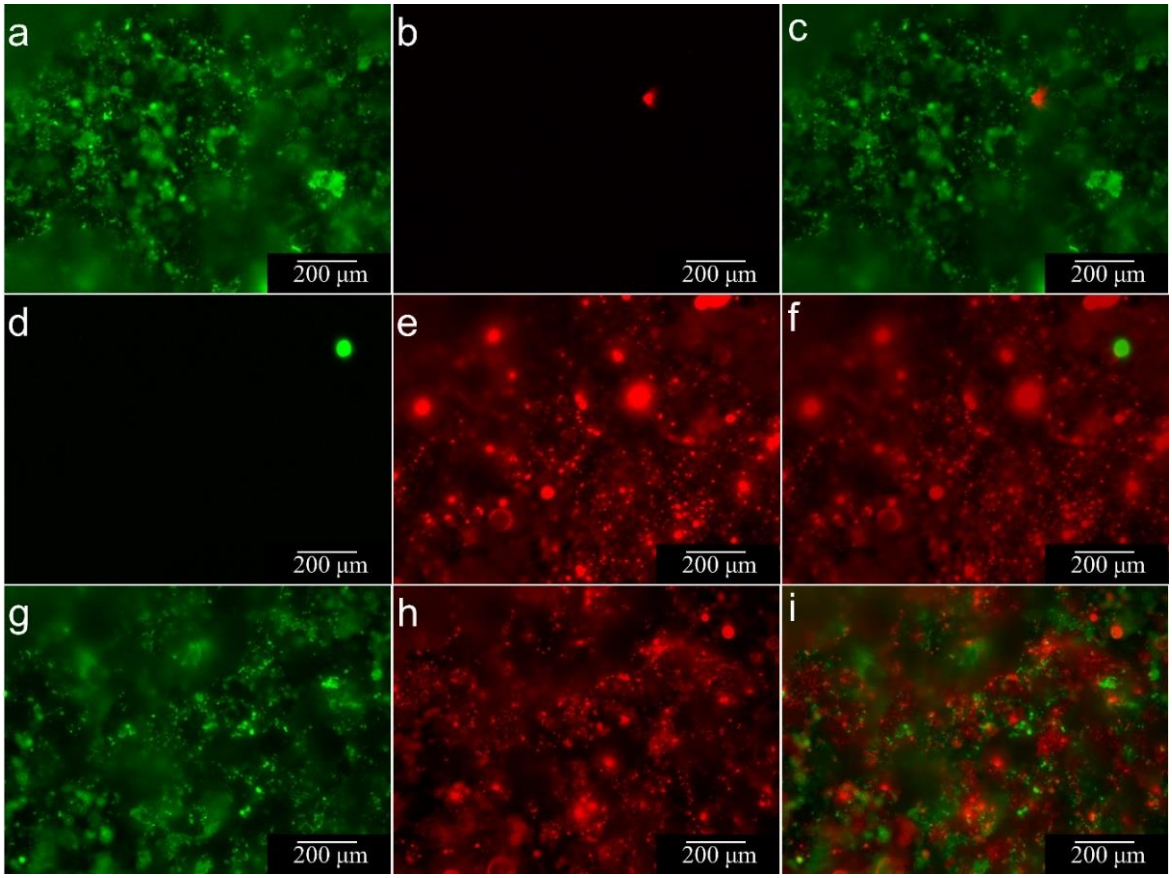

Figure 5.6 Fluorescent photomicrographs of protein immobilization: (a-c) BSA (FITC, green) grafted surface, (d-f) HSA (Rhodamine, red) grafted surface, (g-i) BSA and HSA grafted surface. (a, d, g) observation of fluorescein FITC, (b, e, h) observation of Rhodamine red , (c) merge of (a) and (b), (f) merge of (d) and (e), (i) merge of (g) and (h).

Covalent grafting is expected to be the most efficient and strongest immobilization of biomolecules but requires sufficient functional groups on the surface [50]. Our previous study demonstrated that P(Py-PyCOOH) particles provided abundant binding sites for the covalent grafting of active biomolecules[22]. As showed in Figure 5.1, the P(Py-PyCOOH) particles can be pre-grafted with desired biomolecules such as enzymes, antibodies and growth factors to form modules, and then assembled to the supporting PPy membrane. In order to prove this concept, FITC conjugated bovine serum albumin (BSA) and rhodamine conjugated human serum albumin (HSA) were separately grafted onto the surface of the P(Py-PyCOOH) particles using NHS-EDC coupling. And then these BSA and HAS grafted particles, considered as two modules, were entrapped onto the nanotube side of the PPy membrane.

The results are showed in Figure 5.6. Figure 5.6a and 5.6e demonstrate that, after adequate washing, the BSA or HSA grafted particles were successfully fixed onto the PPy membrane, revealing a uniform fluorescent intensity over the entire surface. Figures 5.6b and 6d prove that both the PPy membrane and the particles have no auto-fluorescence in the exciting lights, and the two emitted fluorescent lights were completely separated under different filters. Further, the PPy membrane loaded with both BSA and HSA grafted particles reveals uniform green and red fluorescent intensity suggesting that two kinds of albumin were successfully immobilized on the nanotube side of the flexible PPy membrane (Fig. 5.6g to 5.6i).

Conventional surface grafting of multiple types of proteins is a cumbersome multi-step process requiring sophisticated techniques to balance the reactions between different proteins that may have different molecular size, steric configuration, reactivity, stability, etc. In contrast, in our modular approach, different biomolecules are separately coupled onto PPy particles in aqueous phase. The quantity and reactivity of the grafted particles can be characterized at this stage, even preserved for future use. To prepare a biofunctional membrane the particles with different functional proteins can be selected according to requirements such as type and quantity, mixed in PBS, and simply dropped onto the PPy membrane with the help of a pipette. This approach therefore makes surface bioactivation easy and straightforward. For example, a NGC loaded with anti-inflammatory drugs and NGFs can be easily fabricated, as well as multi-target biosensors. In fact, the P(Py-PyCOOH) particles can be replaced by other carbon nanomaterials such as carbon nanotubes and graphite or metal oxide particles such as V_2O_5, MnO_2, $NiCo_2O_4$, WO_3, Co_3O_4, and SnO_2, for electronic or energy storage application. The PPy substrate can also be replaced by any surface with micro/nano textures.

5.6 Conclusion

A modular approach has been developed to biofunctionalize micro/nano structured surface. Core-shell structured functional P(Py-PyCOOH) particles were synthesized and grafted with BSA and HSA as model proteins. These bioactive particles can be mixed and easily assembled to the top of a flexible PPy membrane to form a multi-biofunctionalized

conducting surface. The functional particles were firmly immobilized to the surface through physical entanglement with the micro/nano structures on the surface. Such bioactive, electrically conductive and flexible substrate may find applications in sensing, neural prostheses, and medical electrical stimulation. This modular approach may be generalized to other types of bioactive particles and micro/nano structured surfaces.

5.7 Associated content

Supporting information

Flexibility of functionalized PPy membrane and tube (AVI, video file has been filed separately).

Movie 1, movie 2 and movie 3

5.8 Author information

Corresponding author

*Correspondence and requests for materials should be addressed to Ze Zhang.
Ze.Zhang@chg.ulaval.ca

Author contributions

Jifu Mao performed the fabrication of samples, measurements, analysis, and wrote the manuscript. Ze Zhang supervised the work, discussed the results and co-wrote the manuscript. All authors contributed to scientific discussion and manuscript revision.

Notes

The authors declare no competing financial interests.

5.9 Acknowledgement

This work was supported by the Natural Sciences and Engineering Research Council of Canada (262258-2011), the Canadian Institutes of Health Research (MOP106555) and Le

Centre de recherche du CHU de Québec. The first author acknowledges Les Bourses de la Fondation du CHU de Québec aux étudiants. The technical assistance of Stéphane Turgeon, Pascale Chevallier, Andrée-Anne Guay-Bégin and Chaojing Li is greatly appreciated.

References

1. Feiner R, Engel L, Fleischer S, Malki M, Gal I, Shapira A, Shacham-Diamand Y, Dvir T, Engineered hybrid cardiac patches with multifunctional electronics for online monitoring and regulation of tissue function. *Nat. Mater.* 2016, 15: 679–685.

2. Balint R, Cassidy NJ, Cartmell SH, Conductive polymers: Towards a smart biomaterial for tissue engineering. *Acta Biomaterialia*. 2014, 10, (6): 2341-2353.

3. Guimard NK, Gomez N, Schmidt CE, Conducting polymers in biomedical engineering. *Prog. Polym. Sci.* 2007, 32, (8): 876-921.

4. Ramanaviciene A, Kausaite A, Tautkus S, Ramanavicius A, Biocompatibility of polypyrrole particles: an in-vivo study in mice. *J. Pharm. Pharmacol.* 2007, 59, (2): 311-315.

5. Kausaite-Minkstimiene A, Mazeiko V, Ramanaviciene A, Ramanavicius A, Evaluation of chemical synthesis of polypyrrole particles. *Colloids Surf., A.* 2015, 483: 224-231.

6. Sasso C, Beneventi D, Zeno E, Chaussy D, Petit-Conil M, Belgacem N, Polypyrrole and polypyrrole/wood-derived materials conducting composites: A review. *BioResources*. 2011, 6, (3): 3585-3620.

7. Nickels JD, Schmidt CE, Surface modification of the conducting polymer, polypyrrole, via affinity peptide. *J. Biomed. Mater. Res., Part A.* 2013, 101, (5): 1464-1471.

8. Cho Y, Borgens RB, Biotin-doped porous polypyrrole films for electrically controlled nanoparticle release. *Langmuir*. 2011, 27, (10): 6316-6322.

9. Zhang LL, Zhang Z, Electrical field directed electropolymerization of free-standing film of polypyrrole and poly (1-(2-carboxyethyl) pyrrole at the air/liquid interface. *Synth. Met.* 2011, 161, (9): 724-730.

10. Bozgeyik İ, Şenel M, Çevik E, Abasıyanık MF, A novel thin film amperometric urea biosensor based on urease-immobilized on poly (N-glycidylpyrrole-co-pyrrole). *Curr. Appl. Phys.* 2011, 11, (4): 1083-1088.

11. Ko S, Jang J, Controlled amine functionalization on conducting polypyrrole nanotubes as effective transducers for volatile acetic acid. *Biomacromolecules*. 2007, 8, (1): 182-187.

12. Bisht V, Takashima W, Kaneto K, A novel thin film urea biosensor based on copolymer poly (N-3-aminopropylpyrrole- co-pyrrole) film. *Surf. Coat. Technol.* 2005, 198, (1): 231-236.

13. Azioune A, Ben Slimane A, Ait Hamou L, Pleuvy A, Chehimi MM, Perruchot C, Armes SP, Synthesis and characterization of active ester-functionalized polypyrrole-silica nanoparticles: application to the covalent attachment of proteins. *Langmuir*. 2004, 20, (8): 3350-3356.

14. Jiang H, Zhang A, Sun Y, Ru X, Ge D, Shi W, Poly (1-(2-carboxyethyl) pyrrole)/polypyrrole composite nanowires for glucose biosensor. *Electrochim. Acta*. 2012, 70: 278-285.

15. Okner R, Domb AJ, Mandler D, Electrochemical formation and characterization of copolymers based on N-pyrrole derivatives. *Biomacromolecules*. 2007, 8, (9): 2928-2935.

16. Oshima K, Nakamura T, Matsuoka R, Kuwahara T, Shimomura M, Miyauchi S, Immobilization of alcohol dehydrogenase on poly [1-(2-carboxyethyl) pyrrole] film for fabrication of ethanol-responding electrode. *Synth. Met.* 2005, 152, (1): 33-36.

17. Shimomura M, Kuwahara T, Iizuka K, Kinoshita T, Immobilization of alcohol dehydrogenase on films prepared by the electrochemical copolymerization of pyrrole and 1-(2-carboxyethyl) pyrrole for ethanol sensing. *J. Appl. Polym. Sci.* 2010, 116, (5): 2651-2657.

18. Ko S, Jang J, Label-free target DNA recognition using oligonucleotide-functionalized polypyrrole nanotubes. *Ultramicroscopy*. 2008, 108, (10): 1328-1333.

19. Hu WH, Li CM, Dong H, Poly (pyrrole- co-pyrrole propylic acid) film and its application in label-free surface plasmon resonance immunosensors. *Anal. Chim. Acta.* 2008, 630, (1): 67-74.

20. Shimomura M, Miyata R, Kuwahara T, Oshima K, Miyauchi S, Immobilization of glucose oxidase on the films prepared by electrochemical copolymerization of pyrrole and 1-(2-carboxyethyl) pyrrole for glucose sensing. *Eur. Polym. J.* 2007, 43, (2): 388-394.

21. Mao J, Zhang Z, Conductive poly(pyrrole-co-(1-(2-carboxyethyl)pyrrole)) core-shell particles: Synthesis, characterization, and optimization. *Polymer*. 2016, 105: 113-123.

22. Mao J, Zhang Z, One-step reactivity-driven synthesis of core-shell structured electrically conducting particles for biomedical applications. *J. Mater. Chem. B.* 2016, 4, (32): 5429-5436.

23. Pan L, Chortos A, Yu G, Wang Y, Isaacson S, Allen R, Shi Y, Dauskardt R, Bao Z, An ultra-sensitive resistive pressure sensor based on hollow-sphere microstructure induced elasticity in conducting polymer film. *Nat. Commun.* 2014, 5: 3002

24. Zhao Ce, Wu J, Kjelleberg S, Loo JSC, Zhang Q, Employing a Flexible and Low-Cost Polypyrrole Nanotube Membrane as an Anode to Enhance Current Generation in Microbial Fuel Cells. *Small*. 2015, 11, (28): 3440-3443.

25. Wang C, Ding Y, Yuan Y, Cao A, He X, Peng Q, Li Y, Multifunctional, Highly Flexible, Free-Standing 3D Polypyrrole Foam. *Small*. 2016, 12, (30): 4070-4076.

26. Peng T, Sun W, Huang C, Yu W, Sebo B, Dai Z, Guo S, Zhao X-Z, Self-assembled free-standing polypyrrole nanotube membrane as an efficient FTO-and Pt-free counter electrode for dye-sensitized solar cells. *ACS Appl. Mater. Interfaces.* 2013, 6, (1): 14-17.

27. Qi G, Wu Z, Wang H, Highly conductive and semitransparent free-standing polypyrrole films prepared by chemical interfacial polymerization. *J. Mater. Chem. C.* 2013, 1, (42): 7102-7110.

28. Qi G, Huang L, Wang H, Highly conductive free standing polypyrrole films prepared by freezing interfacial polymerization. *Chem. Commun.* 2012, 48, (66): 8246-8248.

29. Mao J, Li C, Park HJ, Rouabhia M, Zhang Z, Conductive Polymer Waving in Liquid Nitrogen. *ACS nano*. 2017.

30. Maeda S, Corradi R, Armes SP, Synthesis and characterization of carboxylic acid-functionalized polypyrrole-silica microparticles. *Macromolecules*. 1995, 28, (8): 2905-2911.

31. Smits F, Measurement of sheet resistivities with the four-point probe. *Bell Syst. Tech. J.* 1958, 37, (3): 711-718.

32. Meng S, Zhang Z, Rouabhia M, Surfactant-templated crystalline polygon nanoparticles of heterocyclic polypyrrole prepared with Fenton's reagent. *Synth. Met.* 2010, 160, (1): 116-122.

33. Blinova NV, Stejskal J, Trchová M, Prokeš J, Omastová M, Polyaniline and polypyrrole: A comparative study of the preparation. *Eur. Polym. J.* 2007, 43, (6): 2331-2341.

34. Machida S, Miyata S, Techagumpuch A, Chemical synthesis of highly electrically conductive polypyrrole. *Synth. Met.* 1989, 31, (3): 311-318.

35. López-García F, Canché-Escamilla G, Ocampo-Flores A, Roquero-Tejeda P, Ordóñez L, Controlled size nano-polypyrrole synthetized in micro-emulsions as PT support for the ethanol electro-oxidation reaction. *Int. J. Electrochem. Sci*. 2013, 8: 3794-3813.

36. Ge H, Qi G, Kang E-T, Neoh KG, Study of overoxidized polypyrrole using X-ray photoelectron spectroscopy. *Polymer*. 1994, 35, (3): 504-508.

37. Dong S, Ding J, Study on polypyrrole film by electrochemical polymerization in aqueous solution. *Synth. Met.* 1987, 20, (1): 119-124.

38. Dyer A, Reynolds J, Skotheim T, Reynolds J, *Handbook of conducting polymers. Conjugated polymers: theory, synthesis, properties, and characterization*. 3rd ed.; CRC Press: Boca Raton, 2007; p 3-75.

39. Mavinakuli P, Wei S, Wang Q, Karki AB, Dhage S, Wang Z, Young DP, Guo Z, Polypyrrole/silicon carbide nanocomposites with tunable electrical conductivity. *J.Phys. Chem. C*. 2010, 114, (9): 3874-3882.

40. Singh A, Salmi Z, Jha P, Joshi N, Kumar A, Decorse P, Lecoq H, Lau-Truong S, Aswal DK, Gupta SK, One step synthesis of highly ordered free standing flexible polypyrrole-silver nanocomposite films at air–water interface by photopolymerization. *RSC Advances*. 2013, 3, (32): 13329-13336.

41. Yuan L, Yao B, Hu B, Huo K, Chen W, Zhou J, Polypyrrole-coated paper for flexible solid-state energy storage. *Energy Environ. Sci*. 2013, 6, (2): 470-476.

42. Xu J, Li M, Wu L, Sun Y, Zhu L, Gu S, Liu L, Bai Z, Fang D, Xu W, A flexible polypyrrole-coated fabric counter electrode for dye-sensitized solar cells. *J. Power Sources*. 2014, 257: 230-236.

43. Wang Z, Tammela P, Strømme M, Nyholm L, Nanocellulose coupled flexible polypyrrole@ graphene oxide composite paper electrodes with high volumetric capacitance. *Nanoscale*. 2015, 7, (8): 3418-3423.

44. Moroder P, Runge MB, Wang H, Ruesink T, Lu L, Spinner RJ, Windebank AJ, Yaszemski MJ, Material properties and electrical stimulation regimens of polycaprolactone fumarate–polypyrrole scaffolds as potential conductive nerve conduits. *Acta Biomaterialia*. 2011, 7, (3): 944-953.

45. Xu H, Holzwarth JM, Yan Y, Xu P, Zheng H, Yin Y, Li S, Ma PX, Conductive PPY/PDLLA conduit for peripheral nerve regeneration. *Biomaterials*. 2014, 35, (1): 225-235.

46. Nguyen HT, Wei C, Chow JK, Nguyen A, Coursen J, Sapp S, Luebben S, Chang E, Ross R, Schmidt CE, Electric field stimulation through a biodegradable polypyrrole-co-polycaprolactone substrate enhances neural cell growth. *J. Biomed. Mater. Res. A*. 2014, 102, (8): 2554-2564.

47. Lee JY, Bashur CA, Milroy CA, Forciniti L, Goldstein AS, Schmidt CE, Nerve Growth Factor-Immobilized Electrically Conducting Fibrous Scaffolds for Potential Use in Neural Engineering Applications. *IEEE T. Nanobiosci*. 2012, 11, (1): 15-21.

48. Nakafuku C, Takehisa S-y, Glass transition and mechanical properties of PLLA and PDLLA-PGA copolymer blends. *J. Appl. Polym. Sci*. 2004, 93, (5): 2164-2173.

49. Passerini N, Craig DQM, An investigation into the effects of residual water on the glass transition temperature of polylactide microspheres using modulated temperature DSC. . *J. Control. Release*. 2001, 73, (1): 111-115.

50. Truong LT, Chikae M, Ukita Y, Takamura Y, Labelless impedance immunosensor based on polypyrrole–pyrolecarboxylic acid copolymer for hCG detection. *Talanta*. 2011, 85, (5): 2576-2580.

CHAPTER VI

GENERAL DISCUSSION AND CONCLUSIONS

6.1 General discussion

Since the synthesis of conductive PPy in 1960s [12], it has received significant attention in biomedical applications and energy storage owing to its inherent electrical conductivity, the ease of synthesis, diversity in chemistry after modification, and biocompatibility [53, 158, 293]. Despite the initial enthusiasm and the extensive investigation, large scale industrial use of pristine PPy is still very limited. The primary cause is the inherently poor mechanical property and processability owing to its unique extensively conjugated and cross-linked molecular structure. In addition, PPy only possesses bioconductivity with no bioinductivity, which is another challenge for PPy when it is applied in biomedical applications. Various strategies have been developed to incorporate biomolecules to biofunctionalize PPy, such as physical adsorption and entrapment [227], doping [294], and covalent immobilization on the copolymers of pyrrole with its derivatives [128, 251, 254, 295]. In general, covalent immobilization is regarded as the most reliable method to attach stable and active biomolecules. Therefore, this thesis explored novel solutions to address these challenging issues. The author for the first time synthesized functional P(Py-PyCOOH) particles via a simple one step emulsion polymerization. The author further synthesized a highly flexible pristine PPy membrane through template assisted interfacial polymerization (TIP), which could become a ground-breaking technology in PPy application. Then the functional particles were grafted with proteins and used as modules to be assembled onto the surface of the micro/nano structured PPy membrane to form a functionalized and flexible PPy membrane. In biological studies, human skin fibroblasts adhered and grew well on the flexible PPy membrane; antigens recognized the antibodies grafted on the functional particles; and two types of biomolecules were co-immobilized onto the functionalized and flexible PPy membrane. The concepts and methodologies used in this thesis cross polymer chemistry, engineering, and biology.

6.1.1 Functional core-shell particles

Poly(pyrrole-co-(1-(2-carboxyethyl)pyrrole)) (P(Py-PyCOOH)), a typical N-functionalized PPy copolymer, was widely used as a substrate for biomolecule immobilization [128, 262, 296], for which a high surface density of functional groups and a sufficient conductivity are both important. However, because the conductivity of Py-COOH homopolymer is low, a decrease

in conductivity is often encountered at high ratio of Py-COOH [255, 258]. Ideally, a core-shell structure may solve this dilemma between reactivity and conductivity because the PPy core would guarantee the conductivity and the PPyCOOH homopolymer shell would provide a high surface functionality. In literatures, four methods are commonly used to construct a core-shell structure [297], including two-step polymerization, emulsion polymerization containing reactive surfactant, step-wise hetero-coagulation, and self-assembly of block amphiphilic polymers. According to Mayo-Lewis equation, the reactivity ratio of comonomers determines how a copolymer is composed, e.g., block vs. random. When r1>1>r2, monomer 1 is consumed firstly, causing a drift in feeding, and eventually ends up with an r2 rich composition. In this work, for the first time, a definite strategy was proposed to build polymeric particles with a core-shell structure by taking the advantages of a lower reactivity of PyCOOH compared to Py (+1.2 V *vs* +0.8 V) and the drift in comonomer feed (see Chapter II). Due to the higher oxidation potential of PyCOOH, a higher feeding of Fe^{3+} is logically expected to initiate the polymerization of PyCOOH monomers. However, considering the optimal ratio of Fe^{3+}/Py (2.33), the ratio of Fe^{3+}/PyCOOH was tested from 1.4 to 4.0 without considering monomer conversion rate [257-259]. Taking into account the yield, conductivity, surface chemistry, and morphology of the obtained particles, experimental parameters including the feeding of $FeCl_3$, ratio of water/oil and Py/PyCOOH, and reaction time were evaluated to define the balanced optimal conditions (Chapter III).

Compared with the classic emulsion polymerization system of PPy [43], a high feeding of oxidant and a low ratio of water were used to increase the reaction of comonomers. Certainly, to some extent, the high feeding of oxidant caused over-oxidation leading to a decrease in conductivity, which however was not significant with respect to the effect of PyCOOH incorporation. It was found that the reaction time can be used as an effective controlling factor to regulate surface and bulk chemistry, conductivity (3.3 $S \cdot cm^{-1}$ - 9.4×10^{-4} $S \cdot cm^{-1}$) and yield (30.5% - 101.3%). Owing to the adhesion and encasing of PPyCOOH homopolymer, the P(Py-PyCOOH) particles present a thread of pea-like structure instead of individual nanoparticles. The feeding ratio of PyCOOH has been used to regulate the quantity of carboxyl groups on surface of the copolymer [257]. Our results confirm that the quantity of functional groups on particles surface will reach the highest level when a shell of PPyCOOH homopolymer is formed, that is, it is unnecessary to excessively increase the feeding of

functionalized monomer to gain more functional groups on particle surface. The key advantage of the reactivity-driven strategy is associated to its simplicity without tedious processes and complicate molecule design. Moreover, this strategy could be used to synthesize core-shell particles with a variety of functional groups via selecting suitable comonomers, such as PyCN, $PyNH_2$, PyPO, and PyOH.

6.1.2 Highly flexible PPy membrane

Inherently conductive polymers such as PPy are known for their stiffness and brittleness because of their extensive conjugation in polymer main chains and the aggregation state resulting in very high surface tension and lattice energy [298]. In addition, PPy is insoluble and infusible due to its cross-linked chains that greatly restricted its processing and application. Because of that, the glass transition temperature (Tg) of PPy is above 100 ^{o}C [299], which is well above room temperature. In fact, PPy, like most other pristine (non-modified) inherently conductive polymers, is normally synthesized either as powder to make composite with other polymers, or to coat as a thin layer on a substrate such as textiles. In other words, pristine heterocyclic conductive polymers cannot be used alone because of their mechanical rigidity and non-processability. However, the mechanical property of the PPy-based composites depends on the nature of the substrates, and becomes brittle because of heavy loading of PPy used to obtain a high conductivity. And even more important, the physicochemical stability of the composite is often inferior to PPy when facing to extreme conditions such as temperature, pH, humidity, and radiation. Thus, in the last decades, efforts have been devoted to preparing single-component PPy materials with proper mechanical property and processability. For example, improvements have been made in synthesizing conductive and stretchable PPy films by EP at low temperature and current [300, 301]. It was demonstrated that the morphology of the electrochemically generated PPy films was significantly affected by dopant anions when the film thickness was more than 1 μm [302]. Using para (toluene sulfonic acid) (pTS) and indigo carmine (IC) as dopants, two types of flexible PPy films with cauliflower-like nodular structures were prepared by EP [303]. Such PPy films are very small and only 4 to 7 μm in thickness. In 1986, via interfacial oxidative polymerization, a small piece of thin, flexible and transparent PPy film was synthesized at the interface of a $FeCl_3$ aqueous solution and a pyrrole benzene or toluene solution [304]. Similarly, a PPy film with a

thickness of 3 to 4 μm also formed at the interface of chloroform and water with $(NH_4)_2S_2O_8$ as oxidant [305]. Noticeably, the flexibility was only obtained in the early phase of polymerization and the film became less conductive and brittle with the progress of polymerization, during which the thickness increased from 1 to 10 μm [306]. To conclude, those flexible PPy films synthesized through EP and interfacial polymerizations were very small in size and extremely thin, leaving the issues of mechanical property and processability unsolved.

In this study, through an innovative combination of $FeCl_3$-MO complex and interfacial polymerization, a template assisted interfacial polymerization or TIP has been developed to prepare a mechanically processable pristine PPy membrane PPy-N. This membrane presents a remarkable softness and flexibility even in liquid nitrogen (Chapter IV). PPy-N membrane, with a nominal thickness of about 0.45 mm, has an asymmetrical morphology on two sides, i.e., a nanotube side formed in water phase and a bubble side formed when facing chloroform. Fascinatingly, after washing and drying, the obtained PPy-N (ϕ 15 cm) exhibited an incredible capability of bending and folding repeatedly without any damage. The flexibility of PPy-N is far superior to any type of pure PPy membranes in literatures [53, 80, 81, 292], and also reaches or exceeds that of the PPy composite membranes [84, 274, 307]. In addition, the PPy-N membrane is mechanically processable, meaning that it can be cut arbitrarily, tied, folded, laminated and rolled into tubes. PPy-N also showed a tensile strength of 90 kPa at 2.5% breaking elongation, which is much higher than that of the 3D PPy foam (18 kPa, 3.3% elongation) [268]. We proposed that the excellent flexibility of PPy-N at both room temperature and -196 °C was because of the uniquely interconnected and multilayered nano/micron structures.

The overall performance of the PPy-N membrane manifests a great potential as electric heating materials. Electric heating elements or appliances are frequently used in industry and daily life such as water heating, deicing, heating clothing or pad, and sport equipment for extremely cold outdoor environment [10, 215, 308]. Composites made of carbon nanomaterials [215], metal nanowires [217] and conducting polymers [10] have been proposed to replace the heavy, corrosion susceptible and less flexible metal wires or fibers in traditional metal-based electric heating devices. The PPy-N exhibits a rapid temperature response and an electric heating

efficiency (42.6 mW $°C^{-1}$) comparable with the PPy composite membranes (28-126 mW $°C^{-1}$)[10] and carbon nanotube composites (2-22 mW $°C^{-1}$) [215, 308]. Compared to conductive composites, the advantages of PPy-N mainly lies in lightweight, low-temperature flexibility, and thermal stability.

When used as biomaterials, PPy-based composites have been widely investigated to mediate electrical signal to stimulate cells [100]. Although the biocompatiblity of PPy was well documented [290, 309], the security of PPy-N synthesized by using MO template should be evaluated before using as a biomaterial. Human skin fibroblasts were cultured on both sides of the PPy-N membrane for 48 hours. Compared to glass coverslips (control), PPy-N was superior in cell attachment owing to its cytocompatibility and the large surface area. The number of cells on the membrane at 48 h was also significantly higher than that on the coverslip, highlighting the potential of PPy-N as cell culture scaffold.

6.1.3 Combination of functionalization and flexibility for PPy

Attempt to prepare a P(Py-PyCOOH) copolymer membrane via TIP ended as a failure after several trials. The causes may be attributed to the low reactivity of PyCOOH monomer and inadequate concentration of Fe^{3+}. As explained in Chapters II and III, a high ratio of Fe^{3+}/comonomers (5.3) was adopted to gain high conductivity and conversion of PyCOOH. The ratio of Fe^{3+}/Py however was only 1.6 in the TIP system. In classic template polymerization of PPy, the ratio of Fe^{3+}/MO is around 2 [53], while it was over 13 in the TIP system. It had not been possible to further increase the feeding of ferric chloride in the TIP because that the $Fe^{3+/}$MO complex template would have had been destroyed. So that the yield of PPy membrane in the TIP was around 6%. Therefore, it is difficult to synthesize flexible P(Py-PyCOOH) copolymer membrane via the TIP method owing to the very low conversion of PyCOOH monomers.

In this work, a straight-forward strategy was developed for the first time to introduce a thin layer of (P(Py-PyCOOH)) particles on PPy-N membrane without changing the flexibility and processability of the membrane. This became possible by taking the advantages of the topology change of the membrane during drying, and the pea-like structure of the P(Py-PyCOOH) particles (Chapter V). It was confirmed that, after drying, the PPy nanotube

network on PPy-N membrane did not swell or disintegrate when being wetted again even under ultrasonic treatment (Chapter IV). Consequently, an ultrasonic bath was safely used to remove unfastened particles. By controlling the feeding of the particles, various coverages to the membrane can be achieved. The nanotube surface of the PPy-N membrane was almost completely covered by the particles after a treatment with 0.27 mg cm^{-2} of particles suspension. After being loaded with particles, the PPy membrane became functionalized and can be cut into different shapes and rolled into tubes of various diameters. These tubes showed exceptional radial compression recovery. Meanwhile, the layer of particles carry abundant carboxyl groups, which can be further modified into active ester [295] and primary and secondary amine [254], showing great modifiability and potential in covalent immobilization of biomolecules. Additionally, other types of materials, such as carbon nanotubes, graphite, metal oxides, could be incorporated onto the surface of the PPy-N membrane to fabricate flexible electrodes for energy storage. Moreover, multi-functional and flexible membranes can be easily prepared.

6.1.4 Grafting biomolecules onto particles surface

To improve the bioinductivity of PPy, it is essential to incorporate biomolecules to PPy scaffold. Using HE as dopant, our group prepared PLA/PPy/HE membranes, which demonstrated the capability to simultaneously improve electrical stability, and cell adhesion and growth [109]. However, physical adsorption and doping may experience uncontrollable loss of biomolecules and decline in biomolecule activity. Fortunately, the P(Py-PyCOOH) copolymer provides the feasibility of immobilizing biomolecules via covalent tethering. By covalent bonding, NGF was chemically immobilized onto the surface of PPyCOOH coated PLGA scaffold that further improved neurite development and neurite length [97]. Especially for biosensor, various biomolecules were covalently grafted onto PPy substrate to form sensing elements such as in the case of enzyme biosensors [263], DNA biosensors [132] and immunosensors [138]. In this work, anti human serum albumin antibody (anti-HSA) was successfully immobilized onto the surface of the P(Py-PyCOOH) particles and remained active to its antigen HSA (Chapter II). In this study, the functional particles were coated onto a PLA membrane first, and then the membrane was activated by NHS-EDC chemistry and grafted with anti-HSA. A different strategy was developed to immobilize two types of

proteins (BSA-FITC and BSA-rhodamine) onto the PPy membrane at the same time (Chapter V). That is, the model proteins were grafted onto surface of the P(Py-PyCOOH) particles first. Then the protein grafted particles were mixed and coated onto freshly prepared wet PPy-N membrane. Compared with conventional methods, this unique strategy demonstrated in Chapter V permits facile immobilization of different types of biomolecules at a controlled ratio onto the PPy membrane, which is significant in biomedical applications.

6.2 General conclusions

The main contributions of this thesis are as follows:

(1) This is the first report on a simple one-step and one-pot emulsion polymerization method to synthesize the core-shell structured electrically conducting polymer particles based on the difference in comonomer reactivity. It was demonstrated that the particles were formed by a core made of the PPy dominated P(Py-PyCOOH) copolymer and a shell composed by the PPyCOOH homopolymer, guaranteeing an appropriate conductivity and a large number of carboxyl groups on surface. A five-step schema was proposed based on the reactivity driven mechanism to explain the formation of the core-shell structure. The functional groups on the surface of the particles proved sufficient to covalently immobilize active antibodies.

(2) The experimental parameters of the one-step emulsion polymerization of P(Py-PyCOOH) particles were optimized. The properties of the copolymers were found inextricably linked with the dosage of Fe^{3+}, solvent system, feeding ratio of PyCOOH and reaction time. Taking into account the yield, conductivity and surface chemical reactivity, a feeding of 80 mmol Fe^{3+} in 100 mL solution and a 25/75 water/chloroform emulsion system are considered optimal. In the presence of sufficient oxidant, it is not feasible to further increase surface carboxyl groups using a feeding ratio of PyCOOH higher than 50%.

(3) This is the first report on a mechanically processable pristine PPy membrane prepared by template-assisted interfacial polymerization (TIP). The membrane exhibited a high flexibility at room temperature as well as in liquid nitrogen (-196 ^{o}C), despite the fact that the glass transition temperature of PPy is above 100 ^{o}C. Without any chemical modification and composition with any other materials, the unique physical structure renders the brittle PPy

extremely flexible in a wide temperature range. Being able to be synthesized in virtually any size, the PPy membrane can be easily manipulated through different processes such as cutting, folding, rolling, laminating and adhesion. This discovery could become a ground-breaking technology in PPy applications.

(4) This is the first report on the preparation of a multi-biofunctional and flexible PPy membrane. The P(Py-PyCOOH) particles were functionalized with different biomolecules and then immobilized onto the nanotube side of the PPy-N membrane, without causing any significant change in membrane flexibility and processablity. This method permits easy immobilization of multiple types of biomolecules or chemical moieties in a controllable fashion.

6.3 Limitations and perspectives

In this thesis, the author has provided solutions to some of the critical issues in pristine PPy application. Unfortunately, there are still some limitations that are:

(1) The conductivity of the PPy particles and PPy-N membranes are lower than that of the PPy materials synthesized by EP, and the conductivity decreases with storage time.

(2) The PPy-N membrane possesses a high flexibility and processability but low tear resistance.

(3) The yield of TIP is low.

In future, new dopants should be explored to increase the conductivity and stability of the PPy particles. Carbon nanotubes and graphene may be incorporated into PPy-N membrane to increase both the conductivity and tear resistance. The Py/$CHCl_3$ solution in the TIP should be recycled after polymerization in order to raise the overall yield and reduce the costs. In next step, such functional and flexible PPy membrane can be grafted with sensing molecules to develop biosensors. The processability, light-weight, high surface area, electrical and electrothermal properties, and low-cost may find this material useful in a wide range of applications such as energy storage, anti-static, and heating. The principle of the TIP may be applied to other conductive polymers as well.

REFERENCES

1. Wan M, *Conducting polymers with micro or nanometer structure*. Springer: 2008; p 1-13.

2. Shirakawa H, Louis EJ, MacDiarmid AG, Chiang CK, Heeger AJ, Synthesis of electrically conducting organic polymers: halogen derivatives of polyacetylene,(CH) x. *J. Chem. Soc., Chem. Commun.* 1977, (16): 578-580.

3. Lange U, Roznyatovskaya NV, Mirsky VM, Conducting polymers in chemical sensors and arrays. *Anal. Chim. Acta*. 2008, 614, (1): 1-26.

4. Das TK, Prusty S, Review on conducting polymers and their applications. *Polym-Plast. Technol. Eng.* 2012, 51, (14): 1487-1500.

5. Ravichandran R, Sundarrajan S, Venugopal JR, Mukherjee S, Ramakrishna S, Applications of conducting polymers and their issues in biomedical engineering. *J. Royal Soc. Interface.* 2010, 7, (Suppl 5): S559-S579.

6. Heeger AJ, Semiconducting and metallic polymers: the fourth generation of polymeric materials. *Synth. Met.* 2001, 125, (1): 23-42.

7. Brédas JL, Scott JC, Yakushi K, Street GB, Polarons and bipolarons in polypyrrole: Evolution of the band structure and optical spectrum upon doing. *Phys. Rev. B.* 1984, 30, (2): 1023-1025.

8. Guimard NK, Gomez N, Schmidt CE, Conducting polymers in biomedical engineering. *Prog. Polym. Sci.* 2007, 32, (8): 876-921.

9. Pan L, Qiu H, Dou C, Li Y, Pu L, Xu J, Shi Y, Conducting polymer nanostructures: template synthesis and applications in energy storage. *Int. J. Mol. Sci.* 2010, 11, (7): 2636-2657.

10. Wang Y, Jiang H, Tao Y, Mei T, Liu Q, Liu K, Li M, Wang W, Wang D, Polypyrrole/poly (vinyl alcohol-co-ethylene) nanofiber composites on polyethylene terephthalate substrate as flexible electric heating elements. *Composites Part A.* 2016, 81: 234-242.

11. Lee JY, Park DW, Lim JO, Polypyrrole-coated woven fabric as a flexible surface-heating element. *Macromol. Res.* 2003, 11, (6): 481-487.

12. Bolto BA, McNeill R, Weiss D, Electronic conduction in polymers. III. Electronic properties of polypyrrole. *Aust. J. Chem.* 1963, 16, (6): 1090-1103.

13. Kanazawa KK, Diaz A, Gill W, Grant P, Street G, Gardini GP, Kwak J, Polypyrrole: an electrochemically synthesized conducting organic polymer. *Synth. Met.* 1980, 1, (3): 329-336.

14. Sasso C, Beneventi D, Zeno E, Chaussy D, Petit-Conil M, Belgacem N, Polypyrrole and polypyrrole/wood-derived materials conducting composites: A review. *BioResources*. 2011, 6, (3): 3585-3620.

15. Balint R, Cassidy NJ, Cartmell SH, Conductive polymers: towards a smart biomaterial for tissue engineering. *Acta biomaterialia*. 2014, 10, (6): 2341-2353.

16. Ateh D, Navsaria H, Vadgama P, Polypyrrole-based conducting polymers and interactions with biological tissues. *J. Royal Soc. Interface.* 2006, 3, (11): 741-752.

17. De Jesus M, Fu Y, Weiss R, Conductive polymer blends prepared by in situ polymerization of pyrrole: A review. *Polym. Eng. Sci.* 1997, 37, (12): 1936-1943.

18. Rao SS, Winter J, Adhesion molecule-modified biomaterials for neural tissue engineering. *Front. Neuroeng.* 2009, 2: 6.

19. Keiji Kanazawa K, Diaz AF, Gill WD, Grant PM, Street GB, Piero Gardini G, Kwak JF, Polypyrrole: An electrochemically synthesized conducting organic polymer. *Synthetic Metals*. 1980, 1, (3): 329-336.

20. Kausaite-Minkstimiene A, Mazeiko V, Ramanaviciene A, Ramanavicius A, Evaluation of chemical synthesis of polypyrrole particles. *Colloids Surf., A*. 2015, 483: 224-231.

21. Ramya R, Sivasubramanian R, Sangaranarayanan M, Conducting polymers-based electrochemical supercapacitors—progress and prospects. *Electrochim. Acta*. 2013, 101: 109-129.

22. Vernitskaya TyV, Efimov ON, Polypyrrole: a conducting polymer; its synthesis, properties and applications. *Russ. Chem. Rev.* 1997, 66, (5): 443-457.

23. Genies E, Bidan G, Diaz A, Spectroelectrochemical study of polypyrrole films. *J. Electroanal. Chem.* 1983, 149, (1-2): 101-113.

24. Asavapiriyanont S, Chandler G, Gunawardena G, Pletcher D, The electrodeposition of polypyrrole films from aqueous solutions. *J. Electroanal. Chem.* 1984, 177, (1-2): 229-244.

25. Sadki S, Schottland P, Brodie N, Sabouraud G, The mechanisms of pyrrole electropolymerization. *Chemical Society Reviews*. 2000, 29, (5): 283-293.

26. Tan Y, Ghandi K, Kinetics and mechanism of pyrrole chemical polymerization. *Synth. Met.* 2013, 175: 183-191.

27. Dong S, Ding J, Study on polypyrrole film by electrochemical polymerization in aqueous solution. *Synth. Met.* 1987, 20, (1): 119-124.

28. Zhang L, Zhang Z, Electrical field directed electropolymerization of free-standing film of polypyrrole and poly (1-(2-carboxyethyl) pyrrole at the air/liquid interface. *Synth. Met.* 2011, 161, (9): 724-730.

29. Li M, Zhu H, Mao X, Xiao W, Wang D, Electropolymerization of polypyrrole at the three-phase interline: Influence of polymerization conditions. *Electrochimica Acta*. 2013, 92: 108-116.

30. Ansari R, Polypyrrole conducting electroactive polymers: synthesis and stability studies. *J. Chem.* 2006, 3, (4): 186-201.

31. Omastová M, Mičušík M, Polypyrrole coating of inorganic and organic materials by chemical oxidative polymerisation. *Chemical Papers*. 2012, 66, (5): 392-414.

32. Omastova M, Trchova M, Kovářová J, Stejskal J, Synthesis and structural study of polypyrroles prepared in the presence of surfactants. *Synthetic Metals*. 2003, 138, (3): 447-455.

33. Machida S, Miyata S, Techagumpuch A, Chemical synthesis of highly electrically conductive polypyrrole. *Synth. Met.* 1989, 31, (3): 311-318.

34. Armes SP, Optimum reaction conditions for the polymerization of pyrrole by iron (III) chloride in aqueous solution. *Synth. Met.* 1987, 20, (3): 365-371.

35. Kudoh Y, Properties of polypyrrole prepared by chemical polymerization using aqueous solution containing $Fe_2(SO_4)_3$ and anionic surfactant. *Synthetic Metals*. 1996, 79, (1): 17-22.

36. Rapi S, Bocchi V, Gardini G, Conducting polypyrrole by chemical synthesis in water. *Synthetic Metals*. 1988, 24, (3): 217-221.

37. Butterworth M, Bell S, Armes S, Simpson A, Synthesis and characterization of polypyrrole–magnetite–silica particles. *Journal of colloid and interface science*. 1996, 183, (1): 91-99.

38. Meng S, Zhang Z, Rouabhia M, Surfactant-templated crystalline polygon nanoparticles of heterocyclic polypyrrole prepared with Fenton's reagent. *Synthetic Metals*. 2010, 160, (1): 116-122.

39. Müller D, Rambo C, Recouvreux D, Porto L, Barra G, Chemical in situ polymerization of polypyrrole on bacterial cellulose nanofibers. *Synth. Met.* 2011, 161, (1): 106-111.

40. Thiéblemont JC, Gabelle JL, Planche MF, Polypyrrole overoxidation during its chemical synthesis. *Synth. Met.* 1994, 66, (3): 243-247.

41. Kudoh Y, Akami K, Matsuya Y, Properties of chemically prepared polypyrrole with an aqueous solution containing Fe2(SO4)3, a sulfonic surfactant and a phenol derivative. *Synth. Met.* 1998, 95, (3): 191-196.

42. Reung-U-Rai A, Prom-Jun A, Prissanaroon-Ouajai W, Ouajai S, Synthesis of highly conductive polypyrrole nanoparticles via microemulsion polymerization. *J. Met., Mater. Miner.* 2008, 18, (2): 27-31.

43. Shi G, Zhang Z, Rouabhia M, The regulation of cell functions electrically using biodegradable polypyrrole–polylactide conductors. *Biomaterials*. 2008, 29, (28): 3792-3798.

44. Yin Z-H, Long Y-Z, Gu C-Z, Wan M-X, Duvail J-L, Current–voltage characteristics in individual polypyrrole nanotube, poly (3, 4-ethylenedioxythiophene) nanowire, polyaniline nanotube, and CdS nanorope. *Nanoscale Res. Lett.* 2009, 4, (1): 63-69.

45. Dubal DP, Caban-Huertas Z, Holze R, Gomez-Romero P, Growth of polypyrrole nanostructures through reactive templates for energy storage applications. *Electrochim. Acta*. 2016, 191: 346-354.

46. Tran HD, Li D, Kaner RB, One-dimensional conducting polymer nanostructures: bulk synthesis and applications. *Adv. Mater.* 2009, 21, (14-15): 1487-1499.

47. Liu J, Wan M, Studies on formation mechanism of polypyrrole microtubule synthesized by template-free method. *J. Polym. Sci., Part A: Polym. Chem.* 2001, 39, (7): 997-1004.

48. Shinde SS, Gund GS, Dubal DP, Jambure SB, Lokhande CD, Morphological modulation of polypyrrole thin films through oxidizing agents and their concurrent effect on supercapacitor performance. *Electrochim. Acta*. 2014, 119: 1-10.

49. Zha Z, Yue X, Ren Q, Dai Z, Uniform polypyrrole nanoparticles with high photothermal conversion efficiency for photothermal ablation of cancer cells. *Adv. Mater.* 2013, 25, (5): 777-782.

50. Liu X, Wu H, Ren F, Qiu G, Tang M, Controllable fabrication of SiO2/polypyrrole core–shell particles and polypyrrole hollow spheres. *Mater. Chem. Phys.* 2008, 109, (1): 5-9.

51. Zhong W, Liu S, Chen X, Wang Y, Yang W, High-yield synthesis of superhydrophilic polypyrrole nanowire networks. *Macromolecules*. 2006, 39, (9): 3224-3230.

52. Lee JY, Bashur CA, Goldstein AS, Schmidt CE, Polypyrrole-coated electrospun PLGA nanofibers for neural tissue applications. *Biomaterials*. 2009, 30, (26): 4325-4335.

53. Zhao C-e, Wu J, Kjelleberg S, Loo JSC, Zhang Q, Employing a flexible and low-cost polypyrrole nanotube membrane as an anode to enhance current generation in microbial fuel cells. *Small*. 2015, 11, (28): 3440-3443.

54. Qi G, Huang L, Wang H, Highly conductive free standing polypyrrole films prepared by freezing interfacial polymerization. *Chem. Commun.* 2012, 48, (66): 8246-8248.

55. Lu Y, He W, Cao T, Guo H, Zhang Y, Li Q, Shao Z, Cui Y, Zhang X, Elastic, conductive, polymeric hydrogels and sponges. *Sci. Rep.* 2014, 4.

56. Wei D, Lin X, Li L, Shang S, Yuen MC-w, Yan G, Yu X, Controlled growth of polypyrrole hydrogels. *Soft Matter*. 2013, 9, (10): 2832-2836.

57. He Y, Wang S, Mu J, Dai L, Zhang Z, Sun Y, Shi W, Ge D, Synthesis of polypyrrole nanowires with positive effect on MC3T3-E1 cell functions through electrical stimulation. *Mater. Sci. Eng., C*. 2017, 71: 43-50.

58. Attia MF, Anton N, Khan IU, Serra CA, Messaddeq N, Jakhmola A, Vecchione R, Vandamme T, One-step synthesis of iron oxide polypyrrole nanoparticles encapsulating ketoprofen as model of hydrophobic drug. *Int. J. Pharm.* 2016, 508, (1–2): 61-70.

59. Liao Y, Wang X, Qian W, Li Y, Li X, Yu D-G, Bulk synthesis, optimization, and characterization of highly dispersible polypyrrole nanoparticles toward protein separation using nanocomposite membranes. *J. Colloid Interface Sci.* 2012, 386, (1): 148-157.

60. Hong J-Y, Yoon H, Jang J, Kinetic study of the formation of polypyrrole nanoparticles in water-soluble polymer/metal cation systems: A light-scattering analysis. *Small*. 2010, 6, (5): 679-686.

61. Bjorklund RB, Liedberg B, Electrically conducting composites of colloidal polypyrrole and methylcellulose. *J. Chem. Soc., Chem. Commun.* 1986, (16): 1293-1295.

62. Pecher J, Mecking S, Nanoparticles of conjugated polymers. *Chem. Rev.* 2010, 110, (10): 6260-6279.

63. Stejskal J, Colloidal dispersions of conducting polymers. *J. Polym. Mater*. 2001, 18, (3): 225-258.

64. Yan F, Xue G, Zhou M, Preparation of electrically conducting polypyrrole in oil/water microemulsion. *J. Appl. Polym. Sci.* 2000, 77, (1): 135-140.

65. Ghalib H, Abdullah I, Daik R, Electrically conductive polystyrene/polypyrrole nanocomposites prepared via emulsion polymerization. *Polym-Plast. Technol. Eng.* 2013, 52, (5): 478-484.

66. Kim MW, Moon IJ, Choi HJ, Seo Y, Facile fabrication of core/shell structured SiO2/polypyrrole nanoparticles with surface modification and their electrorheology. *RSC Advances*. 2016, 6, (61): 56495-56502.

67. Marinakos SM, Novak JP, Brousseau LC, House AB, Edeki EM, Feldhaus JC, Feldheim DL, Gold particles as templates for the synthesis of hollow polymer capsules. Control of capsule dimensions and guest encapsulation. *JACS*. 1999, 121, (37): 8518-8522.

68. Deng J, Peng Y, He C, Long X, Li P, Chan AS, Magnetic and conducting Fe3O4–polypyrrole nanoparticles with core-shell structure. *Polym. Int.* 2003, 52, (7): 1182-1187.

69. Cheng D, Xia H, Chan HSO, Facile fabrication of AgCl@ polypyrrole-chitosan core-shell nanoparticles and polymeric hollow nanospheres. *Langmuir*. 2004, 20, (23): 9909-9912.

70. Yang X, Dai T, Wei M, Lu Y, Polymerization of pyrrole on a polyelectrolyte hollow-capsule microreactor. *Polymer*. 2006, 47, (13): 4596-4602.

71. Wang K, Wu H, Meng Y, Wei Z, Conducting polymer nanowire arrays for high performance supercapacitors. *Small*. 2014, 10, (1): 14-31.

72. Zhang X, Zhang J, Liu Z, Robinson C, Inorganic/organic mesostructure directed synthesis of wire/ribbon-like polypyrrole nanostructures. *Chem. Commun.* 2004, (16): 1852-1853.

73. Hassanzadeh N, Omidvar H, Tabaian SH, Chemical synthesis of high density and long polypyrrole nanowire arrays using alumina membrane and their hydrogen sensing properties. *Superlattices Microstruct.* 2012, 51, (3): 314-323.

74. Nair S, Hsiao E, Kim SH, Fabrication of electrically-conducting nonwoven porous mats of polystyrene–polypyrrole core–shell nanofibers via electrospinning and vapor phase polymerization. *J. Mater. Chem.* 2008, 18, (42): 5155-5161.

75. Yu Y, Ouyang C, Gao Y, Si Z, Chen W, Wang Z, Xue G, Synthesis and characterization of carbon nanotube/polypyrrole core–shell nanocomposites via in situ inverse microemulsion. *J. Polym. Sci., Part A: Polym. Chem.* 2005, 43, (23): 6105-6115.

76. Zhang X, Manohar SK, Narrow pore-diameter polypyrrole nanotubes. *JACS*. 2005, 127, (41): 14156-14157.

77. Jang J, Yoon H, Formation mechanism of conducting polypyrrole nanotubes in reverse micelle systems. *Langmuir*. 2005, 21, (24): 11484-11489.

78. Zang J, Li X, In situ synthesis of ultrafine [small beta]-MnO2/polypyrrole nanorod composites for high-performance supercapacitors. *J. Mater. Chem.* 2011, 21, (29): 10965-10969.

79. Dai T, Yang X, Lu Y, Controlled growth of polypyrrole nanotubule/wire in the presence of a cationic surfactant. *Nanotechnology*. 2006, 17, (12): 3028.

80. Singh A, Salmi Z, Jha P, Joshi N, Kumar A, Decorse P, Lecoq H, Lau-Truong S, Aswal DK, Gupta SK, One step synthesis of highly ordered free standing flexible polypyrrole-silver nanocomposite films at air–water interface by photopolymerization. *RSC Advances*. 2013, 3, (32): 13329-13336.

81. Qi G, Wu Z, Wang H, Highly conductive and semitransparent free-standing polypyrrole films prepared by chemical interfacial polymerization. *J. Mater. Chem. C.* 2013, 1, (42): 7102-7110.

82. Shen M, Han Y, Lin X, Ding B, Zhang L, Zhang X, Preparation and electrochemical performances of porous polypyrrole film by interfacial polymerization. *J. Appl. Polym. Sci.* 2013, 127, (4): 2938-2944.

83. Chen Y, Han M, Tang Y, Bao J, Li S, Lan Y, Dai Z, Polypyrrole–polyoxometalate/reduced graphene oxide ternary nanohybrids for flexible, all-solid-state supercapacitors. *Chem. Commun.* 2015, 51, (62): 12377-12380.

84. Wang Z, Tammela P, Strømme M, Nyholm L, Nanocellulose coupled flexible polypyrrole@ graphene oxide composite paper electrodes with high volumetric capacitance. *Nanoscale*. 2015, 7, (8): 3418-3423.

85. Pan L, Yu G, Zhai D, Lee HR, Zhao W, Liu N, Wang H, Tee BC-K, Shi Y, Cui Y, Hierarchical nanostructured conducting polymer hydrogel with high electrochemical activity. *Proc. Natl. Acad. Sci.* 2012, 109, (24): 9287-9292.

86. Wang Y, Shi Y, Pan L, Ding Y, Zhao Y, Li Y, Shi Y, Yu G, Dopant-enabled supramolecular approach for controlled synthesis of nanostructured conductive polymer hydrogels. *Nano Lett.* 2015, 15, (11): 7736-7741.

87. Luo S-C, Conducting polymers as biointerfaces and biomaterials: a perspective for a special issue of polymer reviews. *Polym. Rev.* 2013, 53, (3): 303-310.

88. Aydemir N, Malmström J, Travas-Sejdic J, Conducting polymer based electrochemical biosensors. *PCCP*. 2016, 18, (12): 8264-8277.

89. De Kroon J, Van der Lee J, IJzerman M, Lankhorst G, Therapeutic electrical stimulation to improve motor control and functional abilities of the upper extremity after stroke: a systematic review. *Clin. Rehabil.* 2002, 16, (4): 350-360.

90. Williams R, Doherty P, A preliminary assessment of poly (pyrrole) in nerve guide studies. *J. Mater. Sci. Mater. Med.* 1994, 5, (6-7): 429-433.

91. Wang X, Gu X, Yuan C, Chen S, Zhang P, Zhang T, Yao J, Chen F, Chen G, Evaluation of biocompatibility of polypyrrole in vitro and in vivo. *J. Biomed. Mater. Res., Part A*. 2004, 68, (3): 411-422.

92. Zhang Z, Roy R, Dugré FJ, Tessier D, Dao LH, In vitro biocompatibility study of electrically conductive polypyrrole-coated polyester fabrics. *J. Biomed. Mater. Res.* 2001, 57, (1): 63-71.

93. Ramanaviciene A, Kausaite A, Tautkus S, Ramanavicius A, Biocompatibility of polypyrrole particles: an in-vivo study in mice. *J. Pharm. Pharmacol.* 2007, 59, (2): 311-315.

94. Shi G, Rouabhia M, Meng S, Zhang Z, Electrical stimulation enhances viability of human cutaneous fibroblasts on conductive biodegradable substrates. *Journal of Biomedical Materials Research Part A*. 2008, 84, (4): 1026-1037.

95. Schmidt CE, Shastri VR, Vacanti JP, Langer R, Stimulation of neurite outgrowth using an electrically conducting polymer. *Proc. Natl. Acad. Sci.* 1997, 94, (17): 8948-8953.

96. Rivers TJ, Hudson TW, Schmidt CE, Synthesis of a novel, biodegradable electrically conducting polymer for biomedical applications. *Adv. Funct. Mater.* 2002, 12, (1): 33-37.

97. Lee JY, Bashur CA, Milroy CA, Forciniti L, Goldstein AS, Schmidt CE, Nerve growth factor-immobilized electrically conducting fibrous scaffolds for potential use in neural engineering applications. *IEEE Trans. Nanobioscience.* 2012, 11, (1): 15-21.

98. Rouabhia M, Park H, Meng S, Derbali H, Zhang Z, Electrical stimulation promotes wound healing by enhancing dermal fibroblast activity and promoting myofibroblast transdifferentiation. *PLoS One*. 2013, 8, (8): e71660.

99. Wang Y, Rouabhia M, Zhang Z, Pulsed electrical stimulation benefits wound healing by activating skin fibroblasts through the TGFβ1/ERK/NF-κB axis. *Biochim. Biophys. Acta, Gen. Subj.* 2016, 1860, (7): 1551-1559.

100. Rouabhia M, Park HJ, Zhang Z, Electrically activated primary human fibroblasts improve in vitro and in vivo skin regeneration. *J. Cell. Physiol.* 2016, 231, (8): 1814-1821.

101. Wang Y, Rouabhia M, Lavertu D, Zhang Z, Pulsed electrical stimulation modulates fibroblasts' behaviour through the Smad signalling pathway. *J. Tissue Eng. Regen. Med.* 2015.

102. Park HJ, Rouabhia M, Lavertu D, Zhang Z, Electrical stimulation modulates the expression of multiple wound healing genes in primary human dermal fibroblasts. *Tissue Eng. Part A*. 2015, 21, (13-14): 1982-1990.

103. Wang Y, Rouabhia M, Zhang Z, PPy-coated PET fabrics and electric pulse-stimulated fibroblasts. *J. Mater. Chem. B.* 2013, 1, (31): 3789-3796.

104. Kai D, Prabhakaran MP, Jin G, Ramakrishna S, Polypyrrole-contained electrospun conductive nanofibrous membranes for cardiac tissue engineering. *J. Biomed. Mater. Res., Part A*. 2011, 99, (3): 376-385.

105. Gilmore KJ, Kita M, Han Y, Gelmi A, Higgins MJ, Moulton SE, Clark GM, Kapsa R, Wallace GG, Skeletal muscle cell proliferation and differentiation on polypyrrole substrates doped with extracellular matrix components. *Biomaterials*. 2009, 30, (29): 5292-5304.

106. Meng S, Zhang Z, Rouabhia M, Accelerated osteoblast mineralization on a conductive substrate by multiple electrical stimulation. *J. Bone Miner. Metab.* 2011, 29, (5): 535-544.

107. Pelto J, Björninen M, Pälli A, Talvitie E, Hyttinen J, Mannerström B, Suuronen Seppanen R, Kellomäki M, Miettinen S, Haimi S, Novel polypyrrole-coated polylactide scaffolds enhance adipose stem cell proliferation and early osteogenic differentiation. *Tissue Eng. Part A*. 2013, 19, (7-8): 882-892.

108. Tessier D, Dao LH, Zhang Z, King MW, Guidoin R, Polymerization and surface analysis of electrically-conductive polypyrrole on surface-activated polyester fabrics for biomedical applications. *J. Biomater. Sci. Polym. Ed.* 2000, 11, (1): 87-99.

109. Meng S, Rouabhia M, Shi G, Zhang Z, Heparin dopant increases the electrical stability, cell adhesion, and growth of conducting polypyrrole/poly (L, L-lactide) composites. *J. Biomed. Mater. Res., Part A*. 2008, 87, (2): 332-344.

110. Weng B, Liu X, Shepherd R, Wallace GG, Inkjet printed polypyrrole/collagen scaffold: A combination of spatial control and electrical stimulation of PC12 cells. *Synthetic Metals*. 2012, 162, (15): 1375-1380.

111. Akkouch A, Shi G, Zhang Z, Rouabhia M, Bioactivating electrically conducting polypyrrole with fibronectin and bovine serum albumin. *Journal of Biomedical Materials Research Part A*. 2010, 92, (1): 221-231.

112. Grill WM, Norman SE, Bellamkonda RV, Implanted neural interfaces: biochallenges and engineered solutions. *Annu. Rev. Biomed. Eng.* 2009, 11: 1-24.

113. Cui X, Hetke JF, Wiler JA, Anderson DJ, Martin DC, Electrochemical deposition and characterization of conducting polymer polypyrrole/PSS on multichannel neural probes. *Sens. Actuators, A*. 2001, 93, (1): 8-18.

114. Cui X, Lee VA, Raphael Y, Wiler JA, Hetke JF, Anderson DJ, Martin DC, Surface modification of neural recording electrodes with conducting polymer/biomolecule blends. *J. Biomed. Mater. Res.* 2001, 56, (2): 261-272.

115. Abidian MR, Martin DC, Experimental and theoretical characterization of implantable neural microelectrodes modified with conducting polymer nanotubes. *Biomaterials*. 2008, 29, (9): 1273-1283.

116. Kim D-H, Abidian M, Martin DC, Conducting polymers grown in hydrogel scaffolds coated on neural prosthetic devices. *J. Biomed. Mater. Res., Part A*. 2004, 71A, (4): 577-585.

117. He W, McConnell GC, Schneider TM, Bellamkonda RV, A novel anti-inflammatory surface for neural electrodes. *Adv. Mater.* 2007, 19, (21): 3529-3533.

118. Wadhwa R, Lagenaur CF, Cui XT, Electrochemically controlled release of dexamethasone from conducting polymer polypyrrole coated electrode. *J. Control. Release*. 2006, 110, (3): 531-541.

119. Richardson RT, Wise AK, Thompson BC, Flynn BO, Atkinson PJ, Fretwell NJ, Fallon JB, Wallace GG, Shepherd RK, Clark GM, Polypyrrole-coated electrodes for the delivery of charge and neurotrophins to cochlear neurons. *Biomaterials*. 2009, 30, (13): 2614-2624.

120. Higgins MJ, Molino PJ, Yue Z, Wallace GG, Organic conducting polymer–protein interactions. *Chem. Mater.* 2012, 24, (5): 828-839.

121. Liu X, Yue Z, Higgins MJ, Wallace GG, Conducting polymers with immobilised fibrillar collagen for enhanced neural interfacing. *Biomaterials*. 2011, 32, (30): 7309-7317.

122. Gomez N, Schmidt CE, Nerve growth factor-immobilized polypyrrole: Bioactive electrically conducting polymer for enhanced neurite extension. *Journal of Biomedical Materials Research Part A*. 2007, 81, (1): 135-149.

123. Gerard M, Chaubey A, Malhotra B, Application of conducting polymers to biosensors. *Biosensors and Bioelectronics*. 2002, 17, (5): 345-359.

124. Malhotra BD, Chaubey A, Singh S, Prospects of conducting polymers in biosensors. *Analytica chimica acta*. 2006, 578, (1): 59-74.

125. Ahuja T, Mir IA, Kumar D, Biomolecular immobilization on conducting polymers for biosensing applications. *Biomaterials*. 2007, 28, (5): 791-805.

126. Fang Y, Ni Y, Zhang G, Mao C, Huang X, Shen J, Biocompatibility of CS–PPy nanocomposites and their application to glucose biosensor. *Bioelectrochemistry*. 2012, 88: 1-7.

127. Soares JC, Brisolari A, Rodrigues VdC, Sanches EA, Gonçalves D, Amperometric urea biosensors based on the entrapment of urease in polypyrrole films. *Reactive and Functional Polymers*. 2012, 72, (2): 148-152.

128. Jiang H, Zhang A, Sun Y, Ru X, Ge D, Shi W, Poly (1-(2-carboxyethyl) pyrrole)/polypyrrole composite nanowires for glucose biosensor. *Electrochim. Acta*. 2012, 70: 278-285.

129. Arora K, Prabhakar N, Chand S, Malhotra B, Immobilization of single stranded DNA probe onto polypyrrole-polyvinyl sulfonate for application to DNA hybridization biosensor. *Sensors and Actuators B: Chemical*. 2007, 126, (2): 655-663.

130. Jiang X, Lin X, Overoxidized polypyrrole film directed DNA immobilization for construction of electrochemical micro-biosensors and simultaneous determination of serotonin and dopamine. *Analytica chimica acta*. 2005, 537, (1): 145-151.

131. Fu Y, Yuan R, Chai Y, Zhou L, Zhang Y, Coupling of a reagentless electrochemical DNA biosensor with conducting polymer film and nanocomposite as matrices for the detection of the HIV DNA sequences. *Analytical letters*. 2006, 39, (3): 467-482.

132. Ko S, Jang J, Label-free target DNA recognition using oligonucleotide-functionalized polypyrrole nanotubes. *Ultramicroscopy*. 2008, 108, (10): 1328-1333.

133. Palecek E, Oscillographic polarography of highly polymerized deoxyribonucleic acid. *Nature*. 1960, 188: 656-657.

134. Sassolas A, Leca-Bouvier BD, Blum LJ, DNA biosensors and microarrays. *Chemical reviews*. 2008, 108, (1): 109-139.

135. Baur J, Gondran C, Holzinger M, Defrancq E, Perrot H, Cosnier S, Label-free femtomolar detection of target DNA by impedimetric DNA sensor based on poly (pyrrole-nitrilotriacetic acid) film. *Analytical chemistry*. 2009, 82, (3): 1066-1072.

136. Kausaite-Minkstimiene A, Ramanaviciene A, Kirlyte J, Ramanavicius A, Comparative study of random and oriented antibody immobilization techniques on the binding capacity of immunosensor. *Analytical chemistry*. 2010, 82, (15): 6401-6408.

137. Ramanavicius A, Finkelsteinas A, Cesiulis H, Ramanaviciene A, Electrochemical impedance spectroscopy of polypyrrole based electrochemical immunosensor. *Bioelectrochemistry*. 2010, 79, (1): 11-16.

138. Hu W, Li CM, Dong H, Poly(pyrrole-co-pyrrole propylic acid) film and its application in label-free surface plasmon resonance immunosensors. *Anal. Chim. Acta*. 2008, 630, (1): 67-74.

139. Chen W, Lei Y, Li CM, Regenerable leptin immunosensor based on protein G immobilized Au-pyrrole propylic acid-polypyrrole nanocomposite. *Electroanalysis*. 2010, 22, (10): 1078-1083.

140. Hu W, Li CM, Cui X, Dong H, Zhou Q, In situ studies of protein adsorptions on poly (pyrrole-co-pyrrole propylic acid) film by electrochemical surface plasmon resonance. *Langmuir*. 2007, 23, (5): 2761-2767.

141. Makaraviciute A, Ramanaviciene A, Site-directed antibody immobilization techniques for immunosensors. *Biosens. Bioelectron.* 2013, 50: 460-471.

142. Truong LTN, Chikae M, Ukita Y, Takamura Y, Labelless impedance immunosensor based on polypyrrole–pyrolecarboxylic acid copolymer for hCG detection. *Talanta*. 2011, 85, (5): 2576-2580.

143. Kwon OS, Park SJ, Jang J, A high-performance VEGF aptamer functionalized polypyrrole nanotube biosensor. *Biomaterials*. 2010, 31, (17): 4740-4747.

144. Bangar MA, Shirale DJ, Chen W, Myung NV, Mulchandani A, Single Conducting Polymer Nanowire Chemiresistive Label-Free Immunosensor for Cancer Biomarker. *Anal. Chem.* 2009, 81, (6): 2168-2175.

145. Minett AI, Barisci JN, Wallace GG, Immobilisation of anti-Listeria in a polypyrrole film. *Reactive and Functional Polymers*. 2002, 53, (2–3): 217-227.

146. Chartuprayoon N, Chartuprayoon Y, Ng J, Nam W, Chen N, Polypyrrole nanoribbon based chemiresistive immunosensors for viral plant pathogen detection. *Anal. Methods*. 2013, 5, (14): 3497-3502.

147. Shirale DJ, Bangar MA, Park M, Yates MV, Chen W, Myung NV, Mulchandani A, Label-Free Chemiresistive Immunosensors for Viruses. *Environ. Sci. Technol.* 2010, 44, (23): 9030-9035.

148. Zinger B, Miller LL, Timed release of chemicals from polypyrrole films. *JACS*. 1984, 106, (22): 6861-6863.

149. Lin Y, Wallace G, Factors influencing electrochemical release of 2, 6-anthraquinone disulphonic acid from polypyrrole. *J. Control. Release*. 1994, 30, (2): 137-142.

150. Thompson BC, Moulton SE, Ding J, Richardson R, Cameron A, O'Leary S, Wallace GG, Clark GM, Optimising the incorporation and release of a neurotrophic factor using conducting polypyrrole. *J. Control. Release*. 2006, 116, (3): 285-294.

151. Bidan G, Lopez C, Mendes-Viegas F, Vieil E, Gadelle A, Incorporation of sulphonated cyclodextrins into polypyrrole: an approach for the electro-controlled delivering of neutral drugs. *Biosens. Bioelectron.* 1995, 10, (1): 219-229.

152. Svirskis D, Travas-Sejdic J, Rodgers A, Garg S, Electrochemically controlled drug delivery based on intrinsically conducting polymers. *J. Control. Release*. 2010, 146, (1): 6-15.

153. George PM, LaVan DA, Burdick JA, Chen CY, Liang E, Langer R, Electrically controlled drug delivery from biotin-doped conductive polypyrrole. *Adv. Mater.* 2006, 18, (5): 577-581.

154. Valero L, Arias-Pardilla J, Cauich-Rodríguez J, Smit M, Otero T, Characterization of the movement of polypyrrole–dodecylbenzenesulfonate–perchlorate/tape artificial muscles. Faradaic control of reactive artificial molecular motors and muscles. *Electrochim. Acta*. 2011, 56, (10): 3721-3726.

155. García-Córdova F, Valero L, Ismail YA, Otero TF, Biomimetic polypyrrole based all three-in-one triple layer sensing actuators exchanging cations. *J. Mater. Chem.* 2011, 21, (43): 17265-17272.

156. Della Santa A, De Rossi D, Mazzoldi A, Performance and work capacity of a polypyrrole conducting polymer linear actuator. *Synth. Met.* 1997, 90, (2): 93-100.

157. Kaneto K, Suematsu H, Yamato K, Training effect and fatigue in polypyrrole-based artificial muscles. *Bioinspir. Biomim.* 2008, 3, (3): 035005.

158. Huang Y, Li H, Wang Z, Zhu M, Pei Z, Xue Q, Huang Y, Zhi C, Nanostructured Polypyrrole as a flexible electrode material of supercapacitor. *Nano Energy*. 2016, 22: 422-438.

159. Wang G, Zhang L, Zhang J, A review of electrode materials for electrochemical supercapacitors. *Chem. Soc. Rev.* 2012, 41, (2): 797-828.

160. Li X, Fang D, Cao Y, Luo Z, Jiang M, Xu W, Xiong C, Template-sacrificed synthesis of polypyrrole nanofibers for lithium battery. *J. Mater. Sci.* 2016, 51, (20): 9526-9533.

161. Simon P, Gogotsi Y, Materials for electrochemical capacitors. *Nat. Mater.* 2008, 7, (11): 845-854.

162. Dubal DP, Kim JG, Kim Y, Holze R, Lokhande CD, Kim WB, Supercapacitors based on flexible substrates: An overview. *Energy Technol.* 2014, 2, (4): 325-341.

163. Jiang L-b, Yuan X-z, Liang J, Zhang J, Wang H, Zeng G-m, Nanostructured core-shell electrode materials for electrochemical capacitors. *J. Power Sources*. 2016, 331: 408-425.

164. Conway B, Birss V, Wojtowicz J, The role and utilization of pseudocapacitance for energy storage by supercapacitors. *J. Power Sources*. 1997, 66, (1): 1-14.

165. Shi C, Zhitomirsky I, Electrodeposition and capacitive behavior of films for electrodes of electrochemical supercapacitors. *Nanoscale Res. Lett.* 2010, 5, (3): 518.

166. Shinde SS, Gund GS, Kumbhar VS, Patil BH, Lokhande CD, Novel chemical synthesis of polypyrrole thin film electrodes for supercapacitor application. *Eur. Polym. J.* 2013, 49, (11): 3734-3739.

167. Sharma RK, Rastogi AC, Desu SB, Manganese oxide embedded polypyrrole nanocomposites for electrochemical supercapacitor. *Electrochim. Acta*. 2008, 53, (26): 7690-7695.

168. Kim J-H, Lee Y-S, Sharma AK, Liu CG, Polypyrrole/carbon composite electrode for high-power electrochemical capacitors. *Electrochim. Acta*. 2006, 52, (4): 1727-1732.

169. Wang H, Bian L, Zhou P, Tang J, Tang W, Core-sheath structured bacterial cellulose/polypyrrole nanocomposites with excellent conductivity as supercapacitors. *J. Mater. Chem. A.* 2013, 1, (3): 578-584.

170. Li J, Que T, Huang J, Synthesis and characterization of a novel tube-in-tube nanostructured PPy/MnO2/CNTs composite for supercapacitor. *Mater. Res. Bull.* 2013, 48, (2): 747-751.

171. Qin T, Liu B, Wen Y, Wang Z, Jiang X, Wan Z, Peng S, Cao G, He D, Freestanding flexible graphene foams@polypyrrole@MnO2 electrodes for high-performance supercapacitors. *J. Mater. Chem. A.* 2016, 4, (23): 9196-9203.

172. Shao M, Li Z, Zhang R, Ning F, Wei M, Evans DG, Duan X, Hierarchical conducting polymer@clay core–shell arrays for flexible all-solid-state supercapacitor devices. *Small*. 2015, 11, (29): 3530-3538.

173. Zhai S, Karahan HE, Wei L, Qian Q, Harris AT, Minett AI, Ramakrishna S, Ng AK, Chen Y, Textile energy storage: Structural design concepts, material selection and future perspectives. *Energy Storage Mater*. 2016, 3: 123-139.

174. Shi Y, Pan L, Liu B, Wang Y, Cui Y, Bao Z, Yu G, Nanostructured conductive polypyrrole hydrogels as high-performance, flexible supercapacitor electrodes. *J. Mater. Chem. A.* 2014, 2, (17): 6086-6091.

175. Liu P, Wang X, Li H, Preparation of carboxylated carbon nanotubes/polypyrrole composite hollow microspheres via chemical oxidative interfacial polymerization and their electrochemical performance. *Synth. Met.* 2013, 181: 72-78.

176. Huang J, Wang K, Wei Z, Conducting polymer nanowire arrays with enhanced electrochemical performance. *J. Mater. Chem.* 2010, 20, (6): 1117-1121.

177. Wu Q-F, He K-X, Mi H-Y, Zhang X-G, Electrochemical capacitance of polypyrrole nanowire prepared by using cetyltrimethylammonium bromide (CTAB) as soft template. *Mater. Chem. Phys.* 2007, 101, (2–3): 367-371.

178. Lei W, He P, Wang Y, Zhang S, Dong F, Liu H, Soft template interfacial growth of novel ultralong polypyrrole nanowires for electrochemical energy storage. *Electrochim. Acta*. 2014, 132: 112-117.

179. Zhao J, Wu J, Li B, Du W, Huang Q, Zheng M, Xue H, Pang H, Facile synthesis of polypyrrole nanowires for high-performance supercapacitor electrode materials. *Prog. Natural Sci. Mater. Int.* 2016, 26, (3): 237-242.

180. Sahoo S, Dhibar S, Das C, Facile synthesis of polypyrrole nanofiber and its enhanced electrochemical performances in different electrolytes. *Express Polym. Lett.* 2012, 6, (12): 965-974.

181. Yang C, Liu P, Wang T, Well-defined core− shell carbon black/polypyrrole nanocomposites for electrochemical energy storage. *ACS Appl. Mater. Interfaces.* 2011, 3, (4): 1109-1114.

182. Yuan W, Han G, Xiao Y, Chang Y, Liu C, Li M, Li Y, Zhang Y, Flexible electrochemical capacitors based on polypyrrole/carbon fibers via chemical polymerization of pyrrole vapor. *Appl. Surf. Sci.* 2016, 377: 274-282.

183. Li P, Shi E, Yang Y, Shang Y, Peng Q, Wu S, Wei J, Wang K, Zhu H, Yuan Q, Cao A, Wu D, Carbon nanotube-polypyrrole core-shell sponge and its application as highly compressible supercapacitor electrode. *Nano Res.* 2014, 7, (2): 209-218.

184. Yang L, Shi Z, Yang W, Polypyrrole directly bonded to air-plasma activated carbon nanotube as electrode materials for high-performance supercapacitor. *Electrochim. Acta*. 2015, 153: 76-82.

185. Hu Y, Zhao Y, Li Y, Li H, Shao H, Qu L, Defective super-long carbon nanotubes and polypyrrole composite for high-performance supercapacitor electrodes. *Electrochim. Acta*. 2012, 66: 279-286.

186. Qi K, Qiu Y, Guo X, Pulse electrochemical incorporation of graphene oxide into polypyrrole films for supercapacitor electrode materials. *Electrochim. Acta*. 2014, 137: 685-692.

187. Li J, Xie H, Li Y, Fabrication of graphene oxide/polypyrrole nanowire composite for high performance supercapacitor electrodes. *J. Power Sources*. 2013, 241: 388-395.

188. Yang C, Zhang L, Hu N, Yang Z, Wei H, Zhang Y, Reduced graphene oxide/polypyrrole nanotube papers for flexible all-solid-state supercapacitors with excellent rate capability and high energy density. *J. Power Sources*. 2016, 302: 39-45.

189. Kashani H, Chen L, Ito Y, Han J, Hirata A, Chen M, Bicontinuous nanotubular graphene–polypyrrole hybrid for high performance flexible supercapacitors. *Nano Energy*. 2016, 19: 391-400.

190. He Y, Bai Y, Yang X, Zhang J, Kang L, Xu H, Shi F, Lei Z, Liu Z-H, Holey graphene/polypyrrole nanoparticle hybrid aerogels with three-dimensional hierarchical porous structure for high performance supercapacitor. *J. Power Sources*. 2016, 317: 10-18.

191. Dong ZH, Wei YL, Shi W, Zhang GA, Characterisation of doped polypyrrole/manganese oxide nanocomposite for supercapacitor electrodes. *Mater. Chem. Phys.* 2011, 131, (1–2): 529-534.

192. Wang N, Zhao P, Liang K, Yao M, Yang Y, Hu W, CVD-grown polypyrrole nanofilms on highly mesoporous structure MnO2 for high performance asymmetric supercapacitors. *Chem. Eng. J.* 2017, 307: 105-112.

193. Li J, Cui L, Zhang X, Preparation and electrochemistry of one-dimensional nanostructured MnO2/PPy composite for electrochemical capacitor. *Appl. Surf. Sci.* 2010, 256, (13): 4339-4343.

194. Cao L, Zhu J, Li Y, Xiao P, Zhang Y, Zhang S, Yang S, Ultrathin single-crystalline vanadium pentoxide nanoribbon constructed 3D networks for superior energy storage. *J. Mater. Chem. A.* 2014, 2, (32): 13136-13142.

195. Yang J, Lan T, Liu J, Song Y, Wei M, Supercapacitor electrode of hollow spherical V2O5 with a high pseudocapacitance in aqueous solution. *Electrochim. Acta*. 2013, 105: 489-495.

196. Bai M-H, Bian L-J, Song Y, Liu X-X, Electrochemical codeposition of vanadium oxide and polypyrrole for high-performance supercapacitor with high working voltage. *ACS Appl. Mater. Interfaces.* 2014, 6, (15): 12656-12664.

197. Hu J, Li M, Lv F, Yang M, Tao P, Tang Y, Liu H, Lu Z, Heterogeneous NiCo2O4@polypyrrole core/sheath nanowire arrays on Ni foam for high performance supercapacitors. *J. Power Sources*. 2015, 294: 120-127.

198. Yang X, Xu K, Zou R, Hu J, A Hybrid Electrode of Co3O4@PPy Core/Shell Nanosheet Arrays for High-Performance Supercapacitors. *Nano-Micro Lett.* 2016, 8, (2): 143-150.

199. Xiong W, Pan X, Li Y, Chen X, Zhu Y, Yang M, Zhang Y, Hierarchical Co3O4@PPy core/shell nanowire arrays on nickel foam for electrochemical energy storage. *Mater. Lett.* 2015, 157: 23-26.

200. Zhou C, Zhang Y, Li Y, Liu J, Construction of high-capacitance 3D CoO@ polypyrrole nanowire array electrode for aqueous asymmetric supercapacitor. *Nano Lett.* 2013, 13, (5): 2078-2085.

201. Wang F, Zhan X, Cheng Z, Wang Z, Wang Q, Xu K, Safdar M, He J, Tungsten oxide@polypyrrole core–shell nanowire arrays as novel negative electrodes for asymmetric supercapacitors. *Small*. 2015, 11, (6): 749-755.

202. Mi H, Zhang X, Ye X, Yang S, Preparation and enhanced capacitance of core–shell polypyrrole/polyaniline composite electrode for supercapacitors. *J. Power Sources*. 2008, 176, (1): 403-409.

203. Liang B, Qin Z, Zhao J, Zhang Y, Zhou Z, Lu Y, Controlled synthesis, core-shell structures and electrochemical properties of polyaniline/polypyrrole composite nanofibers. *J. Mater. Chem. A.* 2014, 2, (7): 2129-2135.

204. Xie Y, Wang D, Ji J, Preparation and supercapacitor performance of freestanding polypyrrole/polyaniline coaxial nanoarrays. *Energy Technol.* 2016, 4, (6): 714-721.

205. Xiong W, Hu X, Wu X, Zeng Y, Wang B, He G, Zhu Z, A flexible fiber-shaped supercapacitor utilizing hierarchical NiCo2O4@polypyrrole core-shell nanowires on hemp-derived carbon. *J. Mater. Chem. A.* 2015, 3, (33): 17209-17216.

206. Thackeray MM, Wolverton C, Isaacs ED, Electrical energy storage for transportation-approaching the limits of, and going beyond, lithium-ion batteries. *Energy Environ. Sci.* 2012, 5, (7): 7854-7863.

207. Barghamadi M, Kapoor A, Wen C, A review on Li-S batteries as a high efficiency rechargeable lithium battery. *J. Electrochem. Soc.* 2013, 160, (8): A1256-A1263.

208. Wang G, Yang L, Chen Y, Wang J, Bewlay S, Liu H, An investigation of polypyrrole-LiFePO 4 composite cathode materials for lithium-ion batteries. *Electrochim. Acta*. 2005, 50, (24): 4649-4654.

209. Kuwabata S, Masui S, Yoneyama H, Charge–discharge properties of composites of LiMn 2 O 4 and polypyrrole as positive electrode materials for 4 V class of rechargeable Li batteries. *Electrochim. Acta*. 1999, 44, (25): 4593-4600.

210. Cui L, Shen J, Cheng F, Tao Z, Chen J, SnO 2 nanoparticles@ polypyrrole nanowires composite as anode materials for rechargeable lithium-ion batteries. *J. Power Sources*. 2011, 196, (4): 2195-2201.

211. Liang C, Fang D, Cao Y, Li G, Luo Z, Zhou Q, Xiong C, Xu W, Polypyrrole-encapsulated vanadium pentoxide nanowires on a conductive substrate for electrode in aqueous rechargeable lithium battery. *J. Colloid Interface Sci.* 2015, 439: 69-75.

212. Li X, Chen Y, Zou J, Zeng X, Zhou L, Huang H, Stable freestanding Li-ion battery cathodes by in situ conformal coating of conducting polypyrrole on NiS-carbon nanofiber films. *J. Power Sources*. 2016, 331: 360-365.

213. Liu R, Liu Y, Kang Q, Casimir A, Zhang H, Li N, Huang Z, Li Y, Lin X, Feng X, Ma Y, Wu G, Synergistic effect of graphene and polypyrrole to enhance the SnO2 anode performance in lithium-ion batteries. *RSC Advances*. 2016, 6, (12): 9402-9410.

214. Xie D, Wang DH, Tang WJ, Xia XH, Zhang YJ, Wang XL, Gu CD, Tu JP, Binder-free network-enabled MoS2-PPY-rGO ternary electrode for high capacity and excellent stability of lithium storage. *J. Power Sources*. 2016, 307: 510-518.

215. Jeong YG, Jeon GW, Microstructure and performance of multiwalled carbon nanotube/m-aramid composite films as electric heating elements. *ACS Appl. Mater. Interfaces.* 2013, 5, (14): 6527-6534.

216. Cheng TC, Cheng ET, Cheng JT, Cheng IY, Medical heating device and method with self-limiting electrical heating element. Google Patents: 2015.

217. Kim T, Kim YW, Lee HS, Kim H, Yang WS, Suh KS, Uniformly interconnected silver-nanowire networks for transparent film heaters. *Adv. Funct. Mater.* 2013, 23, (10): 1250-1255.

218. Kaynak A, Håkansson E, Generating heat from conducting polypyrrole-coated PET fabrics. *Adv. Polym. Tech.* 2005, 24, (3): 194-207.

219. Shang S, Yang X, Tao X-m, Lam SS, Vapor-phase polymerization of pyrrole on flexible substrate at low temperature and its application in heat generation. *Polym. Int.* 2010, 59, (2): 204-211.

220. Hakansson E, Kaynak A, Lin T, Nahavandi S, Jones T, Hu E, Characterization of conducting polymer coated synthetic fabrics for heat generation. *Synth. Met.* 2004, 144, (1): 21-28.

221. Zhu L, Zhang L, Wu L, Sun Y, Bai Z, Xu J, Liang G, Xu W, Conductive cotton fabrics for heat generation prepared by mist polymerization. *Fiber. Polym.* 2014, 15, (9): 1804-1809.

222. Oroumei A, Tavanai H, Morshed M, Electrical resistance and heat generation of polypyrrole-coated polyacrylonitrile nanofibrous and regular fibrous mats. *Polym. Adv. Technol.* 2012, 23, (9): 1302-1310.

223. Zhou J, Mulle M, Zhang Y, Xu X, Li EQ, Han F, Thoroddsen ST, Lubineau G, High-ampacity conductive polymer microfibers as fast response wearable heaters and electromechanical actuators. *J. Mater. Chem. C.* 2016, 4, (6): 1238-1249.

224. Vallejo-Giraldo C, Kelly A, Biggs MJ, Biofunctionalisation of electrically conducting polymers. *Drug Discov.Today*. 2014, 19, (1): 88-94.

225. Dicks J, Cardosi M, Turner A, Karube I, The application of ferrocene-modified n-type silicon in glucose biosensors. *Electroanalysis*. 1993, 5, (1): 1-9.

226. Sanghvi AB, Miller KP-H, Belcher AM, Schmidt CE, Biomaterials functionalization using a novel peptide that selectively binds to a conducting polymer. *Nat. Mater.* 2005, 4, (6): 496.

227. Nickels JD, Schmidt CE, Surface modification of the conducting polymer, polypyrrole, via affinity peptide. *J. Biomed. Mater. Res., Part A.* 2013, 101, (5): 1464-1471.

228. Li JR, Cai M, Chen TF, Jiang L, Enzyme electrodes with conductive polymer membranes and Langmuir-Blodgett films. *Thin Solid Films*. 1989, 180, (1): 205-210.

229. Ekanayake EM, Preethichandra DM, Kaneto K, Polypyrrole nanotube array sensor for enhanced adsorption of glucose oxidase in glucose biosensors. *Biosens. Bioelectron.* 2007, 23, (1): 107-113.

230. Bendrea A-D, Cianga L, Cianga I, Review paper: progress in the field of conducting polymers for tissue engineering applications. *J. Biomater. Appl.* 2011, 26, (1): 3-84.

231. Meng S, Rouabhia M, Zhang Z, Electrical stimulation modulates osteoblast proliferation and bone protein production through heparin-bioactivated conductive scaffolds. *Bioelectromagnetics*. 2013, 34, (3): 189-199.

232. Stewart E, Liu X, Clark G, Kapsa R, Wallace GG, Inhibition of smooth muscle cell adhesion and proliferation on heparin-doped polypyrrole. *Acta biomaterialia*. 2012, 8, (1): 194-200.

233. Garner B, Georgevich A, Hodgson A, Liu L, Wallace G, Polypyrrole–heparin composites as stimulus-responsive substrates for endothelial cell growth. *J. Biomed. Mater. Res.* 1999, 44, (2): 121-129.

234. Ghasemi-Mobarakeh L, Prabhakaran MP, Morshed M, Nasr-Esfahani MH, Baharvand H, Kiani S, Al-Deyab SS, Ramakrishna S, Application of conductive polymers, scaffolds and electrical stimulation for nerve tissue engineering. *J. Tissue Eng. Regen. Med.* 2011, 5, (4): e17-e35.

235. Moreno JS, Panero S, Artico M, Filippini P, Synthesis and characterization of new electroactive polypyrrole–chondroitin sulphate A substrates. *Bioelectrochemistry*. 2008, 72, (1): 3-9.

236. Gelmi A, Higgins MJ, Wallace GG, Physical surface and electromechanical properties of doped polypyrrole biomaterials. *Biomaterials*. 2010, 31, (8): 1974-1983.

237. Wang J, Jiang M, Fortes A, Mukherjee B, New label-free DNA recognition based on doping nucleic-acid probes within conducting polymer films. *Anal. Chim. Acta*. 1999, 402, (1): 7-12.

238. Barisci J, Hughes D, Minett A, Wallace G, Characterisation and analytical use of a polypyrrole electrode containing anti-human serum albumin. *Anal. Chim. Acta*. 1998, 371, (1): 39-48.

239. Ramanavicius A, Habermüller K, Csöregi E, Laurinavicius V, Schuhmann W, Polypyrrole-entrapped quinohemoprotein alcohol dehydrogenase. Evidence for direct electron transfer via conducting-polymer chains. *Anal. Chem.* 1999, 71, (16): 3581-3586.

240. Kontturi K, Pentti P, Sundholm G, Polypyrrole as a model membrane for drug delivery. *J. Electroanal. Chem.* 1998, 453, (1): 231-238.

241. Zhou Q-X, Miller LL, Valentine JR, Electrochemically controlled binding and release of protonated dimethyldopamine and other cations from poly (N-methyl-pyrrole)/polyanion composite redox polymers. *J. Electroanal. Chem.* 1989, 261, (1): 147-164.

242. Hepel M, Mahdavi F, Application of the electrochemical quartz crystal microbalance for electrochemically controlled binding and release of chlorpromazine from conductive polymer matrix. *Microchem. J.* 1997, 56, (1): 54-64.

243. Lee J-W, Serna F, Schmidt CE, Carboxy-endcapped conductive polypyrrole: biomimetic conducting polymer for cell scaffolds and electrodes. *Langmuir*. 2006, 22, (24): 9816-9819.

244. Roy CJ, Leprince L, De Boulard A, Landoulsi J, Callegari V, Jonas AM, Demoustier-Champagne S, Electrosynthesis of pyrrole 3-carboxylic acid copolymer films and nanotubes with tunable degree of functionalization for biomedical applications. *Electrochim. Acta*. 2011, 56, (10): 3641-3648.

245. Janmanee R, Baba A, Phanichphant S, Sriwichai S, Shinbo K, Kato K, Kaneko F, In situ electrochemical-transmission surface plasmon resonance spectroscopy for poly (pyrrole-3-carboxylic acid) thin-film-based biosensor applications. *ACS Appl. Mater. Interfaces.* 2012, 4, (8): 4270-4275.

246. Rapiphun J, Akira B, Sukon P, Saengrawee S, Kazunari S, Keizo K, Futao K, Detection of Human IgG on Poly(pyrrole-3-carboxylic acid) Thin Film by Electrochemical-Surface Plasmon Resonance Spectroscopy. *Jpn. J. Appl. Phys.* 2011, 50, (1S2): 01BK02.

247. Shi W, Cao H, Song C, Jiang H, Wang J, Jiang S, Tu J, Ge D, Poly(pyrrole-3-carboxylic acid)-alumina composite membrane for affinity adsorption of bilirubin. *J. Membr. Sci.* 2010, 353, (1–2): 151-158.

248. Patterson JM, Brasch J, Drenchko P, Synthesis and pyrolysis of some cycloalkano[a]pyrroles1. *J. Org. Chem.* 1962, 27, (5): 1652-1659.

249. Maeda S, Corradi R, Armes SP, Synthesis and characterization of carboxylic acid-functionalized polypyrrole-silica microparticles. *Macromolecules*. 1995, 28, (8): 2905-2911.

250. Rajesh, Bisht V, Takashima W, Kaneto K, A novel thin film urea biosensor based on copolymer poly(N-3-aminopropylpyrrole-co-pyrrole) film. *Surf. Coat. Technol.* 2005, 198, (1–3): 231-236.

251. Bozgeyik İ, Şenel M, Çevik E, Abasıyanık MF, A novel thin film amperometric urea biosensor based on urease-immobilized on poly(N-glycidylpyrrole-co-pyrrole). *Curr. Appl. Phys.* 2011, 11, (4): 1083-1088.

252. Khan W, Kapoor M, Kumar N, Covalent attachment of proteins to functionalized polypyrrole-coated metallic surfaces for improved biocompatibility. *Acta Biomaterialia*. 2007, 3, (4): 541-549.

253. Lee JY, Lee J-W, Schmidt CE, Neuroactive conducting scaffolds: nerve growth factor conjugation on active ester-functionalized polypyrrole. *Journal of the Royal Society Interface*. 2009, 6, (38): 801-810.

254. Ko S, Jang J, Controlled amine functionalization on conducting polypyrrole nanotubes as effective transducers for volatile acetic acid. *Biomacromolecules*. 2007, 8, (1): 182-187.

255. Shimomura M, Miyata R, Kuwahara T, Oshima K, Miyauchi S, Immobilization of glucose oxidase on the films prepared by electrochemical copolymerization of pyrrole and 1-(2-carboxyethyl) pyrrole for glucose sensing. *Eur. Polym. J.* 2007, 43, (2): 388-394.

256. Li W, Qiu T, Wang L, Ren S, Zhang J, He L, Li X, Preparation and electromagnetic properties of core/shell polystyrene@ polypyrrole@ nickel composite microspheres. *ACS Appl. Mater. Interfaces.* 2013, 5, (3): 883-891.

257. Madani A, Nessark B, Brayner R, Elaissari H, Jouini M, Mangeney C, Chehimi MM, Carboxylic acid-functionalized, core–shell polystyrene@ polypyrrole microspheres as platforms for the attachment of CdS nanoparticles. *Polymer*. 2010, 51, (13): 2825-2835.

258. Lee J-W, Serna F, Nickels J, Schmidt CE, Carboxylic acid-functionalized conductive polypyrrole as a bioactive platform for cell adhesion. *Biomacromolecules*. 2006, 7, (6): 1692-1695.

259. Shi W, Cao H, Shen Y, Song C, Li D, Zhang Y, Ge D, Chemically modified PPyCOOH microtubes as an affinity matrix for protein purification. *Macromol. Chem. Phys.* 2009, 210, (17): 1379-1386.

260. Kojima K, Yamauchi T, Shimomura M, Miyauchi S, Covalent immobilization of glucose oxidase on poly [1-(2-carboxyethyl) pyrrole] film for glucose sensing. *Polymer*. 1998, 39, (11): 2079-2082.

261. Şenel M, Nergiz C, Novel amperometric glucose biosensor based on covalent immobilization of glucose oxidase on poly (pyrrole propylic acid)/Au nanocomposite. *Curr. Appl. Phys.* 2012, 12, (4): 1118-1124.

262. Oshima K, Nakamura T, Matsuoka R, Kuwahara T, Shimomura M, Miyauchi S, Immobilization of alcohol dehydrogenase on poly [1-(2-carboxyethyl) pyrrole] film for fabrication of ethanol-responding electrode. *Synth. Met.* 2005, 152, (1): 33-36.

263. Shimomura M, Kuwahara T, Iizuka K, Kinoshita T, Immobilization of alcohol dehydrogenase on films prepared by the electrochemical copolymerization of pyrrole and 1-(2-carboxyethyl) pyrrole for ethanol sensing. *J. Appl. Polym. Sci.* 2010, 116, (5): 2651-2657.

264. Dong H, Li CM, Chen W, Zhou Q, Zeng ZX, Luong JHT, Sensitive amperometric immunosensing using polypyrrolepropylic acid films for biomolecule immobilization. *Anal. Chem.* 2006, 78, (21): 7424-7431.

265. Chu Y-M, Lin C-C, Chang H-C, Li C, Guo C, TiO2 nanowire FET device: Encapsulation of biomolecules by electro polymerized pyrrole propylic acid. *Biosens. Bioelectron.* 2011, 26, (5): 2334-2340.

266. Serafín V, Agüí L, Yáñez-Sedeño P, Pingarrón JM, Determination of prolactin hormone in serum and urine using an electrochemical immunosensor based on poly(pyrrolepropionic acid)/carbon nanotubes hybrid modified electrodes. *Sens. Actuators, B.* 2014, 195: 494-499.

267. Pan L, Chortos A, Yu G, Wang Y, Isaacson S, Allen R, Shi Y, Dauskardt R, Bao Z, An ultra-sensitive resistive pressure sensor based on hollow-sphere microstructure induced elasticity in conducting polymer film. *Nat. Commun.* 2014, 5: 3002

268. Wang C, Ding Y, Yuan Y, Cao A, He X, Peng Q, Li Y, Multifunctional, highly flexible, free-standing 3D polypyrrole foam. *Small*. 2016, 12, (30): 4070-4076.

269. Yuan W, Han G, Chang Y, Li M, Xiao Y, Zhou H, Zhang Y, Li Y, Performance of flexible capacitors based on polypyrrole/carbon fiber electrochemically prepared from various phosphate electrolytes. *Appl. Surf. Sci.* 2016, 387: 902-911.

270. Lu Y, Li T, Zhao X, Li M, Cao Y, Yang H, Duan YY, Electrodeposited polypyrrole/carbon nanotubes composite films electrodes for neural interfaces. *Biomaterials.* 2010, 31, (19): 5169-5181.

271. Yang Y, Wang C, Yue B, Gambhir S, Too CO, Wallace GG, Electrochemically synthesized polypyrrole/graphene composite film for lithium batteries. *Adv. Energy Mater.* 2012, 2, (2): 266-272.

272. Wei H, Wang Y, Guo J, Yan X, O'Connor R, Zhang X, Shen NZ, Weeks BL, Huang X, Wei S, Guo Z, Electropolymerized polypyrrole nanocoatings on carbon paper for electrochemical energy storage. *ChemElectroChem*. 2015, 2, (1): 119-126.

273. Hara S, Zama T, Ametani A, Takashima W, Kaneto K, Enhancement in electrochemical strain of a polypyrrole-metal composite film actuator. *J. Mater. Chem.* 2004, 14, (18): 2724-2725.

274. Yuan L, Yao B, Hu B, Huo K, Chen W, Zhou J, Polypyrrole-coated paper for flexible solid-state energy storage. *Energy Environ. Sci.* 2013, 6, (2): 470-476.

275. Firoz Babu K, Dhandapani P, Maruthamuthu S, Anbu Kulandainathan M, One pot synthesis of polypyrrole silver nanocomposite on cotton fabrics for multifunctional property. *Carbohydr. Polym.* 2012, 90, (4): 1557-1563.

276. Kuhn HH, Characterization and application of polypyrrole-coated textiles. In *Intrinsically Conducting Polymers: An Emerging Technology*, Aldissi, M., Ed. Springer Netherlands: Dordrecht, 1993; pp 25-34.

277. Muller D, Silva JP, Rambo CR, Barra GMO, Dourado F, Gama FM, Neuronal cells' behavior on polypyrrole coated bacterial nanocellulose three-dimensional (3D) scaffolds. *J. Biomater. Sci. Polym. Ed.* 2013, 24, (11): 1368-1377.

278. Aznar-Cervantes S, Roca MI, Martinez JG, Meseguer-Olmo L, Cenis JL, Moraleda JM, Otero TF, Fabrication of conductive electrospun silk fibroin scaffolds by coating with polypyrrole for biomedical applications. *Bioelectrochemistry*. 2012, 85: 36-43.

279. Yu Q-Z, Dai Z-w, Lan P, Fabrication of high conductivity dual multi-porous poly (l-lactic acid)/polypyrrole composite micro/nanofiber film. *Mater. Sci. Eng., B.* 2011, 176, (12): 913-920.

280. Xie J, MacEwan MR, Willerth SM, Li X, Moran DW, Sakiyama-Elbert SE, Xia Y, Conductive core–sheath nanofibers and their potential application in neural tissue engineering. *Adv. Funct. Mater.* 2009, 19, (14): 2312-2318.

281. Laforgue A, Robitaille L, Deposition of ultrathin coatings of polypyrrole and poly (3, 4-ethylenedioxythiophene) onto electrospun nanofibers using a vapor-phase polymerization method. *Chem. Mater.* 2010, 22, (8): 2474-2480.

282. Kaur G, Adhikari R, Cass P, Bown M, Gunatillake P, Electrically conductive polymers and composites for biomedical applications. *RSC Advances*. 2015, 5, (47): 37553-37567.

283. Brigandi PJ, Cogen JM, Pearson RA, Electrically conductive multiphase polymer blend carbon-based composites. *Polym. Eng. Sci.* 2014, 54, (1): 1-16.

284. Huang J, Hu X, Lu L, Ye Z, Zhang Q, Luo Z, Electrical regulation of Schwann cells using conductive polypyrrole/chitosan polymers. *J. Biomed. Mater. Res., Part A*. 2010, 93A, (1): 164-174.

285. Wang Z, Roberge C, Wan Y, Dao LH, Guidoin R, Zhang Z, A biodegradable electrical bioconductor made of polypyrrole nanoparticle/poly(D,L-lactide) composite: A preliminary in vitro biostability study. *J. Biomed. Mater. Res., Part A*. 2003, 66A, (4): 738-746.

286. Shi G, Rouabhia M, Wang Z, Dao LH, Zhang Z, A novel electrically conductive and biodegradable composite made of polypyrrole nanoparticles and polylactide. *Biomaterials*. 2004, 25, (13): 2477-2488.

287. Takano T, Mikazuki A, Kobayashi T, Conductive polypyrrole composite films prepared using wet cast technique with a pyrrole–cellulose acetate solution. *Polym. Eng. Sci.* 2014, 54, (1): 78-84.

288. Collier JH, Camp JP, Hudson TW, Schmidt CE, Synthesis and characterization of polypyrrole–hyaluronic acid composite biomaterials for tissue engineering applications. *J. Biomed. Mater. Res.* 2000, 50, (4): 574-584.

289. Broda CR, Lee JY, Sirivisoot S, Schmidt CE, Harrison BS, A chemically polymerized electrically conducting composite of polypyrrole nanoparticles and polyurethane for tissue engineering. *J. Biomed. Mater. Res., Part A*. 2011, 98, (4): 509-516.

290. Guo B, Glavas L, Albertsson A-C, Biodegradable and electrically conducting polymers for biomedical applications. *Prog. Polym. Sci.* 2013, 38, (9): 1263-1286.

291. Severt SY, Ostrovsky-Snider NA, Leger JM, Murphy AR, Versatile Method for Producing 2D and 3D Conductive Biomaterial Composites Using Sequential Chemical and Electrochemical Polymerization. *ACS Appl. Mater. Interfaces.* 2015, 7, (45): 25281-25288.

292. Peng T, Sun W, Huang C, Yu W, Sebo B, Dai Z, Guo S, Zhao X-Z, Self-assembled free-standing polypyrrole nanotube membrane as an efficient FTO-and Pt-free counter electrode for dye-sensitized solar cells. *ACS Appl. Mater. Interfaces.* 2013, 6, (1): 14-17.

293. Wang J, Li S, Yi F, Zi Y, Lin J, Wang X, Xu Y, Wang ZL, Sustainably powering wearable electronics solely by biomechanical energy. *Nat. Commun.* 2016, 7.

294. Cho Y, Borgens RB, Biotin-doped porous polypyrrole films for electrically controlled nanoparticle release. *Langmuir*. 2011, 27, (10): 6316-6322.

295. Azioune A, Ben Slimane A, Ait Hamou L, Pleuvy A, Chehimi MM, Perruchot C, Armes SP, Synthesis and characterization of active ester-functionalized polypyrrole− silica nanoparticles: Application to the covalent attachment of proteins. *Langmuir*. 2004, 20, (8): 3350-3356.

296. Okner R, Domb AJ, Mandler D, Electrochemical formation and characterization of copolymers based on N-pyrrole derivatives. *Biomacromolecules*. 2007, 8, (9): 2928-2935.

297. Li W-H, Stöver HD, Monodisperse cross-linked core− shell polymer microspheres by precipitation polymerization. *Macromolecules*. 2000, 33, (12): 4354-4360.

298. Dyer A, Reynolds J, Skotheim T, Reynolds J, *Handbook of conducting polymers. Conjugated polymers: theory, synthesis, properties, and characterization*. 3rd ed.; CRC Press: Boca Raton, 2007; p 3-75.

299. Mavinakuli P, Wei S, Wang Q, Karki AB, Dhage S, Wang Z, Young DP, Guo Z, Polypyrrole/silicon carbide nanocomposites with tunable electrical conductivity. *J. Phys. Chem. C.* 2010, 114, (9): 3874-3882.

300. Lee JH, Chung IJ, Electrical conductivity of stretched polypyrrole film. *Synth. Met.* 1993, 53, (2): 245-249.

301. Yamaura M, Hagiwara T, Hirasaka M, Demura T, Iwata K, Structure and properties of biaxially stretched polypyrrole films. *Synth. Met.* 1989, 28, (1-2): 157-164.

302. Silk T, Hong Q, Tamm J, Compton RG, AFM studies of polypyrrole film surface morphology I. The influence of film thickness and dopant nature. *Synth. Met.* 1998, 93, (1): 59-64.

303. Sultana I, Rahman MM, Wang J, Wang C, Wallace GG, Liu H-K, All-polymer battery system based on polypyrrole (PPy)/para (toluene sulfonic acid) (pTS) and polypyrrole (PPy)/indigo carmine (IC) free standing films. *Electrochim. Acta*. 2012, 83: 209-215.

304. Bocchi V, Gardini GP, Chemical synthesis of conducting polypyrrole and some composites. *J. Chem. Soc., Chem. Commun.* 1986, (2): 148a-148a.

305. Lu Y, Shi G, Li C, Liang Y, Thin polypyrrole films prepared by chemical oxidative polymerization. *J. Appl. Polym. Sci.* 1998, 70, (11): 2169-2172.

306. Nakata M, Shiraishi Y, Taga M, Kise H, Synthesis of electrically conductive polypyrrole films by interphase oxidative polymerization. *Die Makromolekulare Chemie*. 1992, 193, (3): 765-771.

307. Xu J, Li M, Wu L, Sun Y, Zhu L, Gu S, Liu L, Bai Z, Fang D, Xu W, A flexible polypyrrole-coated fabric counter electrode for dye-sensitized solar cells. *J. Power Sources*. 2014, 257: 230-236.

308. Isaji S, Bin Y, Matsuo M, Electrical conductivity and self-temperature-control heating properties of carbon nanotubes filled polyethylene films. *Polymer*. 2009, 50, (4): 1046-1053.

309. Feiner R, Engel L, Fleischer S, Malki M, Gal I, Shapira A, Shacham-Diamand Y, Dvir T, Engineered hybrid cardiac patches with multifunctional electronics for online monitoring and regulation of tissue function. *Nat. Mater.* 2016, 15: 679–685.

SCIENTIFIC CONTRIBUTIONS

Publications

1. **Jifu Mao** and Ze Zhang. "*A Novel Modular Approach to Prepare a Multi-Biofunctional Surface by Using Flexible and Electrically Conducting Polypyrrole Membranes and Functional Particles"*(To be submitted)
2. **Jifu Mao**, Chaojing Li, Hyun Jin Park, Mahmoud Rouabhia, Ze Zhang. "*Conductive Polymer Waving in Liquid Nitrogen",* ***ACS Nano***, 2017 (DOI: 10.1021/acsnano.7b05546)
3. **Jifu Mao** and Ze Zhang. "*Conductive Poly(pyrrole-co-(1-(2-carboxyethyl)pyrrole)) Core-shell Particles: Synthesis, Characterization, and Optimization",* ***Polymer*** 2016,105,113-123
4. **Jifu Mao** and Ze Zhang. "*One-Step Reactivity-Driven Synthesis of Core-Shell Structured Electrically Conducting Particles for Biomedical application*", ***J. Mater. Chem. B***, 2016, 4, 5429-5436
5. **Jifu Mao**, Yongliang Wang, Eric Philippe, Denis Desaulniers, Ivan Vesely, Tomas Cianciulli, Jean-Michel Bourget, Ze Zhang, Lucie Germain, Robert Guidoin. "*Handling of Bovine Pericardium to Manufacture Bioprosthetic Heart Valves: Preventing the Pitfalls",* ***Morphologie,*** 2017(101):77-87.
6. Shiyun Meng, **Jifu Mao**, Elizabeth Nicole Rouse, Gaëtan Lebel, Robert R. Reed, David How, Lucie Germain, Ze Zhang, Robert Guidoin. *"Assessment of Red Kangaroo Pericardium As A Material Source for The Manufacture of Percutaneous Heart Valves"*, (2017) (Submitted)
7. Robert Guidoin, **Jifu Mao**, Rachid Zegdi, Jing Lin, Daniel How, Eric Philippe, Tomás Cianciulli, Lu Wang and Ze Zhang. "*Transcatheter Heart Valve Crimping and Expansion: Commentary"*, ***Journal of Medical and Surgical Pathology*** 2017, 2:144
8. Robert Guidoin, Rachid Zegdi, Jing Lin, **Jifu Mao**, Olivier Rochette-Drouin, Daniel How, Xiaoning Guan, Partrick Bruneval, Lu Wang, Lucie Germain, Ze Zhang. "*Transcatheter Heart Valve Crimping and The Protecting Effects of A Polyester Cuff ",* ***Morphologie*** 2017, 100, 234-244

9. Jean-Michel Bourget, Rachid Zegdi, Jing Lin, Paul Wawryko, Yahye Merhi, Channing Convelbo, **Jifu Mao**, Yijun Fu, Tingting Xu, Nina Ostara Merkel, Lu Wang, Lucie Germain, Ze Zhang, Robert Guidoin. "*Correlation between Structural Changes and Acute Thrombogenicity in Transcatheter Pericardium Valves after Crimping and Balloon Deployment*", ***Morphologie*** 2017, 101, 19-32

Oral presentations and posters

1. **Jifu Mao**, Chaojing Li, Hyun Jin Park, Mahmoud Rouabhia, Ze Zhang. (**August 8-11, 2016**) Highly Flexible Free-standing Conductive Polypyrrole Membrane. *37th Canadian High Polymer Forum*. Gananoque, Canada (**Oral Presentation**)
2. **Jifu Mao**, Hyun Jin Park,Yongliang Wang, Mahmoud Rouabhia, Ze Zhang. (**May 17-22, 2016**) A flexible Free-standing Conductive Polypyrrole Membrane with Asymmetric Surface Structures for Biomedical Application. *The 10th World Biomaterials Congress*. Montreal, Canada (**Poster Presentation**)
3. **Jifu Mao** and Ze Zhang. (**May 27-30, 2015**) Chemical Synthesis of Carboxyl Functionalized Polypyrrole Particles and Covalent Attachment of Antibody for Biosensor. *32nd Annual Meeting of The Canadian Biomaterials Society*. Toronto, Canada (**Oral Presentation**)
4. **Jifu Mao** and Ze Zhang. (**June 4-7, 2014**) Covalent Attachment of Antibody to Electrically Conductive Poly(pyrrole-co-(1-(2-carboxyethyl)pyrrole)) Particles. *31st Annual Meeting of The Canadian Biomaterials Society*. Halifax, Canada (**Poster Presentation**)
5. **Jifu Mao** and Ze Zhang. (**May 29 – June 1, 2013**) Synthesis and Characterization of Functionalized Polypyrrole Particles. *30th Annual Meeting of The Canadian Biomaterials Society*. Ottawa, Canada (**Poster Presentation**)
6. **Jifu Mao** and Ze Zhang. (**April 10-13, 2013**) Preparation and Characterization of Functional Polypyrrole Particles. *2013 Annual Meeting of the Society For Biomaterials*. Boston, the United States (**Poster Presentation**)